

FTS THESIS

621.3692 BOG

30001005537081

Bogdanov, Valentin Kanchev
Energy exchange processes in
erbium-doped fluoride
glasses

Energy exchange processes in erbium-doped fluoride glasses

A thesis submitted

by

Valentin Kanchev Bogdanov

For the degree of

Doctor of Philosophy



Optical Technology Research Laboratory,
School of Communications and Informatics,
Victoria University

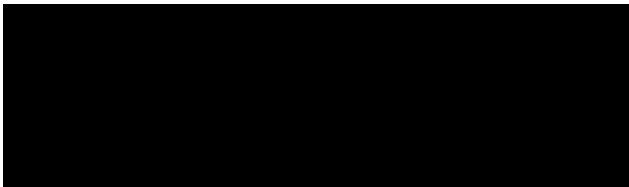
1999

Declaration

I, Valentin Kanchev Bogdanov, declare that the thesis titled,

"Energy exchange processes in erbium - doped fluoride glasses"

is my own work and has not been submitted previously, in whole or in part, in respect of any other academic award.



Valentin K.Bogdanov

Dated the 20th day of September, 1999

Acknowledgments

I would like to thank the former Department of Applied Physics, Victoria University, for the provision of Postgraduate Scholarship for this research.

There are two people without whom this thesis would have not been possible. First of all I would like to thank Professor David Booth who has provided me with superb guidance, advice and encouragement, as well as financial support, throughout this thesis and especially during the time of its writing. The second person to whom I am especially grateful is Keith Gibbs for his constant support and helpful advice. I feel really honoured to have had David and Keith as my supervisors and colleagues.

I am also grateful to Dr Peter Farrell and Dr Greg Baxter for their helpful assistance in various matters during the time of this work.

I also would like to thank my postgraduate student colleagues and other members of OTRL for their friendship and help during the period of this work. In particular, I have had some very helpful discussions with Ian Mitchell, Scott Wade, Chistopher Vale and Darol Garchev, for which I would like to express my gratitude.

Of the technical staff, I also would like to thank Alex Shelamoff for his assistance and technical advice. I am also grateful to all the other academic, technical and administrative staff from the former Department of Applied Physics for their friendly assistance.

All of the materials used in this work were provided by the Amorphous Materials Group, Department of Chemistry, Monash University. I would like to thank Professor Doug MacFarlane, Dr Peter Newman and Dr John Javorniczki for their helpful contribution during our collaborative work.

Finally, I must thank the most important people in my life. I thank my wife Iva and my sons Kaloian and Stefan for their understanding and patience during the course of this PhD. Thank you for being my support and inspiration. I also would like to thank my father Kancho and my mother Ruska who, despite being so far away, really made it all possible. Thank you all for all the love.

Abstract

In recent years there has been considerable interest in cross relaxation processes between ions in rare earth doped glasses and crystals. In particular interest has focused on diode-pumped lasers and optical waveguide amplifiers based on rare earth ions. This thesis is concerned with developing a model, which can explain the population and de-population processes which are responsible for the spectroscopic behaviour of Er^{3+} ions in fluoride glass materials. The model particularly concentrates on Er^{3+} :ZB(L)AN glasses with very heavy Er^{3+} doping levels. Under these circumstances the energy level dynamics can be dominated by non-linear multiple-ion cross relaxation processes.

The work includes CW and pulsed spectroscopic measurements on the glasses that provide data for the model. CW absorption and fluorescence measurements provide absorption cross sections for important pump transitions and data from which an energy level diagram can be constructed. Fluorescence waveforms measured under high-energy short-pulse excitation from a tunable OPO source are used to provide information on the temporal behaviour of the population of a large number of energy levels for a wide range of doping concentrations using five pump wavelengths. These measurements, together with some simplified modelling, are used to obtain a physical understanding of the processes responsible for the various fluorescence features observed. This information is then used to construct a rate equation model consisting of nine simultaneous non-linear differential equations containing fluorescence, multiphonon and cross relaxation terms which can predict the observed population behaviour of the levels quite well. The modelling has allowed identification and quantification of 14 ion-ion cross relaxation processes that are needed to explain the behaviour of these heavily doped materials.

The work has produced is by far the most detailed model of the behaviour of erbium ions in any material to date. The model will find application in the design and optimisation of lasers based on this material.

Table of Contents

	Page:
Declaration	I
Acknowledgments	II
Abstract	III
Table of contents	IV

Chapter 1 *Introduction*

1.1. Introduction	1.1
1.2. Aim and subject of the research	1.2
1.3. Structure of the thesis	1.4

Chapter 2 *Previous work on spectroscopic measurements and laser operation in bulk Er³⁺-doped fluoride materials*

2.1. Introduction	2.1
2.2. The fluorozirconate glass as a host	2.2

2.2.1.	Suitable for high doping concentrations	2.3
2.2.2.	Narrower fluorescence and absorption lines	2.3
2.2.3.	Low phonon-assisted transition rates	2.4
2.2.4.	Suitable host for IR lasers	2.7
2.3.	The dopant ions	2.8
2.3.1.	Rare earths	2.8
2.3.2.	Erbium	2.8
2.3.2.1.	Ion-ion exchange processes in erbium	2.10
2.3.2.2.	Erbium glasses co-doped with other rare earth ions	2.16
2.3.2.3.	Laser action in singly-doped erbium fluoride glasses	2.19
2.3.3.	General comments on energy transfer processes among ions	2.20
2.4.	Conclusions	2.28

Chapter 3 *Experimental arrangements for the measurement of spectroscopic data*

3.1.	Introduction	3.1
3.2.	Preparation of the glass samples	3.2
3.3.	Absorption measurements	3.3
3.3.1	Spectrophotometer measurements	3.3
3.3.2.	CW measurements with laser diode excitation	3.6
	• Experimental arrangement	3.6
	• Results	3.7
3.4.	Fluorescence measurements	3.9
3.4.1.	Experimental arrangement	3.9
3.4.2.	Dependence of the fluorescence intensity on the pump power	3.13
3.4.3.	Fluorescence decay waveforms	3.17
3.5.	Conclusions	3.19

Chapter 4 *Modelling of the population dynamics of the three lowest excited energy levels*

4.1.	Introduction	4.1
4.2.	Experimental results	4.3
4.2.1.	Exponential fits	4.8
	• Fitting of independent exponential rise and decay waveforms to section of a waveform	4.8
	• Fitting of multiple exponential function to a non-exponential decay	4.9
	• Fitting of combined rise and decay function to a waveform	4.10
4.2.2.	Fitting functions, derived from simple rate-equation modelling in low Er^{3+} concentrations	4.12
4.2.3.	Discussion	4.15
	• General observations	4.15
	• Level 2 (${}^4\text{I}_{11/2}$)	4.16
	• Level 1 (${}^4\text{I}_{13/2}$)	4.17
4.3.	Rate equation modelling including non-linear ion-ion exchange terms	4.18
4.3.1.	Direct pumping	4.18
4.3.2.	800nm pumping	4.22
	• Rate-equation modelling	4.22
	• Agreement between the model and the experimental data	4.28
	• Relative importance of the processes modelled	4.31
	• Accuracy of the parameters obtained from numerical fits	4.35
4.4.	Conclusions	4.38

Chapter 5 *Extended model of the population dynamics of erbium excited energy levels with 800nm pump*

5.1.	Introduction	5.1
5.2.	Results	5.5
5.2.1.	800nm pumping	5.5
5.2.1.1.	Fluorescence rise and decay times	5.5
	• Analytical fitting function for Level 5 ($^4S_{3/2}+^2H_{11/2}$)	5.7
	• Multiple exponential fits to the waveforms of Level 5 ($^4S_{3/2}+^2H_{11/2}$) in high Er^{3+} concentrations	5.8
5.2.1.2.	Dependence of the fluorescence rise and decay times on pump density	5.11
	• Processes which result in exponential behaviour of level populations	5.11
	• Processes which result in non- exponential behaviour of level populations	5.13
5.2.2.	Other Pumping Wavelengths	5.16
5.2.2.1.	Fluorescence rise and decay times	5.16
	• Pumping into the $^4I_{13/2}$ level (Level 1) at 1.5 μm	5.17
	• Pumping into the $^4I_{11/2}$ level (Level 2) at 975 nm	5.20
	• Pumping into the ($^4S_{3/2}+^2H_{11/2}$) levels (Level 5) at 520 nm	5.22
	• Pumping into the $^2H_{9/2}$ level (Level 6) at 403 nm	5.24
5.2.2.2.	Dependence of the fluorescence rise and decay times on the pump density	5.26
5.3.	Initial populations	5.28
5.3.1.	Initial population under 800 nm pumping	5.29
5.3.2.	Initial populations for other pumping wavelengths	5.30
5.4.	Analysis and discussions	5.32
5.4.1.	Analysis and discussions in the case of 800 nm pumping	5.32
5.4.1.1.	Level 1 ($^4I_{13/2}$)	5.36
	• Rise	5.36

• Decay	5.38
5.4.1.2. Level 2 (${}^4I_{11/2}$)	5.39
• Rise	5.39
• Decay	5.39
5.4.1.3. Level 3 (${}^4I_{9/2}$)	5.40
5.4.1.4. Level 4 (${}^4F_{9/2}$)	5.40
• Rise	5.41
• Decay	5.48
5.4.1.5. Level 5 (${}^4S_{3/2}+{}^2H_{11/2}$)	5.49
• Rise	5.49
• Decay	5.50
5.4.1.6. Levels 6 (${}^2H_{9/2}$), 7 (${}^2P_{3/2}+{}^2D_{3/2}+{}^2F_{3/2}$) and 8 (${}^4H_{9/2}+{}^4G_{9/2}$)	5.60
5.4.2. Pumping wavelengths other than 800 nm	5.63
5.4.2.1. 1.5 μm pumping (into Level 1)	5.64
5.4.2.2. 975 nm pumping (into Level 2)	5.67
5.4.2.3. 520 nm pumping (into Level 5)	5.71
5.4.2.4. 403 nm pumping (into Level 6)	5.74
5.5. Extended rate-equation model	5.76
5.5.1. Introduction	5.76
5.5.2. Non cross-relaxation constants used in the model	5.77
• Level 4 (${}^4F_{9/2}$)	5.78
• Level 5 (${}^4S_{3/2}+{}^2H_{11/2}$)	5.78
• Level 6 (${}^2H_{9/2}$)	5.78
• Level 7 (${}^2P_{3/2}+{}^2D_{3/2}+{}^2F_{3/2}$)	5.79
• Level 8 (${}^4H_{9/2}+{}^4G_{9/2}$)	5.79
5.5.3. The rate-equation model	5.81
5.5.4. Agreement between model predictions and experimental data	5.83
5.5.5. Accuracy of the parameters obtained from the numerical fits	5.94
5.5.6. Relative contributions of the various processes under 800nm pumping	5.97
• Level 1 (${}^4I_{13/2}$)	5.99
• Level 2 (${}^4I_{11/2}$)	5.99

• Level 4 (${}^4F_{9/2}$)	5.99
• Level 5 (${}^4S_{3/2}+{}^2H_{11/2}$)	5.100
5.6. Conclusions	5.100
Chapter 6 <i>Conclusions</i>	6.1
References	R.1
Symbols and Acronyms	S.1
Publications	P.1

Chapter 1

Introduction

1.1. Introduction

Erbium (Er), together with other rare-earth elements like holmium (Ho) and thulium (Tm), was first made to lase in the 1960s by a group from Bell Telephone Laboratories (Hecht, 1993). The laser transitions took place between energy levels of the relevant three-valent ions in the solid state host. One significant reason for attention to Er^{3+} is its laser transition at a wavelength just beyond $1.5 \mu\text{m}$. This transition is in the so-called "eye-safe" spectral range and therefore is of particular interest for remote-sensing and range-finding applications. Erbium also has another infrared (IR) laser transition at $2.7 \mu\text{m}$, which corresponds to a spectral region of strong water absorption and lasers operating at this wavelength have proved to be very suitable for surgery applications (Hecht, 1993). These laser transitions in erbium have been demonstrated in a number of crystal and glass materials (Koechner, 1992; France, 1991). The issues that affect overall laser performance are rather complicated but include thermal conductivity and properties of relevant energy levels such as lifetime, linewidth and fluorescence efficiency. The fluorescence efficiency and lifetimes are strongly dependent on phonon energy in the material and in the case of glass materials, fluoride-based hosts have been

shown to be of particular importance since they have very low phonon depopulation rates and hence high fluorescence efficiency and long lifetimes.

In recent years there has been a considerable interest in compact, laser-diode pumped, rare-earth laser sources, based on fluoride glasses, for a range of medical, sensor, spectroscopic and communications applications (Zayhowski *et al.*, 1989; Taira *et al.*, 1991; Knowles *et al.* 1992; Laporta *et al.*, 1993; Barnes, 1996). Materials configurations for these diode-pumped lasers include small rods, optical fibres, planar slabs and microchips. The major advantage of the microchip configuration is that single longitudinal mode operation can more easily be obtained since there are normally only a few longitudinal cavity modes within the gain profile. For compact bulk laser configuration such as a microchip, relatively large doping concentrations are normally required to obtain sufficient absorption of the pump radiation in the thin sample (~1 mm) (Laporta *et al.*, 1993). However, as the dopant concentration increases, ion-ion energy transfer processes between the dopant ions become increasingly important. These processes may lead to increased or decreased population of particular energy levels and thus are important for laser performance in highly-doped materials. For this reason the development of any practical device requires a very detailed knowledge for the population dynamics of the energy levels of the rare earth ions in the particular glass host. While, as will be seen in the next chapter, some of the important ion-ion cross-relaxation processes in Er^{3+} -doped fluoride glasses have already been identified, no detailed analysis of particular processes has yet been presented. Certainly, to the best of our knowledge, no values for the rate constants for any ion-ion interaction process in Er^{3+} -doped fluoride glass have been published.

1.2. Aim and subject of the research

A detailed study of all the ion-ion processes which have a significant effect on the population of important Er^{3+} energy levels in heavily-doped $\text{Er}/\text{ZB(L)AN}$ glass is the basic aim of the research described in this thesis. The dominant cross-relaxation processes have been identified and analysed. Values for the corresponding concentration-independent cross-relaxation rate constants have been obtained. A rate-

equation model describing the population behaviour of the erbium energy levels has been developed which is sufficiently detailed to enable optimisation of the design of materials suitable for laser applications. This model is applicable to any doping level and any pumping wavelength and provides a new level of understanding of the behaviour of these materials.

Initially both fluorozirconate and fluoroaluminate glasses were investigated. However, preliminary fluorescence measurements indicated that the fluorozirconates had slightly stronger fluorescence lines than those of similarly-doped fluoroaluminates. This confirmed the observations of Yanagita *et al.* (1989) for similar glasses. Thus it was decided to concentrate the research on fluorozirconate glasses only.

Glass samples required for this research were provided by the Amorphous Materials Group of the Department of Chemistry at Monash University. This Group was able to produce a range of stable fluorozirconate glasses with excellent optical quality and erbium concentration varying from 0.8 mol% to 18 mol%. To the best of our knowledge this is the highest reported erbium concentration in fluorozirconate glasses. As will be seen in the following chapters, these concentrations were high enough to give rise to a large number of cross-relaxation processes at rates that were comparable to other population and depopulation effects. Thus these processes had effects on the fluorescence behaviour at levels which were sufficient to allow determination of their rate constants.

At the time of commencement of this research, CW laser-diode sources with power levels suitable for pumping devices such as microchip lasers were readily available at about 800 nm and to a lesser extent at about 980 nm. A 1 W single junction laser diode at about 805 nm was available in the laboratory and it was decided to concentrate on this source for most CW measurements. Pulsed measurements of the rise and decay of fluorescence from the erbium levels were performed with an optical parametric oscillator (OPO) which could produce 10 ns pulses with energies varying up to 100 mJ over the wavelength range 220 nm to 1800 nm. For consistency, measurements performed with the OPO also concentrated on 800 nm pumping. Pumping at this wavelength was found to give rise to significant populations of a substantial number of erbium levels through cross-relaxation and excited-state-absorption (ESA) processes. Other wavelength between 400 nm and 1500 nm were

used to selectively excite particular levels to study their temporal fluorescence behaviour under direct pumping.

1.3. Structure of the thesis

The work presented in this thesis has been divided into six chapters:

- Chapter 1 contains a brief introduction and describes the aims and motivations of the research.
- Chapter 2 presents an overview of previously reported spectroscopic work on erbium-doped fluoride materials. The main properties of fluorozirconate glasses as a host and the erbium ions as dopant are described. Previously reported ion-ion exchange processes in erbium are described and summarised. This chapter also briefly discusses laser devices based on bulk fluoride glass hosts doped with pure erbium or erbium co-doped with other rare earth ions.
- Chapter 3 describes the experimental arrangements used for all the spectroscopic measurements. This chapter also describes most of the data which was measured. Absorption spectra were recorded using a Cary spectrophotometer and fluorescence spectra of all main lines have been obtained using the 800 nm laser-diode (LD) pump. These measurements have been used to calculate absorption cross-sections and construct a low-resolution energy level diagram for the Er^{3+} ion in these fluorozirconate materials. The fluorescence intensity of various lines has been studied as a function of the erbium concentration and the excitation power. The most important and certainly the most extensive measurements are those of fluorescence rise and decay times of the various levels. The waveforms of ten different fluorescence lines under five different pumping wavelengths (including the main one at 800nm) were measured in samples with erbium concentration from 0.8 mol% to 18 mol%. The substantial change of rise and decay rates of some fluorescence lines with concentration or the non-exponential behaviour of other fluorescence lines were a clear indication of the presence of cross-relaxation processes. The majority of the fluorescence waveform data is not presented directly

in Chapter 3 but is deferred to Chapters 4 and 5 where it is combined with appropriate analysis and discussion.

- Many models for erbium in materials with higher photon energies than fluoride glasses have considered only a relatively small number of lower energy levels. Certainly even in fluoride glasses, most of the excited state population is in the lowest couple of levels. Hence it seems reasonable to see to what extent it is possible to model the behaviour of the glasses with only the involvement of a restricted number of levels. This is done in Chapter 4. The same chapter also introduces the techniques used in the analysis and modelling of the data. This modeling shows that it is not possible to obtain reasonable fits to the complete data set without the involvement of higher levels. It also strongly suggests the involvement of previously unreported three-ion energy exchange processes.
- In Chapter 5 the higher energy levels have also been included in the model. These levels had substantially smaller population than the lower levels under 800 nm pumping and therefore tended to be sensitive indicators of the extent of many cross relaxation processes originating from the lower levels. This chapter contains detailed discussions of the reasons for inclusion of the various non-linear cross-relaxation terms and their effect on the populations of the levels and hence the measured fluorescence waveforms. A comprehensive model including most of the fluorescence levels of erbium has been developed. The cross-relaxation parameters were varied until a single set was obtained which adequately reproduced the observed fluorescence waveforms for the whole range of concentrations used. As a result of this modelling 14 cross-relaxation processes were identified. Six of these fourteen processes had previously been reported for the Er^{3+} ion in some host but very few values of the corresponding rate constants have been reported, none of which were in fluoride glasses.
- Chapter 6 summarises the main results and conclusions from the research.

Chapter 2

Previous work on spectroscopic measurements and laser operation in bulk Er^{3+} -doped fluoride materials

2.1. Introduction

As has already been mentioned, the motivation for this work has been to develop an understanding of materials with very heavy doping concentrations, which are suitable for applications such as miniature lasers or waveguide devices, where the interaction length is small. For such an understanding, knowledge of both the optical characteristics of the glass host and the spectroscopic properties of the dopant ions is necessary. This chapter summarises previous spectroscopic work with erbium ions in fluoride glass hosts. To help the reader understand future discussions regarding the spectroscopic properties of Er^{3+} a very detailed energy level diagram has been supplied as a foldout in the end of the thesis. A table with the absorption wavelengths and the corresponding wavenumbers of some of the excited states of the Er^{3+} ions has also been provided there.

It is very clear from the literature that the fluorescence properties of an active ion are in general strongly dependent on the nature of the host material and so studies of the energy-level processes in the ion are necessarily specific to a particular host. However, because there has been relatively little modelling work on singly-doped erbium materials, and particularly in fluoride hosts, the discussion includes some work

in other crystal and glass host materials as well as some work on co-doped materials. The purpose of the co-dopants in general is to aid in selective excitation of the upper laser level or selective de-population of the lower laser level. Reports on materials co-doped with other ions, especially Yb^{3+} ions, represent a substantial part of the literature on Er^{3+} -doped materials suitable for laser-diode pumping. Such reports, however, have been only very briefly described here as the population behaviour in co-doped materials can be very different from that in materials doped only with Er^{3+} . For example, the addition of Yb^{3+} ions leads to strong coupling of the ${}^2\text{F}_{5/2}$ Yb^{3+} level to the ${}^4\text{I}_{11/2}$ Er^{3+} level, which results in a considerable shortening of the lifetimes of most levels in the erbium system.

2.2. The fluorozirconate glass as a host

Up until mid-seventies, many years after the discovery of the laser, crystal hosts were the dominant materials used for CW laser applications, due mainly to their superior thermal conductivity. One major step in the development of the CW glass lasers was made by Stone and Burrus (1973) with the demonstration of a working laser-diode pumped Nd^{3+} /oxide glass laser. Two years later Poulain *et al.* (1975) introduced the fluorozirconate glasses based on heavy metal fluorides. The initial $\text{ZrF}_4\text{-BaF}_2\text{-NaF}$ (ZBN) system formed an unstable glass. This composition, however, was stabilised with the addition of AlF_3 and LaF_3 and the, now well known, ZBLAN glass was reported for the first time. The interest in these new fluoride glasses and their applications was so overwhelming, that a number of books (Almeida (1987); France (1990), (1991); Aggarwal and Lu (1991)) and a major international symposium series (International Symposium on Halide Glasses) have been dedicated to them. In general, ZBLAN is the designation of these glasses for doping concentrations below 4 mol%. In higher doping concentrations the La^{3+} ions are usually completely substituted by the dopant ions and the glass is referred to as ZBAN. Throughout this thesis a universal naming protocol of ZB(L)AN, describing all glasses (with concentrations from 0.2mol% to 18 mol%), has been used.

The heavy metal structure of these glasses resulted in several important properties, which proved these glasses to be a viable alternative of the popular silica-based glasses in some infrared applications. These properties are outlined below.

2.2.1. Suitable for high dopant concentrations

One consequence of the specific structure of the fluorozirconate glasses is that these glasses could be doped with much higher rare-earth-ion concentrations than the silica-based glasses. The current understanding of the structure of fluoride-based glasses is the subject of some uncertainty. Attempts have been made to describe their structural properties in terms of network forming models which are well accepted for glasses based on silica in which there are strong covalent bonds (France, 1990). However, it seems more accurate to describe the structural properties in terms of the ions being loosely bound by relatively weak electrostatic bonds (Newman, 1999). In this latter model, no network is formed and the possibility for high doping concentrations is easily understood as the ions fit into a much more open easily-modified lattice. The limitation on doping levels is set by the onset of crystallisation. The tendency of some ions to lower their energy state by spontaneous crystal formation is avoided by addition of non-compatible ions to the mix. Thus for increasing dopant levels it is also necessary to make variations to the base glass composition in order to preserve the random glass structure. This has been the basic strategy used in making the glasses in this work. As the doping concentration is increased, some intuition has been necessary in making compensating changes in the composition of the base materials in order to maintain a glass structure. Chapter 3 contains a table which lists the full composition of each glass used in this work and to the best of our knowledge the upper dopant level of 18 mol% is the highest erbium concentration which has been reported in fluoride glasses.

2.2.2. Narrower fluorescence and absorption lines

Experimentally it is observed that the fluorescence linewidth of the erbium transitions in fluoride glasses is narrower than the corresponding transitions in silica glasses (Shinn *et al.*, 1983; Adam and Sibley., 1985; Samek *et al.*, 1992). This is clearly related to the glass structure although the details are not fully understood. The fluorescence lines in solid materials such as glasses are broadened by variations of the electric field at dopant sites within the glass. Thus a reduced inhomogeneous linewidth in erbium-doped glasses is an indication of a narrower range of magnitudes of electric fields at the erbium sites. A model of a loosely-bound electrostatic lattice in fluoride glasses would seem to imply a much a greater variety of dopant sites than would apply in a network environment. However, the immediate environment of the erbium site in fluoride glasses always consists of six fluoride ions and also the electric fields in fluoride glasses are relatively weak. The overall effect can be understood to produce a narrower range of electric field magnitudes.

When considering the absorption and the fluorescence lines of rare-earth dopants in glasses and crystals, it is important to understand that the optical transitions of the trivalent rare-earth ions take place within the 4f shell which is to some extent shielded from outside influences by the filled 5s and 5p shells. This is responsible for the relatively small variation of observed fluorescence spectra for a given ion between different hosts (compared, for example, to the variation for transition metal ions in similar hosts)(Desurvire, 1994).

2.2.3. Low phonon-assisted transition rates

The heavy atoms and weak bonds in fluoride glasses results in relatively low phonon energies. The fundamental phonon energy in these glasses is approximately 500cm^{-1} which is substantially smaller than phonon energies in many other glasses as seen in Table 2.2-1.

Host	Borate	Phosphate	Silicate	Germanate	Tellurite	Fluorozirconate	Sulfide	LaF ₃
$\hbar\omega$ (cm ⁻¹)	1400	1200	1100	900	700	500	350	350

Table 2.2-1 Phonon energies of various glasses and LaF₃ crystal (Reisfeld and Jorgensen, 1987)

This low phonon energy results also in lower multiphonon assisted decay rates for the fluorozirconates as compared to other glasses such as silicates or phosphates. It has been shown (Layne *et al.*, 1977; Reisfeld and Jorgensen, 1977) that the multiphonon assisted decay rate, W_{21} , from level 2 to level 1 varies exponentially with the energy gap between the two levels:

$$W_{21} = a[n(T)+1]^p e^{-b(E_2-E_1)}, \quad (2.2-1)$$

where; p is the number of phonons required to bridge the energy gap (E_2-E_1) and a and b are host-dependent parameters which are considered to be insensitive to the rare earth ion and the particular levels involved. The Bose-Einstein occupational number (which is temperature dependent) for the effective phonon mode is:

$$n(T) = \frac{1}{\frac{\hbar\omega}{e^{kT}} - 1}, \quad (2.2-2)$$

where $\hbar\omega$ is the fundamental phonon energy. Values for the parameters a and b and the phonon energies $\hbar\omega$ for various glasses are available (Reisfeld and Jorgensen., 1987). For fluorozirconate glasses, the values given were $a=1.59 \times 10^{10} \text{ s}^{-1}$ and $b= 5.19 \times 10^{-3} \text{ cm}$. Similar values of $1.88 \times 10^{10} \text{ s}^{-1}$ and $5.77 \times 10^{-3} \text{ cm}$ respectively were obtained for ZBLA glasses by Shinn *et al.* (1983) who also reported multiphonon decay rates in fluoride glasses which were an order of magnitude lower than those observed in germanate and tellurite glasses. They pointed out that the parameters a and b are characteristics only of the glass host and so equation (2.2-1) allows the non-radiative rates for any lanthanide ion in a particular host to be calculated (within a factor of about two). The uncertainty in the estimates of multiphonon rates obtained using equation (2.2-1) was, however, pointed out to be much larger in the case of a very large or very small (one or two phonons) energy gaps. Shinn *et al.* (1983) presented also a very detailed study of the spectroscopic properties of erbium in ZBLAN. Optical absorption and emission spectra were presented and oscillator strengths of the transitions between J manifolds at 300 K and 15 K have been calculated. The non-radiative decay rates were determined as a

difference between the measured and the calculated radiative rates. The predictions of the phenomenological equation (2.2-1), useful in a number of crystals and glasses, was found to be in agreement with the predictions of the Huang-Rhys theory of multiphonon decay at temperatures up to room temperature.

Wetenkamp *et al.* (1992 b) also studied the optical properties of erbium, as well as a variety of other rare earth ions, in ZBLAN glasses. Branching ratios and radiative decay-rates have been calculated for the erbium $^4S_{3/2}$, $^4I_{11/2}$ and $^4I_{13/2}$ levels and these rates have been compared to the experimentally measured ones. Values for the non-radiative decay rates and the parameters a and b in Equation (2.2-1) were obtained. The reported values of $a=1.99 \times 10^5 \text{s}^{-1}$ and $b=2.1 \times 10^{-3} \text{cm}$, however, are substantially different from the values published by Reisfeld and Jorgensen (1987) and Shinn *et al.* (1983). Results from the work of this thesis are consistent with the values given by Reisfeld and Jorgensen (1987) and Shinn *et al.* (1983).

In general, lower fundamental phonon energy leads to lower multiphonon-assisted decay rates for a given energy difference between two levels. This would suggest that the fluorozirconate glasses have smaller multiphonon assisted decay rates than most other glasses in Table 2.2-1. These non-radiative decay rates are directly connected to the fluorescence quantum efficiency of the level and also to the overall lifetime of the level by:

$$\eta = \frac{\sum A_r}{\sum A_r + \omega + \sum A_{ET}} \quad \text{and} \quad \tau = \frac{1}{\sum A_r + \omega + \sum A_{ET}}. \quad (2.2-3)$$

In these equations, η is the fluorescence quantum efficiency, A_r are the radiative spontaneous decay rates to the various lower levels, ω is the multiphonon assisted decay rate, τ is the overall decay time of the level and the A_{ET} terms represent the rates of ion-ion energy transfer processes. Because of the lower multiphonon decay rates, the fluorozirconate glasses should have higher quantum efficiencies and longer decay times than many other glasses.

Indeed, the studies of Yanagita *et al.* (1989) confirmed that the quantum efficiency of erbium-doped ZBLAN glasses was superior to that of similarly doped fluorozirco-aluminate, phosphate, fluorophosphate and tellurite glasses. The radiative and non-radiative properties of each of these glasses were studied and compared. The radiative decay rates of the $^4I_{11/2}$ level were calculated using the Judd-Ofelt theory (see

later in this chapter). The measured decay times for the ${}^4I_{11/2}$ and ${}^4I_{13/2}$ levels were observed to be longest in the ZBLAN glasses. Yanagita *et al.*, however, pointed out that an important advantage of the fluorozirco-aluminate over the ZBLAN glasses was the fact that the former could be doped with up to 20% rare-earth ions (a concentration which was significantly higher than the levels achieved with ZBLAN at that time)

There are some important implications resulting from the higher fluorescence quantum efficiency and the longer decay times in the fluorozirconate glasses. The larger quantum efficiencies would mean that more and stronger fluorescence lines should be observed in fluorozirconate glasses (France, 1991). The longer decay times of the levels, on the other hand, would offer lower threshold for lasing and also greater probabilities for two (or more) photon absorption or cross-relaxation processes, which would increase the possibility of obtaining up-conversion lasing. This was confirmed by Quimby *et al.* (1987) who reported that the up-conversion from infrared to visible light in erbium-doped fluoride glasses is four orders of magnitude more efficient than in silicate or phosphate glasses. An efficient upconversion from red to violet was reported by Pope *et al.* (1997) in erbium-doped fibre. A three-photon excitation process was found to be responsible for this fluorescence.

2.2.4. Suitable host for IR lasers

The relatively small phonon energy and high quantum efficiency of the fluorozirconate glasses makes them especially suitable for IR laser applications. As was pointed out by France *et al.* (1991), if a typical radiative decay time of 10^{-3} s is assumed in fluoride glass, a minimum energy gap of 3100cm^{-1} is required between two levels for the radiative and phonon assisted decay rates to be equal. In other words, in these glasses a quantum efficiency of at least 50% would be present for energy separations greater than 3100 cm^{-1} (fluorescence wavelengths below about $3.2\text{ }\mu\text{m}$). This compares very favourably with similar calculations for oxide glasses and YAG crystals, where the same 50% quantum efficiency is obtained only for wavelengths below $2\text{ }\mu\text{m}$ (Auzel, 1989; France, 1991). A further advantage of the fluorozirconate glasses is their superior transmission in the mid-IR compared to that of silicates or phosphates.

2.3. The dopant ions

2.3.1. Rare earths

Electric dipole transitions between the states of the $4f^N$ electron configuration of an isolated ion are normally forbidden by the parity selection rule. Inside a host, however, this prohibition is avoided due to the non-centrally symmetric interactions of the ions with the surroundings, which mixes states of opposite parity (Auzel, 1989; France, 1991). An important step in developing the theory of transition intensities in rare-earth ions was made by Judd (1962) and Ofelt (1962). In the early 1960s they developed a quantum-mechanical theory of rare-earth-ion doped solid-state media, which allowed estimates to be made of the electric dipole transition strength between any pair of LSJ manifolds. Regardless of the many approximations made by the theory, it has been widely used for calculating the spontaneous emission probabilities of the energy levels in rare earths (Reisfeld and Jorgensen, 1977; Vickers and McFarlane, 1992; Wetenkamp *et al.*, 1992 b).

The basic spectroscopic properties of rare-earth ions in a range of glasses, including fluorides and fluorozirconates, have been comprehensively reviewed (Auzel 1989; Miniscalco, 1993). The energies and line-widths of levels, absorption cross-sections, excited state decay times, radiative and non-radiative rates as well as energy transfer and up-conversion processes in these glasses have been discussed in detail.

2.3.2. Erbium

Laser action and optical amplification in the Er^{3+} ion in a variety of hosts has attracted considerable attention in recent years. Erbium has been of interest because it can be optically pumped at a number of the popular high-power laser-diode wavelengths and its laser wavelengths are in IR spectral regions which are important for optical

communications (Nakazawa *et al.*, 1990; Kimura and Nakazawa, 1992), remote sensing (Hecht, 1993) and medical applications (Pollnau, 1997).

Erbium was first reported to lase in a silicate glass host by Snitzer and Woodcock, (1965). In fluoride glasses, Okada *et al.* (1988) studied the green (550 nm) and red (650 nm) fluorescence lines at erbium doping concentrations up to 15 mol%. Using an 807 nm LD pump, the dependence of the 987 nm, 650 nm and 550 nm fluorescence lines as a function of the pumping power was studied. While the intensity of the 987 nm fluorescence line varied linearly with pump power, the intensity of the other two lines exhibited a quadratic dependence, confirming their up-conversion origin. These results were very similar to the results of our study in a similar experiment (Chapter 5). In another experiment, reported in the same paper, an Argon ion laser at 488 nm as well as the LD were used as a pumping source in a study of the fluorescence intensities of the 550 and 650 fluorescence lines as a function of the erbium concentration. A very different dependence of the fluorescence intensity on the doping concentration was observed in both cases, but no explanation was offered. Our study (Chapter 5) confirmed the presence of cross-relaxation processes, originating from the lower levels, which under 807 nm pumping repopulate the levels responsible for the 650 nm and 550 nm fluorescence lines and thus explain the trend toward a stronger fluorescence intensity in higher concentrations, observed by Okada *et al.* (1988). When the 488 nm pumping of the Ar laser was used, the populations of the higher levels were relatively high, which stimulates various cross-relaxation processes, which were affecting the populations of these levels. The populations of the lower levels, however, are relatively small and the effective rates of the cross-relaxation processes, originating from these levels, were not sufficient to cause a substantial repopulation of the ($^2H_{11/2}+^4S_{3/2}$) and $^4F_{9/2}$ levels. Thus a concentration quenching of the 650 nm and 550 nm fluorescence lines should be observed. This analysis is based on our modelling work, however, it explains well the behaviour of these two fluorescence lines, observed by Okada *et al.*

Calculated oscillator strengths and the spontaneous emission probabilities for excited states in erbium have been reported by Reisfeld *et al.* (1982); Shinn *et al.* (1983); Miniscalco *et al.* (1989); Vickers and McFarlane (1992) and Zou and Izumitani (1993). Especially detailed work has been presented by Vickers and McFarlane (1992),

who reported calculated oscillator strengths for 12 excited energy levels in Er^{3+} , as well as many levels in Ho^{3+} , Tm^{3+} and Pr^{3+} .

2.3.2.1. Ion-ion exchange processes in erbium

Many researchers have studied population quenching, resulting from various ion-ion energy exchange processes that affect the population dynamics of the system. The interest in these processes is almost 50 years old (Dexter, 1953; Inokuti and Hirayama, 1965). The effect of the ion-ion exchange processes becomes significant in high dopant concentrations where the distances between the dopant ions in the host is reduced and an energy exchange can occur between similar ions of the same dopant or different ions in co-doped materials. From Equation (2.2-3) it is clear that if this energy transfer rate A_{ET} is high enough it can completely dominate the other relaxation processes and reduce the fluorescence quantum efficiency. Depending on the particular level involved, these cross-relaxation processes add or remove population from the level and hence can enhance or limit the performance of any practical device.

An energy level diagram for Er^{3+} is presented in Figure 2.3-1 below. For the purpose of visualising and easier identification of the levels a numbering system has been introduced where the $^4I_{15/2}$ level is denoted as Level 0, the $^4I_{13/2}$ level - as

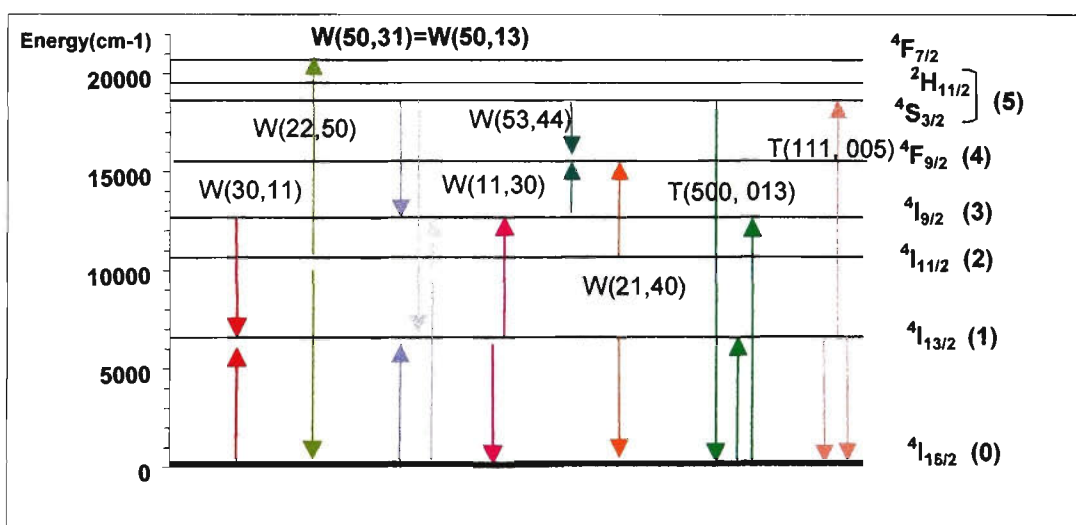


Figure 2.3-1 Energy level diagram for Er^{3+} and cross-relaxation processes reported in Er^{3+} . For designation of cross-relaxation processes and corresponding references - see Table 2.3-1 and the text below.

Level 1 and so on. Level 5 in Figure 2.3-1 consists of three closely spaced energy levels ($^4S_{3/2}$, $^2H_{11/2}$ and $^4F_{7/2}$), which at room temperature are thermally coupled. A brief summary of the cross-relaxation processes reported previously in Er^{3+} is presented in Table 2.3-1.

Process:	Reference:
W(30,11)	Moine <i>et al.</i> , 1989; Knowles and Janssen, 1992; Zou and Izumitani, 1993.
W(22,50)	Moine <i>et al.</i> , 1989; Shi <i>et al.</i> , 1990; Brenier <i>et al.</i> , 1990; Wetenkamp, 1991; Knowles and Janssen, 1992; Lupei <i>et al.</i> , 1993; Zou and Izumitani, 1993; Pollnau, 1997
W(50,31)=W(50,13)	Haixing and Fuxi, 1985; Moine <i>et al.</i> , 1989; Shi <i>et al.</i> , 1990; Brenier <i>et al.</i> , 1990; Wetenkamp, 1991; Knowles and Janssen, 1992; Lupei <i>et al.</i> , 1993; Pollnau, 1997
W(11,30)	Shi <i>et al.</i> , 1990; Yanagita <i>et al.</i> , 1991 Knowles and Janssen, 1992; Lupei <i>et al.</i> , 1993; Zou and Izumitani, 1993 Brunel <i>et al.</i> , 1996; Pollnau, 1997
W(21,40)	Zou and Izumitani, 1993
W(53,44)	Oomen <i>et al.</i> , 1990
T(500,013)	Zhekov <i>et al.</i> , 1990; Georgescu <i>et al.</i> , 1991; Lupei <i>et al.</i> , 1993
T(111,005)	Lupei <i>et al.</i> , 1993

Table 2.3-1 Previously reported ion-ion interaction processes involving Er^{3+} in various materials. Where possible, the papers chosen describe these processes in fluoride-based materials. For the designation of the cross-relaxation processes see Figure 2.3-1 and text below.

In this thesis we discuss a very large number of ion-ion energy exchange processes and have found it convenient to introduce our own nomenclature for describing them. The processes are designated as either two-ion (W) or three-ion (T), followed by up to six numbers indicating (starting levels, finishing levels). The processes, with the energy levels numbered as in Figure 2.3-1, are detailed below:

$$\begin{aligned}
 \mathbf{W(30,11)}: & [^4I_{9/2} + ^4I_{15/2} \rightarrow 2(^4I_{13/2})]; & \mathbf{W(22,50)}: & [2(^4I_{11/2}) \rightarrow ^4S_{3/2} + ^4I_{15/2}]; \\
 \mathbf{W(50,31)}: & [(^2H_{11/2} + ^4S_{3/2}) + ^4I_{15/2} \rightarrow (^4I_{13/2}) + (^4I_{9/2})]; & \mathbf{W(11,30)}: & [2(^4I_{13/2}) \rightarrow ^4I_{9/2} + ^4I_{15/2}];
 \end{aligned}$$

$$\mathbf{W(50,31)}: [(^2\text{H}_{11/2} + ^4\text{S}_{3/2}) + ^4\text{I}_{9/2} \rightarrow 2(^4\text{F}_{9/2})]; \quad \mathbf{W(21,40)}: [^4\text{I}_{11/2} + ^4\text{I}_{13/2} \rightarrow ^4\text{F}_{9/2} + ^4\text{I}_{15/2}];$$

$$\mathbf{T(500,013)}: [(^2\text{H}_{11/2} + ^4\text{S}_{3/2}) + 2(^4\text{I}_{15/2}) \rightarrow ^4\text{I}_{15/2} + ^4\text{I}_{13/2} + ^4\text{I}_{9/2}];$$

$$\mathbf{T(111,005)}: [3(^4\text{I}_{13/2}) \rightarrow 2(^4\text{I}_{15/2}) + (^2\text{H}_{11/2} + ^4\text{S}_{3/2})].$$

In the literature values of the corresponding cross-relaxation constants have been reported for very few of these processes. Table 2.3-2 summarises these reported values for different materials.

Rate Constant:	Value(cm^3/s):	Material:	Er^{3+} (at.%)	Reference:
W(11.30)	1×10^{-18}	Phosphate glass		Nilsson <i>et. al.</i> , 1994
W(11.30)= =W(22,50)	2.6×10^{-18} 3.76×10^{-17}	Si fibre laser	$4 \times 10^{19} \text{cm}^{-3}$ $2 \times 10^{20} \text{cm}^{-3}$	Di Pasquale, 1996
W(11.30)	1.8×10^{-17}	$\text{Y}_3\text{Al}_5\text{O}_{12}$	10	Zhekov <i>et. al.</i> , 1986
W(11.30)	2.5×10^{-17}	$\text{Y}_3\text{Al}_5\text{O}_{12}$	15	Zhekov <i>et. al.</i> , 1984
W(11.30)	1.5×10^{-17}	$\text{Y}_3\text{Al}_5\text{O}_{12}$	16.6	Shi <i>et. al.</i> , 1990
W(11.30)	4×10^{-17}	$\text{Ba}_3\text{Y}_2\text{F}_8$	20	Knowles and Jenssen, 1992
W(11.30)	4×10^{-17}	$\text{Y}_3\text{Al}_5\text{O}_{12}$	33.3	Shi <i>et. al.</i> , 1990
W(11.30)	2.5×10^{-17}	$\text{Y}_3\text{Al}_5\text{O}_{12}$	50	Shi <i>et. al.</i> , 1990
W(11.30)	25.0×10^{-17}	$\text{Y}_3\text{Al}_5\text{O}_{12}$	50	Zhekov <i>et. al.</i> , 1984
W(11.30)	1.3×10^{-15}	$\text{Y}_3\text{Al}_5\text{O}_{12}$	50	Lupey <i>et. al.</i> , 1993
W(22.50)	3.0×10^{-17}	$\text{Y}_3\text{Al}_5\text{O}_{12}$	16.6, 33.3, 50	Shi <i>et. al.</i> , 1990
W(22.50)	5×10^{-17}	$\text{Y}_3\text{Al}_5\text{O}_{12}$	10	Zhekov <i>et. al.</i> , 1986
W(22.50)	0.8×10^{-17}	$\text{Ba}_3\text{Y}_2\text{F}_8$	20	Knowles and Jenssen, 1992
W(22.50)	3.7×10^{-15}	$\text{Y}_3\text{Al}_5\text{O}_{12}$	50	Lupey <i>et. al.</i> , 1993
W(50.31)	1.06×10^{-15}	$\text{Y}_3\text{Al}_5\text{O}_{12}$	50	Georgescu <i>et. al.</i> , 1998

Table 2.3-2 Cross-relaxation rate constants reported as numerical values in the literature for Er^{3+} in different materials

An investigation of the concentration dependence of the fluorescence intensities of Er^{3+} in fluoride glass at room temperature was carried out by Haixing and Fuxi (1985). In their experiments a so-called "infrared fluorescence-enhanced phenomenon" occurred when pumping the $^4\text{S}_{3/2}$ and $^2\text{H}_{11/2}$ levels. In this effect, the intensity of the visible (~540 nm) fluorescence from these levels decreased rapidly with

increasing concentration, in contrast to the 1.56 μm fluorescence from the ${}^4\text{I}_{13/2}$ level which increases its intensity. With pumping of only the ${}^4\text{I}_{11/2}$ and ${}^4\text{I}_{13/2}$ levels, however, the fluorescence of the latter exhibited the usual concentration quenching. The effect of the cross-relaxation process W(50,31) (see Figure 2.3-1 and Table 2.3-1) was proposed as a possible explanation of this behaviour. Our work confirmed the existence of this process, however a three-ion process (T(500,031)) was found to be more important for the population dynamics of the ${}^4\text{S}_{3/2}$ and ${}^2\text{H}_{11/2}$ levels when these levels were pumped directly.

Oomen *et al.* (1990) and Van Dongen *et al.* (1991) paid special attention to the origin of the red (from level ${}^4\text{F}_{9/2}$) and the green (from levels (${}^4\text{S}_{3/2}+{}^2\text{H}_{11/2}$)) upconversion fluorescence in Er^{3+} -doped fluoride glasses as well as to the cross-relaxation processes which affect these fluorescence lines. Fluorescence intensities of these lines as a function of the intensity of the pump were studied in order to determine the origin of the population of the corresponding ${}^4\text{F}_{9/2}$ and (${}^4\text{S}_{3/2}+{}^2\text{H}_{11/2}$) levels. A multiphonon decay from the (${}^4\text{S}_{3/2}+{}^2\text{H}_{11/2}$) levels to the ${}^4\text{F}_{9/2}$ level was found to be the major mechanism responsible for the population of the ${}^4\text{F}_{9/2}$ level in doping concentrations below 1 mol%. In higher concentrations, the cross-relaxation process W(53,44) (see Figure 2.3-1) was found to become increasingly important for the population of the ${}^4\text{F}_{9/2}$ level. A decay with a double time-constant was reported for the green fluorescence line at 545 nm. The initial part of this decay exhibited a time-constant of about 540 μs , which was similar to the "intrinsic" decay time of this (${}^4\text{S}_{3/2}+{}^2\text{H}_{11/2}$) combined level. Here "intrinsic" refers to the decay time measured under direct pumping in doping concentrations which are sufficiently low so that no cross-relaxation processes are affecting the population of the level. The second part of the decay curve exhibited a slower decay rate, equivalent to a time constant of about 1.5 ms. The existence of a cross-relaxation process was suggested as an explanation, however, no further discussions or justification was offered. A similar double decay was observed in the green fluorescence at 550 nm in our experiments with 800 nm pump. An energy transfer process originating from the lower energy levels was shown to repopulate the (${}^4\text{S}_{3/2}+{}^2\text{H}_{11/2}$) levels thus imposing on them a second (and longer) decay time constant. In work reported in later chapters of this thesis, a three-ion cross-

relaxation process originating from the $^4I_{9/2}$ level was found to be responsible for the population of the $^4F_{9/2}$ level in high Er^{3+} concentrations.

A very extensive study of the spectroscopic properties, as well as various energy transfer processes in Er^{3+} -doped ZBLAN, aluminate, gallate and several other glasses was presented by Zou and Izumitani (1993). Spontaneous emission probabilities were calculated (Judd-Ofelt calculation) for a large number of the excited Er^{3+} levels. The red and the green erbium fluorescence lines under 800 nm pumping were studied. Processes involving an excited state absorption and cooperative energy transfer from the $^4I_{13/2}$ and $^4I_{11/2}$ levels were suggested to be responsible for the population of the corresponding $^4F_{9/2}$ and ($^4S_{3/2}+^2H_{11/2}$) levels (see processes W(11,30), W(22,50) and W(21,40) in Figure 2.3-1 and Table 2.3-1).

A study of energy transfer processes in Er^{3+} when used as a co-dopant for Ho^{3+} ions has been reported by Moine *et al* (1989). The strong visible absorption of Er^{3+} has been used to sensitize the Ho^{3+} ions in order to optimise its laser emission at 2 μm . Several cross-relaxation processes were described in detail (see W(30,11), W(22,50) and W(50,31) in Figure 2.3-1 and Table 2.3-1). The fluorescence dynamics in the erbium:holmium co-doped system has been studied in ZBLA, BATY and BIZYT fluoride glasses at room temperature. Numerous concentrations and different selective laser excitations in the visible and infrared spectral ranges were used in order to determine the best concentrations and the most suitable glass for this particular 2 μm laser application.

Various energy exchange processes between erbium ions in highly doped (Er/YAG) were studied by Lupei *et al.* (1990) (see W(22,50), W(50,31), W(11,30), T(500,013) and T(111,005) in Figure 2.3-1 and Table 2.3-1). Data over large concentration (0.1-100 at.% replacement of Er^{3+} for Y^{3+} in YAG) and temperature (10-300 K) ranges were analysed. A three-ion cross-relaxation process (T(500,013)) was found responsible for the quadratic concentration dependence of the decay rate for the coupled $^4S_{3/2}+^2H_{11/2}$ levels at temperatures above 150 K.

Shi *et al.* (1990) presented an extensive study of the effects of energy transfer among the erbium ions on the fluorescence properties of heavily doped (Er/YAG) at room temperature. They report non-exponential decays in high Er^{3+} concentrations of

both ${}^4I_{13/2}$ and ${}^4I_{11/2}$ levels. A rate-equation model was developed and solved numerically. Various two-ion cross-relaxation processes, involving the ${}^4I_{13/2}$, ${}^4I_{11/2}$ and (${}^4S_{3/2}+{}^2H_{11/2}$) levels (see W(22,50), W(50,32) and W(11,30) in Figure 2.3-1 and Table 2.3-1) were analysed and values have been obtained for some of their rate constants. Shi *et al.* obtained values for W(11,30) in Er:YAG which varied between $1.5 \times 10^{-17} \text{ cm}^3\text{s}^{-1}$ and $4 \times 10^{-17} \text{ cm}^3\text{s}^{-1}$ for Er doping levels between 16.6 and 50 at.%. These values can be compared with other results in YAG giving values of W(11,30) of $1.8 \times 10^{-17} \text{ cm}^3\text{s}^{-1}$. (Zhekov *et al.*, 1986; 10 at.% Er^{3+}), $2.5 \times 10^{-17} \text{ cm}^3\text{s}^{-1}$. (Zhekov *et al.*, 1984; 15 at.% Er^{3+}) and $25 \times 10^{-17} \text{ cm}^3\text{s}^{-1}$. (Zhekov *et al.*, 1984; 50 at.% Er^{3+}). The spread of values and particularly the large discrepancy between the latter two values is indicative of the existence of additional processes affecting the ${}^4I_{13/2}$ level. Indeed, in our initial modeling where no account is taken of such processes (see Chapter 4) we obtain a value for W(11,30) of $4 \times 10^{-17} \text{ cm}^3\text{s}^{-1}$ in our fluoride glasses. After the inclusion of additional processes (see Chapter 5), which gave better agreement with the experimental data, a value of $1 \times 10^{-17} \text{ cm}^3\text{s}^{-1}$ was obtained.

For the process W(22,50), Shi *et al.* obtained a consistent value of $3.0 \times 10^{-17} \text{ cm}^3\text{s}^{-1}$ for W(22,50) for the same range of concentrations (16.6 to 50 at.%). This compares to a value of $5.1 \times 10^{-17} \text{ cm}^3\text{s}^{-1}$ obtained by Zhekov *et al.* at (1984). The values obtained for these two cross-relaxation rate-constants (W(22,50) and W(11,30)) would be expected to vary with material structure as they depend on the environment of the Er^{3+} ions. Hence values obtained in YAG can only be used as a guide to values which could be expected in fluoride glasses and direct comparison of YAG values and values obtained in this thesis are not particularly meaningful. Our values of W(11,30) were included above only to illustrate the point about the possible existence of additional processes, beyond the two considered by Shi *et al.* All of the processes presented in this chapter (and others) will be discussed in detail in Chapters 4 and 5.

Throughout this thesis there will be a great deal of discussions of various ion-ion exchange processes. For that reason a comment should be made about the nomenclature used with these processes. Various researchers have taken different approaches with this regard. Wright (1976) uses nomenclature which refers to the detailed mechanisms and uses different names for various energy transfer processes such as "up-conversion", "fluorescence quenching", "sensitisation" and so on. Authors like Chen *et al.* (1989)

and Shi *et al.* (1990) use only general terms like "energy transfer" and "cross-relaxation process". A significant number of processes, some of them involving three ions, will be introduced later in the thesis. Many of these processes are introduced, in our knowledge, for the first time. To avoid any confusion caused by the use of specific effect-related terms for a variety of different processes, it was decided to only use general expressions like "ion-ion exchange process", "energy transfer process" or "cross-relaxation process".

2.3.2.2. Erbium glasses co-doped with other rare earth ions

Erbium ions have often been used together with other rare-earth ions which can be effective in modifying the properties of levels via cross-ion relaxation processes. The relatively low absorption efficiency of Er^{3+} for direct pumping with wavelengths around $1\mu\text{m}$ is one of the reasons for co-doping with Yb^{3+} ions. The Yb^{3+} ion has a much higher absorption cross section at 980 nm , which makes it suitable for laser-diode pumping, and can also be excited using the $1.06\mu\text{m}$ output of a Nd:YAG laser (Hanna *et al.*, 1987).

Gapontsev *et. al* (1982, 1983) have presented data for laser action in the Yb-Er system at $1.55\mu\text{m}$ for a number of glasses (but not including fluorozirconate glasses). Energy accumulation and channels of energy loss were covered in detail. High energy operation using both flashtube and Nd-glass-laser pumping were studied as well as possible applications of these laser systems. This paper is fairly typical of early work on co-doped glass lasers. More recently there has been a considerable volume of work on a wide range of compact Er:Yb laser systems based on bulk glass materials. These lasers cover a similarly wide range of operating regimes from CW to mode locked and the review by Taccheo *et al.* (1996) gives a very good description of the types of system which are possible and their performance.

Of particular interest for the type of materials described in this thesis are glass microchip lasers as this configuration is capable of high power and single longitudinal mode operation and is likely to require high dopant concentration for good pump

absorption in the thin material. The first Er-Yb:phosphate glass microchip laser at 1.5 μm was reported by Laporta *et al.* (1993). A 980 nm LD was used as the pumping source and Er^{3+} and Yb^{3+} doping concentrations of 1×10^{20} ions/ cm^3 (approximately 0.5 mol%) and 2×10^{21} ions/ cm^3 (approximately 10 mol%) were used. A single longitudinal mode output power of 25 mW and slope efficiency of 22% were obtained with a 150 mW pump. The experimental and modeling work by this group on microchip lasers in phosphate hosts has been recently summarised (Laporta *et al.*, 1999). Also, recently, a diode-pumped Er:Yb microchip laser, Q-switched using a semiconductor saturable absorber mirror, has delivered pulse energies up to 4 μJ at repetition rates up to 100kHz (Fluck *et al.*, 1998)

The optical properties of erbium (and holmium) doped thorium-, zinc- and yttrium-based fluoride glasses have been determined by Eyal *et al.* (1987). The Judd-Ofelt intensity parameters Ω_i ($i=2,4,6$) were calculated for these glasses and compared with previously reported values. The radiative decay rates of various transitions between different Er^{3+} and Ho^{3+} levels were also calculated. The multiphonon-assisted decay rates between adjacent levels were obtained as the calculated radiative rates were subtracted from the measured decay rates. Logarithmic plots of these multiphonon-assisted decay rates vs the energy gap between the fluorescing level and the nearest level below produced values for the parameters a and b (see Equation (2.2-1)) for these fluoride glasses. This allowed an equation, similar to Equation (2.2-1) to be used and values for the multiphonon-assisted decay rates to be predicted. A reasonably good agreement between the calculated and predicted multiphonon-assisted decay rates was obtained in the cases where energy gaps larger than 1900 cm^{-1} were involved. In the cases with smaller energy gaps large discrepancies were observed. One such example involved the ${}^2\text{H}_{9/2}$ level and was explained in terms of uncertainty in the multi-phonon rates to the next lowest level due to an uncertainty of the order of KT ($KT \approx 200 \text{ cm}^{-1}$ for their glasses), which was about 10% from the energy gap between these two levels (about 1750 cm^{-1}). Peak cross-sections for laser action and threshold powers for infrared laser emissions have been calculated and compared with data published in the literature. Co-doping with Yb^{3+} is shown to significantly decrease the threshold for laser action. The measured decay times of the main levels in Er^{3+} which were reported Eyal *et al.* (1987) are very close to those reported in this thesis.

Further progress with rare-earth sensitizers was reported by Heuman *et al.* (1988) using Er-doped fluoride-based glass co-doped with chromium and ytterbium. As a result, for the first time, CW erbium laser action at $\lambda=1.6 \mu\text{m}$ in Cr,Yb,Er:fluoroaluminate glass was achieved. A two-step pumping process, via Cr^{3+} and Yb^{3+} , with krypton laser excitation produced an 80 mW laser threshold. It was pointed out that further improvement in the efficiency of the laser was possible by optimisation of the doping concentration and further improving the optical quality of the glass.

The other important emission wavelength of Er^{3+} at $2.7 \mu\text{m}$ has also been extensively studied. Yanagita *et al.* (1989) studied the radiative and non-radiative properties of this transition in a broad range of glasses which included fluorides, fluorophosphates, tellurides and phosphates. The calculated radiative rates were similar for all glasses except for the tellurides where the rates were substantially higher. Two different ways of depopulating the ${}^4\text{I}_{13/2}$ level (which is the lower level for the $2.7 \mu\text{m}$ transition) were tried in an attempt to increase the population inversion between the ${}^4\text{I}_{11/2}$ and ${}^4\text{I}_{13/2}$ levels. First they increased the Er^{3+} concentration without using co-dopants. With these heavily-doped glasses, the most promising results were obtained with the fluorozirco-aluminates which could be doped with Er^{3+} concentrations up to 20 mol%. Shortening of the lifetimes of both ${}^4\text{I}_{11/2}$ and ${}^4\text{I}_{13/2}$ levels due to concentration quenching was observed for dopant levels above about 10 mol%. Depopulating the lower level by co-doping with Ho^{3+} and Tm^{3+} in several glass hosts has shown that holmium ions are preferable for this purpose. The Tm^{3+} ions also tended to depopulate the ${}^4\text{I}_{11/2}$ level.

Other co-dopants for erbium-doped ZBLAN glasses, such as Eu and Pr, have been studied by Wetenkamp *et al.* (1992 a). Praseodymium ions proved to be a particularly good deactivator for the lower level of the erbium transition at $2.7 \mu\text{m}$. Very efficient depopulation of the ${}^4\text{I}_{13/2}$ level of highly-doped Er/ZBLAN glass was demonstrated even with a very small dopant concentration of Pr^{3+} (0.05 mol%).

2.3.2.3. Laser action in singly-doped erbium fluoride glasses

One of the first pulsed lasers operating at wavelength 2.7 μm in erbium-doped ZBLAN at room temperature has been reported by Pollack and Robinson (1988). An erbium concentration of 4 mol% and highly inefficient xenon flash-lamp pumping were used. Although laser action was achieved on the 2.7 μm transition, no stimulated emission was observed from the ${}^4\text{I}_{13/2} \rightarrow {}^4\text{I}_{15/2}$ transition at 1.55 μm .

The first continuous wave operation of an erbium-doped fluoride bulk-glass laser at the 2.7 μm wavelength was reported by Auzel *et al.* (1988b). Doping concentrations up to 8% and pumping at 514 nm were used. Multi-wavelength and tunable operation were demonstrated.

Wetenkamp *et al.* (1992b), also consider the possibility of CW operation of Er^{3+} in ZBLAN in their comprehensive study of the optical properties of rare-earth doped fluorozirconate glasses. They confirmed that CW operation of the ${}^4\text{I}_{11/2} \rightarrow {}^4\text{I}_{13/2}$ transition at 2.7 μm could be realised by depleting the lower ${}^4\text{I}_{13/2}$ level via excited state absorption (ESA) of the pump at 640 nm or 800 nm. They also pointed out that laser action on the ${}^4\text{I}_{13/2} \rightarrow {}^4\text{I}_{15/2}$ transition at 1.55 μm should be possible with direct excitation of the upper level because there is no effective ESA of the pump at around 1.5 μm to deplete this level.

Modelling results for laser operation at approximately 3 μm in $\text{Er}/\text{BaY}_2\text{F}_8$ crystals have been presented by Knowles and Jenssen (1992). These crystals involve doping levels of 1 - 100% Er and 0.1 - 1 % Pr. The advantages and disadvantages of laser action, based on both upconversion deactivation and Pr-deactivation of the lower laser level, have been discussed and compared. It was shown that the upconversion laser should operate with higher efficiency than the quantum defect limited Er/Pr laser at least in CW mode. Possible problems with operating these materials at high inversion levels (such as thermal loading) were pointed out.

During the writing of this thesis, the first diode-pumped laser based on thin samples of heavily-doped Er:fluorozirconate glass of the type investigated in this thesis was reported (Sandrock. *et al.*, 1999). CW laser emission was obtained in the 2.7 μm to

2.8 μm wavelength range. A 970 nm fibre-coupled LD pump and erbium concentrations of up to 8 mol% were used. A CW output power of more than 160 mW and slope efficiency of 10% were achieved. Although they did not have any glasses with doping concentrations exceeding 8 mol%, the authors predicted that optimum performance would be expected at higher concentrations.

Laser action in doped fluoride fibres can be very strong due to the advantage of the high pump intensity and long interaction length which is achieved in this confined geometry. Apart from the traditional wavelengths of 2.7 μm (Brierley and France, 1988; Srinivasan *et al.*, 1999; Poppe *et al.*, 1998) and 1.5 μm (Barnes *et al.*, 1989), laser action in erbium-doped fluoride fibres has been reported at various other wavelengths such as 1.0 μm (Allain *et al.*, 1989), 1.66 and 1.72 μm (Smart *et al.*, 1990), 850nm (Miller *et al.*, 1990) and 540nm (Whitley *et al.*, 1991). Although the motivation for the work described in this thesis has been the development of materials suitable for small diode-pumped bulk glass lasers, the models of material behaviour are equally relevant to the fibre geometry. Indeed, the high pump intensity in the core of fibre lasers and amplifiers is likely to lead to significant excited state populations and strong cross-relaxation processes when high doping concentrations and short lengths are used (Pope *et al.*, 1997).

Various commercial Er^{3+} glass laser systems have already been made available on the market. Q-switched Er^{3+} :phosphosphate lasers at 1.54 μm , pumped by flash tubes, produce output energies of around 5 mJ and are in use for laser rangefinders. CW Er^{3+} :fluorozirconate fibre lasers at 2.7 μm produce output powers up to about 2 W and are used for a wide range of medical applications.

2.3.3. General comments on energy transfer processes among ions

Up to now we have introduced concepts such as two and three-ion energy exchange mechanisms without discussing their fundamental basis. The models that we will develop in later chapters are based on the writing of rate equations. The use of this

approach needs to be justified as such equations cannot be used in all situations. This section will discuss ion-ion energy transfer processes in more detail and introduce a number of concepts which will be used in the justification of the use of rate equations in the modelling processes for the materials used in this thesis.

In discussing ion-ion energy transfer processes it is easier to understand the physics of the situation if we first discuss two-ion processes involving two types of ion in the decay - a donor ion and an acceptor ion. This is the approach followed below even though singly-doped materials have been used exclusively in this thesis and the donor and acceptor ions are therefore of the same type. We will later consider the case of single doping.

Consider a host system containing randomly distributed assemblies of donor and acceptor ions. The various ions interact via coulomb forces and if they are sufficiently close then an interacting system of ions can be described using states of the whole system (Di Bortolo, 1984). The basic mechanism for ion-ion interaction is via electric dipole transitions between multiple-ion states (Watts and Richter, 1972). Some of these transitions result in exchange of excitation energy between the ions. Under the assumption that a short pulse of radiation has excited a small number of donor ions, then, in the absence of acceptor ions or diffusion of energy amongst ions, the donor excitation density, $\Phi(\mathbf{r},t)$, decays simply as $\exp(-t/\tau_0)$, where τ_0^{-1} is the intrinsic donor decay rate due to radiative and internal non-radiative transitions. In the presence of acceptor ions there are three basic regimes in which the temporal behaviour of the donor excitation can be described:

- Direct transfer

A donor ion in the vicinity of acceptor ions can interact with one of them in a direct energy transfer. If the probability for direct energy transfer between donor and acceptor separated by distance R_n is $w(R_n)$ (two-ion process) then the donor excitation density $\Phi(\mathbf{r},t)$ (the probability of finding a donor at position \mathbf{r} at time t in an excited state) is (Weber, 1971):

$$\Phi(\mathbf{r},\tau) = e^{-\tau/\tau_0} \sum_{n=1}^{N_{av}} e^{-w(R_n)\tau} \quad (2.3-1)$$

Here N_a is the number of acceptor ions per unit volume and $N_a v$ is the total number of acceptors in the sample volume v . The observed macroscopic signal will be proportional to the statistical average of Φ over all the donor-acceptor pairs

$$\Phi(t) = \int \Phi(\mathbf{r}, t) d^3 r. \quad (2.3-2)$$

In principle, if one knows the spatial distribution function for the ions and the form of $w(R_n)$ then the above equation can be solved to give an expression for the decay of the excited state population. Such solutions for the decay function for the particular radial dependencies of the transfer rate in the cases of multipolar interactions and exchange coupling have been reported by Inokuti and Hirayama (1965) and by Wright (1976). For multipolar interaction the transfer rate constant is proportional to an inverse power of the donor-acceptor separation, $w(R) = cR^{-s}$ (Weber, 1971). The values of s are 6, 8 and 10 for dipole-dipole, dipole-quadrupole and quadrupole-quadrupole coupling respectively. The general solution (Inokuti and Hirayama, 1965; Weber, 1971; Watts and Richter, 1972) in this case is:

$$\Phi(t) = \exp\left[-\frac{t}{\tau_0} - \frac{4\pi}{3} N_a \Gamma\left(1 - \frac{3}{s}\right) R_0^3 (t/\tau_0)^{3/s}\right], \quad (2.3-3)$$

where $\Gamma(x)$ is the gamma function and R_0 is the critical transfer distance $(c\tau_0)^{1/s}$ defined as the separation at which the probability for energy transfer between donor-acceptor pair is equal to the intrinsic decay probability τ_0^{-1} .

Early in the decay, when $t \ll \tau_0$, the above equation reduces to a decay which is approximately proportional to $(1 - kt^{3/s})$, where $k = (4/3)\pi\Gamma(1 - 3/s)N_a R_0^3 \tau_0^{-3/s}$. The initial decay therefore has a non-exponential time dependence. This can be understood because the number of donors having unexcited acceptors within the critical radius decreases with time. Hence during the decay the average separation of the interacting ions is increasing and a changing decay rate will be observed within the time of the decay. As the decay progresses, the intrinsic decay rate becomes more competitive with that due to energy transfer. The late part of the decay will be predominantly exponential with a rate that is close to the intrinsic decay rate.

- Diffusion Limited transfer

When the donor concentration is increased, donor-donor energy exchange interactions can become important. These donor-donor interactions give rise to energy migration which can be described either as diffusion process or a random walk (resonant exchange or hopping model). Both models lead to similar theoretical results (Di Bartolo, 1984). A diffusion limited transfer is present when the rate of the energy migration process among the donor ions is comparable with the donor-acceptor transfer rate. After excitation of a sample containing a significant density of donors, excited donors in the vicinity of acceptors relax via direct transfer. For excited donors which are at substantial distances from the nearest acceptor, the excitation first diffuses via donor-donor transfer until the excitation reaches a donor sufficiently close to an acceptor for direct relaxation to occur. The time evolution of the excitation is now given by the diffusion equation (Weber, 1971):

$$\frac{\partial \Phi(\mathbf{r}, t)}{\partial t} = D^* \nabla^2 \Phi(\mathbf{r}, t) - \sum v(\mathbf{r} - \mathbf{r}_n) \Phi(\mathbf{r}, t) - \frac{1}{\tau_0} \Phi(\mathbf{r}, t). \quad (2.3-5)$$

Here D^* is the diffusion coefficient and $v(\mathbf{r} - \mathbf{r}_n)$ is the probability for energy transfer from an excited donor to the n^{th} acceptor at position \mathbf{r}_n . Yokota and Tanimoto(1967) have obtained an approximate solution of the above function in the case of dipole-dipole interaction:

$$\Phi(t) = \Phi(0) e^{-t/\tau_0} \exp\left[-\frac{4}{3} \pi^{3/2} N_a (ct)^{1/2} \left(\frac{1 + 10.87x + 15.5x^2}{1 + 8.743x}\right)^{3/4}\right], \quad (2.3-6)$$

where $x = D^* c^{-1/3} t^{2/3}$. This equation assumes that the density of donors is much greater than that of the acceptors and so the average separation of donors is much less than that of acceptors. It also assumes the same value of c for donor-donor interaction and donor-acceptor interaction. At the early part of the decay (for $t \ll c^{1/2} D^{*3/2}$, $x \approx 0$) diffusion is negligible and this equation reduces to equation 2.3-3. In the later part of the decay when $t \rightarrow \infty$, Equation 2.3-6 reduces to an exponential decay with a decay time constant

$$1/\tau = 1/\tau_0 + K_d, \text{ where } K_d \approx 2.7\pi D^{*3/4} N_a c^{1/4}. \quad (2.3-7)$$

The diffusion coefficient is a function of the donor concentration N_d and is given by (Brenier *et al.*, 1990)

$$D^* = 3.375 c N_d^{4/3}. \quad (2.3-8)$$

Using this, K_d becomes

$$K_d \approx 30 c N_a N_d . \quad (2.3-9)$$

In this diffusion-limited decay, the initial part of the decay is non-exponential and the latter part is exponential. The effective late decay rate varies directly with the product of donor and acceptor doping concentrations.

- Fast diffusion

In high donor concentrations when the diffusion constant is large, diffusion is very rapid and leads to a spatial equilibrium of the excitation within the donor system. In this case the variation in the transfer rates for different donor-acceptor pairs is effectively averaged out and a single exponential decay is observed. Under these conditions diffusion is no longer important in limiting the rate of decay and for two-ion interactions, equation 2.3-7 becomes (Watts and Richter, 1972; Brenier *et al.*, 1990):

$$1/\tau = 1/\tau_0 + K_d, \text{ where } K_d \approx UN_a, \quad (2.3-10)$$

where U is a constant. Because of the fast diffusion, the donor (acceptor) excitation is now de-localised over the entire system and the processes now can be described with an average transition rate. This allows a rate-equation analysis to be used (Di Bartolo, 1984). In the terms of a rate-equation model the evolution of the excited donor population in fast diffusion regime can be expressed as:

$$\frac{dN_{d'}(t)}{dt} = -\frac{N_{d'}(t)}{\tau} - KN_a(t)N_{d'}(t), \quad (2.3-11)$$

where $N_{d'}$ denotes excited donor ion concentration and K is a constant which determines the rate of the process.

In general, a regime of fast diffusion is thought to be present only in higher concentrations where the diffusion rate is sufficiently high. However, rate-equation analysis has been successfully used also in relatively low concentrations. Watts and Richter (1972) report that for Yb^{3+} ions in a $\text{Y}_{1-x-y}\text{Yb}_x\text{Ho}_y\text{F}_3$ crystal, the fast diffusion regime is noticed at about 0.3 mol% and it completely dominates the direct transfer above 3 mol%. Chen *et al.* (1989) successfully used rate-equation models for heavy metal fluoride glasses with combined Er^{3+} and Tm^{3+} concentration of about 1 mol%. Laporta *et al.* (1993) also reported successful rate-equation modelling of both erbium and ytterbium processes in Er-Yb phosphate glass laser with Er^{3+} concentration of only about 0.05 mol% (and Yb^{3+} concentration of about 5 mol%).

In many other papers that use rate-equation modelling it is not clear exactly what evidence exists for believing that the fast diffusion regime is applicable. This is partly because even when one is not strictly in the fast diffusion regime, rate equations can be used still as an approximation (Wright, 1976). It is also because the value of D^* depends on both N_d and c (see equation 2.3-8). This latter dependence on c means that the diffusion coefficient is a function of the energy transfer probability at a particular separation and hence a function of the transition concerned. Hence in principle, different ion-ion interaction processes in a particular material could satisfy the requirements for fast diffusion to varying degrees. It should also be noted that inhomogeneous broadening, common in most glasses, can lead to reduced overlap integrals and hence lower values of c than applies in crystals. Thus, the situation is very much dependent on the details of the material and the processes being considered. In the end, rate equations tend to be used and the justification in a particular situation tends to be that they work in the sense that models agree with measurements. If the fast diffusion regime can be shown to apply for a particular energy level it is reasonable to assume that the regime applies to all levels in a particular material.

The distinguishing feature of the fast diffusion regime is that, provided only a single energy exchange process is active, one will observe a single exponential decay constant over the entire decay period. This is thus the best test for applicability of rate equations. If many processes are affecting a particular level during a decay then one will in general not see a single exponential decay, even if fast diffusion applies.

Before going on to discuss the evidence for the applicability of rate equations to the modelling of this thesis, we first digress to consider the effect on the preceding discussions of a having only a single dopant. In this case, $N_a = N_d$ and for the case of slow diffusion, Equation 2.3-9 becomes: $K_d \approx 30 c N_d^2$. Thus for two-ion interaction in the diffusion limited regime, the decay rate is proportional to concentration squared. Physically, in the case of single-ion doping, diffusion can be thought of as a resonant energy transfer (ion hopping) mechanism that can temporarily store the excitation energy prior to eventual decay via direct energy transfer to some other state in another dopant ion. For two-ion interactions in a singly-doped material, diffusion-limited decay will be characterised by a late decay rate which is proportional to concentration squared. In the case of fast diffusion, the two-ion decay rate is proportional to dopant

concentration (Equation 2.3-10) and pure exponential decays are observed. Often these concentration dependencies are used as an indication of the presence of either fast diffusion or diffusion-limited decay (Brenier *et al.*, 1990; Moine *et al.*, 1989). However, it must be stressed that this is only true if two-ion processes dominate the decay. Fong and Diestler (1972) presented an elegant analysis of many body dipole-dipole processes for energy transfer between ions in crystals. They showed that provided energy conserving interactions are possible (and there is fast diffusion) pairwise energy transfer will predominate at high dilution while higher order n-body processes can dominate at high doping levels. They also showed that in the fast diffusion regime, n-body processes will have decay rates which depend on $N_d^{(n-1)}$. Thus one can indeed be in the fast diffusion regime and still observe decay rates proportional to concentration squared. Such a situation would indicate the existence of dominant three-ion decay processes. The essential test for fast diffusion is thus whether or not a single exponential decay is observed and not the concentration dependence of the decay. Fong and Diestler (1972) also show that many body mechanisms are particularly important in rare earth ions because of the narrow widths of the $4f^n$ crystal states for which overlap of donor emission and acceptor absorption spectra (and hence pairwise energy transfer) is minimised. Later in this thesis we will introduce a number of three-ion processes to explain certain features of our experimental fluorescence data. Some of these three-ion processes have been previously reported by other workers in erbium-doped materials (Lupei *et al.*, 1990; Lupei, 1993, Georgescu *et al.*, 1991; Zhekov *et al.*, 1990) and others are introduced for the first time in this thesis.

We now return to a discussion of the reasons why we have used rate equations to model the behaviour of the glasses used in this thesis. The dopant concentrations used in our work are very high (up to 18 mol%) and thus it is reasonable to expect that the fast diffusion regime will apply, particularly at the higher concentrations.

This assumption of fast diffusion was supported by a number of observations that were interpreted as an indication that a fast diffusion regime is dominant in the observed fluorescence behaviour of the different energy levels. In the complex situation which occurs for heavily doped Er^{3+} :fluoride glasses used in this thesis, the best way to minimise the number of processes affecting a particular level is to observe the decay when the level is directly pumped. Under these circumstances, the populations of other

levels tend to be lower and competing cross relaxation processes tend to be minimised. The fluorescence from some of the levels ($^4I_{9/2}$ and $^2H_{9/2}$) exhibited exponential decays for all concentrations and pumping conditions (see Tables 5.2-1, 5.2-2, 5.2-8). Insufficient data was collected for the $^4F_{9/2}$ level to test its behaviour under direct pumping. However, some data is available at low concentrations and this shows pure exponential decays (see Table 5.2-9). The fluorescence from levels $^4I_{13/2}$ and $^4I_{11/2}$ exhibited non-exponential decays, but only under pumping conditions where they are heavily populated (for non-exponential behaviour see Tables 5.2-1, 5.2-6, 5.2-7 for the $^4I_{11/2}$ level and Tables 5.2-4, 5.2-5 and 5.2-7 for the $^4I_{13/2}$ level). The large population in this case can result in more than one significant energy transfer process and this would explain the observed non-exponential decay. When populated with a smaller number of ions these two levels exhibited pure exponential decays for all concentrations (the relative populations and the population dynamics under various pumping conditions would be discussed in Chapter 4 and Chapter 5; for exponential behaviour see Tables 5.2-4, 5.2-5, 5.2-8 for the $^4I_{11/2}$ level and Tables 5.2-1, 5.2-2 and 5.2-8 for the $^4I_{13/2}$ level). This exponential behaviour is typical of the fast diffusion regime. Another important indication with regard to the origin of the observed non-exponential behaviour was that the non-exponential decays of the fluorescence lines from these two levels were observed only in the highest doping concentrations. This is quite opposite to what one would expect under the diffusion limited regime where non-exponential decays occur at low concentrations (Wright, 1976). Such non-exponential decays in only low concentrations have been observed, for example, by Watts and Richter (1972).

In this thesis the measured decay rate of the fluorescence from the $^4S_{3/2}+^2H_{11/2}$ levels will be shown to exhibit a quadratic dependence of the dopant concentration (see Chapter 5). As previously explained, this dependence can be typical of the diffusion limited transfer regime for two-ion processes (see Equation 2.3-9). However, as was also pointed out, the decays observed in the diffusion-limited regime have a non-exponential initial part, followed by a later exponential part. For singly-doped Er^{3+} : BIZYT and BATY glasses, Moine *et al.* (1989) have observed a quadratic dependence of lifetime for the same $^4S_{3/2}+^2H_{11/2}$ levels in concentration varying from 0.1-28 %. They interpret their data as being in the diffusion-limited regime. However, the data is also consistent with a three-ion process, as there is no evidence presented of early non-

exponential decay. In all our experiments (for all concentrations) only pure exponential decays, typical of the fast diffusion regime, were observed.

Thus, we have shown that under appropriate experimental conditions, pure exponential decay has been observed with the ${}^4I_{13/2}$, ${}^4I_{11/2}$, ${}^4I_{9/2}$, ${}^4F_{9/2}$, ${}^4S_{3/2}+{}^2H_{11/2}$ and ${}^2H_{9/2}$ levels of our heavily-doped erbium glasses. Thus we believe that these materials are operating in the fast diffusion regime and the use of rate equations to describe the processes is appropriate. However, as it will become clear later in the thesis, the ultimate justification of our rate equation approach was that it provided a clear physical understanding and interpretation of the energy exchange processes and their effects on the temporal behaviour of the populations of the levels involved in the modelling. This understanding allowed successful predictions to be made of the complex population dynamic for all the main fluorescence levels under various pumping conditions and for the whole range of concentrations used. A detailed rate equation analysis of our $Er^{3+}/ZBAN$ glass system under various pumping conditions is presented later in the thesis in Chapters 4 and 5.

2.4. Conclusion

Erbium-doped fluoride glasses have been extensively studied because of their suitability for IR laser applications. High erbium concentrations in these glasses have been a subject of a particular interest because of the more effective pump absorption (Laporta *et al.*, 1993) and the lower threshold for CW lasing (Auzel *et al.*, 1988b). The high erbium concentration, however, would increase the rates of various cross-relaxation processes and thus strongly affect the population dynamics of the lasing levels. Depending on the levels involved and the nature of the cross-relaxation process, their effect on laser action can be either positive or negative. Certainly their effect is positive in the case of the 2.7 μm Er:fluorozirconate laser reported by Sandrock *et al.*, (1999). While various cross-relaxation processes have already been discussed in the literature, very few values for the cross-relaxation rate constants of these processes have been published in crystals and, to the best of our knowledge, no value has been published for fluorozirconate glasses. It is evident that for further progress in this area, a detailed understanding of the dynamics of the dominant cross-relaxation processes in

erbium-doped ZB(L)AN glasses and knowledge of the values of the corresponding cross-relaxation rate constants is required. The exponential decay forms of the measured fluorescence lines from the 6 lower excited levels in our glasses under appropriate pumping conditions are a strong indication that rate equations could be used in the modelling process.

Chapter 3

Experimental arrangements for the measurement of spectroscopic data

3.1. Introduction

A set of 11 erbium doped ZB(L)AN glasses with doping concentration varying from 0.2 mol% to 18 mol% was produced by the Amorphous Materials Group of the Department of Chemistry at Monash University, Melbourne, Australia. This wide range of doping levels was required so that the concentration dependence of fluorescence behaviour would be evident and changes would be significant enough to allow differentiation between the various non-linear processes.

Absorption and fluorescence spectra were taken for each of the glasses under CW excitation. The spectra were used to identify suitable pumping wavelengths and calculate absorption cross-sections. Fluorescence spectra were used to identify strong fluorescence lines and study the pump power and concentration dependence of fluorescence intensity. Extensive measurements of the time dependence of fluorescence were also made using a tunable high intensity 10 ns OPO source. The rise and decay waveforms of the main fluorescence lines under 5 different pumping wavelengths were

recorded. Due to the large number of samples and fluorescence waveforms, less important fluorescence lines were studied in only four or five samples, chosen to cover the full range of concentrations. The analysis of the fluorescence waveforms provided important information about the main cross-relaxation processes and their effect on the population of the corresponding levels. A comprehensive presentation and discussion of this fluorescent waveform data is deferred to Chapters 4 and 5.

3.2. Preparation of the glass samples

The glass hosts were based on a standard $\text{ZrF}_4\text{-BaF}_2\text{-LaF}_3\text{-AlF}_3\text{-NaF}$ (ZB(L)AN) composition that was prepared from highly purified fluorides, obtained from BDH and Morita and then re-sublimed to further remove OH and oxide impurities (MacFarlane *et. al*, 1997). The glass sample preparation involved batching in a nitrogen-filled dry box and subsequent melting in an electrically heated furnace, attached to the dry box. At lower doping levels, compositions were typical of those used in standard ZBLAN glasses with small amounts of erbium added. As the erbium doping level was progressively increased, compositional changes were made to the glass host when devitrification was encountered. At the lowest doping levels, the Er^{3+} ion was substituted for La^{3+} . Above 4 mol% doping, when the La^{3+} concentration was zero, it was necessary to decrease the ZrF_4 and NaF contents to avoid crystallisation. Increasing the barium content as the erbium content increases was also found to be important, the effect being to produce a substantially different Zr/Ba ratio at the highest Er^{3+} doping levels. The composition and the Er^{3+} concentration of the most stable glasses are presented in Table 3.2 -1.

Slab samples were prepared from 6 gr batches melted in glassy carbon crucibles at above 1000°C , held for 1 hour and then poured into a brass mould with a rectangular shaped cavity (20x10x5 mm), followed by annealing for 2 hours. A brass lid was placed over the mould to reduce the likelihood of crystallisation in the glasses with higher erbium concentration. The mould temperature was maintained at approximately 20°C below the glass transition temperature.

ZrF ₄	BaF ₂	AlF ₃	NaF	LaF ₃	ErF ₃	Er ³⁺ [$\times 10^{20}$]
53	20	3	20	4	0	0
53	20	3	20	3.8	0.2	0.37
53	20	3	20	3.6	0.4	0.74
53	20	3	20	3.2	0.8	1.48
53	20	3	20	2.4	1.6	2.98
53	20	3	20	0.8	3.2	5.96
53	20	3	20		4	7.46
51	23	4	16		6	11.0
51	21	4	16		8	14.7
48	22	4	16		10	18.6
45	25	4	14		12	22.5
46	23	3	14		14	26.1
44	24	3	13		16	29.6
43	23	3	13		18	33.4

Table 3.2 -1 Compositions of the ZB(L)AN glasses (in mol%) and Er³⁺ concentrations (in cm⁻³)

The glass slabs were then polished on two surfaces. The final dimensions of the glass samples were 20mm x 10mm x 1mm.

3.3. Absorption measurements

Two different measurements were performed in order to study the absorption of the studied samples. The main absorption measurements in the UV-Vis-NIR region were carried out with a Spectrophotometer. Additional absorption measurements were made in the region of 800 nm using a CW laser diode source.

3.3.1. Spectrophotometer measurements

Spectrometer measurements were performed using a Cary 1750 with a wavelength resolution of 1 nm and spectral slit width of 2 nm. One typical absorption

spectrum is presented in Figure 3.3-1. From this spectrum, it can be seen that the absorption line at 800nm is a relatively weak compared to most other absorption lines. A closer investigation reveals that the absorption at 802 nm is approximately two times smaller than the absorption at 403 nm, three times smaller than that at 975 nm, 7 times smaller than that at 1.53 μm and 19 times smaller than the absorption at 520 nm. However, the availability of powerful LD sources for CW and pulse excitation at about 800nm was considered a good justification for choosing this wavelength as the main pumping wavelength for this study.

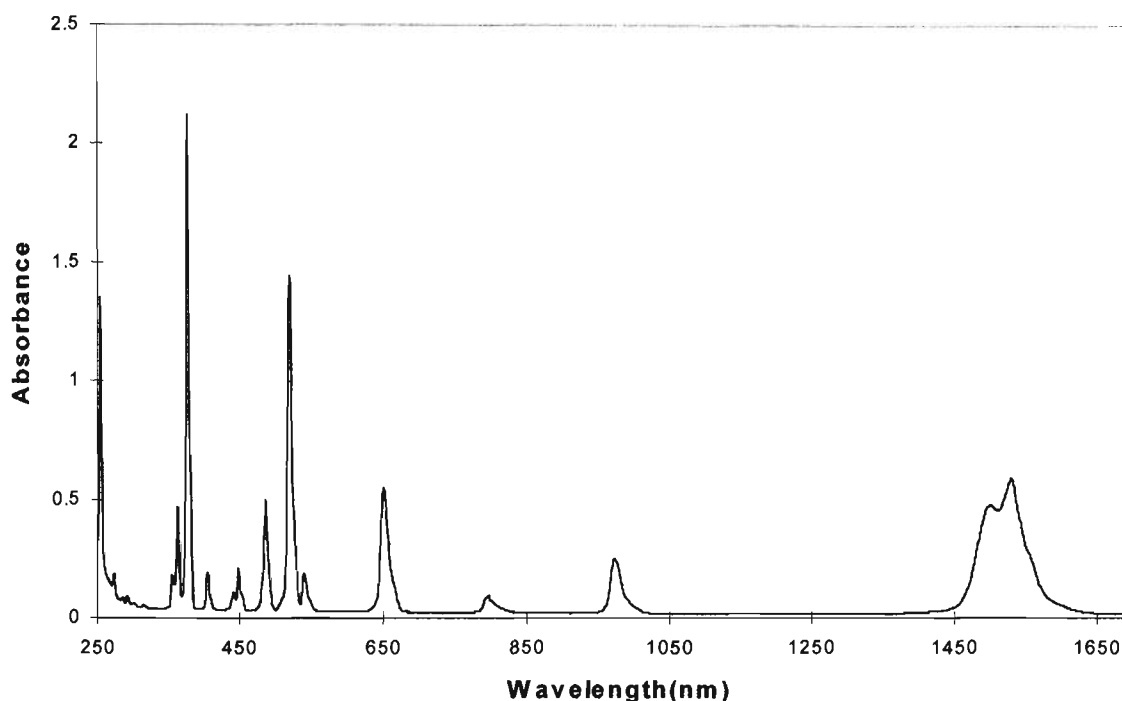


Figure 3.3-1 A typical absorption spectrum (16 mol% Er^{3+} /ZB(L)AN)

The absorption spectra of the other samples were very similar to the spectrum presented above. A summary of the wavelengths of the absorption peaks and the energies of the corresponding levels is presented in Table 3.3-1 below. This table is based mostly on our absorption measurements, however for completeness data from Zhong *et al.* (1992) for higher energy levels (UV fluorescence below 300 nm) have also been included. The level assignments used in Table 3.3 follow those of Zhong *et al.* (1992). A close look at the energies of various levels reveals that many of the levels are resonantly spaced. For instance, within the energy of the fundamental phonon, which in ZBLAN glasses is $\approx 500 \text{ cm}^{-1}$ (Zou X. and Izumitani T., 1993), the difference between

the energies of the ${}^4I_{15/2}$, ${}^4I_{13/2}$, ${}^4I_{9/2}$, ${}^4S_{3/2}$, ${}^2H_{9/2}$, (${}^2P_{3/2}+{}^2D_{3/2}+{}^4F_{3/2}$) and even the ${}^4D_{7/2}$ level are approximately the same ($\approx 6500 \text{ cm}^{-1}$, corresponding to $\lambda \approx 1.5\mu\text{m}$). The levels ${}^4I_{15/2}$, ${}^4I_{11/2}$, ${}^4F_{7/2}$ and (${}^2P_{3/2}+{}^2D_{3/2}+{}^4F_{3/2}$) are also approximately equally spaced with an energy gap of about 10300 cm^{-1} (corresponding to approximately $1 \mu\text{m}$). Similarly levels ${}^4I_{15/2}$, ${}^4I_{9/2}$, ${}^2H_{9/2}$ and (${}^4H_{9/2}+{}^4G_{9/2}$) are also approximately equally spaced with energy difference of about 12500 cm^{-1} , corresponding to a transition with a wavelength of about 800 nm - the same as the main pumping wavelength in the present study. These resonant spacings between the levels has a significant effect on the dynamics of their populations, giving rise to overlapping fluorescence lines, excited state absorptions (ESA) and a complex set of cross-relaxation processes. The effects of these resonant spacings will be discussed in detail in the next two chapters.

Wavenumber ($\times 10^3 \text{ cm}^{-1}$)	Absorption λ (nm)	Linewidth FWHM(nm)	Energy level	Reference:
0			${}^4I_{15/2}$	
6.55	1527	70	${}^4I_{13/2}$	our work
10.30	975	16	${}^4I_{11/2}$	our work
12.56	796	20	${}^4I_{9/2}$	our work
15.39	650	13	${}^4F_{9/2}$	our work
18.59	538	8	${}^4S_{3/2}$	our work
19.23	520	8	${}^2H_{11/2}$	our work
20.70	483	8	${}^4F_{7/2}$	our work
22.37	447	6	${}^4F_{5/2}$	our work
22.78	439	6	${}^4F_{3/2}$	our work
24.81	403	5	${}^2H_{9/2}$	our work
26.52	377	7	${}^4G_{11/2}$	our work
27.62	362	4	${}^2G_{9/2}+{}^2K_{15/2}$	our work
28.33	353	6	${}^2G_{7/2}$	our work
31.85	314	6	${}^2P_{3/2}+{}^2D_{3/2}+{}^4F_{3/2}$	our work
33.28	300		${}^2K_{13/2}$	Zhong <i>et al.</i> ,1992
34.16	298		${}^2D_{7/2}$	Zhong <i>et al.</i> ,1992
34.94	286		${}^2D_{5/2}$	Zhong <i>et al.</i> ,1992
36.67	273		${}^4H_{9/2}+{}^4G_{9/2}$	Zhong <i>et al.</i> ,1992
39.49	253		${}^4D_{7/2}$	Zhong <i>et al.</i> ,1992

Table 3.3-1 Peak absorption wavelengths and corresponding energies of some of the excited states of the Er^{3+} ions in ZB(L)AN.

Spectrometer data was used to obtain the absorption coefficient at 802 nm for the various glasses and this data is presented in Table 3.3-2. The absorption cross section at this wavelength is obtained from the slope of the plot of absorption coefficient against erbium concentration.

3.3.2. CW measurements with laser diode excitation

- Experimental arrangement

A study of the absorption coefficient of the glasses was then also carried out with the pumping LD. This source was a Sony SLD304XT LD which could produce a continuous wave (CW) output of up to 1 W at a wavelength which was temperature tunable between about 802nm and 807nm. The output spectrum consisted of about 6 modes with a total spectral width of about 2 nm (FWHM). The normal operating power of the laser diode at 802nm was 600 mW. The setup of the experiment, where the LD was used to measure the absorption coefficient of the glasses is presented in Figure 3.3-2.

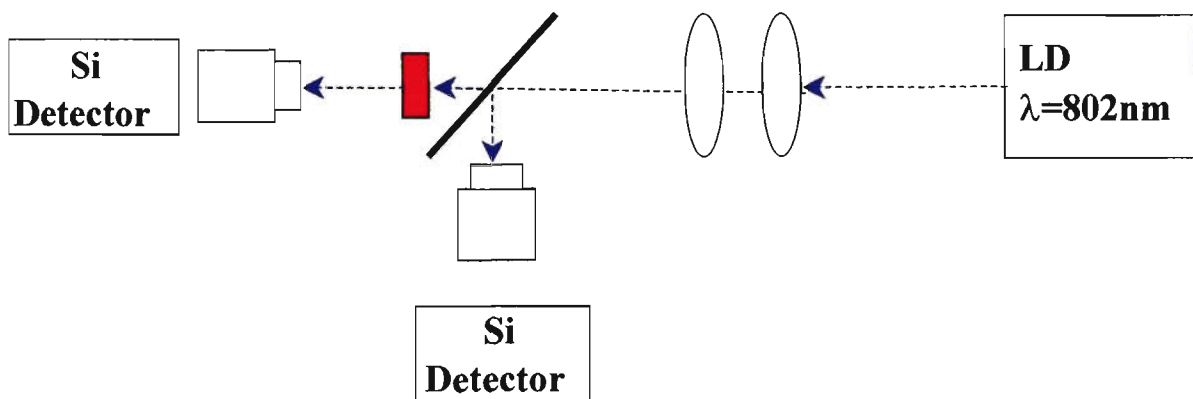


Figure 3.3-2 Absorption measurement setup using the LD source.

In the above setup a pair of convergent lenses was used to focus the divergent beam from the LD. To avoid instabilities due to back reflections into the LD, optical elements in Figure 3.3-2 were tilted slightly off-axis. To monitor the power of the LD a very thin glass slide was used to reflect a small part of the beam (the reflection of both surfaces was estimated at approximately 8% of the whole beam) towards a silicon

detector. A second silicon detector was used to measure the power of the remaining unabsorbed pump beam after passing through the sample.

- **Results**

The results of both LD and spectrophotometer measurements of the absorption coefficients of the glasses at 802nm are shown in Table 3.3-2 and Figure 3.3-3. The two sets of data appear consistent within experimental error and follow a reasonable straight line. It should be noted that at the lowest concentration, the absorption in a 1 mm thick sample is only about 1.5% and so the uncertainties in estimates of absorption coefficient are greater at low doping concentration. This is the reason why only LD data is presented for the lowest three concentrations. The major cause of the deviations from linearity is believed to be thickness variations that could be as much as about 10% across some samples. The data in Table 3.3-2 have been corrected for reflection losses at the surfaces but not for a small amount of scattering loss at these surfaces (due to the limited polishing facilities available) which was visually evident but difficult to quantify.

Er³⁺ (mol%)	Absorption coefficient α (cm⁻¹)	
	LD	Spectrophotometer
0.8	0.150	
1.6	0.250	
3.2	0.440	
4	0.580	0.550
6	0.765	0.680
8	0.990	1.030
10	1.310	1.220
12	1.375	1.380
14	1.610	1.530
16	1.785	1.860
18	2.070	2.040

Table 3.3-2 Measured absorption coefficients at 802 nm in Er³⁺/ZB(L)AN. The uncertainty is less than 10% (see text).

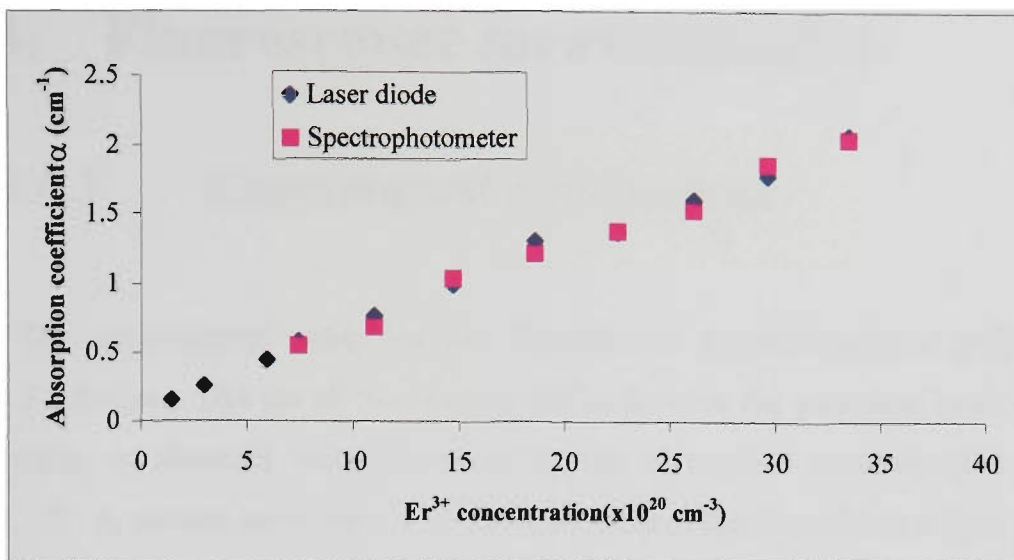


Figure 3.3-3 Plot of the absorption coefficients obtained for Er/ZB(L)AN glasses with both laser diode and spectrophotometer as a function of the Er³⁺ concentration.

A linear regression fit to the data of Figure 3.3-3 (including the origin) gives a slope of $6.26 \times 10^{-22} \text{ cm}^2$ with a standard error of $0.09 \times 10^{-22} \text{ cm}^2$. Thus the 95% confidence limits on the erbium absorption cross section at 802 nm in our host glasses are $(6.08 - 6.44) \times 10^{-22} \text{ cm}^2$.

No detailed measurements of the peak absorption cross-sections were carried out for the other pumping wavelengths used. Approximate values, estimated from the ratio between the amplitude of the absorption peaks at these wavelengths and the one at 802 nm, were used instead (see Table 3.3-3).

Pumping λ	1.53 μm	975 nm	802 nm	520 nm	403 nm	Source:
σ ($\times 10^{-21} \text{ cm}^2$)	4.7	2.0	0.63	11.5	1.4	This work
	5.00	2.15	0.644			Miniscalco, 1993

Table 3.3-3 Summary of the absorption cross-sections in Er/ZB(L)AN glasses for the different pumping wavelengths used.

All cross sections used in later calculations are expected to be accurate to better than 10%. These cross sections are considered sufficiently accurate for use in the modeling calculations of later chapters in this thesis. For comparison, the cross sections reported by Miniscalco (1993) for similar wavelengths in Er³⁺:ZBLAN glass are also included in Table 3.3-3. The two sets of values agree within 10%.

3.4. Fluorescence measurements

3.4.1. Experimental arrangement

The experimental setup for the fluorescence measurements is presented in Figure 3.4-1 below. The set of two lenses, which focuses the pumping beam onto the glass sample, is identical with the set from the absorption measurement setup in Figure 3.3-2. A second set of lenses was used to collect the fluorescence light from the glass sample and focus it onto the entrance slit of a Jarrell-Ash 0.25 m monochromator. Three gratings were used with this monochromator to cover the wavelength range of the fluorescence measurements (see Table 3.4-1). For most of the measurements in the visible and near infrared, 150 μm slits were used giving a spectral resolution of up to about 1 nm. In a few instances of weak fluorescence lines, slit width up to 500 μm were used. Measurements of fluorescence at 2.7 μm also used 500 μm slits and hence the spectral resolution for these measurements is about 7 nm.

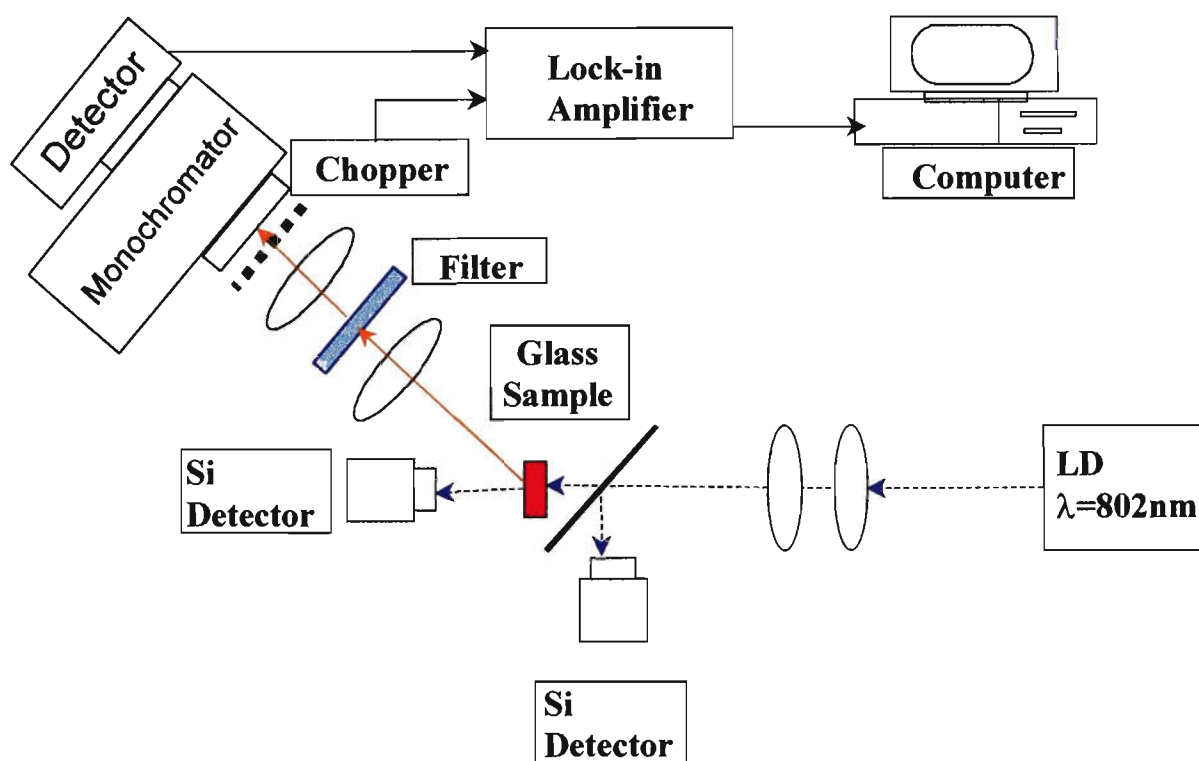


Figure 3.4-1 Absorption (at 802nm) and fluorescence measurement setup

Spacing (grooves/mm):	Blazed for λ :	Spectral range :	Reciprocal linear dispersion (nm/mm):
1180	500 nm	350 nm - 1000 nm	3.3
590	1.0 μm	700 nm - 1.8 μm	6.6
295	2.1 μm	1.3 μm - 3.8 μm	13.2

Table 3.4-1 Gratings used with the 0.25 m Jarrel-Ash monochromator

In addition to the monochromator, optional filters were sometimes used to remove unwanted spectral components such as higher orders of visible lines when measuring in the IR or to provide additional rejection of nearby pump radiation. Several detectors were used to cover the total fluorescence wavelength range. The main characteristics of these detector/amplifier systems are presented in Table 3.4-2. A Stanford SR530 lock-in amplifier was used to improve the signal-to-noise ratio of the fluorescence signals. The signal from the lock-in amplifier then was sampled using a 12-bit A/D recording system and stored in a PC.

Detector :	Wavelength range:	Response time
Photomultiplier (Hamamatsu; R928, R632)	200nm - 900nm 200 nm - 1100 nm	Depends on a load resistor (< 10 ns with 50Ω)
PbS (Graseby, PS1-0-01)+Amplifier	1 μm - 3 μm	150 μs
InGaAs (Fermionics, FD300)+Amplifier	900 nm -1700 nm	10 μs
InAs (EG&G, J12TE2-8B6-R01M)+Amplifier	1.5 μm - 3.5 μm	10 μs

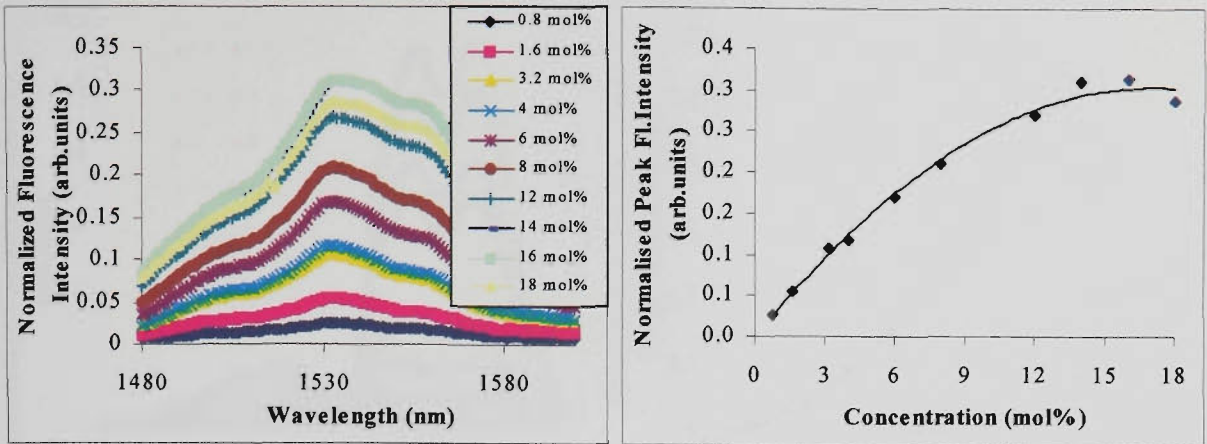
Table 3.4-2 Wavelength range and response time of the detector systems used.

Some of the measured fluorescence curves, normalised for the absorbed pump power at 802 nm are presented in Figures 3.4-2 and 3.4-3. These spectra have been approximately corrected for re-absorption of the fluorescence within the sample by assuming that the emitted light traverses half the sample thickness before exiting the glass (using an absorption coefficient appropriate to the wavelength concerned). In fact these corrections produce only a relatively small change in shape of the fluorescence spectra. The spectra have also been corrected for the spectral response of any filters used in these measurements. The difference in the spectral response of the gratings and

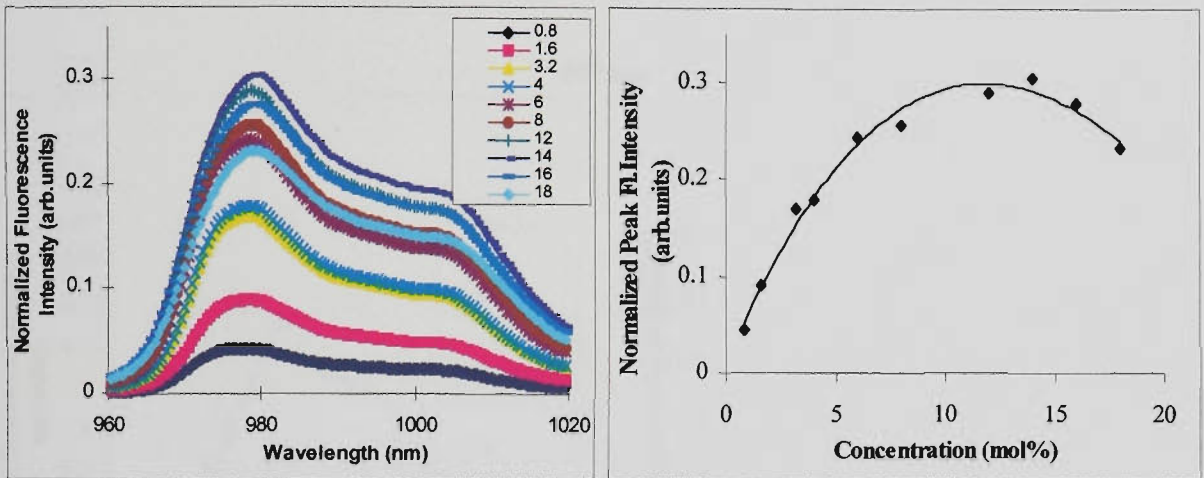
the detectors used in the recording of these fluorescence curves was generally small (within a few percent over the line-widths of the curves) and was ignored. One obvious feature in all of the spectra is the substructure, caused by the presence of the Stark splitting of the levels. These Stark levels, however are not very well resolved at room temperature, where they tend to overlap, forming essentially a homogeneously-broadened quasi-continuum (France *at. el.*, 1991) which, as far as a narrow linewidth pumping source is concerned, can be treated as a single level. Thus, for the purpose of this study, the substructure of the energy levels has been ignored. In the case of the green fluorescence, the two well pronounced peaks at 520-530 nm and 540-550 nm represent two separate energy levels (level $^2H_{11/2}$ and level $^4S_{3/2}$). The energy separation of these levels is small ($\sim 700 \text{ cm}^{-1}$) and they are strongly coupled by phonons and hence they are treated as a single level in the modeling of later chapters.

Also shown in Figures 3.4-2 and 3.4-3 is the variation of peak fluorescence intensity with doping concentration for five of the main fluorescence lines. It will be shown in later chapters that the levels responsible for these fluorescence lines include the bulk of the excited state population. All of the fluorescence intensities peak somewhere between 10 and 15 mol% Er^{3+} doping concentration. Since the effect of changes in pump absorption has already been removed, an overall increase or decrease in fluorescence with doping level is indicative of the existence of non-optical pumping mechanisms which increase or decrease the total number of excited ions. This implies the existence of cross-relaxation processes involving the ground state. The existence of a peak in the fluorescence variation with doping level suggests a balance between cross-relaxation processes which both populate and de-populate the ground state. As will be seen in the following chapters, the variation in energy level population with doping concentration in these highly doped glasses is very complex and does require cross-relaxation processes involving the ground state for an adequate explanation.

1.53 μm



980 nm



655 nm

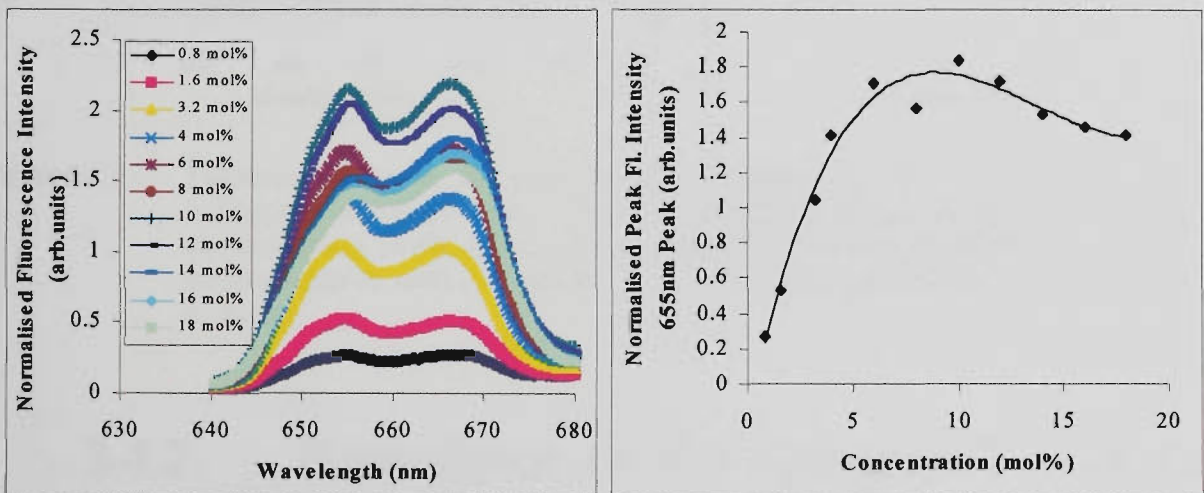
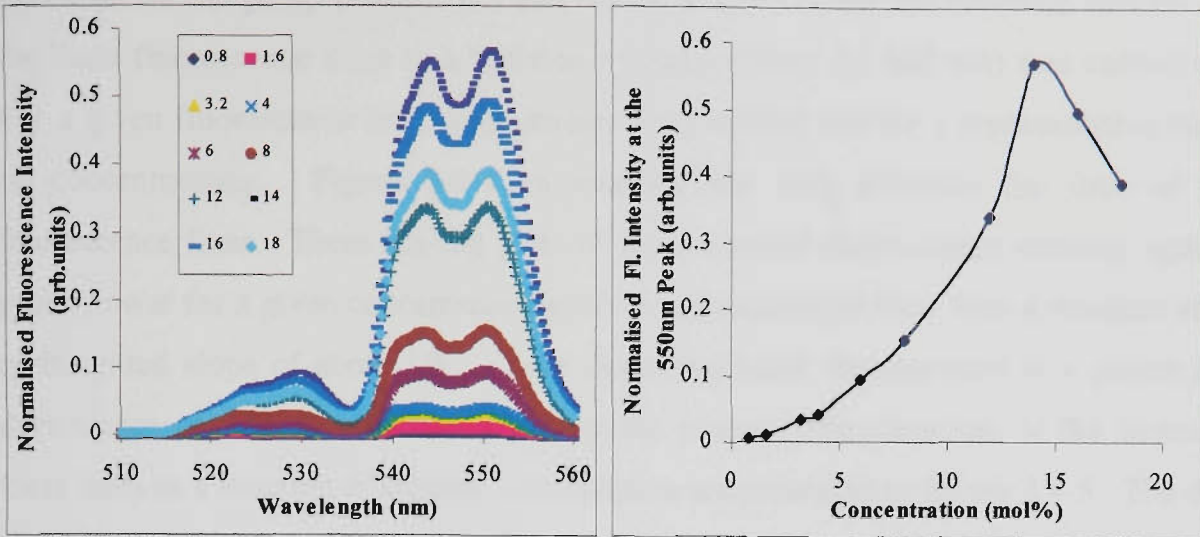


Figure 3.4-2 Fluorescence spectra and peak fluorescence intensity vs Er³⁺ concentration for the indicated fluorescence lines. These intensities have been normalised by dividing by absorbed pump power and the fluorescence spectra have been adjusted to compensate for re-absorption within the sample. The curves on the right hand figures are only guide to the eye.

530 / 550nm



407 nm

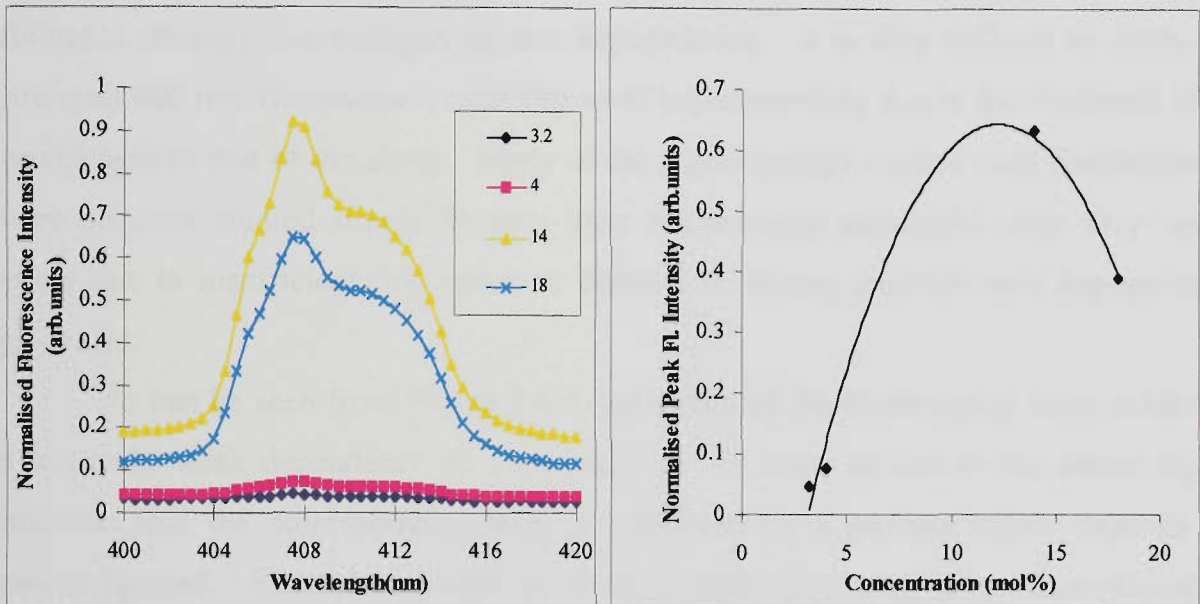


Figure 3.4-3 Fluorescence spectra and peak fluorescence intensity vs Er³⁺ concentration for the indicated fluorescence lines. These intensities have been normalised by dividing by absorbed pump power and the fluorescence spectra have been adjusted to compensate for re-absorption within the sample. The curves on the right hand figures are only guide to the eye.

3.4.2. Dependence of the fluorescence intensity on pump power

One way to obtain information about the processes affecting the population of a particular level is to study the dependence of the intensity of the fluorescence lines from

this level on the pump power. For this reason a study of the fluorescence intensity of the main fluorescence lines as a function of pump power (at 802 nm) was carried out. For a given fluorescence line, these studies were carried out for a representative range of concentrations. Figure 3.4-4 summarises the data obtained for four of the fluorescence lines. These log-log plots of the measured fluorescence intensity against pump power for a given concentration gave excellent straight lines with a standard error of the fitted slope of about 1%. These slopes represent the exponent in a power law dependence of fluorescence intensity on pump power. The variations of the slopes of these lines as a function of erbium concentration are presented in Figure 3.4-5. The data of figure 3.4-5 include at least one fluorescence line from each of the five lowest energy excited states except for the $^4I_{9/2}$ level. This latter level is not included as it does not fluoresce strongly due to rapid phonon depopulation. It is also difficult to study the strongest 800 nm fluorescence from this level experimentally due to the closeness of its wavelength to that of the pump. Many of the higher energy excited state fluorescences were also not studied simply because their fluorescence intensities were very weak, either due to insufficient population or because of strong multi-phonon depopulation processes.

As can be seen from Figure 3.4-5, the slopes of the fluorescence lines exhibited a relatively weak dependence on concentration. A slope of two in the above figure indicates that the corresponding level is populated by a process which depends on power squared. Examples include an excited state absorption or a cross-relaxation process such as W(11,30) and W(22,50) (see foldout energy level diagram) which require two pump photons for the excitation of a single ion. A slope of one in Figure 3.4-5 is produced if each excited ion is a result of absorption of a single photon. A slope of less than one results if, on average, more than one excited state is produced for a given pump photon, indicating that additional pumping mechanisms, which are not dependent on the initial absorption, are also active.

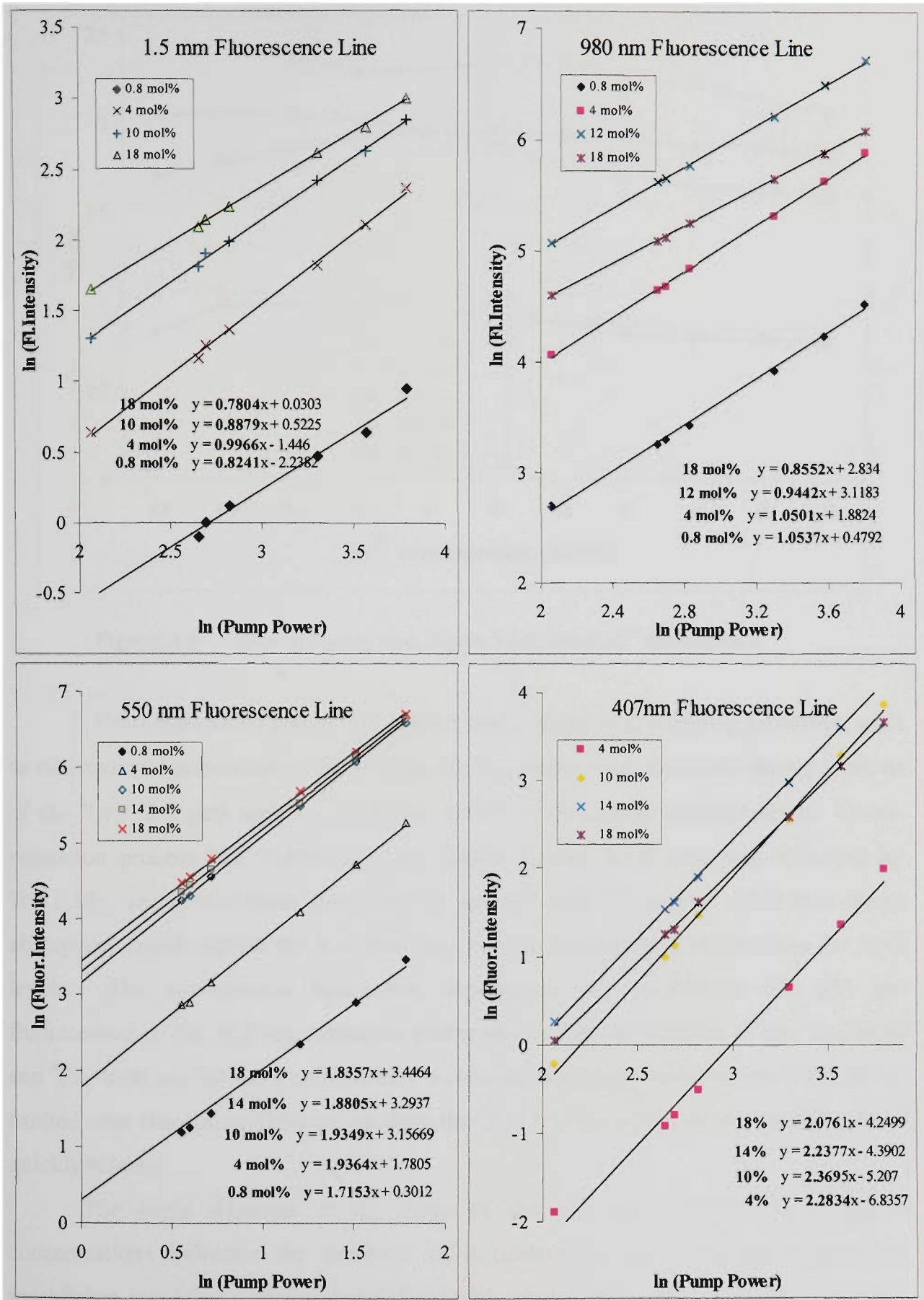


Figure 3.4-4 Log/Log plots of the fluorescence intensity of the indicated fluorescence lines vs 800 nm pump power for a range of erbium concentrations.

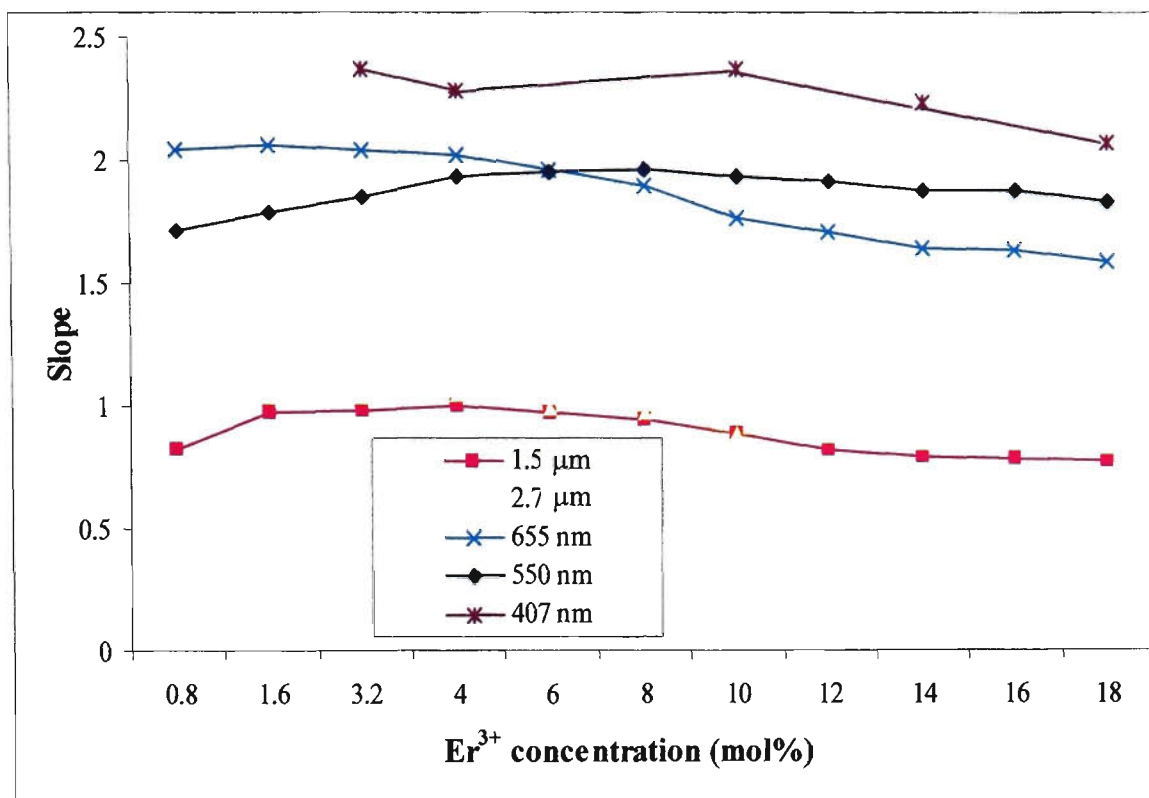


Figure 3.4-5 Slope of log-log plots (Figure 3.4-4) versus Er^{3+} concentration

From the results above it is evident that a single step pumping processes, such as radiative and non-radiative decay from the $^4\text{I}_{9/2}$ pump level, dominate the populations of the $^4\text{I}_{11/2}$ (2.7 μm) and $^4\text{I}_{13/2}$ (1.5 μm) levels at all doping concentrations. Cross-relaxation process like T(300,011) (see foldout energy level diagram), followed by W(11,30), which contribute ions from the ground state via process other than direct absorption, could explain the less than one slope in the higher concentrations for both levels. The approximate square-law dependence of the 540 nm and 655 nm fluorescence on the 800 nm excitation power shows that populations of the $^4\text{S}_{3/2}$ level and $^4\text{F}_{9/2}$ level are basically produced by a cross-relaxation process such as W(22,50) or excited state absorption of the pump from the $^4\text{I}_{11/2}$ level to which the pumped $^4\text{I}_{9/2}$ level quickly relaxes.

The slight decrease in the slope of the 655 nm fluorescence at higher concentrations indicates the presence of a contribution from additional pumping mechanism involving a level populated by single photon processes. A slope higher than two, exhibited by the weak 407 nm fluorescence, showed that while the bulk of the population of the $^2\text{H}_{9/2}$ level was coming from ESA of the pump from the $^4\text{I}_{9/2}$ level,

there was also a contribution involving a three-stage ESA or three-ion cross-relaxation process such as T(333,008) (see foldout energy level diagram).

The origin of the non-integer slopes at lowest doping concentrations is not at present clear. As has already been mentioned, the population dynamics of this system is very complex and the combined effect of the various cross-relaxation processes is very difficult to predict without a very detailed model. The processes responsible for the populations of each individual energy level will be discussed in more detail in Chapter 5 when such a model is developed.

3.4.3. Fluorescence decay waveforms

Probably the most important measurements for an understanding of the energy level processes in these materials involved a study of the temporal behaviour of the excited state fluorescence after pumping with a very short pulse. The experimental arrangement for this study is shown in Figure 3.4-6.

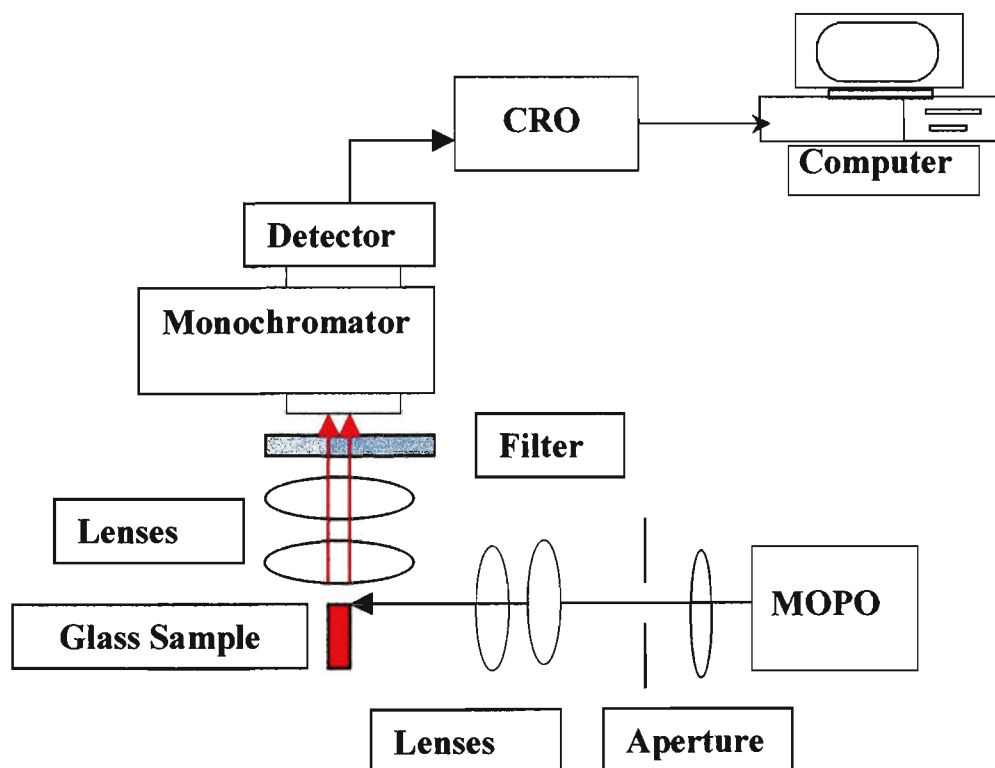


Figure 3.4-6 Experimental setup for fluorescence waveform measurements

The excitation source was a narrow linewidth ($\sim 0.2 \text{ cm}^{-1}$ in the visible) Spectra Physics optical parametrical oscillator (MOPO) of pulse length about 10 ns, repetition rate of 10 Hz, output energy of up to 100mJ and a wavelength tunable between 220 nm and 1.8 μm . The idler beam at 802 nm from this system had a transverse mode structure which could often be quite complicated. In some of the early measurements this beam was simply focused onto the target sample. In later experiments an optical system, consisting of a diverging lens, an aperture and two focusing lenses as shown in the figure, was used to obtain more uniform pumping.

The pumping spot was typically 1 - 4 mm in diameter and was carefully placed very close to the edge of the sample to minimize the distance traveled by the fluorescence light within the sample and help avoid fluorescence trapping. The fluorescence was collected from the side of the sample (at 90° to the pump beam) to reduce the amount of pump light entering the monochromator. For the pulsed measurements, the monochromator used was a 275 mm focal length Jarrell-Ash MonoSpec 27. This system used the same filters and detectors as were previously used for the CW fluorescence measurements. A Tektronix TDS 320C digital storage oscilloscope was used to average and record the fluorescence waveforms. Typically, recorded fluorescence signals used an average of 256 waveforms.

A very large number of fluorescence rise and decay waveforms were recorded. These waveforms were recorded for all the main fluorescing levels for all concentrations and for 5 different excitation wavelengths; 1.5 μm , 975 nm, 800nm, 520nm and 403nm. Once recorded, the fluorescence waveforms were analysed by fitting appropriate mathematical functions and extracting the values of coefficients together with standard errors of these coefficients. In some cases the waveforms, or sections of them, were fitted with functions representing a simple single exponential rise or decay. In many cases, however, more complicated functions were found necessary. For example, when the rise and decay time constants are comparable in magnitude, the data cannot be sectioned to separate the rise and decay portions and it is necessary to fit a single function involving both rise and decay components to the whole waveform. In other cases decays needed to be fitted by multiple exponential functions involving multiple decay time constants representing different decay processes. A detailed

discussion of the fitting functions, the values of parameters obtained from the fitting and their interpretation will be presented in Chapter 4 and Chapter 5.

3.5. Conclusion

This chapter has presented all the experimental arrangements used for data collection in sufficient detail to allow the reader to appreciate the main features and limitations of that data. The compositions of the Er^{3+} -doped glasses have been presented as have their absorption spectra. The absorption spectra were used to calculate an energy level diagram and obtain values of absorption cross sections at the various pump wavelengths used in the measurements.

CW fluorescence measurements have been made to study the fluorescence spectra under 802 nm excitation and to obtain information about pumping and energy exchange processes in the glasses from the pump power dependence of the fluorescence intensity. These measurements indicate that both ESA and cross-relaxation processes are significant at the doping levels used in these glass materials.

The experimental arrangement for making fluorescence waveform measurements using very short pulses with high energy density has been described. The data obtained from these measurements, its interpretation and its use in developing a rate equation model of the energy level processes is the subject of the next two chapters.

Chapter 4

Modelling of the population dynamics of the three lowest excited energy levels

4.1 Introduction

In this chapter we discuss the development of a model of the population dynamics of the three lower energy levels of our Er^{3+} -doped ZB(L)AN glasses. This model is developed and refined by comparing model outputs with measured fluorescence waveforms. The model outputs gave the predicted temporal behaviour of the population of the levels and the measured fluorescence intensities were presumed to be proportional to the populations of the levels from which the fluorescence originated. Various processes were included in or excluded from the model and the cross-relaxation rate constants, characterising these processes, were varied until good agreement was obtained with the set of measured waveforms.

The current work has been concentrated mainly on the use of 800 nm pumping and the modelling, presented in this chapter, concentrates mainly on this pumping wavelength. Measurements with other pumping wavelengths, however, have been also considered in order to help elucidate some of the processes in the modelling. When a pumping wavelength was chosen so that an energy level was directly excited by the pump, the term "direct pumping" is used in association with the data for this level. The Er^{3+} energy level diagram in Figure 4.1-1 shows that a pump with wavelength of about 800 nm will initially put the majority of the excited ions in Level 3 ($^4I_{9/2}$). In addition, there will also be a small number of ions initially excited to higher levels due to possible excited state absorption from the $^4I_{9/2}$ level or from the $^4I_{11/2}$ level into which the $^4I_{9/2}$ level rapidly decays. However, the number of ions excited to these upper levels

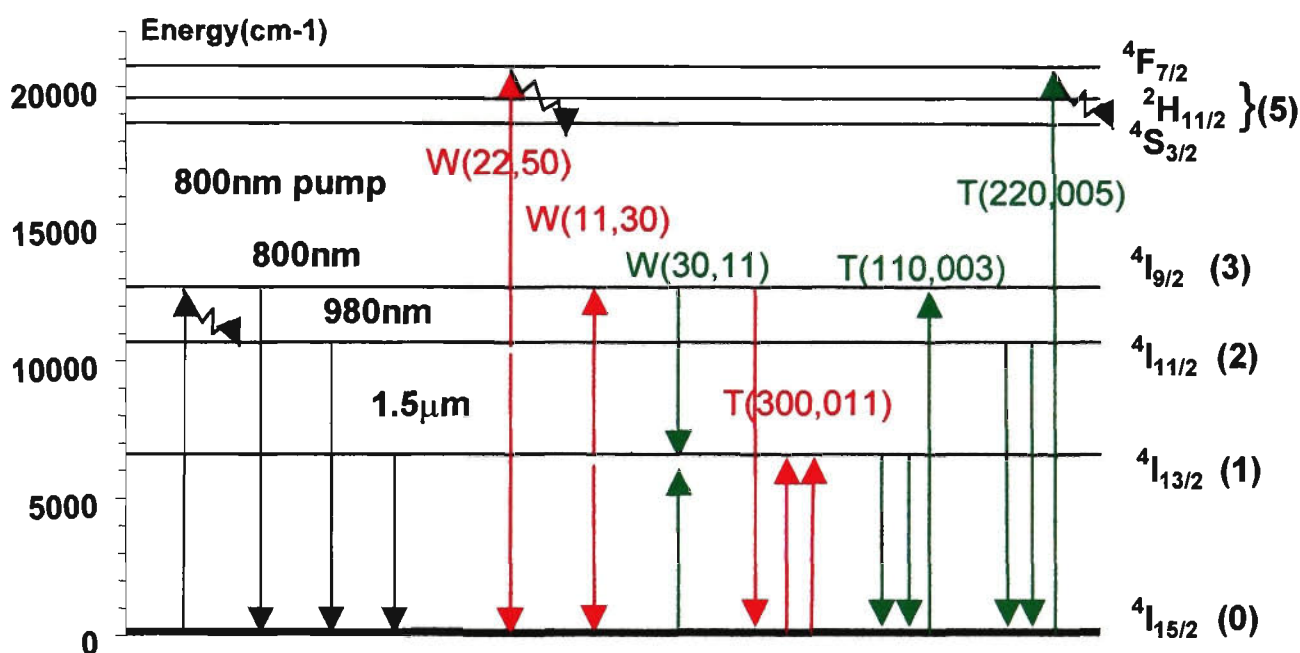


Figure 4.1-1 Energy level diagram for Er^{3+} , fluorescence and multiphonon transitions and cross-relaxation processes in $\text{Er}/\text{ZB(L)AN}$ glasses. For designation of the cross-relaxation processes-see text of Chapter 2.

under our pumping conditions represents a small fraction of the total excited state population. Thus, to a first approximation, it can be assumed that with an 800 nm pump the bulk of the excited ions are in the three lowest excited energy levels ($^4I_{9/2}$, $^4I_{11/2}$, $^4I_{13/2}$). Hence it was considered useful to start with a model which considered only

these levels. As pointed out in Chapter 2, such a model has proved suitable for use in glasses with higher phonon energies.

The levels considered in this modelling are designated as: $0(^4I_{15/2})$, $1(^4I_{13/2})$, $2(^4I_{11/2})$ and $3(^4I_{9/2})$. The $^4S_{3/2}+^2H_{11/2}$ and $^4F_{7/2}$ levels are included in Figure 4.1-1 only for completeness in that some of the processes, which affect Levels 0 – 3 and which are considered in the model, involve these levels also. The radiative transitions under consideration are shown together with the important multiphonon decays from the $^4I_{9/2}$, $^4F_{7/2}$ and $^2H_{11/2}$ levels. As previously described in Chapter 2, the cross-relaxation processes presented are designated as either two-ion (W) or three-ion (T), followed by up to six numbers indicating starting levels and finishing levels.

4.2 Experimental results

As was mentioned in Chapter 3, the recorded rise and decay waveforms of most of the fluorescence lines were fitted with exponential functions, representing filling and emptying of the levels. A summary of the results for the three lowest energy excited states (Level 3 ($^4I_{9/2}$), Level 2 ($^4I_{11/2}$), Level 1 ($^4I_{13/2}$)) is presented in Table 4.2-1, where the appropriate time-constants are given. This table is rather complicated in that it contains several series of numbers which are calculated in different ways and which in general should not be compared with each other as they have different physical meanings. They are presented in one table as they represent different ways of comparing trends in the same set of data and in the long run presentation in a single table helps one obtain an overview of the trends. Each of the sets of data, which are differentiated by colour, will be described in the following pages. Before presenting a discussion of the various trends in the fluorescence waveforms it is worth reiterating and expanding a comment which has been made earlier. In a situation where one is dealing with a complex set of non-linear processes, there is nothing fundamental in a particular fluorescence waveform or a rise and decay constant for a particular level. These waveforms and time constants are function of the pumping energy density (number of excited ions) and wavelength (pump level) and quite different waveforms can be obtained as these parameters are varied. If the measurements are to be useful they must be reduced to a model which can be used to predict the response of the doped

glass under any form of excitation. Hence the real output of the work of this thesis is the model which is progressively developed and presented in its final form in Chapter 5. The waveforms obtained under particular excitation conditions are merely the basic data which is used in the development of the model. The various time constants which are listed in the table of this chapter (and also in Chapter 5) are one step further removed from being fundamental material data, in that they have been introduced as a way of presenting a summary of trends in a much more compact and easy to comprehend way than would be provided by just attaching a large set of measured waveforms. It has to be appreciated in considering the data contained in the tables that there is not, for example, only one decay time for Level 1 but as many decay times as there are pumping conditions.

To reinforce the points made above, Table 4.2-2 below presents comparable sets of time constants to those displayed in Table 4.2-1 but for different excitation conditions. Table 4.2-1 was produced using the focused idler output from the MOPO without spatial filtering and the energy and spot size in the beam were approximately 24 mJ and 8 mm² respectively. These parameters can be used to calculate an average energy density for the excitation but it was clear that there were spatial hot spots in the unfocused beam due to its unavoidable complex mode structure which varied considerably from day to day. There was a concern that even though hot spots were not visually evident in the predominantly green visible fluorescence from the focused beam that they might still be present. The burn pattern on a polaroid film placed at the position of the target material looked reasonably uniform but was not completely circular. Hence a second set of fluorescence waveforms were measured for which an aperture was used to select a fairly uniform part of the idler beam and this was focused onto the sample with a similar average power density to that used in the previous measurements. For this second set of measurements the energy of the focused beam was about 5 mJ and the spot size was about 2.5 mm². These excitation conditions were as uniform as was possible to obtain with the MOPO and polaroid film burns were both uniform and circular. The two sets of measurements represented by data summarised in Tables 4.2-1 and 4.2-2 are both valid and both used in the discussions which follow. Since the excitation used in the second set of measurements was considered more uniform and better characterised by the average energy density, this set of waveforms

was generally used to compare measured and modelled data. The model has been applied to both excitation conditions and the measured waveforms have been compared with model outputs for both sets of data. The agreement between model and measurement is very similar for the two data sets. However, the examples presented in the thesis were mostly from the second data set.

For completeness, two other differences between the two sets of data should be mentioned. The faster components of the 1.5 μm waveforms are more faithfully recorded in the second set of data as an InGaAs detector system with a 10 μs response time was used for this set and a PbS detector system with a response time of 150 μs was used with the initial set. The second obvious difference is that the first data set covered a slightly larger range of measured concentrations than was the case with the second. The second set tended to focus on a more detailed study of the 1.5 μm fluorescence with the faster detector.

Another consequence of the more uniform spatial distribution of the focused pump spot in the second set of data is that the shot-to-shot variability of the waveforms would be expected to be a little less. The recorded fluorescence waveforms are averages of (usually) 256 individual waveforms produced at the 10 Hz pulse repetition rate of the MOPO. There is obvious fluctuation in the waveform from pulse to pulse which is partly due to variation in excitation produced by variations in the pump beam. While it is difficult to make comparisons under different excitation conditions and on different days due to the presence of various other noise sources in the detector outputs, we have tended to prefer the second set of data in the belief that it would have a lower total "noise" in the recorded waveform. Repeated measurements of fluorescence waveforms under the more uniform excitation conditions indicated an improved overall repeatability of the fitted time constants in Table 4.2-2 of about 20%.

		800 nm pump		975 nm pump		1.5 μm pump		
Fluor. λ (Level)	Er (mol%)	Rise (μs)	Decay (ms)	Rise (ms)	Decay (ms)	Rise (ms)	Decay (ms)	
820 nm Level 3 (⁴ I _{9/2})	0.4	Inst.	7.9 μs					
	1.6		9.0 μs					
	4		7.6 μs					
	10		6.9 μs					
	14		6.2 μs					
	18		6.0 μs					
980 nm Level 2 (⁴ I _{11/2})	0.4	7.7	7.7	Inst.				
	0.8				7.8			
	1.6	7.8	8.0			5.9	9.7	
	4	7.5	8.3			8.2	5.1	11.9
	8	6.9	NE(2.4+7.9)					
	10	6.9	NE(2.5+9.9)			NE(1.5+8.4)	1.6	12.1
	14	6.2	NE(1.7+9.5)					
	18	5.8	NE(1.5+7.7)			NE(0.5+5.8)	0.4	7.4
1.5 μm Level 1 (⁴ I _{13/2})	0.8	25*(±28) (8.0)	9.3*(±2) (8.1)	54*(±117) (8.0)	9.1*(±1.6) (8.7)	Inst.	10.9	
	1.6	21*(± 8) (8.0)	10.0*(±0.8) (8.7)					
	4	8.6 (8.0)	12.9 (8.6)	7.4 (8.0)	15.4 (9.3)			NE(1.0+9.5)
	8	Fast + 3.7	12.3					
	10	Fast + 0.8	14	2.2	16.6			NE(0.8+6.6)
	14	Fast + 0.5	14.1					
	16	Fast Only	10.2					
	18	Fast Only	7.3	0.5	7.8			NE(0.5+5.7)

Table 4.2-1

Data set 1(1.5 μm PbS detector): Measured fluorescence rise and decay time constants for the indicated levels and for the pump wavelengths as shown. Inst.- faster than the response of the detector. NE – non-exponential, Fast – Fast component (see text), **Black numbers** - obtained from fits with a single (or double) exponential function (see text), **Blue numbers** – obtained from fits with combined exponential rise and decay function (see text). **Red Numbers** –decay time constants of fluorescing and "filling" levels calculated using an analytical fitting function obtained from a simple 2-level rate-equation model (see text), * - large uncertainties (± standard error). Approximate pump conditions: ~24 mJ, ~ 8 mm² spot area, λ = 802 nm.

Fluor.λ (Level)	Er (mol%)	800nm pump		1.5μm pump	
		Rise (μs)	Decay (ms)	Rise (ms)	Decay (ms)
980nm Level 2 (⁴ I _{11/2})	1.6	7.0	8.4	6.3	12.9
	18	4.8	NE(1.5+7.2)	0.85	8.9
1.5μm Level 1 (⁴ I _{13/2})	0.4	21.6*(± 3.4) (8.0)	10.6 (8.7)	Inst.	9.5
	0.8	17.6(8.0)	10.6 (9.1)		10.0
	1.6	14.8 (8.0)	12.1 (10.4)		10.3
	4	10.9 (8.0)	13.5 (10.6)		9.0
	8	Fast + 4.9	12.4		
	10	Fast + 3.7	15.7		NE(1.8+13.2)
	14	Fast + 1.2	15.0		NE(1.2+9.9)
	18	Fast Only	6.6		NE(0.8+7.4)

Table 4.2-2 Data set 2 (1.5 μm InGaAs detector) - Measured fluorescence rise and decay time constants for the indicated levels and for the pump wavelengths as shown. Inst.- faster than the response of the detector. NE – non-exponential, Fast – Fast component (see text), **Black numbers** - obtained from fits with a single (or double) exponential function (see text), **Blue numbers** – obtained from fits with combined exponential rise and decay function (see text). **Red Numbers** –decay time constants of fluorescing and "filling" levels calculated using an analytical fitting function obtained from a simple 2-level rate-equation model (see text), * - large uncertainty (± standard error). Approximate pump conditions: 5 mJ, 2.5 mm² spot area, λ = 802 nm.

We now return to a discussion of the data contained in Tables 4.2-1 and 4.2-2. For a proper understanding of these tables, there are a number of issues, related to the way these time constants have been obtained and the way they should be interpreted, that need to be discussed in more detail.

4.2.1 Exponential fits

- **Fitting of independent exponential rise and decay functions to sections of a waveform (black numbers in Table 4.2-1 and Table 4.2-2)**

A meaningful fit to an experimental waveform is relatively easily obtained for the case of a fast rise, followed by a much slower decay (for an example of such a waveform see 980 nm fluorescence of Figure 4.3-1). This is the case with Level 1 (${}^4I_{13/2}$) and Level 2 (${}^4I_{11/2}$) under direct pumping (with a 10 ns MOPO pump pulse, the rise of population of directly-pumped levels can be treated as effectively instantaneous in comparison to the timescales of other processes). A similar situation applies with Level 2 (${}^4I_{11/2}$) under 800 nm pumping where the multi-phonon decay from Level 3 (${}^4I_{9/2}$) populates Level 2 (${}^4I_{11/2}$) with a time constant of about 8 μ s. The decay times of both Level 1 (${}^4I_{13/2}$) and Level 2 (${}^4I_{11/2}$) are about 10 ms so the rise and the decay in these cases do not significantly affect each other and the simple exponential functions $(1-Ae^{(-t/\tau)})$ and $Ae^{(-t/\tau)}$ were fitted to the measured rise and the decay waveforms respectively. The values obtained from such fits represent the actual time constants for increase or decrease of population of the corresponding level and are written in normal black type in the tables above. Although each fit had a standard error of the fitted decay time of less than 5% (often less than 1%), the overall repeatability of the rise and decay times, obtained from the fits, was significantly worse. One factor affecting the repeatability was the selection of the part of the waveform which was to be actually fitted. Even in the case of waveforms that very closely followed a single exponential decay, this choice, in the presence of noise, was observed to affect the fitted decay by up to 5%. However, the major reason for variability in the decay times was the effect of pumping variations discussed above which, even under the best conditions, resulted in the time constants only being reproducible to about 20%. For this reason, the standard errors obtained for the fitted parameters are not quoted in the tables.

- **Fitting of multiple exponential functions to a non-exponential decay (NE followed by black numbers in Table 4.2-1 and Table 4.2-2)**

When discussing the fitting procedures another very important case is the one of non-exponential decays (designated as NE in Table 4.2-1 and Table 4.2-2), such as the decays of the $^4I_{11/2}$ and $^4I_{13/2}$ levels under direct pumping at high Er^{3+} concentrations (see Figure 4.2-1).

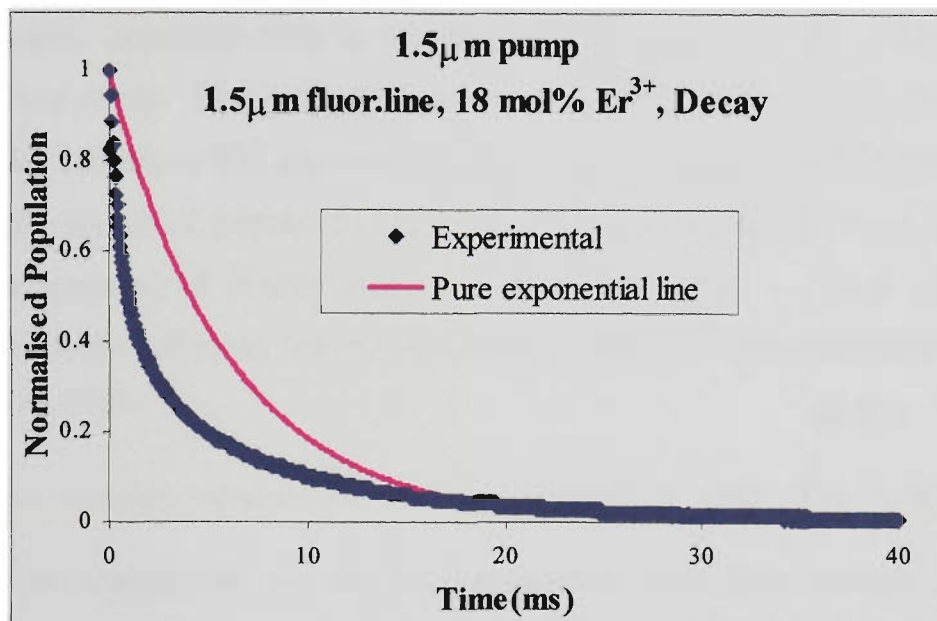


Figure 4.2-1 An example of a non-exponential fluorescence decay. A decay with a single exponential time constant is presented for comparison

These decays were characterised by fitting with a function, containing two-exponentials:

$$Ae^{(-t/\tau_1)} + Be^{(-t/\tau_2)} \quad (4.2.1)$$

An examination of either the 980 nm or 1.5 μm fluorescence waveforms under direct pumping shows that the instantaneous decay rates could vary up to a factor of 10 during the time of the decay. The fits of double exponential decays to the measured waveforms were generally very good with a standard error of the fitted decay times for a particular waveform of up to a few percent. The overall repeatability was again around 20%. The fitted values, obtained in this way, do not represent the time constants of any particular process, but are rather associated with a number of processes that together cause the particular non-exponential behaviour of the population of the level.

These non-exponential decays will be shown later to provide a very good indication of the nature of the processes which are important in determining the population and de-population of the level concerned.

- **Fitting of combined rise and decay function to a waveform (blue numbers in Table 4.2-1 and Table 4.2-2)**

Another important case to be considered is that of a non-instantaneous rise followed by a decay. This was observed with the fluorescence waveforms of Level 1 ($^4I_{13/2}$) under 800 nm or 975 nm pumping (see 1.5 μm fluorescence of Figure 4.3-1). In this case the source of population for Level 1 ($^4I_{13/2}$) is Level 2 ($^4I_{11/2}$), which has a decay time constant of similar magnitude to that of Level 1 ($^4I_{13/2}$). Under these circumstances, the following function was initially fitted to the fluorescence waveforms:

$$A(1-e^{(-t/\tau_r)})e^{(-t/\tau_d)} \quad (4.2.2)$$

This function consists of two time-dependant parts: The first, $(1-e^{(-t/\tau_r)})$, represents an exponential rise of the fluorescence (with time constant τ_r) and the second, $e^{(-t/\tau_d)}$, corresponds to an exponential decay (with time constant τ_d). It is important to realise that the time constants obtained from these fits are just the time constants associated with the waveform being characterised and not necessarily the time constants of any physical process responsible for populating or de-populating the level. If $\tau_r \ll \tau_d$ then the values of τ_r and τ_d obtained from fitting the expression above will be very similar to the time constants of the "filling" and "emptying" of the corresponding level. In this case τ_r and τ_d will also be very close estimates of the apparent rise time (0 - 63%) and decay time constants (100% - 36%) of the measured waveforms. However, τ_r and τ_d will more accurately characterise the rise and decay than the apparent time constant to the extent that the rise and decay are occurring simultaneously and this interaction is taken into account. When τ_r is not very much less than τ_d , however, a careful distinction should be made between the apparent time constants of the waveform (0 - 63% etc.), the time constants obtained from expression 4.2.2 and the "emptying" and "filling" time constants of the fluorescing level since these can be very different. The reason is that in this case the "filling" and "emptying" time constants of a level

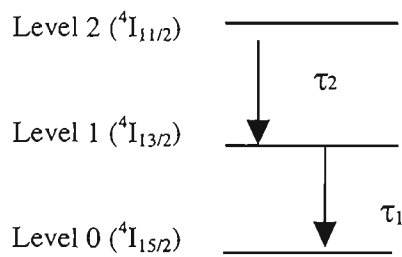
strongly interact in determining the rise and decay time constants of the waveform. This problem is particularly evident when the "filling" and "emptying" time constants are very similar or when the time constant of the "filling" process is longer than that of the "emptying" process. In these cases the time constants obtained from expression 4.2.2 represent neither the filling and emptying processes, nor the traditional definition of rise and the decay constants of the fluorescence waveform. In this case the physical interpretation of the decay times obtained from fitting expression 4.2.2 is rather complex but nevertheless these time constants are useful in demonstrating trends in the fluorescence waveforms.

For Er^{3+} doping levels higher than 1.6 mol% very good fits of expression 4.2.2 to the measured waveform ($R^2 > 0.999$) and small standard errors for the time constants (~ few %) were obtained. For Er^{3+} doping levels below 1.6 mol%, the fits of expression 4.2.2 to the fluorescent waveforms still appeared reasonable ($R^2 > 0.99$). However, the fitted parameters were characterised by larger standard errors. These time constants are indicated in Tables 4.2-1 and 4.2-2 by the inclusion of an asterisk and also by adding the standard error of the fitted parameter. These relatively large uncertainties arise from the fitting process because the partial derivatives of the function with respect to the variable parameters become very small when the τ_r of expression 4.2.2 becomes large. This problem is worst for the A and τ_r parameters and so under these conditions A and τ_r have a much larger range of possible fitted values than does τ_d . Physically what this means is that when τ_r is large (this happens when the filling and emptying time constants are nearly equal) one can balance the effect of amplitude A and rise time τ_r . That is, one can fit a given waveform quite well with either a small A and small τ_r or with a large A and large τ_r . Thus the values in the table which include an asterisk are considered very unreliable and are included only for completeness. Under the conditions being discussed here, the value of time constant of the decay is generally much better defined than that of the rise. These values have still been included in the tables with an asterisk if they are dependent on unreliable values of τ_r . In summary, the problems with fitting an expression such as 4.2.2 to the waveforms is that the constants obtained do not, in general, have any physical meaning and also do not always characterise the rise and decay time constants determined by just considering the rising

and decaying sections of the measured waveforms. This is the reason for considering an alternative form of fitting function in the next section.

4.2.2 Fitting functions, derived from simple rate-equation modelling in low Er^{3+} concentrations (red numbers in Table 4.2-1 and Table 4.2-2)

In this section we consider a form of exponential fitting function for which, at least in low doping concentrations, the decay time constants obtained have physical significance for a particular level. We first derive this function by considering a general case in which a level with some initial population decays into another level which is also decaying with a different time constant. This situation applies for the case of Level 2 (${}^4\text{I}_{11/2}$) and Level 1 (${}^4\text{I}_{13/2}$) with 975 nm pumping. It also applies to these levels under 800 nm pumping since the directly pumped Level 3 (${}^4\text{I}_{9/2}$) decays very rapidly into Level 2 (discussed later in this chapter) and therefore in both cases Level 2 (${}^4\text{I}_{11/2}$) could be considered of having effectively an instantaneous rise, compared to its rate of decay. This situation is shown schematically below:



If now only low Er^{3+} concentrations are considered the effect of the cross-relaxation processes would be negligible and the simplified system of rate-equations for Level 2 (${}^4\text{I}_{11/2}$) and Level 1 (${}^4\text{I}_{13/2}$) in this case would be:

$$\frac{dn_2(t)}{dt} = -(A_2 + \omega_2)n_2(t) \quad \text{and} \quad (4.2.3)$$

$$\frac{dn_1(t)}{dt} = -A_1 n_1(t) + (b_{21} A_2 + \omega_2)n_2(t),$$

where n_i is the population of Level i , normalised with respect to the Er^{3+} concentration.

$A_{1,2}$ and $\omega_{1,2}$ are the radiative and multiphonon decay rates of Level 1 (${}^4I_{13/2}$) or Level 2 (${}^4I_{11/2}$) respectively and b_{21} is the branching ratio for fluorescence from Level 2 (${}^4I_{11/2}$) to Level 1 (${}^4I_{13/2}$).

It should be noted that the measured fluorescence waveforms involve a detector voltage rather than a normalised population. The above equations, however, contain only linear terms and, in the absence of detector non-linearity, the measured voltage will be directly proportional to the population of the levels. Equations 4.2.3 can be solved analytically and the solution for n_1 is readily shown to be:

$$n_1(t) = \frac{(\omega_2 + b_{21} A_2) n_{20} (e^{(-A_1 t)} - e^{-(A_2 + \omega_2) t})}{((A_2 + \omega_2) - A_1)} \quad (4.2.4)$$

Written in terms of decay-times this becomes:

$$n_1(t) = C \frac{\tau_1 \tau_2 (e^{(-t/\tau_1)} - e^{(-t/\tau_2)})}{(\tau_1 - \tau_2)} \quad (4.2.5)$$

In this equation, $\tau_1 = 1/A_1$ and $\tau_2 = 1/(A_2 + \omega_2)$, where $\tau_{1,2}$ are the fluorescence decay times of levels 1 and 2 respectively. $C = n_{20}(\omega_2 + b_{21}A_2)$, where n_{20} is the initial normalised population of Level 2 (${}^4I_{11/2}$). Although equation 4.2.5 has been derived for the specific case of Levels 1 and 2, the only requirement is for constant τ_1 and τ_2 and hence the equation is likely to be applicable to any similar situation where ion-ion cross-relaxation processes are not too significant and the decay times of the levels can be approximated by a single effective constant for each level.

If an equation of the form of 4.2.5 is fitted to the measured fluorescence waveforms for an applicable pair of levels, then the constants obtained can be interpreted in terms of decay time constants associated with the "filling" and "emptying" levels. In fact the above equation can be readily written in the form of equation 4.2.2 as

$$n_1(t) = C \frac{\tau_2 \tau_1}{\tau_1 - \tau_2} (1 - e^{\frac{-t}{\tau_1 - \tau_2}}) e^{(-t/\tau_1)} \quad (4.2.6)$$

Comparing equations 4.2.2 and 4.2.6 one can see that they have identical form and that

$$A = C \frac{\tau_2 \tau_1}{\tau_1 - \tau_2}, \quad \tau_r = \frac{\tau_2 \tau_1}{\tau_1 - \tau_2} \quad \text{and} \quad \tau_d = \tau_1 \quad (4.2.7)$$

An inspection of equations 4.2.7 makes it clear why problems were encountered in fitting equation 4.2.2 to the measured fluorescence waveforms for the low doping level glasses where $\tau_1 \sim \tau_2$. Under these circumstances, both τ_r and A vary rapidly for small changes in $(\tau_1 - \tau_2)$. This is the reason why the uncertainty in the fitted values of τ_r were much higher than those of τ_d (see page 4-11 and Tables 4.2-1 and 4.2-2).

The problems encountered in fitting equation 4.2.2 to the fluorescence waveforms will still apply when trying to fit equation 4.2.5. The problem of large uncertainties only exists when $\tau_1 \sim \tau_2$ and for situations in which this applies, the problems can be alleviated by fixing one of the decay times. Such an action may seem somewhat arbitrary but it can be reasonable in some situations and it does allow one to characterise the trends in the fluorescence waveforms under these circumstances. As can be seen from Table 4.2-1, the measured fluorescence decay time of Level 2 ($^4I_{11/2}$) in several low Er^{3+} concentrations, where the effects of possible cross-relaxation processes are minimised, was consistently around 8 ms. To limit the number of fitting parameters when fitting equation 4.2.5 to the fluorescence waveforms at low doping levels, τ_2 was fixed at 8.0 ms. Under this approximation, good fits of the equation to the measured fluorescence waveform were obtained for the low Er^{3+} concentrations (the high Er^{3+} concentrations will be discussed later in this chapter) and the decay time constants from these fits are represented in red in Table 4.2-1 and Table 4.2-2.

Before going on to discuss the meaning of the trends characterised by the time constants of Figures 4.2-1 and 4.2-2, it is worth considering one more point about the fitted time constants which will be useful in later discussions of the data. This concerns a somewhat surprising effect on the measured waveforms of a situation in which τ_2 is larger than τ_1 . An appreciation of this situation will assist later (Chapter 5) in an understanding of the fluorescence behaviour of level 4 ($^4F_{9/2}$). Equation 4.2.5 is symmetrical with respect to interchange of τ_1 and τ_2 . This means that the only effect of a change in sign of $(\tau_1 - \tau_2)$ is to swap the positions of τ_1 and τ_2 in the equation. We have already seen that for $\tau_1 > \tau_2$, the rise of the n_1 waveform is determined by τ_2 and the decay by τ_1 . When $\tau_1 < \tau_2$, this situation is reversed and we get the surprising situation that the rise of the n_1 waveform is determined by the decay time constant of n_1 and the decay of the waveform is determined by the decay time constant of Level 2 which is responsible for the "filling" of Level 1.

4.2.3 Discussion

Now that the main issues associated with the fitting of the fluorescence waveforms and interpretation of fitted time constants have been discussed, we proceed to consider the interpretation of the data summarised in Tables 4.2-1 and 4.2-2.

- **General observations**

The first observation concerns the data for the fluorescence at approximately 800 nm from Level 3 ($^4I_{9/2}$). In our fluorescence waveform measurements the fluorescence at about 800 nm from the $^4I_{9/2}$ level was weak and could be detected only with direct pumping into this level. To avoid interference with the scattered pump radiation, the fluorescence was measured at a slightly longer wavelength (820 nm). In addition to the $^4I_{9/2}$ to $^4I_{15/2}$ transition which gives fluorescence at wavelengths in the 800 nm region, there are 4 other higher levels which may fluoresce at similar wavelengths via transitions to levels above the ground state (see Chapter 5, Figure 5.1-2). To avoid any problems in interpreting the current fluorescence waveforms, the measurements were made using very weak pumping so that excited state populations were small. These measured fluorescence waveforms exhibited single exponential decays with decay-times varying between 9 μ s and 6 μ s over the concentration range (a PMT with a rise time of less than 0.5 μ s was used for this measurement). As multiphonon processes dominate the $^4I_{9/2}$ decay (Shinn *et al.*, 1983; Zou *et al.*, 1993) it would be expected that the rise times of the $^4I_{11/2}$ level at the different Er^{3+} concentrations would correspond to these decay times. The data for the rise of the population of Level 2 ($^4I_{9/2}$) in Table 4.2-1 and Table 4.2-2 are consistent with this expectation.

Another feature of the data in the tables is the substantial variations in rise and decay times as well as a trend to non-exponential behaviour of Level 1 ($^4I_{13/2}$) and Level 2 ($^4I_{11/2}$) in higher Er^{3+} concentration, especially under direct pumping. These variations are a good indication of the existence of ion-ion interaction processes.

- **Level 2 (${}^4I_{11/2}$)**

The behaviour of Level 2 (${}^4I_{11/2}$) under direct (975 nm) or 800 nm pumping reveals the features one might expect after the discussions of the previous pages. The rise is virtually instantaneous under direct pumping and very fast (of order of 8 μ s) in the case of 800 nm pumping. The decay-rates in both cases were as expected in low Er^{3+} concentration (see expected values of A_2 and ω_2 in Table 4.3-4). In high Er^{3+} concentration non-exponential behaviour was observed, most probably due to presence of cross-relaxation processes such as W(22,50) (see Figure 4.1-1). The effect of W(22,50) would be expected to be greatest during the initial part of the decay when the number of excited ions is greatest. This is consistent with the observed decay constants for this level in higher doping levels.

The temporal behaviour of the population of the ${}^4I_{11/2}$ level under 1.5 μ m pumping was also as expected. The long rise time constant of the 980 nm fluorescence in low Er^{3+} concentrations, and its decrease at higher Er^{3+} doping concentrations, was a good indication that the population of Level 2 (${}^4I_{11/2}$) in this case originates from Level 1 (${}^4I_{13/2}$), possibly via the cross-relaxation process W(11,30). This cross-relaxation process shifts some of the initial population from Level 1 (${}^4I_{13/2}$) to Level 3 (${}^4I_{9/2}$), from which the ions rapidly decay into Level 2 (${}^4I_{11/2}$) via a multiphonon process. As is the case with time constants at high doping concentrations under 800 nm pumping, the time constants describing the decay of Level 2 (${}^4I_{11/2}$) at these higher doping levels under 975 nm pumping were somewhat longer than those expected in the absence of cross relaxation processes (see typical parameters in Table 4.3-3). However, although cross relaxation processes are likely to be responsible for the increased time constants, it is difficult to make any quantitative conclusions from this difference. As was pointed out in an earlier discussion, the time constants listed in Tables 4.2-1 and 4.2-2 are only fits of exponential functions to the available fluorescence data. In general they have no direct connection with the actual physical processes (radiative or non-radiative) behind this data and, hence, are of limited value in obtaining quantitative information on the processes occurring in the glasses. A quantitative discussion requires a model to describe the redistribution of the population which should take into

account the presence of variety of cross-relaxation processes. This leads to a system of rate-equations that are too complex to solve analytically.

- **Level 1 (${}^4I_{13/2}$)**

Level 1 (${}^4I_{13/2}$) also exhibited some interesting features. One of these was the observation of a fast component in the rise of its population with 800 nm pumping. Although the measurement of this fast component (“Fast” in Table 4.2-1 and Table 4.2-2) was detector limited ($\sim 10 \mu\text{s}$), the most noticeable feature was its contribution to the overall rise of the level population. Whilst this fast contribution was virtually absent at low Er^{3+} concentration, it completely dominated the rise-waveform at the highest Er^{3+} concentration used.

The temporal behaviour of the population of Level 1 (${}^4I_{13/2}$) under direct pumping was as expected. In low Er^{3+} concentration the fluorescence could be described with exponential decays with rates close to those expected in the absence of cross relaxation processes (see Table 4.3-3). The non-exponential behaviour at high Er^{3+} concentration indicated the presence of cross-relaxation process originating from this level, such as W(11,30).

The temporal behavior of the population of Level 1 (${}^4I_{13/2}$) with 975 nm pumping in low Er^{3+} concentrations has been discussed previously. The long fitted rise-times and large uncertainties (blue values) are a consequence of the fact that $\tau_2 \approx \tau_1$. The decay time constants (red or blue values) are reasonably matched to those which would be expected in the absence of cross relaxation processes.

When the decays of Level 1 (${}^4I_{13/2}$) are considered under either 800 nm or 975 nm pumping in higher Er^{3+} concentrations ($\geq 4 \text{ mol}\%$), the non-exponential decay of Level 2 (${}^4I_{11/2}$) makes equation (4.2.5) not applicable. This is why no red values for fits of this equation to the measured fluorescence waveforms are included in Tables 4.2-1 and 4.2-2 for Er^{3+} concentrations higher than 4 mol%. The exponential fits have still been presented, despite the fact that they do not represent physical processes. The fact that the fitted decay time constants for Level 1 (${}^4I_{13/2}$) increased slightly with Er^{3+} concentrations is consistent with the presence of cross-relaxation processes. The increase in decay time constant of Level 1 at higher concentrations is consistent with the

action of a process such as W(11,30) which can initiate a re-cycling of the population from Level 1 to Level 3 and back again to Level 1 via Level 2. This slows down the eventual decay of Level 1 to the ground state. Finding a proper fitting function that includes such processes is difficult because the differential equations which describe the level populations are non-linear and do not have an analytical solution. The general situation, in which non-linear processes are significant, will be treated numerically and discussed later in this chapter as well as in Chapter 5.

4.3 Rate equation modelling including non-linear ion-ion exchange terms

4.3.1 Direct pumping

As can be seen from Figure 4.1-1 there is a variety of competing ion-ion interaction processes which could possibly affect the populations of the three lowest excited energy levels. In order to try to simplify matters, the modelling below initially concentrates on examining the behaviour of the population of Level 1 (${}^4I_{13/2}$) and Level 2 (${}^4I_{11/2}$) under direct pumping where the processes W(22,50) and W(11,30) are expected to play a dominant role. By using direct pumping the effects of processes that involve significant populations of other levels are minimised. Both W(22,50) and W(11,30) processes are well known (see Chapter 2, Table 2.3-1); however, to our knowledge, no estimates of the cross-relaxation coefficients in fluoride glasses have been previously published.

The behaviour of the population of each of the ${}^4I_{13/2}$ and ${}^4I_{11/2}$ levels under direct pump was first modelled by an equation, which assumed the dominance of a single two-ion cross-relaxation process:

$$\frac{dn(t)}{dt} = -\frac{n(t)}{\tau} - 2Kcn^2(t) \quad (4.3.1)$$

where τ represents the reciprocal of the combined radiative and multiphonon decay rates (it is the measured decay time in low Er^{3+} concentration, where the cross-

relaxation processes have negligible effect on the population dynamics) and K is the cross-relaxation coefficient corresponding to either $W(22,50)$ or $W(11,30)$. The level populations in the rate-equations are again normalised with respect to the total Er^{3+} concentration: $n_i = N_i / C$, where C is the Er^{3+} concentration. The initial normalised population n_0 of each pumped level was determined from:

$$n_0 = \sigma E / h\nu S, \quad (4.3.2)$$

where σ is the appropriate absorption cross-section for the level, E is the energy of the pump pulse, $h\nu$ is the pump photon energy and S is the pumped area of the sample. In this calculation of the initial populations of the directly pumped levels, the possible presence of excited state absorption (ESA) is ignored. This is justified since the population of the levels from which the ESA originates is very much smaller than that of the ground state. Thus the populations produced by ESA is very much smaller than that of the levels which are directly pumped from the ground state.

The calculated initial populations for the various pump wavelengths were:

$$\begin{aligned} n_1(0) &= (2 \pm 1) \times 10^{-3} \quad (\text{for } \sigma_{1.5\mu\text{m}} = 4.7 \times 10^{(-21)} \text{ cm}^2, E_{1.5\mu\text{m}} = 6 \text{ mJ}, S = 10 \pm 5 \text{ mm}^2), \\ n_2(0) &= (1 \pm 0.5) \times 10^{-3} \quad (\text{for } \sigma_{980\text{nm}} = 2.0 \times 10^{(-21)} \text{ cm}^2, E_{980\text{nm}} = 14 \text{ mJ}, S = 13 \pm 7 \text{ mm}^2), \\ n_3(0) &= (5 \pm 2.5) \times 10^{-4} \quad (\text{for } \sigma_{800\text{nm}} = 6.3 \times 10^{(-22)} \text{ cm}^2, E_{800\text{nm}} = 5 \text{ mJ}, S = 2.5 \pm 1 \text{ mm}^2). \end{aligned}$$

The absorption cross-sections were determined from appropriate absorption measurements (see Chapter 3, Table 3.3-3). The main source of uncertainties in the calculation of the above initial population was the uncertainty in the area of the pumped spot S , caused by the non-uniform spatial distribution of the pump energy within the spot. The estimate of the area of the pumped spot was further complicated by the non-linear nature of the visualisation of the spot via polaroid film burns or IR cards.

From the values of the initial populations of the various levels under direct pumping it becomes obvious that in all the cases the ground state population was not significantly perturbed by the pump energy density used. At the same time, however, as it will be seen later in the chapter, these initial populations are quite sufficient to give rise to significant non-linear effects due to cross-relaxation processes.

Having calculated the initial population, the decays of both Level 1 (${}^4I_{13/2}$) and Level 2 (${}^4I_{11/2}$) could be modelled with the explicit solution of (4.3.1). As was pointed out earlier, the actual experimental curves to be fitted did not represent normalised

population, but a voltage proportional to fluorescence intensity (which is proportional to the instantaneous population of the level). The ratio between the measured voltage and the normalised population could be estimated from the initial point and thus the experimentally measured curves were scaled appropriately so that they represent normalised population.

The solution of equation (4.3.1) is:

$$n(t) = - \frac{1}{2KC\tau - \frac{(1 + 2n_o \tau KC)}{n_o} \exp(t/\tau)} \quad (4.3.3)$$

or after some simplification:

$$n(t) = - \frac{1}{K'\tau - (\frac{1}{n_o} + K'\tau) \exp(t/\tau)} \quad (4.3.4)$$

where $K'=(2KC)$. This function was fitted to the appropriately-scaled experimental fluorescence waveforms from the $^4I_{13/2}$ and $^4I_{11/2}$ levels and estimates of the appropriate cross-relaxation parameters ($K = W(11,30)$ or $K = W(22,50)$) were obtained. The values obtained in this way, for a range of doping concentrations, are summarised in Table 4.3-1 below. We have at this stage assigned the K values to W(11,30) and W(22,50) on the presumption that these processes are dominant. This assignment will be further discussed later.

Er (mol%)	0.8	4	10	14	18
W(11,30)($\times 10^{(-17)} \text{cm}^3 \text{s}^{-1}$)		1.0 \pm 0.5	2.3 \pm 1.2	4.0 \pm 2	4.3 \pm 2.2
W(22,50) ($\times 10^{(-17)} \text{cm}^3 \text{s}^{-1}$)	1.7 \pm 0.9		3.0 \pm 1.5		7.1 \pm 3.6

Table 4.3-1 Estimate of cross-relaxation coefficients in Er/ZB(L)AN glasses obtained from direct pumping measurements under the assumption that a single two-ion cross-relaxation process dominates all others in its contribution to the non-linear terms. The uncertainties arise mainly from the estimate of the initial population produced by the non-uniform pump beam.

Although the values in this table are subject to uncertainties mainly due to the uncertainties of about 50% in the estimate of the initial populations used in the fitting,

there is an obvious trend to increased values at higher Er^{3+} concentrations (Figure 4.3.1).

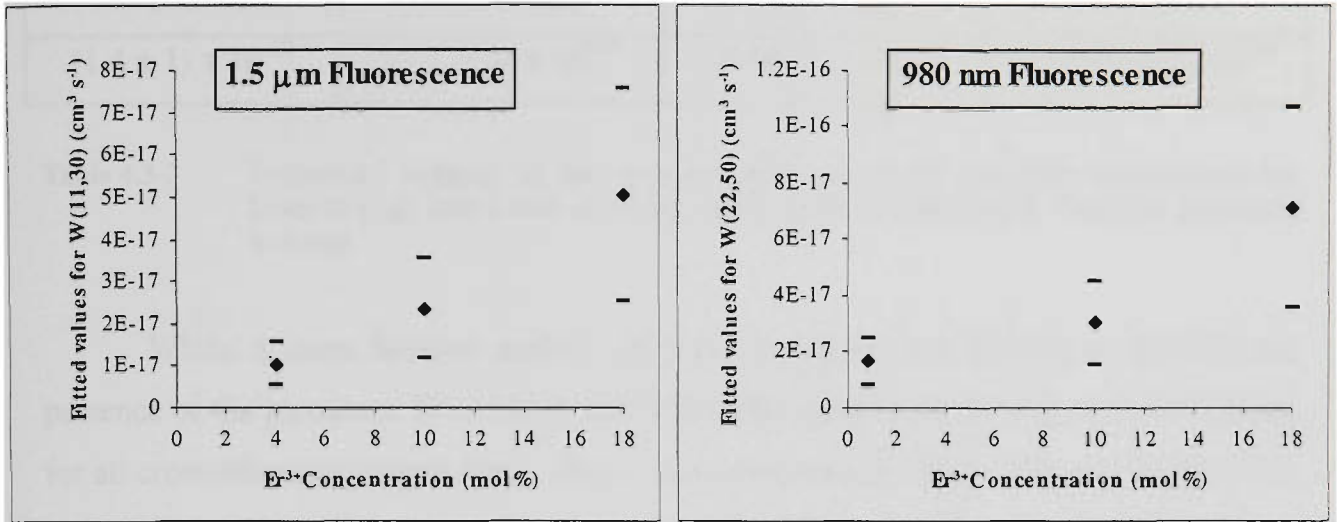


Figure 4.3-1 Fitted values and their uncertainties for the cross-relaxation parameters $W(11,30)$ and $W(22,50)$ for different doping concentrations of Er^{3+}

The most probable reason for this trend was the presence of additional cross-relaxation processes, such as $T(110,003)$ and $T(220,005)$ (Figure 4.1-1). Although three ions are needed for these interactions, their probability could be appreciable since only the ground level and relatively highly populated excited levels are involved in the case of direct pumping. The populations of the levels, in the case where these particular three ion processes are included, can be described by the equation:

$$\frac{dn(t)}{dt} = -\frac{n(t)}{\tau} - 2WCn^2(t) - 2TC^2n^2(t)n_0(t) \quad (4.3.5)$$

For the present case where the ground state is not significantly perturbed ($n_0 \sim 1$), the solution is similar to Equation (4.3.4), however K in this case can be expressed as $K=W+CT$. Here W and T are cross-relaxation coefficients, corresponding to the two and three-ion processes described above.

A plot of the K values from Table 4.3-1 against the Er^{3+} concentration (similar to Figure 4.3-1) was fitted with a straight line and so values for $W(11,30)$ and $T(110,003)$ (for $1.5 \mu\text{m}$ pumping) and for $W(22,50)$ and $T(220,005)$ (for 975 nm pumping) were obtained. The limited data set, however, resulted in fairly large uncertainties in the fitted parameters, as shown on Table 4.3-2:

W(22,50)	T(220,005)	W(11,30)	T(110,003)
$(1.4 \pm 1) \times 10^{-17}$	$(1.2 \pm 1) \times 10^{-38}$	$(-0.06 \pm 1) \times 10^{-17}$	$(1.4 \pm 0.8) \times 10^{-38}$

Table 4.3-2 Preliminary estimate of the cross-relaxation parameters and their uncertainties for Level 1 (${}^4I_{13/2}$) and Level 2 (${}^4I_{11/2}$) under direct pumping with three-ion processes included

Whilst a more detailed analysis of these processes was needed to confirm the presence of the processes T(110,003) and T(220,005) and to obtain more reliable values for all cross-relaxation parameters. The values presented in Table 4.3-1 and Table 4.3-2 were useful as a starting point for the modelling of ${}^4I_{13/2}$ and ${}^4I_{11/2}$ levels with 800 nm pumping.

4.3.2 800 nm pumping

- **Rate equation modelling**

For the 800 nm pump (the exact wavelength was 801 nm), the decays of the ${}^4I_{13/2}$ and ${}^4I_{11/2}$ levels are less concentration dependent than with a direct pump (see Table 4.2-1 and Table 4.2-2). This could be due to the reduced importance of the three-ion processes T(110,003) and T(220,005) resulting from the relatively smaller initial populations of these levels (see $n_1(0)$, $n_2(0)$, $n_3(0)$ above). However, since the aim was the design of a general model it was decided that all the cross-relaxation processes in Figure 4.1-1 should be included. With all of the four lowest energy levels populated, the system of four coupled non-linear differential rate equations, describing the behaviour of the system with 800 nm pump are as follows:

$$\frac{dn_1(t)}{dt} = -(A_1 + \omega_1)n_1(t) + (b_{21}A_2 + \omega_2)n_2(t) + b_{31}A_3n_3(t) + 2W(30,11)Cn_0(t)n_3(t) + 2T(300,011)C^2n_3(t)n_0^2(t) - 2W(11,30)Cn_1^2(t) - 2T(110,003)C^2n_1^2(t)n_0(t)$$

$$\frac{dn_2(t)}{dt} = -(A_2 + \omega_2) n_2(t) + (b_{32} A_3 + \omega_3) n_3(t) - 2W(22,50)C n_2^2(t) - 2T(220,005)C^2 n_2^2(t) n_0(t)$$

$$\frac{dn_3(t)}{dt} = -(A_3 + \omega_3) n_3(t) + W(11,30) C n_1^2(t) - W(30,11) C n_3(t) n_0(t) - T(300,011) C^2 n_3(t) n_0^2(t) + T(110,003) C^2 n_1^2(t) n_0(t)$$

$$n_0(t) + n_1(t) + n_2(t) + n_3(t) = 1 \quad (4.3.6)$$

In the last equation, the population excited to levels higher than Level 3 (e.g. by T(220,005)) has been ignored. In the above equations $n_1(t)$, $n_2(t)$, $n_3(t)$ are the normalised populations of the $^4I_{13/2}$, $^4I_{11/2}$ and $^4I_{9/2}$ levels; A_i and ω_i are the radiative and multiphonon decay rates of the i -th level; b_{ij} is the branching ratio from i -th to j -th level; C is the Er^{3+} concentration of the sample and $W(30,11)$, $W(11,30)$, $W(22,50)$, $T(300,011)$, $T(110,003)$ and $T(220,005)$ are the cross-relaxation rate constants for the ion-ion interaction processes shown in Figure 4.1-1. The values of the radiative and multiphonon parameters used are given in Table 4.3-3 below.

Parameter:	Value:	Source:
A_1	100 s^{-1}	Our work [c.f. Shinn <i>et al.</i> , (1983); Zou and Izumitani (1993); Wetenkamp <i>et al.</i> , 1992]
A_2	118 s^{-1}	Our work [c.f. Zou and Izumitani (1993); Shinn <i>et al.</i> , (1983)]
A_3	140 s^{-1}	Our work [c.f. Zou and Izumitani (1993)]
ω_1	0 s^{-1}	Our work [c.f. Shinn <i>et al.</i> , (1983); Zou and Izumitani (1993)]
ω_2	9 s^{-1}	Our work [c.f. Shinn <i>et al.</i> , (1983); Zou and Izumitani (1993); Wetenkamp <i>et al.</i> , (1992)]
ω_3	125000 s^{-1}	Our work [c.f. Zou and Izumitani., (1993)]
b_{20}	0.88	Zou and Izumitani (1993); Wetenkamp <i>et al.</i> , (1992)
b_{21}	0.12	Zou and Izumitani (1993); Wetenkamp <i>et al.</i> , (1992)
b_{30}	0.77	Zou and Izumitani (1993); Wetenkamp <i>et al.</i> , (1992)
b_{31}	0.22	Zou and Izumitani (1993); Wetenkamp <i>et al.</i> , (1992)
b_{32}	0.01	Zou and Izumitani (1993); Wetenkamp <i>et al.</i> , (1992)

Table 4.3-3 Values of the parameters used in the rate-equation models

The above values have been obtained from a combination of our measurements and reported radiative rates of the levels in very similar glasses (see Shinn *et al.*, 1983; Wetenkamp *et al.*, 1992; Zou *et al.*, 1993) in the following manner:

- Level 1 (${}^4I_{13/2}$):

The consistent values of about 100 s^{-1} , measured for the decay rate in low Er^{3+} concentrations (0.4 - 1.6 mol%) under direct pumping with $1.5\ \mu\text{m}$ excitation (Table 4.2-2), were an indication that ion-ion exchange processes were not significant in those Er^{3+} concentrations. Therefore (Equation 2.2-3) this decay rate represents only the sum of the radiative and multiphonon-assisted decay rates. All of the reported radiative rates for this level were equal or higher than the measured one (109 s^{-1} -Shinn *et al.*, 1983; 100 s^{-1} -Wetenkamp *et al.*, 1992; 142 s^{-1} -Zou *et al.*, 1993). For this reason it was assumed that the measured rate is actually the radiative one and the multiphonon-assisted decay rate for Level 1 (${}^4I_{13/2}$) is zero.

- Level 2 (${}^4I_{11/2}$):

An average decay rate of 128 s^{-1} was measured in several measurements in low Er^{3+} concentration (0.8 mol%, Table 4.2-1)). The reported rates (Shinn *et al.*, 1983; Wetenkamp *et al.*, 1992; Zou *et al.*, 1993) were similar with an average of 118.5 s^{-1} . Since no cross-relaxation processes were evident in this low Er^{3+} concentration, a multiphonon-assisted decay rate of 9 s^{-1} was calculated by subtracting the reported radiative rate from the measured decay rate. Reported branching ratios were all very similar (Shinn *et al.*, 1983; Wetenkamp *et al.*, 1992; Zou *et al.*, 1993) and typical values of $b_{20}=0.88$ and $b_{21}=0.12$, were assumed.

- Level 3 (${}^4I_{9/2}$):

The average radiative decay reported by Shinn *et al.* (1983) and Zou *et al.* (1993) was 140 s^{-1} . Since, however, our measured decay rate of the population of Level 3 in low Er^{3+} concentration (0.4 mol%) was consistently around 125000 s^{-1} (Table 4.2-1) it is clear that the observed decay of Level 3 was governed almost entirely by the multiphonon-assisted decay to Level 2 (${}^4I_{11/2}$). This was consistent with the fact that fluorescence from Level 3 could only be detected under direct pumping. Branching ratios typical of those quoted by Wetenkamp *et al.* (1992) and Zou *et al.* (1993) were assumed.

The system of differential equations (4.3.7) was solved using fourth-fifth order Runge-Kutta routines (Maple software). The solutions obtained provided waveforms which could be compared to the measured fluorescence waveforms recorded using MOPO excitation at 800 nm. This comparison was done after first normalising the two waveforms to the same peak amplitude. The methodology adopted was to vary the rate constants of the various cross relaxation processes and compare the resulting numerical solution waveforms to the measured ones. In this way it was possible to determine which processes needed to be included for acceptable fits and also the optimum values of these necessary constants. It was also possible to vary the constants around their optimum values and obtain estimates of their uncertainty by investigating the sensitivity of the fit to changes in the rate constants. This latter process gives only approximate estimates of the uncertainties as the parameters can only be varied one at a time. A full study with simultaneous random variations was impractical because of the numerical calculations involved. Studies of uncertainty are mostly relevant to Chapter 5 where more complete models are involved. We now proceed to discuss how the various processes affect the waveforms and why it is necessary to include certain processes if one is to obtain reasonable fits to the measured data.

The most challenging task for the modelling was to explain the fast rise of the population of Level 1 ($^4I_{13/2}$). This fast rise, dominant at high Er^{3+} concentrations (see Table 4.2-1 and Table 4.2-2), would suggest a cross-relaxation process originating from the $^4I_{9/2}$ level, as this is the only level with both a fast time dependence and a substantial population during the initial 10 - 20 microseconds. Two cross-relaxation processes were prime candidates for causing this rise - $W(30,11)$ and $T(300,011)$. These processes involve the same two levels, however $T(300,011)$ is a three-ion process and therefore its rate should have a stronger dependence on the Er^{3+} concentration. Being a three-ion process, $T(300,011)$ would be expected to have somewhat smaller probability than the two-ion process $W(30,11)$. However, considering the high Er^{3+} concentrations used and also the fact that the process originates from the highly populated (compared to all other excited levels) Level 3, the effect of $T(300,011)$ on the system could still be appreciable. Here it should be mentioned that the effect of another three-ion process, $T(330,113)$, was also considered. Both processes were almost identical with respect to their net effect on the populations of the levels being considered. They both have

similar concentration dependence and also the effective result from both of them was that two ions, one from both the ground level and one from Level 3, were delivered to Level 1. However, T(330,113) required two ions from Level 3 and only one from the ground level, while, T(300,011) involved two ions from the heavily populated ground level and only one from the much less populated Level 3. Thus, it was likely that T(330,113) would have lower probability than T(300,011) and hence the former has been excluded from any further consideration.

Despite these considerations, only the previously reported (see Chapter 2, Table 2.3-1) two-ion process W(30,11) (see Figure 4.1-1) was initially included in the model as a possible source of the fast rise of the population of Level 1 ($^4I_{13/2}$). The inclusion of this two-ion process W(30,11) alone (without the three-ion process T(300,011)) gave reasonable fits to the decay of the $^4I_{13/2}$ fluorescence for the 1.6 mol% and 18 mol% Er^{3+} concentrations, but not for the intermediate range of Er^{3+} concentrations (10 mol%). Another problem with the inclusion of only W(30,11) was that reasonable fits at 18 mol% also required a value for the rate constant of the reverse process W(11,30) which was ten times greater than the value determined from direct pumping measurements at 1.5 μm (see Table 4.3-2). The reason for the need to include this large value was the following: the absence of a fast component of the rise of Level 1 ($^4I_{13/2}$) in low Er^{3+} concentration (see Table 4.2-1 and Table 4.2-2) required a relatively low value of W(30,11). This value, however, appeared to be too small in high Er^{3+} concentrations where it resulted in a rise of Level 1 which was substantially slower than the experimentally observed one. A sufficiently large value of W(11,30) could "compensate" for that. Such a large value of W(11,30) results in a decay rate of the population of Level 1 which completely dominates the population waveform of the level after the initial 10-20 microseconds. The overall effect is that a waveform similar to the observed one is produced. Thus a large value for W(11,30) could be used together with the value for W(30,11), which satisfies the low Er^{3+} concentration, to produce an acceptable waveform also in the high Er^{3+} concentrations. This large value, however, in addition to being inconsistent with the direct pumping measurements, also resulted in a high population of the $^4I_{11/2}$ level and too fast a decay rate of that level via the process W(22,50). Higher energy levels in the system were also affected. In reality, with the inclusion of the two-ion process W(30,11) and the exclusion of the three-ion

process T(300,011) we were unable to obtain a set of parameters which can give a self-consistent fit to the fluorescence data of all the levels.

The inclusion of T(300,011) and the exclusion of W(30,11), on the other hand, gave both good agreement to the waveforms at both high and low Er^{3+} concentrations when used in conjunction with a value of W(11,30) which was consistent with that determined from direct pumping. There were no problems with the ${}^4\text{I}_{11/2}$ and higher levels but the agreement with the waveforms for the ${}^4\text{I}_{13/2}$ level at intermediate Er^{3+} concentrations was still poor. We return to a discussion of this latter point later but it was clear from the modeling of the fluorescence waveforms that no agreement was possible without the inclusion of the T(300,011) process. The necessity of including the three-ion process is a significant result of the modelling. The fact that we have fitted the data without inclusion of the two-ion process W(30,11) does not necessarily mean that it is not present. However it does indicate that the three-ion process T(300,011) is dominant over the range of Er^{3+} concentrations used.

Aside from the comments mentioned above, no particular problems were encountered with the modelling of the population of Level 2. Reasonable fits to the measured waveforms could be obtained with the inclusion of W(22,50) (using a value consistent with that obtained from direct pumping) or with the inclusion of both W(22,50) and T(220,005). With the data from just these lowest excited levels, it is not possible to distinguish between these cases. The only indication that there may be some influence of a process like T(220,005) is the increase in the constant (assumed to be W(22,50)) obtained with fitting the direct pumping measurements at 980 nm (see Table 4.3-1).

Solving numerically the equations (4.3.6) for different values of the cross-relaxation coefficients allowed values to be obtained that produced the best fits to the experimental waveforms (see Table 4.3-4). Two sets of parameters were found which produced satisfactory fits to the experimental fluorescence waveforms from Level 1 (${}^4\text{I}_{13/2}$) and Level 2 (${}^4\text{I}_{11/2}$) at both high and low concentrations. The first (Model 1) corresponds to the presumption that under 800 nm pumping the contribution of the three-ion processes T(110,003) and T(220,005) is negligible. The second (Model 2), on the other hand, includes these two processes and thus represents an attempt to develop a

more comprehensive model of our three-level system. Following the above discussions, both sets of parameters included T(300,011) and excluded W(30,11).

Parameter:	W(22,50) (cm ³ /s)	W(11,30) (cm ³ /s)	T(300,011) (cm ⁶ /s)	T(220,005) (cm ⁶ /s)	T(110,003) (cm ⁶ /s)
Model 1	5x10 ⁽⁻¹⁷⁾	4x10 ⁽⁻¹⁷⁾	0.4x10 ⁽⁻³⁸⁾	0	0
Model 2	1x10 ⁽⁻¹⁷⁾	1x10 ⁽⁻¹⁷⁾	1x10 ⁽⁻³⁸⁾	2.5x10 ⁽⁻³⁸⁾	0.6x10 ⁽⁻³⁸⁾

Table 4.3-4 Cross-relaxation coefficients for Er/ZB(L)AN glasses, determined from numerical modelling of fluorescence waveforms for Levels 1 and 2 only. W(30,11) excluded from the model. The accuracy of parameters is to within a factor of about two (see text below)

- **Agreement between the model and the experimental data**

Some of the measured waveforms (corresponding to Set 2 - the data in Table 4.2-2) together with the model predictions for 1.6 mol% and 18 mol% are presented in Figure 4.3-2. Only the predictions of Model 2 have been plotted, since the predictions of Model 1 are very close and, within the resolution possible with visual inspection of the fits, indistinguishable from the ones of Model 2. This figure shows that both models predicted well the behaviour of Level 2 (⁴I_{11/2}) and Level 1 (⁴I_{13/2}) in both Er³⁺ concentrations. The predicted decays of Level 2 (⁴I_{11/2}) for both Er³⁺ concentrations as well as of Level 1 (⁴I_{13/2}) for 1.6 mol% were in very good agreement with the experimental waveforms. The predicted rate of the decay of Level 1 (⁴I_{13/2}) for 18 mol% was slightly lower than the experimental one. The rising portions of the waveforms for both levels and both concentrations were also modelled reasonably well. This is quite obvious for the experimental rise of Level 2 (⁴I_{11/2}) on Figure 4.3-2, which despite of being slightly noisy, has been fitted quite satisfactorily. The predicted rise of Level 1 (⁴I_{13/2}) was faster than the experimental one. It should, however, be noted that the experimental rise has been measured with an InGaAs detector system and is affected by the detector response time of about 10 μs. Thus the actual rate of rise may well be faster than shown by the experimental data in the figure and could well agree with the prediction of the model.

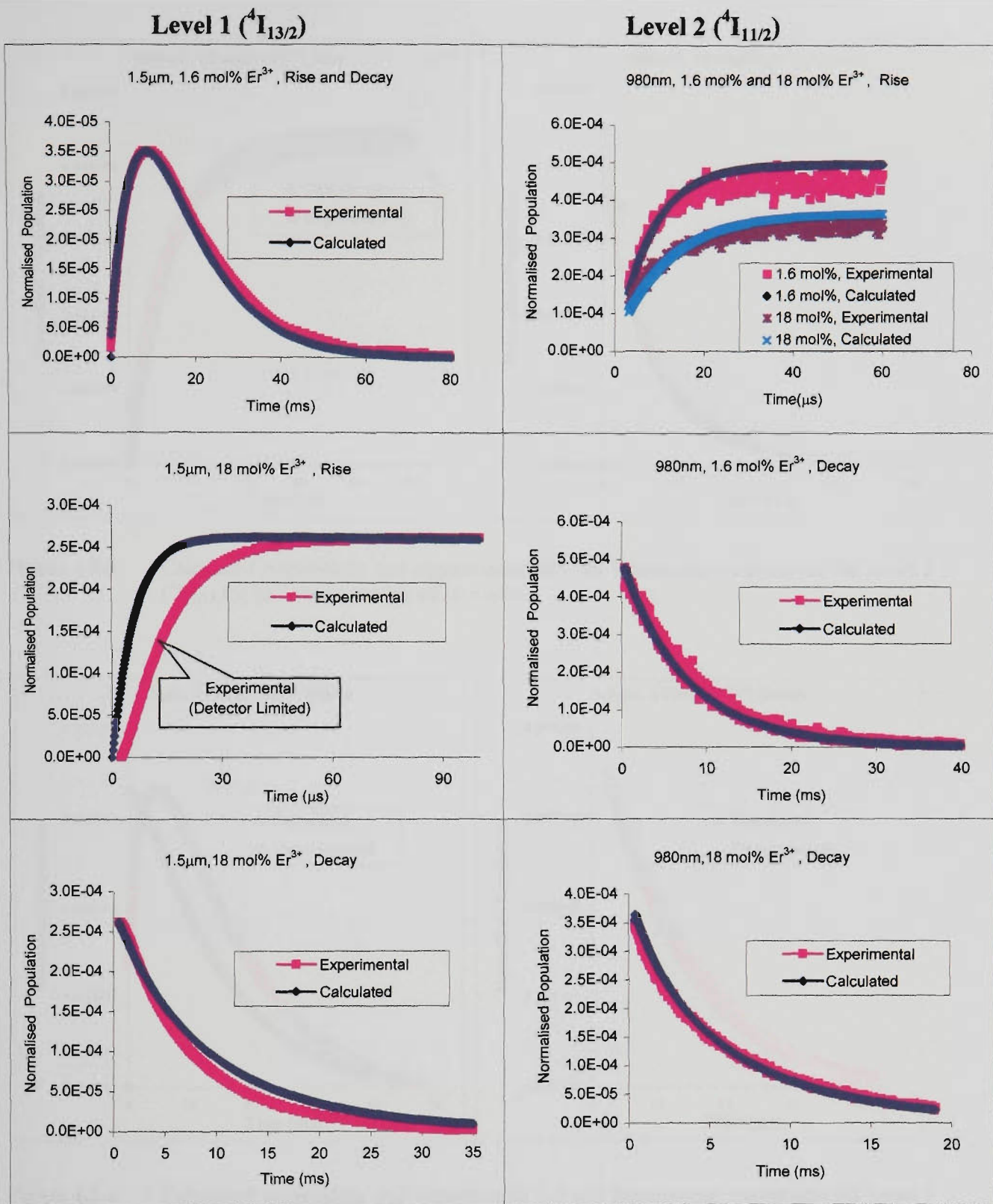


Figure 4.3-1 Calculated populations (Model 2) and experimental fluorescence waveforms for Level 1 (${}^4I_{13/2}$, 1.5 μm fluorescence) and Level 2 (${}^4I_{11/2}$, 980 nm fluorescence) levels for Er^{3+} concentrations of 1.6 mol% and 18 mol%. Predictions of Model 1 identical with Model 2 (see text)

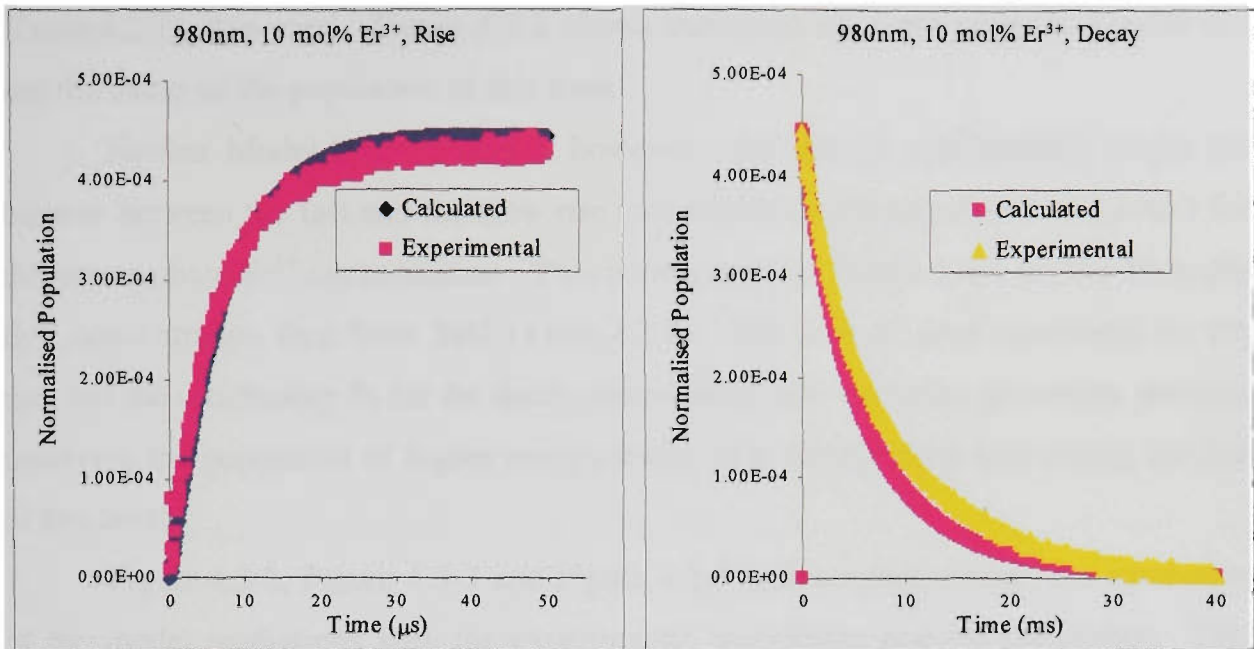


Figure 4.3-3 Calculated populations and experimental 980 nm fluorescence waveforms for Level 2 ($^4I_{11/2}$) for Er^{3+} concentration of 10 mol%

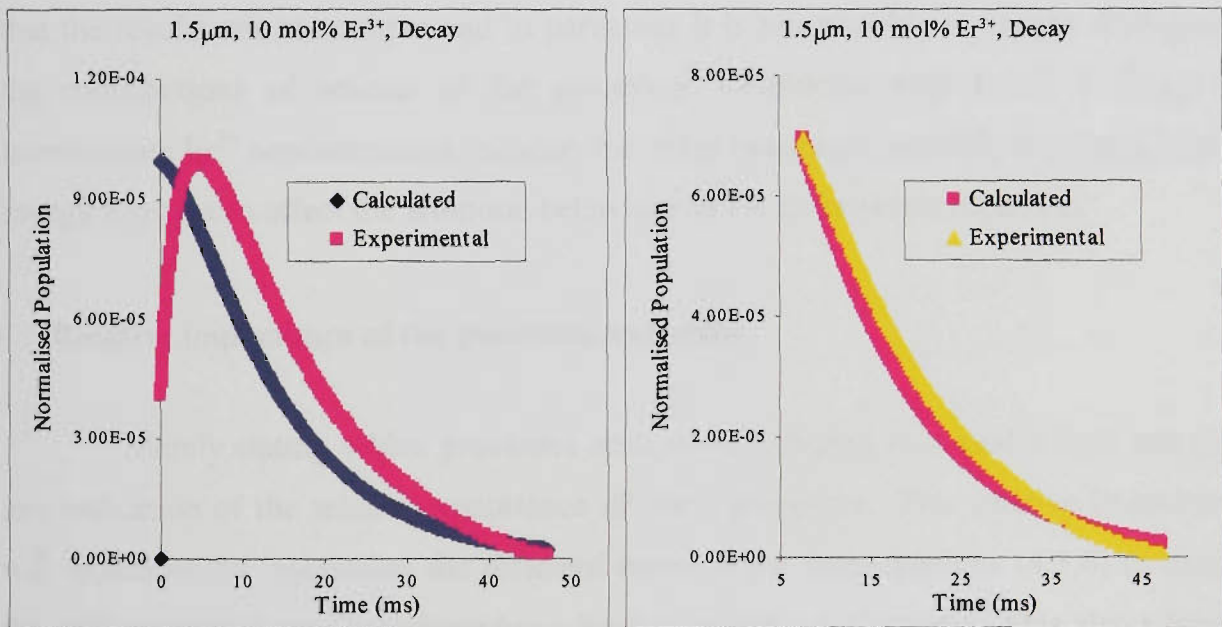


Figure 4.3-4 Calculated populations and experimental 1.5 μm fluorescence waveforms for Level 1 ($^4I_{13/2}$) for Er^{3+} concentration of 10 mol%

The predicted and the experimental waveforms were compared also for the intermediate Er^{3+} concentration of 10 mol%. In order to check the applicability of the models for predicting the temporal behaviour of the population of Level 2 ($^4I_{11/2}$) for this intermediate Er^{3+} concentration, the data from the Set 1 measurements

(Table 4.2-1), was used. Figure 4.3-3 shows that good fits were obtained for the rise and the decay of the population of this level.

Neither Model 1 nor Model 2, however, was able to satisfactorily model the balance between the fast and the slow rise components in the population of Level 1 for the intermediate Er^{3+} concentration. This is illustrated in Figure 4.3-4 for the 10 mol% Er^{3+} concentration data from Set2 (Table 4.2-2). The lack of good agreement for the rise, but the satisfactory fit for the decay was an indication that other processes, possibly involving the population of higher energy levels, play an important role during the rise of this level.

Figure 4.3-2, Figure 4.3-3 and Figure 4.3-4 indicate that overall, the agreement of the model predictions with the experimental waveforms is quite reasonable. This shows that despite the complexity of the modelled system and the limitations of including only three-levels in the models, they predicted the essential features of the dynamics of the level populations. The biggest problem with this modelling to date is that the results are not unique and in particular it is not possible to clearly distinguish the contributions of several of the processes. Problems with Level 1 ($^4\text{I}_{13/2}$) at intermediate Er^{3+} concentrations indicate that other processes, possibly involving higher energy levels, also affect the temporal behaviour of the three levels modelled.

- **Relative importance of the processes modelled**

Merely stating which processes need to be included in a model does not give any indication of the relative importance of these processes. This relative importance was examined by integrating the different terms in the rate-equations (4.3.6) to obtain the total number of ions contributed to a level by a particular process. This also allowed the two models from Table 4.3-4 to be further compared. The integrated normalised populations of Level 1 ($^4\text{I}_{13/2}$) and Level 2 ($^4\text{I}_{11/2}$), contributed by each term of equations (4.3.6), were plotted. These plots are shown for Er^{3+} concentrations of 1.6 mol% and 18 mol% in Figure 4.3-5 and Figure 4.3-6. The columns in the figures represent the magnitude and sign of the contributions of the terms indicated by the annotations, to the population of the particular level for both models 1 and 2. Some smaller contributions

are not obvious in the figures and arrows have been used to indicate the position where they are plotted.

Some general observations regarding Level 1 (${}^4I_{13/2}$) and Level 2 (${}^4I_{11/2}$) under 800 nm pumping can be made by examining Figure 4.3-5 and Figure 4.3-6:

- The contributions of the terms $\omega_1 n_1$ and $b_{32} A_3 n_3$ are very small and have not been plotted on the diagrams.
- The observed negligible difference between the two models in low Er^{3+} concentration is understandable since in this Er^{3+} concentration the additional three-ion processes, considered by Model 2 (T(110,003) for Level 1(${}^4I_{13/2}$) and T(220,005) for Level 2 (${}^4I_{11/2}$) - see Table 4.3-4) make a very small contribution to the overall population.
- Whilst the overall population of ions going into Level 2 (${}^4I_{11/2}$) drops slightly in high Er^{3+} concentration, the population of ions going into Level 1 (${}^4I_{13/2}$) dramatically increases, due to the effect of process T(300,011). This three-ion process bypasses Level 2 (${}^4I_{11/2}$), populating Level 1 (${}^4I_{13/2}$) directly, and at the same time excites a substantial amount of previously unexcited ions from the ground level.

Some specific observation can also be made for Level 1 (${}^4I_{13/2}$) under 800 nm pumping:

- As expected in low Er^{3+} concentration, the population of Level 1 (${}^4I_{13/2}$) is mainly due to radiative and multiphonon decay from Level 2 (${}^4I_{11/2}$). Even though the radiative rate dominates the depopulation of Level 2, the value of the branching ratio for the transition to Level 1 makes the contribution of this radiative decay comparable with that of the multiphonon decay. The contribution of the radiative decay from Level 3 to Level 1 (${}^4I_{13/2}$) is negligible.
- In high Er^{3+} concentration the population of this level comes mainly from the three-ion cross-relaxation process T (300,011). In both Er^{3+} concentrations (1.6 mol% and 18 mol%) the depopulation of Level 1 (${}^4I_{13/2}$) is mainly via radiative decay ($-A_1 n_1$) to Level 0 (${}^4I_{15/2}$).
- The inclusion of the three-ion process T(110,003) in Model 2 does not mean the effect of the two-ion process W(11,30) is negligible. Even in the highest Er^{3+} concentration used, the contributions of both processes to the depopulation of Level 1 (${}^4I_{13/2}$) are comparable.

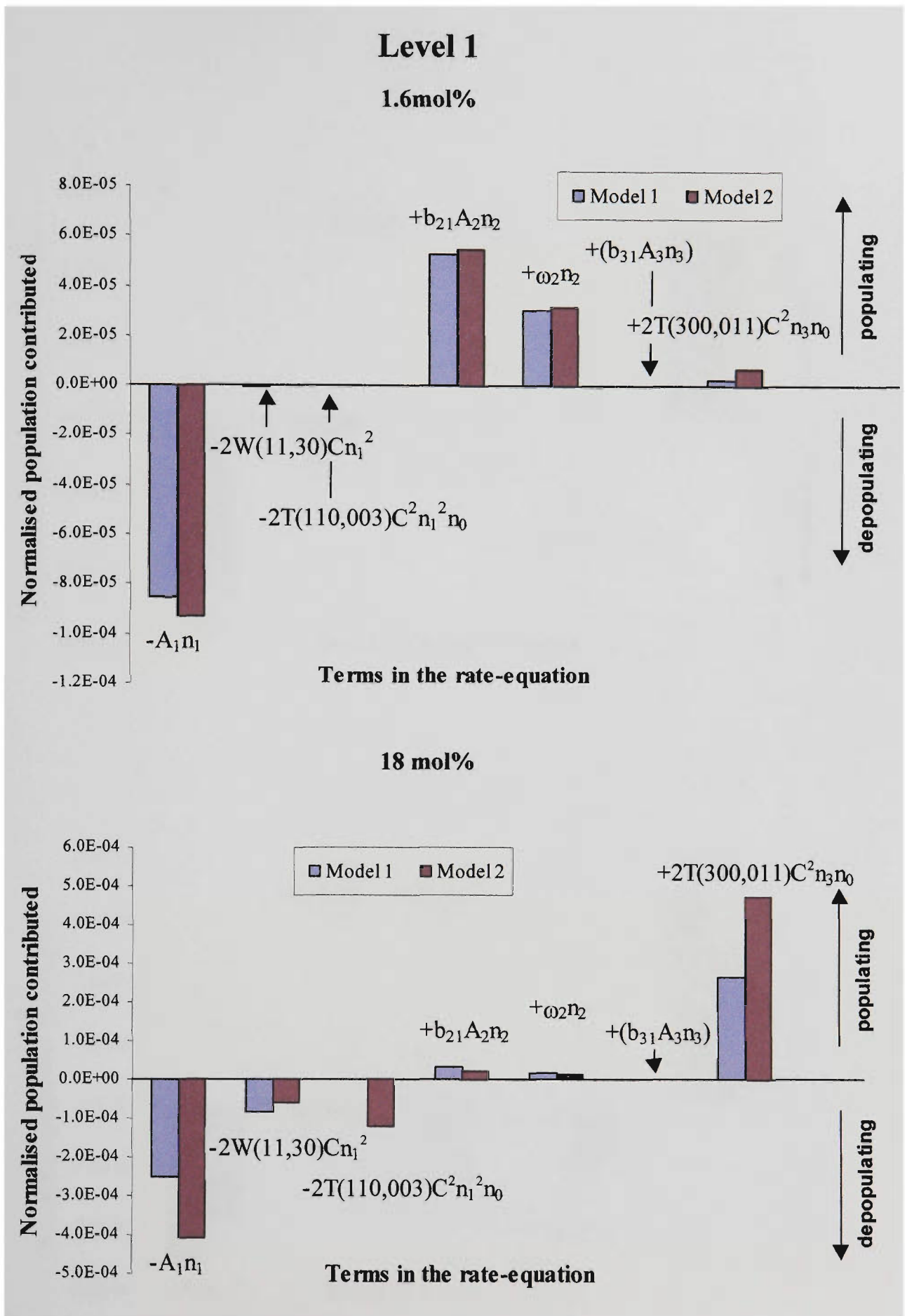


Figure 4.3-5 Integrated contribution of the different terms in equations (4.3.6) to the normalised population of Level 1 ($^4I_{13/2}$) at 1.6 mol% and 18 mol%, 800 nm pumping.

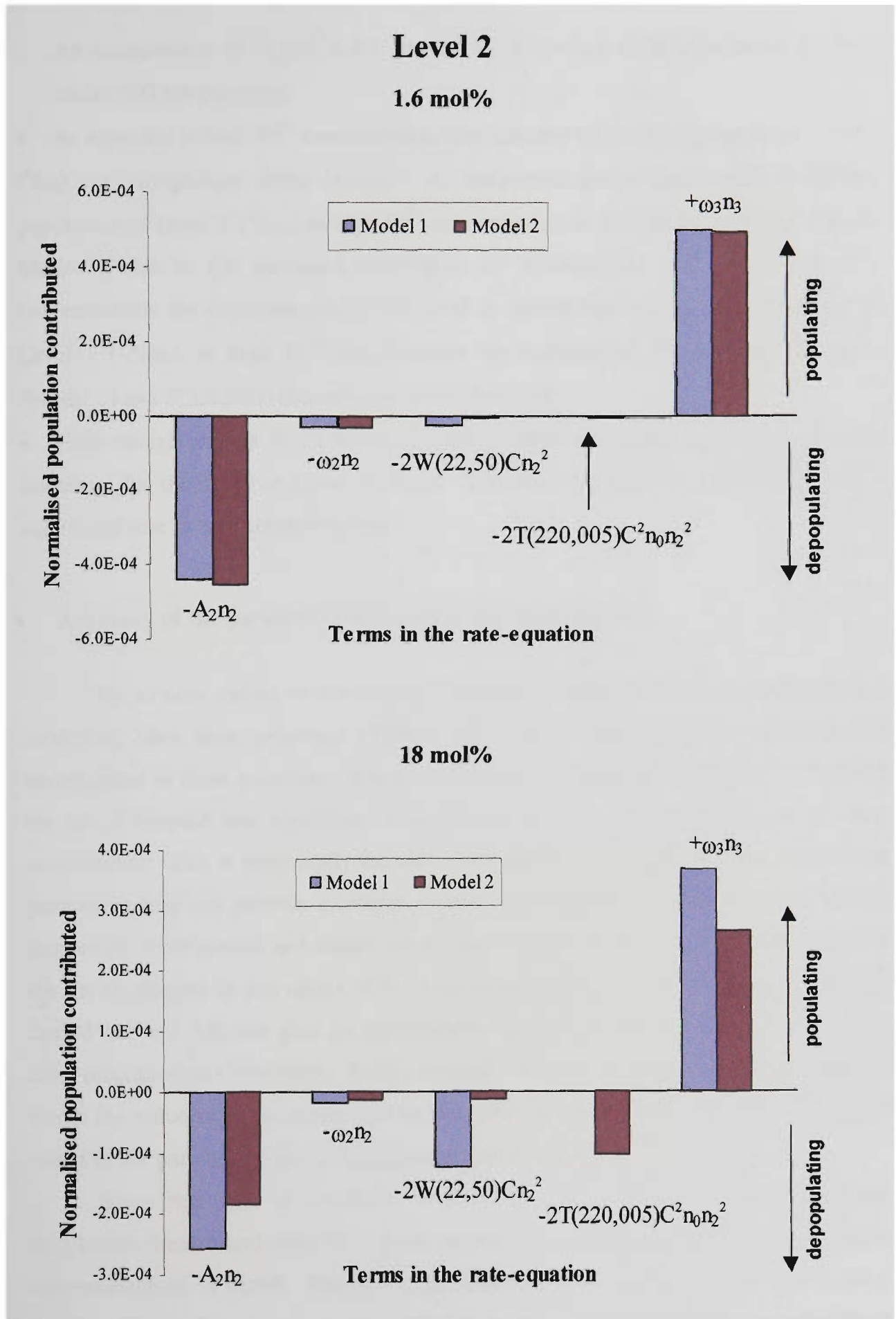


Figure 4.3-6 Integrated contribution of the different terms in equations (4.3.6) to the normalised population of Level 2 (${}^4I_{11/2}$) at 1.6 mol% and 18 mol%, 800 nm pumping.

An examination of Figure 4.3-6 reveals the following trends for Level 2 (${}^4I_{11/2}$) under 800 nm pumping:

- As expected in both Er^{3+} concentrations the majority of the ions come from Level 3 (${}^4I_{9/2}$) via multiphonon decay ($+\omega_3n_3$). As mentioned above, the overall normalised population of Level 2 (${}^4I_{11/2}$) in high Er^{3+} concentration is smaller for Model 2 than for Model 1 due to the increased importance of T(300,011). Whilst in both Er^{3+} concentrations the depopulation of this level is mainly due to the radiative decay to Level 1 ($-A_2n_2$), in high Er^{3+} concentration the contribution of processes W(22,50) (Model 1) and T(220,005) (Model 2) is also substantial.
 - Even though process W(22,50) is included in Model 2, it does not seem to be very important for the decay of Level 2 (${}^4I_{11/2}$). The three ion process T(220,005) plays a significant role in high concentrations.
- **Accuracy of the parameters obtained from numerical fits**

Up to now values of the various parameters obtained from the rate equation modelling have been presented (Table 4.3-4) without any discussion of the likely uncertainties in these quantities. Because of the use of numerical techniques for solving the set of coupled rate equations, it is difficult to give a reliable estimate of these uncertainties. This is particularly the case when one considers that fitting a given set of parameters may not provide a unique solution to the problem of matching a limited number of experimental and model waveforms. However a study of the sensitivity of the fits to changes in the values of the various parameters in a particular set is readily carried out and this can give an approximate estimate of the accuracy of the quoted cross relaxation rate constants. In this context, "accuracy" simply means the extent to which the value of a parameter can be determined from the modelling, i.e. different values of the parameters can be distinguished in the quality of the final fits.

Since this type of treatment is only approximate and involves significant calculation, these calculations have been carried out only for Model 2 and for a doping concentration of 18 mol%. The results are expected to be very similar for both models and the effects of the cross relaxation processes are expected to be most significant at the highest available doping concentration. In this study every parameter was

independently varied by factor of 0.5, 0.75, 1.5, 2 and in some cases 3. For every value of the particular parameter, the predicted fluorescence waveforms for both Level 1 (${}^4I_{13/2}$) and Level 2 (${}^4I_{11/2}$) were calculated. These predicted waveforms were then normalised to unity and compared to the similarly-normalised experimental curves. The sum of the square of the differences (SSD) was then calculated and divided by the number of points involved. This provided a quantitative measure of the quality of the corresponding fit. The data obtained in this way is shown schematically in the plots of Figure 4.3-7.

In Figure 4.3-7 the "chosen" value for a particular cross-relaxation rate constant is the one considered to give the best fits of the modelled to the experimental curves. These are the values which are used in the final version of the models (Table 4.3-4). These values, however, are not necessarily the ones which gave the smallest SSD for a particular Level in a particular Er^{3+} concentration. For example, the column charts for all three-ion parameters in the figure for Level 1 (${}^4I_{13/2}$) would suggest that the values needed for a good fit of Level 1 (${}^4I_{13/2}$) are larger than the chosen ones. It needs, however, to be remembered that the best value of a parameter should provide self-consistent fits for both levels. Therefore larger values of the three ion-parameters should not be used since they would produce a greater error in the fit for Level 2 (${}^4I_{11/2}$) (see the charts for Level 2 (${}^4I_{11/2}$) in Figure 4.3-7).

A lack of sensitivity of the SSD to the value of a particular cross-relaxation parameter generally means that the corresponding cross-relaxation process is not important for that particular level. This is the case, for example, with the parameter $W(22,50)$ if only Level 1 (${}^4I_{13/2}$) is considered. However, once Level 2 (${}^4I_{11/2}$) has also been considered it becomes obvious that process $W(22,50)$ is of significant importance for Level 2 (${}^4I_{11/2}$) and therefore for the whole system. Even though it is not so obvious in Figure 4.3-7 because of the overall scale of the graph, a change of factor of 2 in the $W(22,50)$ rate constant more than doubles the SSD for Level 2 (${}^4I_{11/2}$).

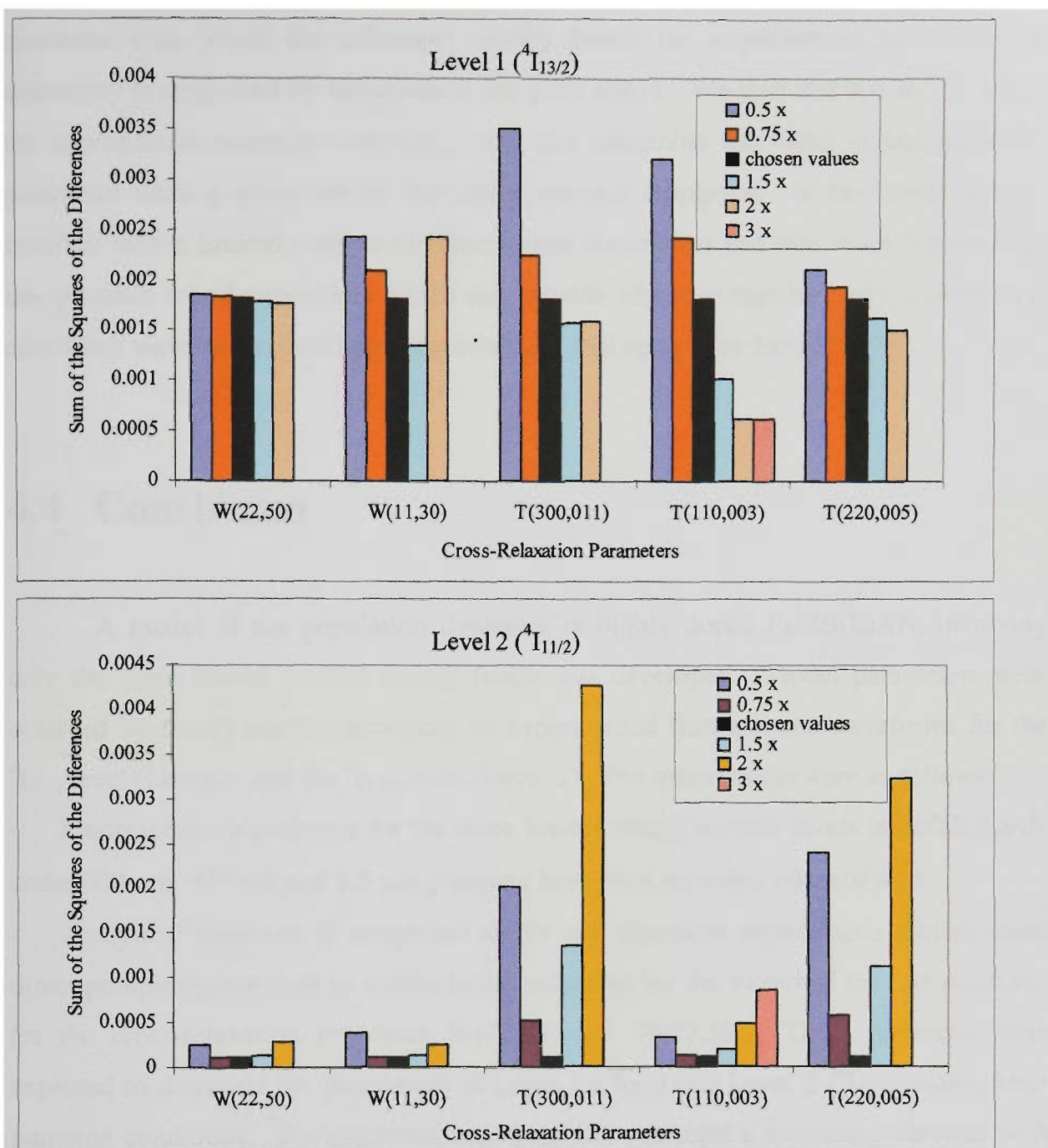


Figure 4.3-7 Sensitivity of the fits of Model 2 to changes in the cross-relaxation parameters (calculated for 18 mol%)

The overall conclusion from Figure 4.3-7 is that the estimates of the values for the cross-relaxation parameters obtained from the numerical modelling are close to the optimum values of these parameters. Whilst being by no means a measure of the absolute uncertainties in the values of these cross-relaxation parameters, this approach gives a good indication of the sensitivity of the model to changes in these values and thus could be used as a qualitative estimate of the uncertainties involved. A change in values of the parameters by a factor of two certainly produces a noticeable change in the

closeness with which the calculated curves match the experimental ones and this sensitivity is supported by variations in the SSD above. We thus use this as a guide to the approximate accuracy with which one can determine the value of any particular parameter from a given set by the fitting process employed. If the fitting process involves only a limited number of fluorescence waveforms and thus there is more than one possible set of parameters which can provide adequate matching of measured and calculated waveforms, then larger uncertainties will apply (see Table 4.3-4).

4.4 Conclusion

A model of the population dynamics in highly doped Er/ZB(L)AN, involving only the three lowest excited energy levels was developed. Model parameters were obtained by fitting model predictions to experimental fluorescence waveforms for the $^4I_{11/2}$ level (Level 2) and the $^4I_{13/2}$ level (Level 1). The main results were as follows:

- Fluorescence waveforms for the three lowest energy excited levels in Er/ZB(L)AN under 800 nm, 975 nm and 1.5 μm pumping have been recorded and analysed.
- Analytical solutions of simplified single rate equations representing a level under direct pumping were used to obtain initial estimates for the values of the rate constants for the cross-relaxation processes W(11,30) and W(22,50). These processes were expected to dominate the population of Level 1 ($^4I_{13/2}$) and Level 2 ($^4I_{11/2}$) under direct pumping conditions. The estimated rate constants exhibited a monotonic increase with Er^{3+} concentration. This is interpreted as a strong indication of the existence of the previously unreported three ion processes T(110,003) and T(220,005). The three-ion and the two-ion processes, however, affect the same levels in similar ways and could not be clearly distinguished within the limited models under consideration.
- A rate-equation model of the complete system, including all four lowest energy levels (the ground level and the three lowest excited energy levels) was presented. The number of cross-relaxation processes, most of which were nonlinear, made analytical solution of this model impossible and numerical routines were used.
- The use of only previously-reported two-ion cross relaxation processes (see W(22,50), W(11,30) and W(30,11) in Figure 4.1-1 and Chapter 2, Table 2.3-1) was not

sufficient for satisfactory explanation of the observed population behaviour of Level 1 ($^4I_{13/2}$). The numerical modelling showed that with an 800 nm pump another three ion process, T(300,011), dominates the rise of the population of the $^4I_{13/2}$ level in high Er^{3+} concentrations. This process, to our knowledge, has not previously been reported.

- Rate constants for the cross-relaxation processes W(22,50), W(11,30), T(300,011), T(220,005) and T(110,003) have been determined for the system Er/ZB(L)AN.
- The sensitivity of the model fits to changes in the values of the above cross-relaxation parameters, as well as the relative contribution of these processes to the population of the $^4I_{13/2}$ and $^4I_{11/2}$ levels have been studied.
- The numerical model developed generally predicted well the decay waveforms of the $^4I_{13/2}$ and $^4I_{11/2}$ levels in both 1.6 mol% and 18 mol% Er^{3+} concentration. However, this model was unable to satisfactorily predict the fine balance between fast and slow rise in the population of the $^4I_{13/2}$ level in the intermediate Er^{3+} concentrations of 10 mol%. This fact together with the observation of very strong green fluorescence in intermediate and high Er^{3+} concentrations was an indication of the presence of appreciable populations in some of the higher energy levels which were unaccounted for in the model developed in this chapter.

In summary, the dynamics of the $Er^{3+}/ZB(L)AN$ system in high Er^{3+} concentrations is very complex with many competing cross-relaxation processes taking place. The limited model presented above has attempted to identify and quantify only the processes that dominate the population dynamics of the three lowest excited energy levels for 800 nm pumping. While predicting quite well the main features of the measured fluorescence waveforms over the whole range of Er^{3+} concentrations, this model was unable to predict the observed behavior in intermediate Er^{3+} concentrations. It also failed to clearly identify the contributions of the two and the three-ion cross-relaxation processes in the system. The model needs to be refined by inclusion of higher energy levels and the processes necessary to explain the measured fluorescence waveforms for these levels. The inclusion of higher levels will impose much tighter restrictions on a possible self-consistent set of rate constants and should improve the reliability of the parameters obtained from the model. It would be expected that inclusion of higher energy levels with relatively small populations could provide sensitive indicators of the extent of processes coupling these and lower levels.

Chapter 5

Extended model of the population dynamics of erbium excited energy levels with 800nm pump

5.1. Introduction

In the previous chapter we introduced a rate equation model involving the three lowest excited energy levels in $\text{Er}^{3+}/\text{ZB(L)AN}$ glasses. This model was able to successfully predict the general population behaviour of these levels. This model also confirmed the complexity of the system in the high Er^{3+} concentrations used. A number of cross-relaxation processes were identified and the model was able to provide approximate values for the corresponding rate constants. There was also a strong indication that the high doping concentrations give rise to previously unidentified

energy exchange processes, which have a significant effect on the population of the two lowest excited levels. Some of these processes affect particular levels in similar ways and so it was difficult to distinguish them from each other and to study their contribution with the limited model under consideration. There also was some evidence that these processes excite an appreciable amount of population to the higher excited energy levels. This relatively small, compared to the lower levels, population is expected to be very sensitive to the doping concentration and the relevant cross-relaxation processes involving the particular levels. In other words, the study of the fluorescence from the upper levels could provide a sensitive means of distinguishing and studying the individual contribution of two or more competing processes originating from the lower levels.

The understanding from the previous chapter was that with the 800nm pumping used, most of the excited population is in the first three excited levels and that the processes discussed in the last chapter were the ones which dominate the population dynamics. The introduction of more levels and other cross-relaxation processes will simply allow refinement of the previous model. This should improve the accuracy of prediction for all levels and over the full range of concentrations. The use of other MOPO wavelengths to directly pump higher excited levels may also highlight additional processes which are important under these excitation conditions and also lead to a better overall understanding of the population behaviour of the Er^{3+} system.

To aid the discussions of energy levels and processes in this chapter an extended Er^{3+} energy level diagram is presented in Figure 5.1-1. For easier reference while reading this chapter, this diagram has also been reproduced as a foldout diagram at the back of the thesis. While many other processes are discussed in this chapter, this diagram includes all the processes which are found to be important in modelling the observed fluorescence behaviour.

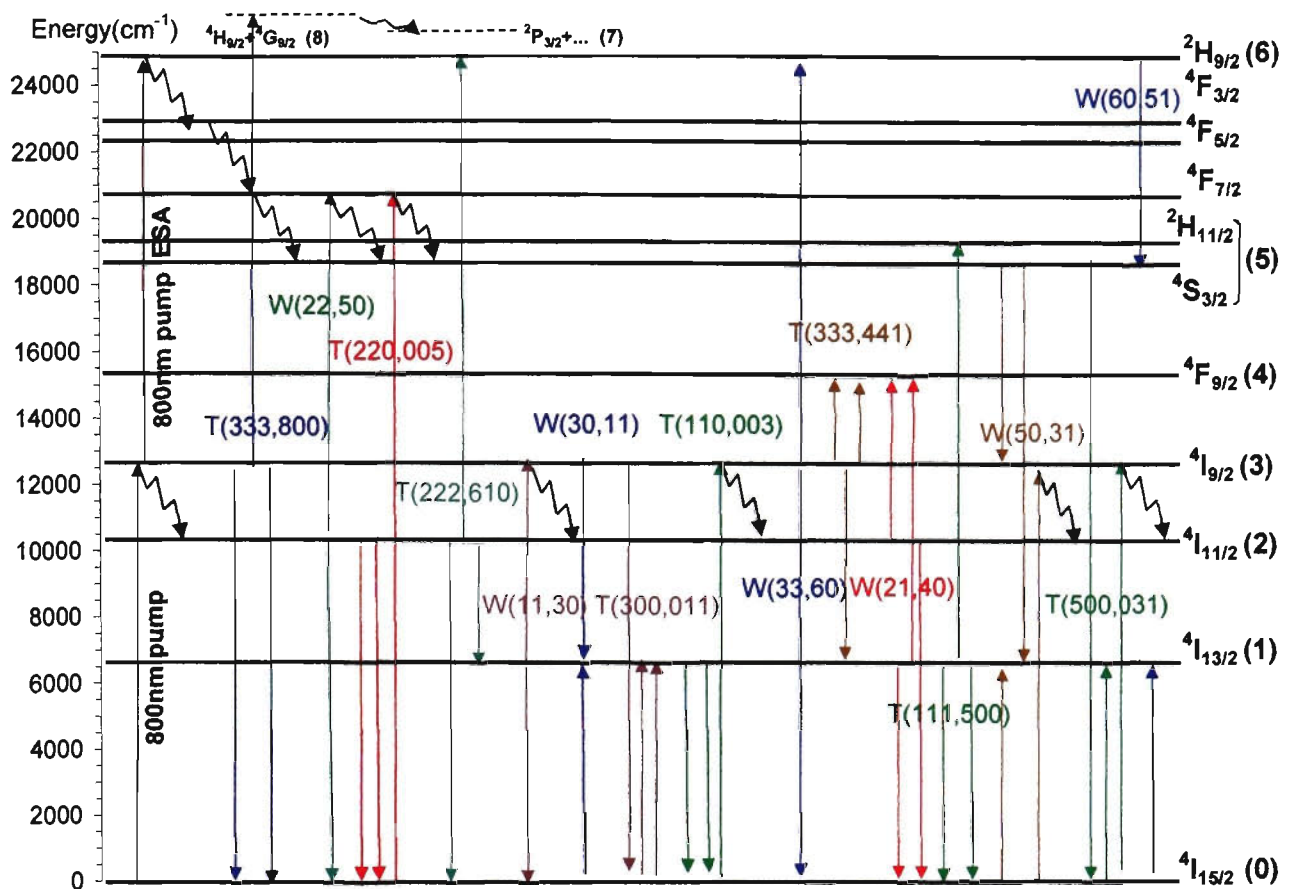


Figure 5.1-1 Energy level diagram, multiphonon (↘) and cross-relaxation processes in Er/ZBAN glasses (In order to allow the use of this diagram as an easily accessible reference it has been attached as a foldout diagram at the end of the Thesis)

Table 3.3-1 (Chapter 3) shows the energy, ground state absorption wavelength and assignment of each of the energy levels included in Figure 5.1-1. This table is important for the process of modelling as it allows estimation of energy mismatch involved in cross-relaxation processes. It also allows one to anticipate which transitions will give rise to overlapping fluorescence lines. Table 5.1-1 presents the possible transition assignments for the fluorescence lines observed under various pumping conditions. The bold numbers correspond to transitions which have been identified with a reasonable degree of certainty. The plain numbers represent possible, but not clearly identified transitions.

Before proceeding further with the material of this chapter it may help the reader to understand a little more of its structure. The basic approach taken is to first present results of waveform characterisation using time constants derived from various types of

<i>Fluorescence Line (nm):</i>	~2.7μm	~1.5 μm	~980	830-850	801-820	~698
<i>Source Level:</i>	<i>Terminating Level:</i>					
$^4I_{15/2}$						
$^4I_{13/2}$		$^4I_{15/2}$				
$^4I_{11/2}$	$^4I_{13/2}$		$^4I_{15/2}$			
$^4I_{9/2}$					$^4I_{15/2}$	
$^4F_{9/2}$						
$^4S_{3/2} + ^2H_{11/2}$	$^4I_{9/2}$	$^4I_{9/2}$		$^4I_{13/2}$	$^4I_{13/2}$	
$^4F_{7/2}$			$^4I_{11/2}$			$^4I_{13/2}$
$^4F_{5/2} + ^4F_{3/2}$	$^4S_{3/2} + ^2H_{11/2}$	$^4F_{9/2}$	$^4I_{9/2}$		$^4I_{11/2}$	
$^2H_{9/2}$	$^4F_{7/2}$	$^4S_{3/2} + ^2H_{11/2}$			$^4I_{9/2}$	$^4I_{11/2}$
$^4G_{11/2} + ^4G_{9/2} + ^2K_{15/2} + ^4G_{7/2}$	$^4F_{5/2} + ^4F_{3/2}$	$^4F_{7/2}$		$^4F_{9/2}$		$^4I_{9/2}$
$^2P_{3/2} + ^2D_{3/2} + ^4F_{3/2}$	$^4G_{11/2} + \dots$	$^2H_{9/2}$	$^4F_{7/2}$		$^4S_{3/2} + ^2H_{11/2}$	

<i>Fluorescence Line (nm):</i>	~655	540-555	520-530	~488	~468	~454	400-410	~383
<i>Source Level:</i>	<i>Terminating Level:</i>							
$^4I_{15/2}$								
$^4I_{13/2}$								
$^4I_{11/2}$								
$^4I_{9/2}$								
$^4F_{9/2}$	$^4I_{15/2}$							
$^4S_{3/2} + ^2H_{11/2}$		$^4I_{15/2}$	$^4I_{15/2}$					
$^4F_{7/2}$				$^4I_{15/2}$	$^4I_{15/2}$			
$^4F_{5/2} + ^4F_{3/2}$	$^4I_{13/2}$					$^4I_{15/2}$		
$^2H_{9/2}$		$^4I_{13/2}$					$^4I_{15/2}$	
$^4G_{11/2} + ^4G_{9/2} + ^2K_{15/2} + ^4G_{7/2}$				$^4I_{13/2}$				$^4I_{15/2}$
$^2P_{3/2} + ^2D_{3/2} + ^4F_{3/2}$		$^4I_{9/2}$	$^4I_{9/2}$		$^4I_{11/2}$		$^4I_{13/2}$	

Table 5.1-1 Transitions responsible for the fluorescence lines in Er³⁺/ZB(L)AN glasses under 802nm, 1.5 μm, 980 nm, 520 nm and 403 nm pumping. Bold numbers - identified transitions, plain numbers - possible, but not confirmed transitions.

rise and decay functions with 800 nm pumping. This is followed by a discussion of the effect of pump intensity on the time constants and then data of this type for 800 nm pumping. After this comes a similar section which covers these topics for other pump wavelengths. Once all the measurements have been presented, a discussion of the main processes responsible for the observed fluorescence behaviour is presented for 800 nm pumping - one level at a time. Similar discussions follow for the other pump wavelengths and then the information derived from these discussions is used to construct an extended energy level model. The predictions of this model are then compared to the measured fluorescence waveforms to obtain values of the various cross-relaxation rate constants.

5.2. Results

5.2.1. 800nm pumping

5.2.1.1. Fluorescence rise and decay times

The basic trends associated with the changes in the fluorescence waveforms for the three lowest excited energy levels were already identified in Chapter 4. This discussion also identified and quantified the important cross-relaxation processes. In Chapter 4 the point was made that the basic data which was used in fitting model predictions to experimental measurements was the fluorescence waveforms. An attempt was made to summarise the waveform changes by tabulating the rise and decay times obtained from the waveforms via various fitting procedures. Table 5.2-1 and Table 5.2-2 presented below summarise the rise and decay data for all waveforms studied with the 800 nm pump. These tables include and extend the data of Figures 4.2-1 and 4.2-2 and represent a more comprehensive picture of the behaviour of the system under pulsed pump excitation.

The most important issues about the fitting procedures and the interpretation of the rise and decay data in both tables below were already discussed in Chapter 4. These considerations also apply to Table 5.2-1 and Table 5.2-2 and other similar tables

presented later in this chapter. For the 800 nm (as well as for the 1.5 μm) pump wavelength, two set of measurements are to be presented. As was also mentioned in Chapter 4, the main purpose of the second set of measurements (Set 2) was to improve the spatial distribution of the pump beam and to allow better time resolution of the IR measurements with the use of the InGaAs detector system (response time approximately 10 μs).

In addition to the 800 nm, 980 nm and 1.5 μm fluorescence lines, discussed in Chapter 4, there are two relatively strong lines (520-550 nm and 407 nm) and three relatively weak lines (655nm, 450nm, 383nm) which have also been presented in the above tables. All these fluorescence lines clearly originated from excited states above Level 3 ($^4\text{I}_{9/2}$). Unlike the fluorescence from the lower levels, they showed mainly exponential decays. This was partially (but not entirely) due to the fact that these levels have a relatively small population. The smaller population would make the probability for up-conversion processes much smaller.

An interesting detail was the presence of a fast component in the rise of both 655nm (originating from Level 4 ($^4\text{F}_{9/2}$)) and 407nm (from Level 6 ($^2\text{H}_{9/2}$)) fluorescence lines. In these fluorescence waveforms the rate of this fast rise did not change much, but its contribution to the amplitude of the total waveform increased markedly with Er^{3+} concentration.

The other two lines; 540 nm (from Level 5 ($^4\text{S}_{3/2}+^2\text{H}_{11/2}$)) and 383 nm (from level $^4\text{G}_{11/2}$), were characterised by a single rise time constant and a two-component decay. The longer decay component had time constants of milliseconds which indicated possible contributions from lower levels which had similar decay times. The strong green fluorescence lines in the region of 540 nm were found to have a rather complicated behaviour with varying concentration. The corresponding ($^4\text{S}_{3/2}+^2\text{H}_{11/2}$) levels (Level 5) played a key role in several of the important cross relaxation processes which are needed to explain the observed fluorescence behaviour of a number of the levels. An understanding of the physical processes responsible for the behaviour of the fluorescence decay of Level 5 is aided by first considering the expected analytical form of the decay under conditions where a single cross-relaxation process is dominant.

- **Analytical fitting function for Level 5 (${}^4S_{3/2}+{}^2H_{11/2}$)**

An approximate analytical solution can be obtained for low Er^{3+} concentrations where the cross-relaxation process $W(22,50)$ is mainly responsible for the long component in the decay of Level 5 (see discussions of Level 5 later in the Chapter). Level 2 has a single exponential decay with a rate which is effectively constant with doping level up to about 4 mol% (see 980 nm fluorescence line in Table 5.2-1 and Table 5.2-2). Under these circumstances, the normalised population of Level 2 (${}^4I_{11/2}$) can be expressed as $n_2=n_{20} \exp(-t/\tau_2)$ and the normalised rate-equation for Level 5 can be written as:

$$\frac{dn_5(t)}{dt} = -(A_5 + \omega_5)n_5(t) + WCn_{20}^2 e^{(-2\frac{t}{\tau_2})} = -\frac{n_5(t)}{\tau_5} + WCn_{20}^2 e^{(-2\frac{t}{\tau_2})}.$$

Here τ_5 is the decay time constant of Level 5 which would apply in the absence of cross-relaxation processes and C is the doping concentration. The solution in the case that Level 5 has an initial normalised population n_{50} (the population rises in less than 10 μs) can be written as

$$n_5(t) = +n_{50} e^{(-\frac{t}{\tau_5})} - WCn_{20}^2 e^{(-2\frac{t}{\tau_2})} \frac{\tau_2 \tau_5}{(2\tau_5 - \tau_2)} (e^{(-2\frac{t}{\tau_2})} - e^{(-\frac{t}{\tau_5})}).$$

When $\tau_2 \gg \tau_5$, this simplifies to

$$n_5(t) = n_{50} e^{(-\frac{t}{\tau_5})} + WC \tau_5 n_{20}^2 (1 - e^{(-\frac{t}{\tau_5})}) \exp(-\frac{t}{\tau_2/2}). \quad (5.2.1-0)$$

A fitting function, similar in form to Equation 5.2.1-0, was used to fit the experimental decays of the fluorescence from Level 5 for doping concentrations up to 4 mol%. The fitted values for τ_5 and $\tau_2/2$ actually represent the decay time constant of Level 5 without the effect of $W(22,50)$ and one-half the decay time constant of Level 2 respectively. These parameters ($\tau_2/2$ not τ_2) are included in the appropriate columns of Table 5.2-1, Table 5.2-2 and Table 5.2-3 in red. It is obvious from the decreasing values of τ_5 that even in these lower concentrations other effects are present which reduce the decay time below that expected from fluorescence and multiphonon processes.

- **Multiple exponential fits to the waveforms of Level 5 ($^4S_{3/2}+^2H_{11/2}$) in high Er^{3+} concentrations**

A fitting function including two waveforms, each consisting of an exponential rise and decay (see Chapter 4, expression 4.2.2), was used for higher Er^{3+} concentrations where the decay of Level 2 ($^4I_{11/2}$) is non-exponential and an explicit solution for Level 5 ($^4S_{3/2}+^2H_{11/2}$) is difficult to obtain. Such a function presumes two independent population and depopulation mechanisms are active for this level - with both population and depopulation processes possibly acting simultaneously during the decay phase of the waveform (see later discussion for justification of this). Some of the parameters obtained from fitting these functions had large uncertainties. This is not surprising considering the large number of fitting parameters. The decay time constants (denoted in blue in Table 5.2-1, Table 5.2-2 and Table 5.2-3) obtained with this function are meant to give some idea of the trends in the decays which are present in the waveforms. The uncertainties limit their value but it is clear that there is a trend to decreasing decay times with increasing doping concentration. The rise times for level 5 listed in the table are not obtained using the fitting functions above. They were obtained by recording the rising portion of the waveform with a fast photomultiplier and fitting a single exponential to the rise. They therefore characterise well the appearance of the rising portion of this green fluorescence waveform.

Two other fluorescence lines were also detected, but are not presented in Table 5.2-1 and Table 5.2-2. The first had a peak intensity at about 553-555 nm and the other at 830 nm. The main decay time constants of these lines were similar to that of the green fluorescence line at 520 – 550 nm. However, there was also a virtually instantaneous initial rise (<25 ns) and an initial decay with a time constant of a few microseconds. Inspection of the energy level diagram in Figure 5.1-1 and Table 5.1-1 indicated that the fluorescence in these two regions could actually consist of overlapping lines originating from different levels. Fluorescence in the region of 830 nm can originate from either the Level 5 ($^4S_{3/2}$) \rightarrow Level 1 ($^4I_{13/2}$) or Level 6 ($^2H_{9/2}$) \rightarrow Level 3 ($^4I_{9/2}$) transitions. These same two levels (Level 5 and Level 6) can also produce fluorescence in the green region (Level 5 ($^4S_{3/2}$) \rightarrow Level 0 ($^4I_{15/2}$) and Level 6 ($^2H_{9/2}$) \rightarrow Level 1 ($^4I_{13/2}$)). As the $^2H_{9/2}$ level (Level 6) can be populated during the pump

Fl.Line(nm):	1.5 μ m	980	820	655	540	450	407	383
	Level 1	Level 2	Level 3	Level 4	Level 5	⁴ F _{3/2} + ⁴ F _{3/2}	Level 6	⁴ G _{11/2} +..
	R+D							
Rise								
Mol%	ms	μ s		Init.+Late (μ s)	μ s	ns	Inst. + ns	
0.4		7.7	Inst.		8.5			
0.8	24.7*(8.0)			98			215	
1.6	21.0*(8.0)	7.8		109	9		189	
4	8.6 (8.0)	7.5		5 + 106	8.2	1900	140	
8	Fast + 3.7	6.9					141	
10	Fast + 0.8	6.9		5.4 + 111	3.8	367	145	<500ns
12							154	
14	Fast + 0.5	6.2		4.2 + 100	2.4		132	
16	Fast only						118	
18	Fast only	5.8		5.1	2.1	263	130	<500ns
Decay								
					(R ₁ +D ₁)+(R ₂ +D ₂)			Init., Late
					D1 D2			
Mol%	ms	ms	μ s	ms	μ s ms	μ s	μ s	μ s ms
0.4		7.7	7.9		454, 2.6		7.7	
0.8	9.3*(8.1)			NE(1.2+5.3)			8.3	
1.6	10.0*(8.7)	8	9.0	NE(2.2+5.5)	295, 2.5		8	
4	12.9 (8.6)	8.3	7.6	6.6	75, 3.2	8.9	7.6	
6		8.2					6.6	
8	12.3	NE (2.4+7.9)					5.8	
10	14	NE (2.5+9.9)	6.9	5.4	70*, 2.7	8.6	5.1	71, 1.4
12							4.6	
14	14.1	NE (1.7+9.5)		4.4	15, 1.0*		3.5	
16	10.2						3.1	
18	7.3	NE (1.5+7.7)	6.0	2.8	32*, 1.7	5.9	2.7	27, 0.86

Table 5.2-1 Data set 1 (1.5 μ m PbS detector): Measured fluorescence rise and decay time constants for the indicated levels with 800 nm pumping. Inst.- faster than the response of the detector. NE – non-exponential, Fast – Fast component (see text), **Black numbers** - obtained from fits with a single (or double) exponential function (see text), **Blue numbers** – obtained from fits with combined exponential rise and decay functions (see text). (R₁+D₁)+(R₂+D₂) – initial (Rise + Decay) form, followed by a secondary (Rise + Decay) form. **Red Numbers** –these are obtained from fits of analytic expressions which contain parameters which have some physical significance in terms of population or depopulation processes for particular levels (see text of chapters 5 and 4), * - large uncertainties. Approximate pump conditions:~24 mJ, ~8 mm² spot area, $\lambda_{\text{pump}} = 802\text{nm}$

Fl.Line (nm):	1.5 μ m	980	655	540	407
	(Level 1)	(Level 2)	(Level 4)	(Level 5)	(Level 6)
	R+D				
	Rise				
Mol%	ms	μ s	μ s	μ s	ns
0.4	21.6*(8)				
0.8	17.6*(8)				
1.6	14.8 (8)	7.0	4.1+103	9.1	
4	10.9 (8)				
6					
8	Fast +4.9				
10	Fast + 3.7				
12					
14	Fast + 1.2				
16					
18	Fast only	4.8	4.8	2.8	Inst.+135
	Decay				
				(R ₁ +D ₁)+(R ₁ +D ₁)	
Mol%	ms	ms	ms	μ s + ms	μ s
0.4	10.6(8.7)				
0.8	10.6(9.1)				
1.6	12.1 (10.4)	8.4	NE(1.8+5.7)	258, 2.5	9
4	13.5 (10.6)				
6					
8	12.4				
10	15.7				
12					
14	15				
16					
18	6.6	NE(1.5+7.2)	2.7	D ₁ D ₂ 8.4*, 1.1	2.5

Table 5.2-2 Data set 2 (1.5 μ m InGaAs detector): Measured fluorescence rise and decay time constants for the indicated levels and for 800 nm pumping. Inst.- faster than the response of the detector. NE – non-exponential, Fast – Fast component (see text), **Black numbers** - obtained from fits with a single (or double) exponential function (see text), **Blue numbers** – obtained from fits with combined exponential rise and decay function (see text). (R₁+D₁)+(R₂+D₂) – initial (Rise + Decay) form, followed by a secondary (Rise + Decay) form. **Red Numbers** –these are obtained from fits of analytic expressions which contain parameters which have some physical significance in terms of population or depopulation processes for particular levels (see text of chapters 5 and 4). * - large uncertainties. Approximate pump conditions: ~24 mJ, ~ 8 mm² spot area, $\lambda_{\text{pump}} = 802$ nm

pulse by direct ESA, this is likely to be the origin of the virtually instantaneous rise. Thus it is likely that these fluorescence lines, which have much longer rise time (2-9 μs), provide information on the population of Level 6, rather than Level 5.

5.2.1.2. Dependence of the fluorescence rise and decay times on pump density

- **Processes which result in exponential behaviour of level populations**

- Radiative and phonon-assisted decays

It is known that the radiative and phonon-assisted decay rates from a level do not depend on the population of the level. This is easily understood if a decay of a level with some initial population is considered. If no cross-relaxation processes are involved the rate equation of the level looks like:

$$\frac{dN(t)}{dt} = -(A + \omega)N(t). \quad 5.2.1-1$$

Normalisation to the Er^{3+} concentration C produces:

$$\frac{dn(t)}{dt} = -(A + \omega)n(t), \quad \text{with } n(t) = N(t)/C. \quad 5.2.1-2$$

Here the term multiplying $n(t)$ is the rate of the decay and it obviously does not depend on the concentration or the population of the level. The solution of this equation is

$n(t) = n(0)e^{-(A+\omega)t}$, where $n(0)$ is the initial normalised population and the decay time constant is $1/(A + \omega)$.

- Inclusion of a two-ion cross-relaxation process involving the ground level

If a two-ion cross-relaxation process that involves the ground level is present, Equation 5.2.1-1 will become:

$$\frac{dN(t)}{dt} = -(A + \omega)N(t) - WN_0(t)N(t), \quad 5.2.1-3$$

where $N_0(t)$ is the absolute population of the ground level. However, as was discussed in Chapter 4, the population of the ground level is not significantly perturbed by the pump pulses used in this work and therefore $N_0(t) \approx N_0(0) \approx C$. The normalised

population of the ground level would then be $n_0(t) \approx n_0(0) \approx 1$ and the equation 5.2.1-3 can be simplified:

$$\begin{aligned} \frac{dn(t)}{dt} &= -(A + \omega)n(t) - WCn_0(0)n(t) = -(A + \omega)n(t) - WCn(t) \\ &= -((A + \omega) + WC)n(t) \end{aligned} \quad \mathbf{5.2.1-4}$$

The solution now is : $n(t) = n(0)e^{-((A+\omega)+WC)t}$ and the decay is still exponential. The rate $((A+\omega)+WC)$ does not depend on the initial population of the level, however it is now a linear function of the concentration C.

Similar behaviour to the above results if ions from the level are involved in a two-ion process with another level (not the ground state) which has a very long decay time constant (much longer than that of the level under consideration). The normalised population of the second level, n_1 , will not be equal to 1. However, during the decay of $n(t)$, $n_1(t) \approx n_1(0) \approx \text{constant}$. Equation (5.2.1-4) then becomes

$$\frac{dn(t)}{dt} = -(A + \omega)n(t) - WCn_1n(t) = -((A + \omega) + WCn_1)n(t). \quad \mathbf{5.2.1-4b}$$

While the decay of the level under consideration will be still exponential, the rate of the decay now will also depend on the population of the other level involved in the cross relaxation process.

- Three-ion cross-relaxation process involving two ions from the ground level

A similar situation to the one discussed above arises in the case of a three-ion cross-relaxation process if two of the ions are from the ground level (see T(300,011) or T(500,013) in Figure 5.1-1). Equation (5.2.1-3) then becomes

$$\frac{dN(t)}{dt} = -(A + \omega)N(t) - TN_0^2N(t).$$

Normalising the populations then gives:

$$\begin{aligned} \frac{dn(t)}{dt} &= -(A + \omega)n(t) - TC^2n_0^2n(t) = -(A + \omega)n(t) - TC^2n(t) \\ &= -((A + \omega) + TC^2)n(t) \end{aligned} \quad \mathbf{5.2.1-5}$$

The decay is again exponential. Its rate $((A+\omega)+TC^2)$ would be still independent of the population of the level, but would exhibit a quadratic dependence on the doping concentration C.

- **Processes which result in non- exponential behaviour of level populations**

- Two-ion process with both ions originating from the same level

If now a two-ion process where both ions originate from the same level is considered (see W(11,30) and W(22,50)), the rate equation for this level would be

$$\frac{dN(t)}{dt} = -(A + \omega)N(t) - WN^2(t) .$$

After normalisation this becomes

$$\frac{dn(t)}{dt} = -(A + \omega)n(t) - Wcn^2(t) . \quad 5.2.1-6$$

This case has already been discussed (see Chapter 4. Equation (4.3.3) and the analytical

$$\text{solution is } n(t) = -\frac{1}{K'\tau - \exp(t/\tau)(\frac{1}{n(0)} + K'\tau)} . \quad 5.2.1-7$$

Where $K'=2WC$ and $\tau=1/(A+\omega)$. The obvious conclusion is that the decay is not exponential any more. This conclusion, however, could be seen even without solving Equation (5.2.1-6). This equation can be written as:

$$\frac{dn(t)}{dt} = -(A + \omega + Wcn(t))n(t) . \quad 5.2.1-8$$

It is now obvious that the decay cannot be exponential and that the decay rate will vary during the duration of the decay.

A similar discussion could be applied in two other cases:

- Two-ion cross-relaxation process with ions from different levels not including the ground level (other than the case considered with Equation 5.2.1-4b) (e.g. see W(21,40) in Figure 5.4-1).

- Three-ion cross-relaxation process with two interacting ions being from the same level (see process T(220,005) in Figure 5.4-1).

- Three-ion cross-relaxation process with three interacting ions being from the same level (see T(111,005) and T(333,008) on Figure 5.1-1).

The normalised rate equations for the above three cases are:

$$\frac{dn_i(t)}{dt} = -(A_i + \omega_i)n_i(t) - Wcn_i(t)n_j(t) = -(A_i + \omega_i + Wcn_j(t))n_i(t) , \quad 5.2.1-9$$

$$\frac{dn_i(t)}{dt} = -(A_i + \omega_i)n_i(t) - TC^2 n_i^2(t) = -(A_i + \omega_i + TC^2 n_i(t))n_i(t), \text{ and } \mathbf{5.2.1-10}$$

$$\frac{dn(t)}{dt} = -(A + \omega)n(t) - TC^2 n^3(t) = -(A + \omega + TC^2 n^2(t))n(t) \quad \mathbf{5.2.1-11}$$

The analytical solutions are more complex than (5.2.1-7), however from an inspection of the equations it is obvious that the decay is dependant not only of the concentration, but also of the population of the level and hence a non-exponential decay would be expected.

These above conclusions depend obviously on the relative magnitudes of the various terms in the equations. In the case where higher-order terms in $n(t)$ are of negligible magnitude compared to the linear term, then the decay will remain exponential.

If the pump energy density is varied in the experiments for measuring the fluorescence waveforms, the populations of the levels and the relative importance of the terms in the rate-equations will be varied. Thus a study of the effect of the pump energy density on the measured rise and decay waveforms would provide an indication of the presence or absence of cross-relaxation process. It will also provide information on the type of cross-relaxation processes involved.

An additional limited set of experiments was performed to study the dependence of the rise and the decay times of the measured fluorescence lines on the energy of the pump pulse (spot size unchanged). The results are shown in Table 5.2-3. Some conclusions from this data are presented below.

The data in Table 5.2-1 and Table 5.2-2 suggested the presence of two components in the rise of the fluorescence line at 407 nm. The initial instantaneous rise is followed by another relatively fast rise with a time constant of about (130-200 ns). These later measurement of the 407 nm fluorescence line (Table 5.2-3) for various pump energies and concentrations confirmed the presence of these two components (in low Er^{3+} concentrations). The contribution of the second component to the overall amplitude of the rise of this fluorescence line increased dramatically and completely dominated the high concentrations, especially when higher pump energy was used. Its rate, however, exhibited only a weak dependence on concentration (see Table 5.2-3, Table 5.2-1 and Table 5.2-2) and pump energy (see Table 5.2-3).

800nm pumping (into $^4I_{9/2}$ level)				
Fluor. Wavelength	Er Concentration	Pump Energy	Rise	Decay
nm	mol%	mJ	μs	μs
383	14	20	<1	NE(141 + 1.7 ms)
407	0.4	20	Inst. + <1 μs	
	1.6	20	Inst. + <1 μs	9.5
	4	20	127ns	
	14	20	124ns	4.3
	18	29	141ns	
		8	142ns	
	1.9	200ns		
520 (R ₁ +D ₁)+(R ₂ +D ₂)			R ₁	D ₁ D ₂
	0.2	29	11	450 , 2.6ms
	0.8	29	13	446 , 3.0ms
	4	30	14	71 , 2.0ms
		8	14	97 , 2.0ms
	10	30	4.3	50* , 4.0ms
		8	5.3	49* , 4.5ms
	18	28	1.8	8.7* , 2.9ms
8		1.3	3.8* , 3.3ms	
655			Initial, Late	
	4	21	1.2 , 105	7.3ms
		7	0.9 , 127	7.1ms
	18	27	2.5	5.0ms
		7	2.9	6.9ms
800nm	18	29	Inst.	5.7
		4	Inst.	5.0
	0.4	29	Inst.	7.8
		1	Inst.	7.2, 7.1, 7.5, 8.7 ^R
980nm	0.2	1	7.2	7.4ms
	0.8	29	7.6	7.6ms, 7.7ms, 8.0ms ^R
		1	7.6	7.8ms, 7.9ms, 7.6ms, 7.8ms ^R

Table 5.2-3 Rise and decay-time constants of the main fluorescence lines under 802nm pumping as a function of the pumping energy. Inst.- faster than the response of the detector. NE – non-exponential, **Black numbers** - obtained from fits with a single (or double) exponential function (see text), **Blue numbers** – obtained from fits with combined exponential rise and decay function (see Exponential fits to the waveforms of Level 5 in high concentrations). (R₁+D₁)+(R₂+D₂) – initial (Rise + Decay) form, followed by a secondary (Rise + Decay) form. **Red Numbers** –decay time constants calculated using an analytical fitting function (see equation 5.2.1-0), * - large uncertainties (Standard error in the order of 100% or more). ^R - repeatability check. The irradiated spot size was approximately constant with an area of approximately 15 mm².

The rise time of the strong green fluorescence at 520 nm decreased with concentration from about 11 μs to about 2 μs , but did not show any substantial

sensitivity to the pump energy. Similarly, the decay of the same fluorescence line exhibited strong concentration dependence, however no substantial variation in the decay-rates was detected for different pump energy at any particular concentration.

A similar lack of substantial effect with variation of pump energy density was evident in the rise of the red fluorescence at 655 nm. The decay time, however, increased from about 5 ms to about 7 ms for about a factor of 4 decrease in the pump energy used. Variation of the pump energy density also did not have any substantial effect on the rise or decay of the fluorescence from Level 3 (at about 800 nm). The data for the 980 nm fluorescence in Table 5.2-3 also shows no significant variation in rise or decay time constants for a factor of 29 change in pump energy density. However, this data only covers very small doping concentrations.

5.2.2. Other Pumping Wavelengths

5.2.2.1. Fluorescence rise and decay times

While the present study concentrated on 800nm pumping, the study of other pumping wavelengths is also important for a comprehensive understanding of the dynamics of the $\text{Er}^{3+}/\text{ZB(L)AN}$ system. The lack of a suitable CW pump source prevented the study of the dependence of the fluorescence intensity as a function of the Er^{3+} concentration for different pump wavelengths. The availability of the MOPO pulsed source, however, allowed an extensive study of the temporal behaviour of the major excited energy levels under 1.5 μm , 975 nm, 520 nm and 403 nm pumps to be performed. The fitting procedures have been already discussed in Chapter 4 as well as in the previous sections of this chapter. The results are presented in the tables below. This following section discusses only the main trends in the data presented in the relevant tables. The origin of the observed fluorescence lines and the particular cross-relaxation processes which are responsible for the observed population dynamics are discussed in later sections.

• Pumping into the $^4I_{13/2}$ level (Level 1) at 1.5 μm

As was mentioned in relation to 800nm pumping, the initial measurements of the 1.5 μm fluorescence, including those presented in Table 5.2-4 below, were performed

Fl.Line:	1.5 μm	980	800-820	655	520-550	407		
(nm)		R+D		R+D	(R ₁ +D ₁)+(R ₂ +D ₂)	(R ₁ +D ₁)+(R ₂ +D ₂)		
	Rise							
		R	Slightly NE	R	R ₁	R ₂	R ₁	R ₂
Mol%		ms	μs		μs	ms	μs	μs
0.8	Inst.							
1.6		5.9	0.6	2.7ms	16	4.9		
4		5.1	0.9	1.1ms	22	5.7	11	898
8			1.4					
10		1.6	1.4	532 μs	13*	1.7	10.5	837
14			1.4					
18		0.4	1.8	209 μs	3.6*	0.48	5.7	382
		Decay						
		D	Init., Late	D	D ₁	D ₂	D ₁	D ₂
Mol%	ms	ms	ms	ms	μs	ms	μs	ms
0.8	10.9							
1.6		9.7	0.14 + 4.5	5.1	414	6.3		
4	NE(1.0+9.5)	11.9	NE(1.8+5.1)	6.2	525	4.8	167	3.54
8			NE(1.1+3.8)					
10	NE(0.8+6.6)	12.1	NE(0.5+2.9)	4.7	58*	4.5	178	2.88
14			NE(0.5+2.9)					
18	NE(0.5+5.7)	7.4	NE(0.2+1.4)	2.6	60*	2.6	108	1.8

Table 5.2-4 Data set 1 (1.5 μm PbS detector) - Rise and decay time constants of the main fluorescence lines under 1.5 μm pumping. Inst.- faster than the response of the detector. NE – non-exponential, **Black numbers** - obtained from fits with a single (or double) exponential function, **Blue numbers** – obtained from fits with combined exponential rise and decay function. (R₁+D₁)+(R₂+D₂) - initial (Rise + Decay) form followed by a secondary (Rise + Decay) form. * - large uncertainties (Standard error in the order of 100% or more).

Fl.Line(nm):	1.5 μ m	980	655	520-550	407
		R+D	R+D		
	<i>Rise</i>				
Mol%		ms	μ s		
0.4	Inst.				
0.8					
1.6		6.3	612	R+D ₁ +D ₂ R=10.3 μ s	
4					
8					
10					
14					
18		0.85	432	(R ₁ +D ₁)+(R ₂ +D ₂) R1=4.3 μ s, R2=2.0ms	(R ₁ +D ₁)+(R ₂ +D ₂) R1=9.3 μ s,R2=0.7ms
		<i>Decay</i>			
Mol%	ms	ms	ms		
0.4	9.5				
0.8	10				
1.6	10.3	12.9	5.6	R+D ₁ +D ₂ D1=580 μ s,D ₂ =6.1ms	
4	9				
10	NE(1.8+13.2)				
14					
18	NE(0.8+7.4)	8.9	3.5	(R ₁ +D ₁)+(R ₂ +D ₂) D1=76* μ s,D2=3.1ms	(R ₁ +D ₁)+(R ₂ +D ₂) D1=18 μ s,D2=1.9ms

Table 5.2-5 Data set 2 (1.5 μ m InGaAs detector) - Measured fluorescence rise and decay time constants for 1.5 μ m pumping. Inst.-faster than the response time of the detector; NE-non-exponential decay; **Black numbers** - obtained from fits with a single (or double) exponential function, **Blue numbers** - obtained from fits with combined exponential rise and decay function. R+D₁+D₂ - rise, followed by a two-component decay; (R₁+D₁)+(R₂+D₂) - initial (Rise + Decay) form, followed by a secondary (Rise + Decay) form. * - large uncertainties (Standard error in the order of 100% or more).

with a PbS detector system with a resolution of about 150 μs . At a later stage during the research an InGaAs detector with a much better time response of about 10 μs became available. A second set of measurements (Set 2) with 1.5 μm pumping was performed with the new InGaAs detector. The results from this second set of measurements are presented in Table 5.2-5.

As can be seen in both tables, the decay of Level 1 ($^4I_{13/2}$) exhibited a non-exponential behaviour under direct pumping. This was expected since the cross-relaxation processes are much more significant under direct pumping because of the higher population produced in the level. The long rise in the fluorescence of 980nm line from the $^4I_{11/2}$ level and the fact that it changed markedly with Er^{3+} concentration, indicated that a cross-relaxation process is probably involved in populating this level.

A relatively weak fluorescence line between 800 and 820 nm was also detected. The line was characterised by a fast non-exponential rise with a rate which did not change much with concentration. In the lowest Er^{3+} concentration the rise was followed by two well distinguished (sequential) decays with time constants of 0.14 ms and 4.5 ms. At higher concentrations a long (1 - 2 ms) non-exponential decay was observed.

The red fluorescence line at 655 nm from the $^4F_{9/2}$ level was also observed with 1.5 μm pumping. This fluorescence displayed a long (0.2 - 2 ms), strongly concentration-dependent, rise and a long decay time constant which decreased slowly with concentration.

The relative strong green fluorescence between 520 nm and 550 nm was also measured. Two well-defined sequential structures, each consisting of rise and decay, were observed within this waveform. The first temporal structure was characterised by a rise with a time-constant of about 20 μs , which did not change much with concentration, and a decay with a time constant that decreased from 500 μs in low concentration to about 50 μs in high concentration. The second structure was characterised by a slow rise with a time constant that rapidly decreased with concentration and a slow decay with a time constant that decreased from 6.3 ms to 2.6 ms for a tenfold increase in the erbium concentration.

A waveform of two (rise + decay) structures was also observed in the relatively weak line at about 407 nm. The rise and the decay rates of the initial (rise+decay) structure were similar to those of the green fluorescence. The second rise exhibited

little dependence of the Er^{3+} concentration, while the second decay was characterised by time constants which were roughly double that of those for the second structure in the green fluorescence.

- **Pumping into the $^4\text{I}_{11/2}$ level (Level 2) at 975 nm**

The decay time-constants which attempt to characterise the waveforms for the study of the glasses under 975nm pumping are presented on Table 5.2-6. As with 800 nm pumping at low concentrations, there is a slow rise of the population for Level 1 followed by a slow decay. As with similar data in Chapter 4, two ways of characterising the waveforms and the colour notation have been used.

The temporal behaviour of the population of Level 2 was as expected. The rise was virtually instantaneous and the decay was non-exponential in high Er^{3+} concentrations.

The fluorescence between 830 - 850 nm (the peak was measured at about 850 nm) and the green fluorescence line between 510 nm and 560 nm (see Figure 3.4-3 for spectrum) exhibited similar temporal behaviour. A virtually instantaneous initial rise was followed by another rise with a time constant of a few microseconds and non-exponential decays. Another fluorescence line with a peak at 801 nm was also observed. This line had a very similar decay to the fluorescence at ~ 830 - 850 nm but only an instantaneous rise. This line is not presented in table 5.2-6.

The behaviour of the red fluorescence line at 655 nm was similar to the case with 800nm pumping. This line displayed a concentration-independent rise with a time constant of about 100 μs and a long exponential decay with a rate which increased slightly with concentration.

Two relatively weak lines around 488 nm and 450 nm, as well as the slightly stronger 407 nm line, were also detected. The 488 nm fluorescence displayed an instantaneous rise, followed by a non-exponential decay with an overall decay time constant of the order of a few milliseconds. The 407 nm fluorescence exhibited similar behaviour to that at 450 nm. These lines featured a fast rise with a time constant of a few microseconds followed by a non-exponential decay. An initial instantaneous component of the rise was also detected, but only in low Er^{3+} concentrations.

Fl.Line(nm):	1.5 μ m R+D	980	830-850 ~500-560	655	488	407 ~450
	Rise					
			Inst+			
Mol%	<i>ms</i>		μs	μs		μs
0.4		Instant.			Instant.	
0.8	54*(8.0)		4.1	88		Inst.+3.6
1.6						
4	7.4(8.0)		4.0	85		Inst.+2.3
6						
8						
10	2.2		3.8	111		3.4
12						
14						
16						
18	0.46	2.3	82	1.0		
	Decay					
						Init., Late
Mol%	<i>ms</i>	<i>ms</i>	$\mu s + ms$	<i>ms</i>	<i>ms</i>	$\mu s, ms$
0.4						
0.8	9.1*(8.7)	7.78	NE (211+0.86)	NE (0.6+4.6)	NE(0.26+1.2)	NE 33, 0.6
1.6					NE(0.19+1.6)	
4	15.4(9.3)	8.23	NE (111+4.8)	7.5		NE 60, 2.5
6						
8						
10	16.6	NE (1.5+8.4)	NE (109+2.0)	4.3	NE(0.52+2.6)	NE 126, 1.4
12						
14						
16						
18	7.8	NE (0.5+5.8)	NE (100+1.3)	2.0	NE(0.15+1.2)	NE 162, 0.7

Table 5.2-6 Measured fluorescence rise and decay time constants for 975nm pumping. Inst.-faster than the response time of the detector; NE-non-exponential decay; **Black numbers** - obtained from fits with a single (or double) exponential function, **Blue numbers** - obtained from fits with combined exponential rise and decay function; **Red Numbers** - decay time constants of fluorescing and "filling" levels calculated using an analytical fitting function obtained from a simple 2-level rate-equation model (see Equation 4.2.5), * - large uncertainties

▪ **Pumping into the ($^4S_{3/2}+^2H_{11/2}$) levels (Level 5) at 520 nm**

The results of the study with 520nm pumping are presented on Table 5.2-7. The infrared line at 1.5 μm was measured using the InAs detector system which had a response time of about 10 μs .

The population of Level 1 exhibited a relatively fast rise, varying from a few hundred microseconds at low concentrations to less than 10 μs at high concentrations. As in the case of the 800 nm pumping, the long decay of Level 2 affects the decay of Level 1 and the fits with single exponential functions produced time constants of up to almost 16 ms (the blue numbers). Fitting with the analytically derived function (see Chapter 4, Equations (4.2.3)-(4.2.5) allowed an estimate of about 10 ms (see red numbers) to be obtained for the radiative decay rate of Level 1. At high Er^{3+} concentrations non-exponential decays were observed.

The rate of the rise of the population of Level 2 (980 nm fluorescence line), determined from the measurements of the fluorescence line at 980nm, was similar to the rise of Level 1 (1.5 μm fluorescence line). At high erbium concentration there was also a small additional contribution in the rise of Level 2 with a time constant decreasing from about 220 μs (10mol%) to about 70 μs (18mol%). The decay of the fluorescence from Level 2 was exponential with a decay time-constant of about 8 ms in low Er^{3+} concentration. Non-exponential behaviour was observed at high Er^{3+} concentration.

The red fluorescence line at 655nm exhibited a rise time, decreasing from about 150 μs to about 6 μs with increasing concentration and a decay time decreasing from about 600 μs to about 90 μs over the whole range of Er^{3+} concentrations. An additional second component of the decay with a time constant of a few milliseconds was observed at high erbium concentrations.

Fl.Line: (nm)	1.5 μ m	980	698	655	520-550 (~800-840)	468(~400) (R ₁ +D ₁)+(R ₂ +D ₂) or R+D	410 R+D
	Rise						
		Init., Late				R₁,R₂	
Mol%	μ s	μ s	μ s	μ s		μ s	μ s
0.2		457	Inst. + 159	149	Instant.	R1=(Inst.+12), R2=166	Inst.
0.4	412						
0.8	267	318		153		R1=(Inst.+7), R2=59	Inst.
1.6							
4	38	37	3.4	109		R=(Inst.+2.1)	Inst.+2.6
8							
10	10	10 + 223	5	19		R=(Inst.+1.6)	3.7
14		<10 + 125					
18	< 10	<10 + 66	1.8	5.6	Inst.	2.3	
	Decay						
			Init., Late	Init., Late		D₁,D₂	Init., Late
Mol%	ms	ms	μ s	μ s	ms	μ s	μ s
0.2		7.9	550	605	531	D1=18, D2=318	38, 343
0.4	13.5 (9.7)	(8)					
0.8	15.6 (10.9)	7.7(8)		456	404	D1=20, D2=290	45, 246
1.6							
4	14.7 (10.3)	9.2(8)	37	190	45	D=27	30
8							
10	NE(1.1+9.4)	8.7	11.5	141 + 3.3	8.7	D=6.3	13
14		NE(3.8+10.5)					
18	NE(0.4+3.9)	NE(1.7+7.6)	4.7	93 + 1.4	3.2	D=2.6	4.6

Table 5.2-7 Measured fluorescence rise and decay time constants for 520 nm pumping. Inst.-faster than the response time of the detector; NE-non-exponential decay; ~ - fluorescence line with similar temporal behaviour, **Black numbers** - obtained from fits with a single (or double) exponential function, **Blue numbers** - obtained from fits with combined exponential rise and decay function; R₁+R₂+D - two-component rise followed by a decay. R₁+D₁+R₂+D₂ - initial (Rise + Decay) form, followed by a secondary (Rise + Decay) form. **Red Numbers** -decay time constants of fluorescing and "filling" levels calculated using an analytical fitting function obtained from a simple 2-level rate-equation model (see Equation 4.2.5).

A fluorescence line at 698 nm was also detected with 520 nm pumping. At low concentration, this fluorescence exhibited an instantaneous rise followed by a second component of the rise with a time constant of about 160 μ s. In high Er³⁺ concentrations, it exhibited a fast rise with a time-constant of a few microseconds. The decay time constant of this fluorescence line decreased sharply with Er³⁺ concentration, varying from 500 μ s to a few microseconds.

The green fluorescence line at 520-550 nm showed similar temporal behaviour to the near IR line at 800-840 nm. An instantaneous rise followed by an exponential decay with a time-constant which varied with concentration from about 530 μ s to 3 μ s

was observed. This behaviour was very similar to that of the green fluorescence under 800 nm pumping.

A fluorescence line at 468 nm was also observed under 520 nm pumping. Two (rise + decay) waveforms could be clearly distinguished within the decay of this fluorescence line in low Er^{3+} concentration. The contribution of the second waveform, which had rise and decay time-constants of a few hundred of microseconds, diminished in higher concentrations. A single waveform, consisting of a very fast rise (time constant smaller than the response time constant of the detector) and a single exponential decay was observed in these higher erbium concentrations.

Two overlapping fluorescence lines with different fluorescence intensity were detected around 400 nm. The first was relatively weak, had a maximum fluorescence intensity at around 400nm and its waveforms were similar to those of the 468 nm fluorescence. The second fluorescence line had a peak at around 410 nm and was somewhat similar to the fluorescence line at 698 nm, especially in high Er^{3+} concentrations. In low Er^{3+} concentrations the 410 nm waveform exhibited an instantaneous rise followed by a two-component decay with time constants of several tens and several hundreds of microseconds. A waveform with a rise time-constant of about 2 μs and a decay with a time constant of about 5 μs was observed in high Er^{3+} concentrations.

▪ Pumping into the $^2\text{H}_{9/2}$ level (Level 6) at 403 nm

The fitting results from our measurements with a 403 nm pump are presented in Table 5.2-8. The temporal behaviour of the 1.5 μm and 980 nm fluorescence lines was similar to that observed with 520 nm pumping. Rise time constants of about a few hundred microseconds were observed at low Er^{3+} concentrations and these rise-time constants decreased significantly with increased doping concentration. The decays, however, were exponential and did not show any substantial concentration dependence.

The fluorescence line at 698 nm, detected with 520 nm pumping, was also observed with 403 nm pumping. This line was characterised by a very fast rise and a decay that varied from about 7 μs to about 2 μs over the whole range of erbium concentrations. Two other lines, a weak fluorescence line at 450 nm and a relatively

Fl.Line:	1.5mm	980	698	655	553	520-540	450	407
(nm)				R+D		~800-840	weak	
	Rise							
Mol%	μs	μs		μs		μs		
0.2		337	Inst.	162	Inst.	6.3	< 1 μs Scatered Pump Interfer.	Inst.
0.4		301		140		3.8		
0.8	<260	203				6.4		
1.6	<180					9.0		
4	< 150	45		2.5+98		5.4		
6		36				5.3		
8		24						
10	< 150	15		0.9		3.8		
12		15						
14		11						
16		10		0.8		2.0		
18	< 150	9		0.8		1.2		
	Decay							
					Init , Late			
Mol%	ms	ms	μs	μs	μs	μs	μs	μs
0.2		7.8	6.7	600	9.2 , 525	527		5.8
0.4		7.9		604		554	7.7	
0.8	13.5(8.9)	8.1(8)			9.3 , 348	427	5.6	5.4
1.6	14.0(8.1)	8.3(8)			9.5 , 156	212	5.5	
4	15.9(9.3)	8.6(8)	8.3	259	9.1	47	5.6	6.2
6		8.9			6.9	27		
8		7.8			7.0	18.6		
10	18.1(10.0)	9.6(8)	3.7	168	7.2	15.3	5.0	4.7
12		9.8						
14		9.4			5.6		4.0	3.5
16		8.8		168	5.3	7.4		
18	9.8(7.9)	8.3(8)	1.8	154	3.4	6.2	3.2	2.7

Table 5.2-8 Measured fluorescence rise and decay time constants for 403 nm pumping. Inst.-faster than the response time of the detector; Init.+Late - two-component decay; ~ - fluorescence line with similar temporal behaviour, **Black numbers** - obtained from fits with a single (or double) exponential function, **Blue numbers** - obtained from fits with combined exponential rise and decay function; **Red Numbers** -decay time constants of fluorescing and "filling" levels calculated using an analytical fitting function obtained from a simple 2-level rate-equation model (see Equation 4.2.5). The measurements of the rise of the 450 nm fluorescence line were affected by pump interference.

strong fluorescence at about 410nm, both exhibited similar temporal behaviour to the 698 nm fluorescence.

The waveform of the red fluorescence line at about 655 nm exhibited a complex dependence on Er^{3+} concentration. The rise time was reasonably constant at about 160 μs for concentrations of up to 4 mol%. A second component of the rise of this fluorescence with a much smaller time constant of about 1 μs was evident at higher concentrations (10 - 18 mol%). This faster component did not show any concentration dependence, but its contribution increased markedly and it completely dominated the rise at the highest Er^{3+} concentrations. The decay of this red fluorescence was exponential and exhibited only moderate concentration dependence, decreasing from about 600 μs to about 150 μs over the whole range of Er^{3+} concentrations.

The green fluorescence at 520-550 nm showed similar behaviour to that at 800-840 nm with a rise time constant varying from about 6 μs to about 2 μs and a decay time constant decreasing from about 530 μs to about 6 μs for the whole range of Er^{3+} concentrations.

As was the case with 800 nm pumping, fluorescence at 553-555 nm was detected. This fluorescence exhibited an instantaneous (detector-limited) rise and a two-component decay. The initial decay component was characterised by a decay time constant which decreased from about 9 μs to about 3 μs for the whole range of Er^{3+} concentrations. The second component was observed only in low Er^{3+} concentrations and had a time constant decreasing from 525 μs (0.2 mol%) to 156 μs (1.6 mol%).

5.2.2.2. Dependence of the fluorescence rise and decay times on the pump density (540 nm and 650 nm pumping)

A limited set of data for the effect of the pump energy density on the fluorescence waveforms of some selected lines was obtained for the 540 nm and 650 nm pumping wavelengths. 540 nm was chosen as the pump wavelength simply to allow easy observation of the fluorescence at 520 nm. In fact the exact pumping wavelength in this band is not considered significant as the energy is redistributed very quickly by phonon

processes. The data obtained during these measurements is summarised in the Table 5.2-9 below.

540nm pumping (into ($^4S_{3/2} + ^2H_{11/2}$) levels)				
Fluor. Wavelength	Er ³⁺ Concentration	Pump Energy	Rise	Decay
nm	mol%	mJ	μs	μs
655	0.2	30	162	603
		0.3	178	580
	18	23	6.7	Initial + Late 311 + 3.1 ms
		0.5	7.4	162
520	0.2	3	Inst.	522
	0.4	30	Inst.	478
		2	Inst.	479
		0.3	Inst.	525
	18			Slightly NE:
		40	Inst.	3.4
		7	Inst.	3.9
		0.5	Inst.	4.1
650nm pumping (into $^4F_{9/2}$ level)				
Fluor. Wavelength	Er Concentration	Pump Energy	Rise	Decay
nm	mol%	mJ	μs	μs
655	0.4			
		33	Inst.	156
		0.3	Inst.	157
	< 0.1	Inst.	219	
800	0.2	32	6.2	146
		0.3	5.8	152
	4	3	6.5	145
	18	3	5.5	138
		0.3	5.0	142

Table 5.2-9 Fluorescence rise and decay times as a function of concentration and energy density for 540 nm and 650 nm pumping wavelengths. NE –slightly non-exponential decay. Inst.-faster than the response time of the detector; Black numbers - obtained from fits with a single (or double) exponential function, Blue numbers – obtained from fits with combined exponential rise and decay function. The irradiated spot was approximately constant with an area of approximately 20 mm²(540 nm pump) and 15 mm²(650 nm pump).

This study of the ($^4S_{3/2} + ^2H_{11/2}$) levels under direct pumping was important for the identification of the types of processes involved in the observed strong concentration dependence of the decay rate of these levels (see also Table 5.2-7). It can be seen from

the table above that the green fluorescence (520 nm) under direct pumping showed similar behaviour to that observed for this fluorescence with the 800 nm pump (see Table 5.2-1 and Table 5.2-2). The decay time constant decreased from about 520 μs to about 3.5 μs over the whole range of concentrations. However, the change in the pump energy density did not have any significant effect on the decay.

The $^4\text{F}_{9/2}$ level, which is directly under the level excited by the pump, was also studied under 540 nm pumping. The rise of the red fluorescence line at 655nm, originating from $^4\text{F}_{9/2}$ level, exhibited a significant dependence on the Er^{3+} concentration, but not on the pumping energy density. The decay exhibited only a moderate dependence on the concentration as well as on the pumping energy density (in high Er^{3+} concentration). A long decay time component (3.1 ms) appeared in the decay of this fluorescence in high Er^{3+} concentrations with the highest energy density used in this experiment.

To obtain some information for the intrinsic decay time constant of the $^4\text{F}_{9/2}$ level, the red fluorescence from this level was studied in a very low erbium concentration under direct pumping at 650 nm (see Table 5.2-9). A significant change in the pumping energy density produced very little effect on the decay time constant of the level. The $^4\text{I}_{9/2}$ level, which is directly under the pumped $^4\text{F}_{9/2}$ level, displayed no dependence on the pump energy density nor on concentration.

5.3. Initial populations

Many of the effective cross-relaxation rates of the processes, responsible for the particular temporal behaviour of the levels, depend on the initial population of these levels. Thus calculating the initial population of the levels under various pumping conditions is an important stage of the modelling process. Despite the substantial uncertainties involved in these calculations, especially when ESA is involved, the values obtained are considered as a reasonable starting point for the numerical modelling and the discussions presented in the following sections.

5.3.1. Initial population for 800 nm pumping

There are two levels which are populated during the pump pulse; Level 3 ($^4I_{9/2}$) via direct absorption of pumping energy by ground state ions, and Level 6 ($^2H_{9/2}$) via ESA from Level 3. While the initial population of Level 3 can be easily calculated (see Equation (4.3.2)), this is not the case for the initial population of Level 6. The problem is that the ESA cross-section is difficult to measure. It is, however, possible to obtain an approximate estimate of the ESA cross-section from Level 3 to Level 6 as discussed below.

The integrated absorption cross section (σ^i) for a transition between two states (1 and 2) can be shown to be given by (Hilborn, 1982):

$$\sigma^i = \frac{1}{4} \frac{g_2}{g_1} \lambda_{21}^2 A_{21} .$$

Here A_{21} is the spontaneous emission rate from state 2 to state 1, g_1 and g_2 are the degeneracy factors of the two states and λ_{21} is the transition wavelength. With the narrow bandwidth pumping used in the present measurements, the absorption cross section (σ_{12}^λ) at the pumping wavelength (λ) rather than the integrated one is needed. If one makes the assumption that the fluorescence line-widths for two transitions are similar, then the ratio of monochromatic absorption to integrated absorption cross sections for these two transitions should also be similar. With this assumption,

$$\sigma_{36}^\lambda = \sigma_{03}^\lambda \frac{\sigma_{36}^i}{\sigma_{03}^i} .$$

Here the three levels under consideration are denoted 0($^4I_{15/2}$), 3($^4I_{9/2}$) and 6($^2H_{9/2}$). The necessary parameters for estimating the ratio of integrated cross-sections are available from Shinn *at al* (1983) for Er^{3+} in ZBLA glasses ($A_{30} = 90.6 \text{ s}^{-1}$ and $A_{63} = 11.9 \text{ s}^{-1}$). Since $g_0=16$, $g_3=10$ and $g_6=10$:

$$\sigma_{03}^i / \sigma_{36}^i = \frac{g_3 / g_0}{g_6 / g_3} \frac{A_{30}}{A_{63}} \approx 5 . \quad 5.3.1-1$$

The peak cross-section at 802nm was measured to be $\sigma_{03}^{800nm} = 6.3 \times 10^{(-22)} \text{ cm}^2$ (see Chapter 3). Therefore a very approximate value of σ_{36}^{800nm} is $\sim 1 \times 10^{(-22)} \text{ cm}^2$. The expression $n_{30} = E \sigma_{03} / h\nu S$ for calculating the initial normalised population per unit

volume for Level 3 under 800nm pumping was already introduced in Chapter 4. Applied to the initial population of Level 6 this gives:

$$n_{60} = E\sigma_{36}^{800\text{nm}} n_{30} / h\nu S \text{ no.} \quad 5.3.1-2$$

Using $\sigma_{36}^{800\text{nm}} / \sigma_{03}^{800\text{nm}} \approx 0.2$ and $n_{30}/n_0 \approx n_{30} \approx 0.0005$ (for 800 nm pumping with the pumping energy density used in this experiment - see Chapter 4), we obtain $n_{60}/n_{30} \approx 1 \times 10^{(-4)}$ or $n_{60} \approx n_{30} \times 1 \times 10^{(-4)} \approx 5 \times 10^{(-8)}$.

The main source of uncertainty in n_{30} was due to the uncertainty in the estimate of the irradiated area caused by the non-uniform spatial distribution of the pump beam and the non-linear nature of the visualisation of the spot via polaroid film burns or IR cards. However in this calculation of n_{60} , the effect of this uncertainty is probably exceeded by the uncertainty caused by the assumption of equivalence between the ratio of the monochromatic and integrated absorption cross-sections for two transitions. While in these circumstances it is difficult to estimate the overall uncertainty of n_{60} , the actual value can be expected to be within an order of magnitude of that estimated above.

5.3.2. Initial populations for other pumping wavelengths

The calculations for the initial populations of Level 3 ($^4I_{9/2}$), Level 2 ($^4I_{11/2}$) and Level 1 ($^4I_{13/2}$) in the case of a direct pumping with 800 nm, 980 nm and 1.5 μm respectively were already discussed in Chapter 4. The initial populations of Level 5 and Level 6 under direct pumping were calculated in a similar way. Analysis similar to that in the previous section was used to calculate the initial populations of levels populated by ESA in the case of all pumping wavelengths other than 800 nm. As in the case with 800 nm pumping, the main source of uncertainties in the calculated values for the initial populations of the directly pumped levels was the uncertainty of about 50% in the estimate of the area of the pumping spot. As mentioned previously, this uncertainty is caused by the non-uniform spatial distribution of the pump energy and the non-linear nature of the visualisation of the spot. In the estimate of the initial populations of the ESA-populated levels, a much larger uncertainty is expected (see previous section).

This was even further complicated in the case of the multi-step ESA under 1.5 μm and 975 nm pumping. Here no information was available about the spontaneous emission rates from levels such as $^2\text{H}_{11/2}$, $^4\text{F}_{7/2}$ and $^2\text{P}_{3/2}$ to the lower levels and the corresponding monochromatic ESA cross-sections were simply assumed equal to the monochromatic ground absorption cross-sections. Initial populations due to ESA were not calculated in the case of 403nm and 520nm pumping, where the destination levels were high up in the energy level diagram and no fluorescence data was available for modelling. The values of the monochromatic ground state absorption cross-sections in our glasses have already been discussed in Chapter 3. All radiative rates used in the calculations are from Shinn *et al.* (1983). The results of the calculations are presented in Table 5.3-1 below.

Pumping Wavelengths:							
1.5 μm		975 nm		520 nm		403 nm	
h ν (cm $^{-1}$)	6670	h ν (cm $^{-1}$)	10260	h ν (cm $^{-1}$)	19230	h ν (cm $^{-1}$)	24800
E $_{\text{pump}}$ (mJ)	6	E $_{\text{pump}}$ (mJ)	14	E $_{\text{pump}}$ (mJ)	16	E $_{\text{pump}}$ (mJ)	1.5
S(mm 2)	10 \pm 5	S(mm 2)	13 \pm 7	S(mm 2)	16 \pm 8	S(mm 2)	4 \pm 2
σ_{01} ($\times 10^{-21}$ cm 2)	4.7	σ_{02} ($\times 10^{-21}$ cm 2)	2	σ_{05} ($\times 10^{-21}$ cm 2)	11.5	σ_{06} ($\times 10^{-21}$ cm 2)	1.4
n$_{10}$ ($\times 10^{-3}$)	2\pm1	n$_{20}$ ($\times 10^{-3}$)	1\pm0.5	n$_{50}$ ($\times 10^{-3}$)	3\pm1.5	n$_{60}$ ($\times 10^{-3}$)	0.2\pm0.1
g $_0$	16	g $_0$	16				
g $_1$	14	g $_2$	12				
g $_3$	10	g $_5$	8				
A $_{10}$ (s $^{-1}$)	73.5	A $_{20}$ (s $^{-1}$)	90				
A $_{31}$ (s $^{-1}$)	29	A $_{52}$ (s $^{-1}$)	NA				
σ_{01}/σ_{13}	4	σ_{02}/σ_{25}	1 A				
n$_{30}$ ($\times 10^{-6}$)	1	n$_{50}$ ($\times 10^{-6}$)	1				
g $_5$	12	g $_7$	4				
σ_{35}/σ_{13}	1 A	σ_{57}/σ_{25}	1 A				
n$_{50}$ ($\times 10^{-9}$)	0.5	n$_{70}$ ($\times 10^{-9}$)	1				

Table 5.3-1 Values of the parameters used and the initial populations of levels (populated directly or via ESA) calculated for various pumping wavelengths. For assignment of the levels – see Foldout Table. NA – not available, A – assumed.

5.4. Analysis and discussions

At this point all the tables of data summarising the features of the measured fluorescence decay curves have been presented. The following sections analyse this data in order to identify the main processes behind the observed temporal behaviour of the population of the levels. A comprehensive rate equation model including all eight levels on the Foldout Diagram was developed. The details of this model will be presented in the next section. The process of analysis comprised numerical solutions of this model being constantly plotted and compared to the observed fluorescence waveforms. This allowed the effect of the inclusion of various cross-relaxation processes on the population dynamics of the affected levels to be studied.

5.4.1. Analysis and Discussions in the case of 800 nm pumping

An extensive modelling process was undertaken to study the implications of different cross-relaxation processes on the temporal behaviour of the populations of all the affected levels in the $\text{Er}^{3+}/\text{ZB(L)AN}$ system under 800 nm pumping. The three lowest energy levels and some of the cross-relaxation processes important for their observed temporal behaviour were already discussed in Chapter 4. These discussions, however, were limited within the frame of the three-level model considered there. That is why all the processes (see Foldout Diagram) were reconsidered in order to test the validity of our previous conclusions within the framework of the eight-level system with very complex interactions among all of the levels. Because of these interactions, the arguments for or against a particular process which is thought to be affecting a given level, were often derived not only from the implications for this level, but also from the consequent effects on other levels. These other levels very often had smaller populations and were thus more sensitive to variations in cross relaxation processes.

Hence a consideration of the temporal behaviour of the populations of the higher levels ($^4F_{9/2}$, $^4S_{3/2}+^2H_{11/2}$, $^2H_{9/2}$ etc.) added a new dimension to the modelling process.

The two figures below (Figure 5.4-1 and Figure 5.4-2) show various cross-relaxation processes which will be discussed later in this section. Figure 5.4-1 shows all of the processes considered important in the overall modelling. All of the processes in this figure have a very small energy mismatch of less than 550cm^{-1} , which is the approximate energy of the fundamental phonon of the ZB(L)AN glass. A colour code has been used which groups the processes in accordance to the level mostly affected. However, because of the complex interconnections among the populations of all energy levels, a process affecting a particular level also affects other levels. Thus the colour code should be regarded only as an approximate indicator.

Figure 5.4-2 shows other possible cross-relaxation processes that have been considered at different stages of the modelling process. For various reasons, however, they have been discarded and omitted from the final model. Nevertheless, these cross-relaxation processes and all the related discussions have been considered important for a good understanding of the modelling process. For simplicity it was decided to structure the discussion level by level, starting from the lowest energy level ($^4I_{13/2}$) and moving up level by level.

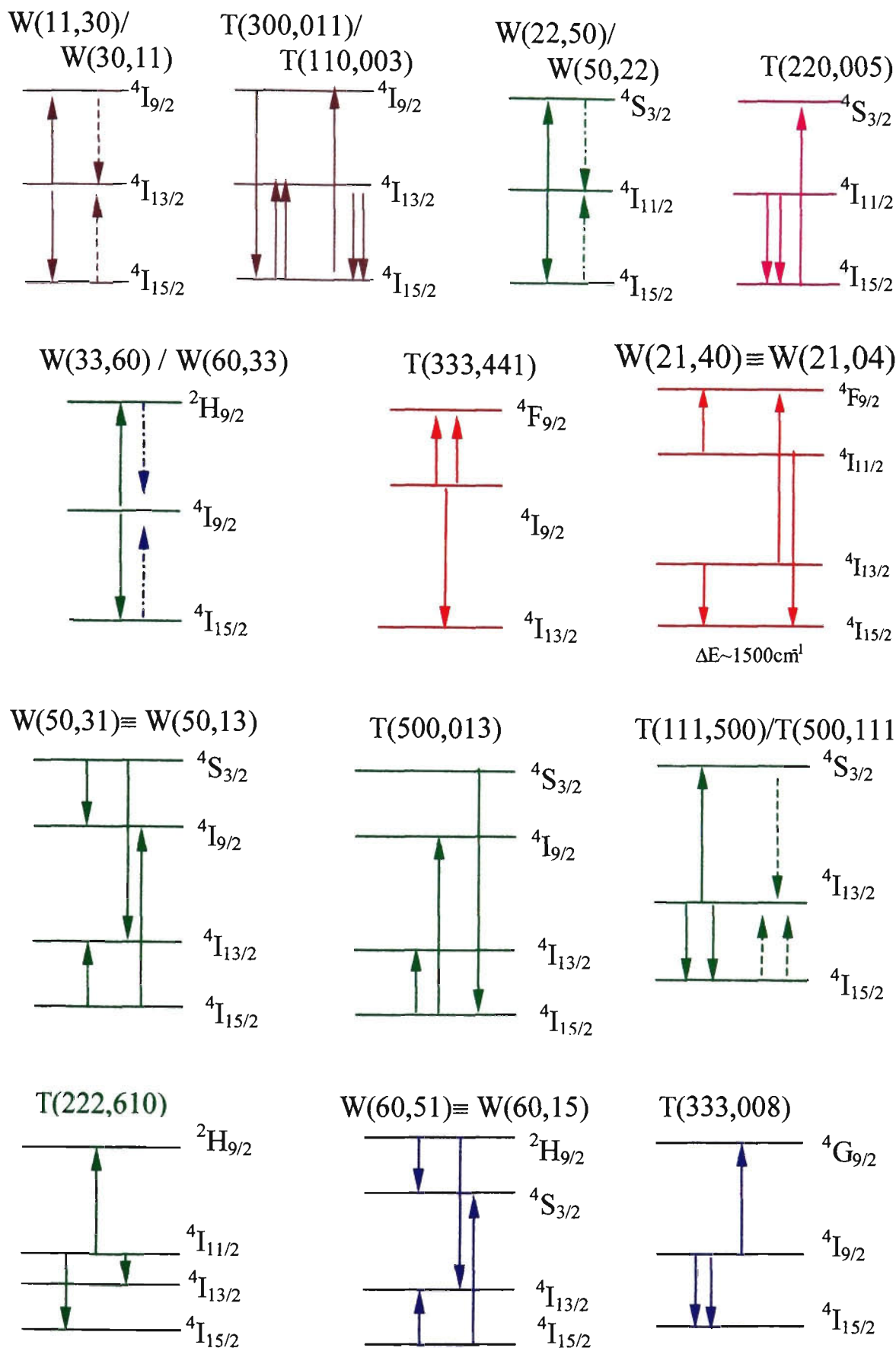


Figure 5.4-1 Cross-relaxation processes included in the extended model: - - - possible, but not very important cross-relaxation processes. The colour relates to the level mostly affected: Level 1- ■ Level 2- ■ Level 4- ■ Level 5- ■ Level 6- ■. For all processes presented the energy mismatch ΔE is $\leq 550\text{cm}^{-1}$ (except where indicated).

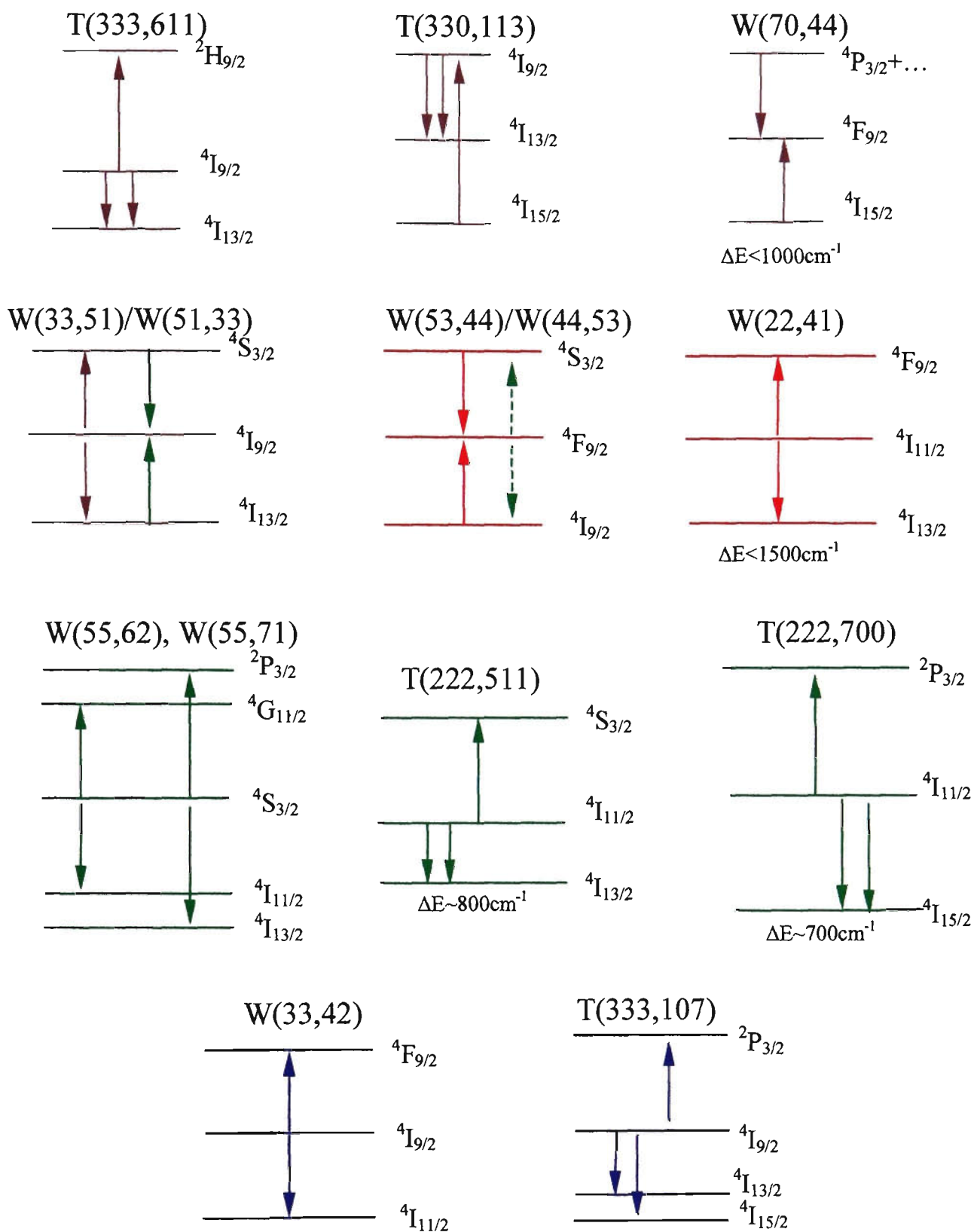


Figure 5.4-2 Cross-relaxation processes omitted from the extended model; - - - - possible, but not important cross-relaxation processes. The colour relates to the level predominantly affected: Level 1- ■ Level 2- ■ Level 4- ■ Level 5- ■ Level 6- ■. For all processes presented the energy mismatch ΔE is $\leq 550 \text{ cm}^{-1}$ (except where indicated).

5.4.1.1. Level 1 ($^4I_{13/2}$)

- Rise

The numerical analyses of the rise of Level 1 under 800 nm pumping indicated that in low Er^{3+} concentration it is relatively slow (see Table 5.2-1 and Table 5.2-2) and originates mainly from the radiative and non-radiative decay from Level 2. In higher Er^{3+} concentrations there is also a contribution from Level 5 via processes T(500,013).

As was pointed out in Chapter 4, the most notable feature in the rise of the population of Level 1 was the presence of a fast component with contribution to the overall rise that was minimal in low concentrations, but increased dramatically and completely dominated at the highest Er^{3+} concentrations. It was also pointed out in Chapter 4 that the origin of this fast rise was Level 3. There were two reasons for this conclusion. Level 3 decays with a rate which is appropriate to explain the rise of Level 1. Also only Level 3 has a population which is large enough to have a significant effect on the relatively large population of Level 1 under 800 nm pumping.

The previously reported cross-relaxation process W(30,11) (see Figure 5.4-1) was not able to model the remarkable change in the contribution of this fast rise component with doping level. Process W(33,51) (see Figure 5.4-2) was also considered. As will be discussed later in the chapter, the Level 5 waveform is the result of a fine balance between two components, the relative magnitude of which change with concentration. While somewhat more successful than process W(30,11) in modelling the rise of Level 1, process W(33,51) contributed a significant population to Level 5 and in doing so increased the contribution of the initial component of the waveform in a manner which was inconsistent with observation. Hence W(33,51) has been excluded from the model.

The lack of success in explaining the initial component of the rise of Level 1 via two-ion process indicated that consideration of a three-ion process was necessary. A three-ion process has a sufficiently strong concentration dependence to explain the observed rate of change of the waveform with doping level. In addition, as the decay of Level 3 was not strongly dependent on doping concentration or pumping energy density (see Table 5.2-3), the required process would need to be such that the population of Level 3 was not substantially disturbed.

The three ion process T(333,611) (Figure 5.4-2) was able to successfully model the fast rise of Level 1. However, its contribution to Level 6 was substantial and since virtually all of the population of this level decays quickly to Level 5 the initial decay of Level 5 was again inconsistent with observation. The population of Level 4 was also affected in a manner inconsistent with its observed fluorescence waveform. Thus process T(333,611) cannot play a very significant role and has been discarded from the model.

Another three ion process, T(333,441) (Figure 5.4-2), could also be incorporated at a level which explained the observed rise of Level 1. However, in this process out of every three ions in Level 3 two are excited to Level 4 and only one is contributed to Level 1. The result, apart from overpopulating Level 4, is that to successfully model the rise of Level 1, this process had to be used with a relatively large rate constant. This large rate constant caused the redistribution of a substantial amount of population from Level 3. This strongly affected not only the decay of Level 3 but also the system as a whole. Virtually all the population of Level 3 decays non-radiatively into Level 2 and whenever the population of Level 3 is affected, the population of Level 2 is also affected. Higher levels such as Level 5 and Level 4 were also affected in ways which are inconsistent with observed fluorescence waveforms. For these reasons, T(333,441) cannot be included in the model, except at a smaller rate (i.e. a small value of the relevant rate constant).

It should also be pointed out that processes such as T(333,441), T(333,611), and even W(33,51) are likely to be less probable when compared to similar process including ions from the ground state. The main reason for this is that with the pumping conditions of our experiments, the normalised population of any excited level was several orders of magnitude smaller than that of the ground state (see Table 5.5-1). The probability of all these cross-relaxation processes is a function of the distance between neighbouring ions, and therefore on the population of the levels involved. This does not mean that these processes are not present at all in the dynamics of the system. In the higher doping levels used in this study even a very small normalised population corresponds to an appreciable absolute population. Thus while these processes are less probable, their presence is still considered possible.

Both three ion processes T(330,113) and T(300,011) (see Figure 5.4-1) were found to satisfy well both the rate and magnitude of the contribution of the fast rise with doping concentration. In line with the discussion from the previous paragraph, process T(300,011) involves two ions from the ground level and therefore it was considered to have a higher probability than T(330,113). For that reason alone, process T(300,011) was introduced and T(330,113) was excluded from the model.

- Decay

When modelling the decay of Level 1 there were three initial considerations to be taken into account:

(a) No substantial concentration quenching was exhibited by this level when pumped with 800 nm. The decay time constant decreased from 9 ms to about 7 ms and the decay remained exponential over the whole range of Er^{3+} concentrations used. Under direct pumping at 1.5 μm where a larger number of ions are excited to Level 1 (compare n_{10} (1.5 μm pump) and n_{30} (800nm pump) from section 4.3.1) this was not the case. Under these conditions non-exponential behaviour was observed with the initial decay rate being up to 10 times faster than the later one.

(b) With the use of T(300,011), the fast rise of Level 1 was adequately modelled. The fine balance in the decay-waveform of Level 5, which will be discussed later, was also achieved. Although the rise was satisfactorily modelled, there remained some inconsistency in the decay behaviour of Level 1. This decay depends on W(11,30) and use of a value consistent with that obtained from direct pumping resulted in a modelled decay which was longer than that observed. Also such a value resulted in a decay of Level 2 which was shorter than that observed. The solution to these problems could not be found in a simple increase in the value of the rate constant for the process W(11,30). Such an increase would have affected the decay of Level 1 at low concentration. There was clearly a need for a process which had the effect of producing a redistribution of population between these two levels - moving some ions from Level 1 back into Level 2.

(c) The final consideration involved the modelling from Chapter 4, which gave not only an initial estimate of the cross-relaxation process W(11,30) but also a

strong indication for the presence of the three-ion process T(110,003) (see Figure 5.4-1).

The overall conclusion from points (a) - (c) above was that the three-ion process T(110,003) also needed to be involved in the model. The numerical modelling including all 8 levels confirmed this conclusion.

While the inclusion of only the three-ion process T(110,003) was able to explain the main features of the population of the Level 1 over the whole range of concentrations, the modelling of this population at lower concentrations was slightly improved by the inclusion of a mixture of W(11,30) and T(110,003). Despite the fact that the improvement was only marginal, both processes have been included in the model.

5.4.1.2. Level 2 ($^4I_{11/2}$)

- Rise

As was already discussed in Chapter 4, the rise of Level 2 was consistent with the measured decay time of Level 3 (800 nm pump level) which is directly above Level 2. This consistency of these two rates indicated that a direct decay (in this case a phonon-assisted one) from Level 3 is responsible for the build up of the population in Level 2.

- Decay

As can be seen in Table 5.2-1 and Table 5.2-6, the decay of Level 2 had a time constant of about 8 ms in low concentrations and a non-linear decay in high concentration. This non-linear decay was especially evident under direct pumping, where a two-exponential fit gave a ratio between the initial and the late decay-rate of the order of 10:1. As will be discussed later in this chapter (see late decay of Level 5), a combination between the two-ion cross-relaxation process W(22,50) and the three-ion cross-relaxation process T(220,055) (see Figure 5.4-1) was found to best satisfy the observed waveforms for both the temporal behaviour of the populations of Level 2 and Level 5 for the whole range of Er^{3+} concentrations. Both processes involve two ions from Level 2 and the rate equation for Level 2 had the form:

$$\begin{aligned}\frac{dn_2(t)}{dt} &= -(A_2 + \omega_{21})n_2(t) - WCn_2^2(t) - TC^2n_2^2(t) = \\ &= -[(A_2 + \omega_{21}) + (WC + TC^2)n_2(t)]n_2(t).\end{aligned}$$

In line with the discussions in Section 5.2.1.2 (see equations 5.2.1-9 to 5.2.1-11) a non-exponential behaviour could be expected in high concentrations and under heavy pumping conditions where the term $(WC+TC^2)n(t)$ starts to dominate the term $(A+\omega)$. The experimental data in Table 5.2-1 and Table 5.2-6 confirmed that to be the case. It turns out that Level 5 provides a more sensitive indicator of the balance between $T(220,005)$ and $W(22,50)$ and so this matter will be further discussed in the section dealing with Level 5.

5.4.1.3. Level 3 (${}^4I_{9/2}$)

As has been mentioned before, Level 3 decays almost entirely non-radiatively (via multiphonon assisted decay) into Level 2. For that reason its fluorescence is very weak and it was detected only under direct pumping at 800nm. As shown in Table 5.2-1, with direct pumping the decay rate of this level did not show a substantial variation with concentration. This decay rate decreased only slightly from about 9 μ s to about 6 μ s over the whole range of concentration used. This was an indication of the fact that cross-relaxation processes involving the population of this level do not substantially affect the level.

5.4.1.4. Level 4 (${}^4F_{9/2}$)

Level 4(${}^4F_{9/2}$) is another level which decays mainly via multiphonon assisted decay (compare A_4 and ω_4 in Table 5.5-2). Its relatively weak fluorescence suggests that it has a small population in almost all pumping conditions except for the case of direct pumping. There are two consequences of this, the first is that the red fluorescence at about 655 nm is relatively difficult to measure and the second is that the population of this level is very sensitive to contributions from any processes – radiative or non-

radiative. All this made the modelling of the temporal behaviour of the population of Level 4 both difficult and important.

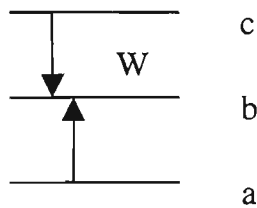
- Rise

There are two distinctive components in the rise of Level 4 – an initial and later rise. The initial rise has a time constant that is independent on the Er^{3+} concentration but its contribution to the total rise increases significantly in high concentrations. This dramatic change in the contribution suggests that a cross-relaxation process is involved.

A combination of two processes was considered to explain the initial rise. First a cross-relaxation process populates a level somewhere above Level 4. This would explain the changing contribution with concentration. Secondly, the level populated in this manner then populates Level 4. There are two possible ways for this population to find its way to Level 4 that could explain the observed lack of change of the time constant with concentration. One way is a multi-phonon-assisted or radiative decay from this higher level to Level 4. Since the time constant of the fast rise was about 5 μs and the level directly above Level 4 (Level 5) had a multiphonon decay time of about 2 ms, it is not possible that this multiphonon decay is responsible for the fast component in the rise of Level 4. A radiative decay from a level above Level 4, initially populated from a cross-relaxation process, looked like the most probable source for this fast rise. Level 6 was a very good candidate to represent this hypothetical source-level. Its decay (see Table 5.2-1 and Table 5.2-2) was of the same order of magnitude as the fast rise, only slightly changing from about 8 μs to about 3 μs over the whole range of Er^{3+} concentrations. There was also a strong indication that a cross-relaxation process is involved in the population of Level 6, since it also had a fast component in its rise. The contribution of this fast component to the rise of Level 6 increased significantly with Er^{3+} concentration. More thorough analysis, however, showed this explanation to be highly unlikely. A later discussion will show that the fast rise of UV fluorescence at about 400 nm, which was initially thought to be associated with Level 6, is more likely to emanate from another level. Also, virtually all the ions from Level 6 reached Level 5 via multi-phonon assisted decay (compare A_6 and ω_6 in Table 5.5-2). The branching ratio of the radiative decay from Level 6 to Level 4 was also very small (about 0.01) and hence radiative decay from Level 6 has negligible effect on the population of Level 4.

Virtually all ions which populate Level 6 subsequently decay to Level 5 and of these approximately 20% decay via a multi-phonon assisted process to Level 4. This is the mechanism of the second and slower component of the rise of Level 4. It is not possible for the tiny contribution from the radiative decay from Level 6 to compete with the substantial slow component in the rise of Level 4 due to the multi-phonon decay of Level 5. So if a radiative decay was to be responsible for the fast component in the rise of Level 4 it had to come from a well-populated level higher up in the system.

There is, however, another possible explanation for this fast component. A direct population from a cross-relaxation process involving the ground level (such as W(70,44) (see Figure 5.4-2)) was also considered. A schematic diagram for the general case of such a process is:



This case has previously been discussed (see Equation 5.2.1-4), but only with reference to the decay of level c. If level a is the ground level, level c has an exponential decay with a time constant of τ_c , level b has a decay time constant $1/(A_b + \omega_b) = \tau_b$ and W is the only cross-relaxation process affecting level b, the normalised population of level b could be expressed as:

$$n_b(t) = 2 \frac{WC n_{c0} \tau_b \tau_c}{(\tau_b - \tau_c)} (-e^{-t/\tau_c} + e^{-t/\tau_b})$$

If one considers a case such as W(70,44), providing $\tau_b \gg \tau_c$ this equation simplifies to

$$n_b(t) = 2WC n_{c0} \tau_c (1 - e^{-t/\tau_c}) e^{-t/\tau_b}$$

Applied to W(70,44) this equation predicts a rise of Level 4 which depends on the decay time constant of level 7. However, the decay time of Level 7 is around five hundred microseconds (Table 5.5.-3) and so an explanation of the rise of Level 4 based on the process W(70,44) is not possible.

A similar process W(61,44) was also considered and later disregarded. Even though the lower level involved in this process is not the ground state, its population is

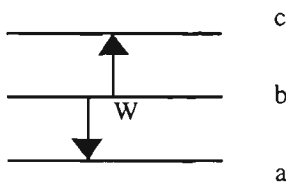
effectively constant during the rise of Level 4 as its decay time is long compared to other times being considered. However, the fast rise of Level 4 was evident in concentrations as low as 4 mol%, where the rise time of Level 1 was still of the order of 10 ms (the fast rise component of Level 1 becomes evident in concentrations above 8 mol%). The low population of Level 1 during the first several tens of microseconds is an indication of an extremely low probability of process W(61,44) (it should also be remembered that Level 6 also has a relatively small population for all Er³⁺ concentrations). Therefore this process was also disregarded.

The group from Phillips Research Laboratories in the Netherlands (Oomen *et al.*, 1990; van Dongen *et al.*, 1991) also considered the problem of the population of the ⁴F_{9/2} level (Level 4) under CW 800 nm excitation. They considered that the population of this level arose from non-radiative relaxation of Level 5 at low concentration (< 1 mol%). At higher concentrations (up to 5 mol%) they ascribed the increased population of this level to the process W(53,44). This conclusion was based on an examination of the power dependence of the emission intensities of the levels. We disagree with their conclusion that the population of Level 4 at higher concentrations can be explained by this process. We have data covering a larger concentration range than the Phillips group and we also have data on the time resolved fluorescence following rapid pulsed excitation. Our data does not support their conclusion. The rise time of Level 5 is similar to that of Level 4. An analytical solution of this system where the populating (Level 5) and populated level (Level 4) rise with similar time constants was somewhat more complex and difficult to express in terms of rise+decay exponential functions. Numerical modelling (including all 8 levels) showed that while the process W(53,44) was reasonably successful in modelling the rate of the fast rise of Level 4, it was not able to predict the observed change in the contribution of this fast rise to the overall rise of the level as the concentration was increased.

Another possible explanation for the fast rise of Level 4 involves direct population from the process W(33,42) (see Figure 5.4-2). Below we discuss this process in some detail before concluding that it does not explain the observed fluorescence data. The reason for the negative conclusion is simply that the numerical modelling does not give results which are consistent with the observed fluorescence waveforms. However, an understanding of what is happening is assisted by some more

approximate modelling so that one can use analytic expressions for the behaviour of the populations of the levels. We first consider a general two-ion process of the type represented by W(33,42) and then go on to apply the results to this particular process.

If a two-ion cross-relaxation process W, with two ions originating from the same level b, is populating another level c the process could be represented on the diagram below:



An assumption can be made that the decay of level b is not disturbed significantly during its exponential decay via radiative and multi-phonon processes. That would mean that not only the particular cross-relaxation process under consideration, but also all other processes affecting this level, are weak enough not to disturb its decay significantly during the time of the observation. The assumption that level b is not affected too much would mean that the normalised population of level b could be written as $n_b(t) = n_{b0}e^{-t/\tau_b}$, where $\tau_b=1/(A_b+\omega_b)$ is the decay time of level b in the absence of cross-relaxation processes.

One more assumption could also be made in order to simplify the analysis. This is that the process W is the only process which affects level c during its rise. If now $\tau_c=1/(A_c+\omega_c)$ is the decay time of level c in the absence of cross-relaxation processes, it can be shown (see Section 5.2.1.1) that in the absence of initial population on level c its normalised population can be expressed as:

$$n_c(t) = -\frac{WCn_{b0}^2\tau_c\tau_b}{2\tau_c - \tau_b} (e^{-t/(\tau_b/2)} - e^{-t/\tau_c})$$

To analyse the implications of this expression for the rise and decay of level c, it is useful to consider two limiting cases:

(i) If $\tau_b \gg \tau_c$, the above equation simplifies to

$$n_c(t) \approx +WCn_{b0}^2\tau_c(1 - e^{-t/\tau_c})e^{-t/(\tau_b/2)} \quad 5.4.1-1$$

In other words if $\tau_b \gg \tau_c$ level c will rise with a time constant which is approximately equal to its own decay time constant. The decay time constant of level c is expected to be approximately half that of level b.

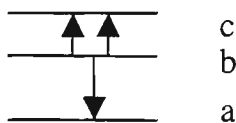
(ii) Similarly it can be shown that if $\tau_b \ll \tau_c$ the population of level c can be written as

$$n_c(t) \approx + \frac{1}{2} W C n_b^2 \tau_b (1 - e^{-t/(\tau_b/2)}) e^{-t/\tau_c} \quad . \quad 5.4.1-2$$

Thus in the case, when $\tau_b \ll \tau_c$, the population of level c rises with a time constant approximately equal to one-half of the decay time constant of level b and decays with its own decay time constant.

It is the second of the above two cases ($\tau_b \ll \tau_c$) that indicates that a direct population of Level 4 via a two-ion cross-relaxation process originating from a single level could be responsible for the fast rise component of Level 4. Level 3 in the $\text{Er}^{3+}/\text{ZB(L)AN}$ system is the ideal candidate for this source level (see process W(33,42) in Figure 5.4-2). It is highly populated and has a decay rate, which is very similar to the rate of the fast component in the rise of Level 4. The relatively constant decay rate of Level 3 with concentration indicates that this level has not been affected strongly by any cross-relaxation processes. Thus the main assumption for deriving the above analytical expressions is satisfied. Apart from that, the intrinsic decay rate of Level 4 is much slower than the rate of its fast rise. Therefore during the initial part of the rise of Level 4 the other assumption is also satisfied, since the process W is the only source of population of Level 4 and the only process which affects Level 4. And as a final consideration it should be remembered that Level 3 has a decay-time that is much smaller than the decay time of Level 4. Thus the conclusion reached above for the case when $\tau_b \ll \tau_c$ is valid, i.e. Level 4 should rise with a time constant roughly equal to one-half of the decay time constant of Level 3. The experimental data in Table 5.2-1 is consistent with this analysis. Thus it is possible for process W(33,42) to explain the rapid rise of the population of Level 4. However, this is not the full story and one needs to check also that it can explain the changes in shape of the fluorescence waveform (i.e. changing contribution of the fast rise to the overall rise) of Level 4 with concentration. Before considering this it is useful to consider one more process which is somewhat similar in its effect on Level 4 to W(33,42).

The general case of a three-ion cross-relaxation process such as T(333,441) (see Figure 5.4-1) can be represented using the energy level diagram below:



Under the same assumptions that applied to level b for the two-ion case discussed above, the rate equation for level c is now:

$$\begin{aligned} \frac{dn_c(t)}{dt} &= -(A_c + \omega_c)n_c(t) + 2TC^2 n_b^3(t) = \\ &= -n_c(t)/\tau_c + 2TC^2 n_{b0}^3 e^{-t/(\tau_b/3)}. \end{aligned} \quad 5.4.1-3$$

The solution to this equation is:

$$n_c(t) = -\frac{2TC^2 n_{b0}^3 \tau_c \tau_b}{3\tau_c - \tau_b} (e^{-t/(\tau_b/3)} - e^{-t/\tau_c}). \quad 5.4.1-4$$

The amplitude of the population of level c now depends on the square of the concentration. It can be seen that when $\tau_b \gg \tau_c$ the population of level c would rise with a time constant approximately equal to that of its own decay and would decay with a time constant which is three times smaller than that of level b. Similarly, when $\tau_b \ll \tau_c$, the population of level c rises with a rate which is three times faster than the decay rate of level b and decays with its own decay rate. An inspection of Table 5.2-1 would show that the rate of the fast rise of Level 4 is slower than one third of the decay rate of Level 3. However in Table 5.2-3 the rates of rise of Level 4 at high concentrations are approximately equal to one third of the decay rate of Level 3. It should be remembered that the analysis above is based on analytic expressions which are only approximate. Thus the conclusions about the ratios between the various rates should be considered as only approximate and more indicative of trends rather than interpreted in terms of exact values. Therefore, on the basis of the analyses above, both W(33,42) and T(333,441) could contribute to the fast component of the rise of the population of Level 4.

It is difficult to decide which of the possible processes should be included in the model to account for the fast rise of Level 4. Aside from the effects on Level 4, processes W(33,42) and T(333,441) have effects on different other levels in the system. However, this does not help in distinguishing between them as these effects are

relatively small. The only way to make a decision is to examine independently the effects of processes such as W(53,44), W(33,42) and T(333,441) on the shapes of the predicted fluorescence waveforms using the numerical model. Choices can then be made to get the best correspondence between measurement and model. If the inclusion of only one process can give a reasonable fit between measurement and model, then combinations of processes do not need to be considered.

The numerical modelling revealed that processes W(53,44) and W(33,42) were unable to explain the change in the contribution of the fast component to the overall rise of Level 4 with doping concentration. If their cross-relaxation constants were large enough to correctly predict the relative contribution of this fast rise at high Er^{3+} concentrations then the contribution at low concentrations was too large. Similarly, if the rate constants were small enough to correctly predict the contribution at low concentrations, the contribution at high concentrations was too small. Process T(333,441) (see Figure 5.4-1), on the other hand, was able to model the rate of the fast component of the rise as well as its contribution to the total rise of Level 4 at all concentrations. Since this is the only process which gives a fit between measurement and model and because this fit is quite good, this is the only process affecting the fast rise of level 4 which has been included in the final model.

Apart from the initial fast rise, there was also a late component of the rise waveform of Level 4 that exhibited a time constant of about 100-110 μs which did not change much with concentration. The rate of this late component of rise was somewhat surprising since it was assumed that this rise originates from Level 5 via radiative and multiphonon-assisted decays. Under these circumstances, one would expect that the population of Level 4 would rise with a time constant determined by the decay of Level 5 and decay with its own decay time constant. However, because of the repopulation effects of cross-relaxation processes such as W(22,50) and T(220,005), the overall decay time constant of Level 5 is in the order of several milliseconds. This is substantially longer than the expected intrinsic decay time constant of Level 4 (see Table 5.5-2). This is then the situation covered by the discussion of Chapter 4 (see section 4.2.2, page 4-14, with $\tau_1 < \tau_2$). Under these conditions, waveform rise and decay time constants appear to be interchanged and the population of Level 4 rises with the intrinsic decay time constant of Level 4 and decays with the decay time constant of

Level 5. However, the decay time constant exhibited by Level 4 was actually longer than that exhibited by Level 5. This appears to contradict the requirement above that $\tau_1 < \tau_2$. In fact what is happening is that the long decay time of Level 4 is produced by ion-ion cross relaxation processes which are effective well after the first few hundred microseconds when the population of Level 4 is rising. Thus during the rise interval, the rates of filling and emptying of Level 4 do in fact satisfy the criterion encapsulated in the requirement that $\tau_1 < \tau_2$. Thus the time constant of the latter component of the rise of the population of Level 4 is due to the intrinsic (no ion-ion repopulation) decay process for Level 4.

- Decay

The discussions from the last section about the late rise component of Level 4 raised issues about the decay of Level 4 as well as its rise. As was pointed, under the assumption that the decay from Level 5 is the dominant population mechanism for Level 4, the decay rate of Level 4 might be expected to follow the decay rate of Level 5. However, an inspection of Table 5.2-1 reveals that the decay of the population Level 4 has a longer decay time-constant than that of Level 5. This was considered as a strong indication that a cross-relaxation process is contributing a long-decay-time component to the population of Level 4. The slow rate of this component was a strong indication that a cross-relaxation process involving the lower Level 1 or Level 2 is involved (they are the only levels with decay rates of similar magnitude). The only other possible explanation would involve a level high up in the system with a decay time constant exceeding 6 ms, which radiatively decays into Level 4. In all the fluorescence data obtained under various pumping conditions there was no indication of the existence of such a level.

Another important observation was that the most significant differences between the rates of decay of Level 4 and Level 5 were observed under 800 nm and 980 nm pumping. Level 2 seemed to be directly involved in this long-term repopulation of Level 4. The cross-relaxation process W(22,41) (see Figure 5.4-2) was one possible mechanism for this repopulation. However there was a significant energy mismatch in this process ($\sim 1300 \text{ cm}^{-1}$). Also, can be seen from Equation 5.4.1-1, a process of this type would impose on Level 4 a decay time constant of about half of the decay time

constant of the Level 2, from which the population originates. In reality, however, in some cases Level 4 exhibited a decay time constant virtually equal to that of Level 2. It is clear that two or three ion process of the type of W(11,30) or T(111,500) (see Figure 5.4-1) would not be able to contribute population with such a large time-constant. In order to do that, the ions in the cross-relaxation process had to originate from two different levels, each level having a long decay time constant. In this situation, the observed decay rate of Level 4 would be somewhat less (50 - 100%) than that of the shorter of the two levels involved in initiating the cross relaxation process. Two processes with identical outcomes, W(21,40) and W(21,04) (see Figure 5.4-1), offered one possible explanation of this phenomena. These processes were invoked by Zou and Izumitani (1993) to explain why the decay times of the ${}^4F_{9/2}$ level (Level 4) were longer than the decay times of the ${}^4S_{3/2}+{}^2H_{11/2}$ level (Level 5) in higher Er^{3+} concentrations in a similar glass system. These two processes involve the two lowest levels, Level 1 and Level 2, each of them contributing only one ion. The energy mismatch ($\sim 1500\text{ cm}^{-1}$) in this processes is rather substantial. However, they appeared to offer the only reasonable explanation of the observed temporal behaviour of the population of Level 4. Their inclusion in the numerical model fitted reasonably well the observed fluorescence waveforms. Thus the balance between the contribution from process W(21,40):W(21,04) and the decay from Level 5 determines the overall decay rate of Level 4.

5.4.1.5. Level 5 (${}^4S_{3/2}+{}^2H_{11/2}$)

- Rise

When discussing the rise of the population of Level 5 (${}^4S_{3/2}+{}^2H_{11/2}$), the next higher level in the model, Level 6 (${}^2H_{9/2}$), and all the closely spaced levels between levels 5 and 6 (${}^4F_{3/2}$, ${}^4F_{5/2}$, ${}^4F_{7/2}$) need to be considered. The largest energy gap between any two of these levels is less than 1700 cm^{-1} , which leads to a multiphonon decay-time of less than $1\text{ }\mu\text{s}$. (Section 2.2.3, Chapter 2). Because of the close proximity of these levels all the ions cascade down from level to level via multiphonon-assisted decays with very small radiative emission. In these circumstances almost the entire population of Level 6 decays non-radiatively to Level 5, which explains the fact that the rate of rise of the

population of Level 5 is consistent with the decay rate of Level 6 for all Er^{3+} concentrations.

- Decay

There are two components in the decay waveform of this level (fitted by $(R_1+D_1)+(R_2+D_2)$ in the tables) that are especially well resolved in high Er^{3+} concentration, where their rates are substantially different. The decay of the initial component varies dramatically with concentration, decreasing from about 500 μs to about 5 μs over the whole range of Er^{3+} concentration. The second component exhibited much longer decay time-constant of several milliseconds, which did not vary much with Er^{3+} concentration. Both decay components will be discussed separately.

- Initial decay

The first component of the overall decay of Level 5 is related to the population, which Level 5 obtains via fast multiphonon-assisted decay from Level 6. After this relatively fast-rising initial population from Level 6, Level 5 decays predominantly with its own decay rate (including cross relaxation processes which involve ions originating from Level 5). In low Er^{3+} concentration this decay is predominantly radiative (see Table 5.5-2 and Table 5.2-7). Later discussions will reveal that a cross-relaxation process also affects this initial decay of Level 5, causing the rapid decrease of its time constant in higher Er^{3+} concentrations. However, as can be seen from the experimental data (see Table 5.2-3 and Table 5.2-9), the observed rates did not depend very much on the energy density of the pump, staying relatively constant for a particular concentration. Another important feature was that the increase of the decay rate with Er^{3+} concentration was not linear. A relatively small increase in the decay rate in concentrations up to about 0.8 mol% was followed by a much faster change above this level. A plot of the relevant data in Table 5.2-7 (Figure 5.4-3) showed an approximate quadratic dependence of the decay rates on the Er^{3+} concentration. A log-log plot of the change in decay rate (0.2 mol% used as a reference) produced a quite good straight line with a best-fit slope of 2.02.

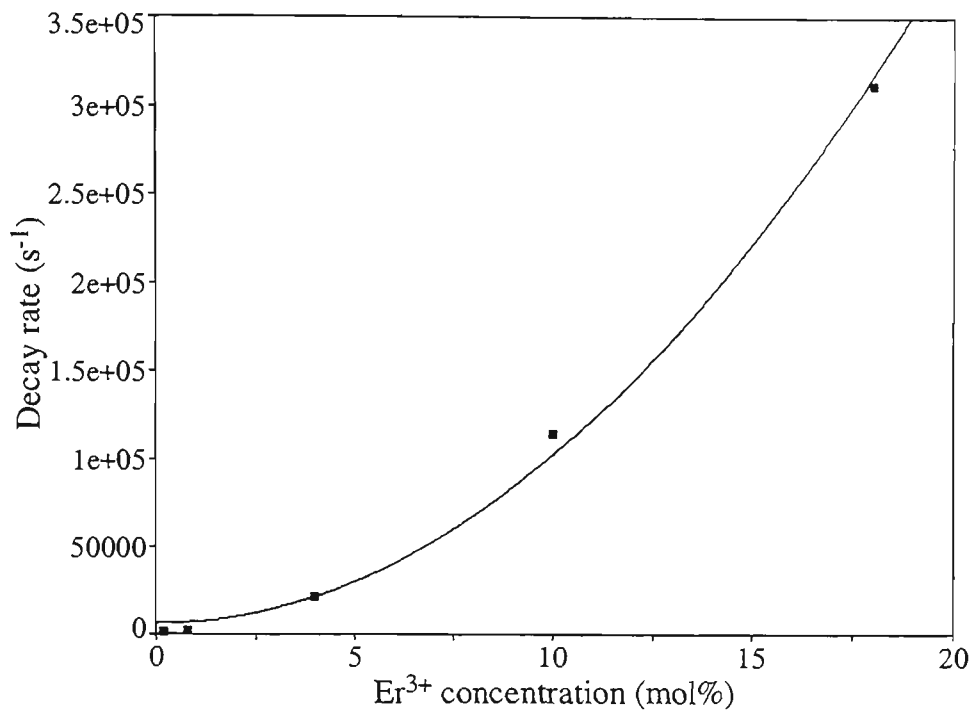


Figure 5.4-3 Experimentally obtained decay rates for the population of Level 5 (${}^4S_{3/2}+{}^2H_{11/2}$) vs Er^{3+} concentration. The solid line is a fit of the function $Y=A+BX^2$ to this data.

Data from direct pumping (Table 5.2-7) with 520 nm wavelength was used in Figure 5.4-3. This was done to avoid complications due to other cross relaxation effects which were evident with 800 nm pumping. Despite the fact that the decay rates for Level 5 under direct pumping varied substantially with doping concentration, the decay waveforms showed a single exponential decay for all doping concentrations.

As discussed in Chapter 2, this single exponential decay and quadratic concentration dependence of the decay rate is consistent with the operation of three-ion decay processes in the fast diffusion regime. Considering all of the points raised in the preceding paragraph, it was possible that two different cross-relaxation processes were responsible for the observed concentration dependence of the initial decay-rate of the green fluorescence under 800 nm pumping. The well known process $W(50,31)\equiv W(50,13)$ (see Figure 5.4-1 and Figure 2.3-1 from Chapter 2) could explain the lower concentration dependence of the decay rate at lowest Er^{3+} doping levels. This is a two-ion process involving the ground level and according to our previous analysis (Equation 5.2.1-3), the resulting decay would be exponential with a decay-rate which varies linearly with Er^{3+} concentration.

Another process should also be mentioned here. As our previous analyses showed, a two-ion process could have a similar effect on Level 5 to that of $W(50,31)$ if

it includes not the ground level, but another level with decay time much longer than that of Level 5 (see Equation 5.2.1-4b). Process W(51,33) (see Figure 5.4-2) is a good example of such a process. Since the decay time of Level 1 under 800 nm pumping is much longer than that of Level 5 (see Table 5.2-1, Table 5.2-2), the population of Level 1 can be considered constant for the time of the initial decay of Level 5 and as a result the Level 5 decay would be exponential. However, when this process was studied with the extended numerical model (which will be presented later in the chapter) its rate exhibited a surprisingly non-linear dependence on the Er^{3+} concentration. The reason for this is the sharp increase in the population of Level 1 in high concentrations due to process T(300,011). In fact the decay rate of Level 5, resulting from process W(51,33), was such a non-linear function of the Er^{3+} concentration that, even used alone, this process could explain the dramatic increase in the decay rate over the whole range of concentrations with 800nm pumping. W(51,33), however, failed to explain the observation that the measured decay rates of Level 5 for a particular concentration were very similar under different pumping conditions. These decay rates do not seem to depend on the population of the level (see Table 5.2-1 for 800 nm pumping, Table 5.2-7 for 520 nm pumping and Table 5.2-8 for 403 nm pumping). For example a W(51,33) cross-relaxation rate constant appropriate for 800nm pumping would completely deplete Level 5 under 1500 nm pumping when Level 1 is much more heavily populated. Other processes such as W(51,42), which include Level 1 or Level 2 instead of the ground level, were also discarded for similar reasons.

The quadratic concentration dependence of the rate of the decay of Level 5 in high Er^{3+} concentration was a clear indication that a higher order cross-relaxation process was involved. The previous discussions from Chapter 2 as well as this chapter (Equations 5.2.1-8 to 5.2.1-11) concluded that the quadratic dependence could be caused by a three-ion cross-relaxation process. The other important conclusion of the discussions in the present chapter was that the only way Level 5 could exhibit an exponential decay in the presence of three-ion process was if two of the ions originated from the ground level. There are only two cross-relaxation processes, which satisfy that condition. Processes T(500,111) and T(500,013) (see Figure 5.4-1) were both able to model the strong concentration dependence of the initial decay-rate of Level 5. Process T(500,013) has been used to explain similar quadratic dependence of the decay rate on

the concentration in the case of Er-doped YAG by Georgescu et al. (1991). The numerical modelling of our glass system confirmed that both processes predicted reasonably well the balance of the population of the levels affected under 800nm pumping with the predictions of T(500,013) being only marginally better than the ones of process T(500,111). Under 520 nm pumping, however, process T(500,111) contributed too large a population to Level 1. As a result the population of Level 1 rose and decayed with a much faster rate than that measured, especially in high Er³⁺ concentrations. Process T(500,013) on the other hand, was able to model well the observed similar rates of rise for Level 2 and Level 1 for the 520 nm and 403 nm pumping (see Table 5.2-7, Table 5.2-8). For all these reasons, only process T(500,013) was left in the final model.

The conclusion from the discussions above was that only two cross-relaxation processes were likely to be responsible for the observed rates of the initial decay of the population of Level 5. However, while there was no doubt about the strong effect of the three-ion process, dominating the high concentrations, there was some degree of uncertainties about the importance of process W(50,31) in low Er³⁺ concentrations. An analytical fit of the appropriate function to the experimental data was considered as a possible way to resolve the effect of the two- and the three-ion processes in low concentration. In these circumstances the rate equation for Level 5 was:

$$\frac{dn_5(t)}{dt} = -(A + \omega)n_5(t) - WCn_0n_5(t) - TC^2n_0^2n_5(t) = -((A + \omega) + WCn_0 + TC^2n_0^2)n_5(t).$$

Here the term $((A + \omega) + WCn_0 + TC^2n_0^2)$, which multiplies $n_5(t)$ is the rate of the exponential ($n_0 \sim 1$) decay of Level 5 in this case. The values of these rates determined from the experimental waveforms were plotted against the doping concentration to obtain values for the cross-relaxation constants W and T. A good fit of the function $Y=A+BX+CX^2$ to the data for the rates of the decay of Level 5 for various concentrations was obtained (see Figure 5.4-3). However, the limited set of data resulted in very large uncertainties, especially for parameter B, which represented the cross-relaxation constant W (see Table 5.4-1). The value of T (for process T(500,013)) obtained from this fit was $2.1 \times 10^{-38} \text{ cm}^6 \text{ s}^{-1}$. This value is very close to the one obtained from the numerical modelling, presented later in the chapter.

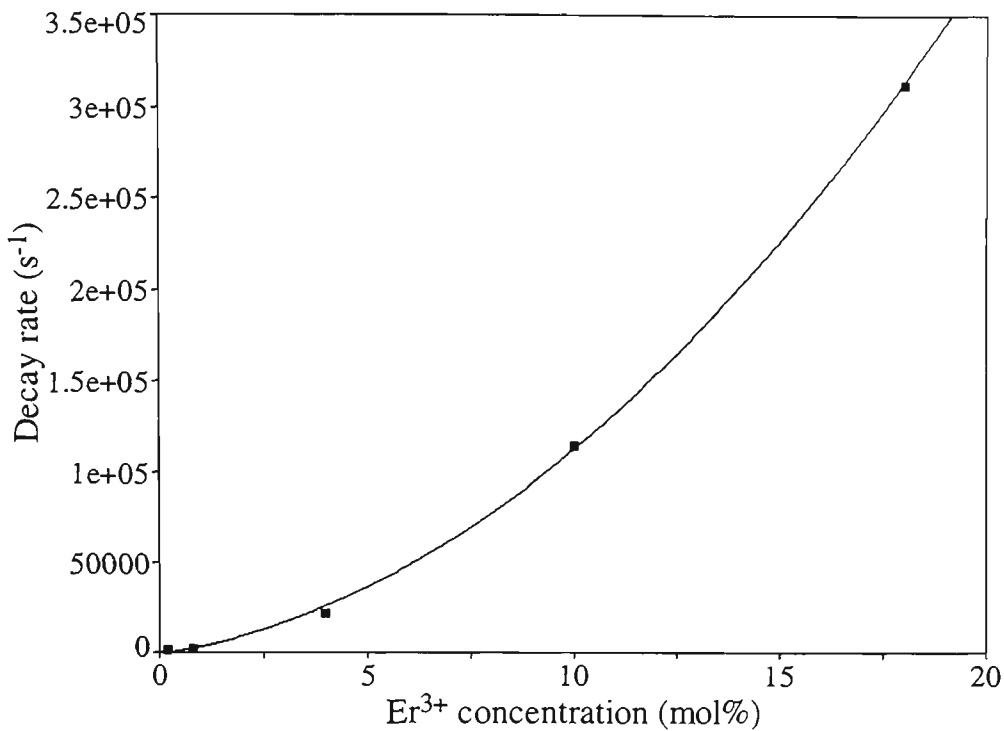


Figure 5.4-3 Fitting the function $Y=A+BX+CX^2$ to the plot of the experimental decay rates of the initial decay of Level 5 vs Er^{3+} concentration

Parameters:	Value:	Standard Error:
A	-828.0	2716.9
B	3657.8	935.9
C	765.8	50.6

Table 5.4-1 Fitting parameters for Figure 5.4-3

- Late Decay

A late decay with a time constant between 2 ms and 4.5 ms was consistently observed in the decay of the green fluorescence in all 800nm pumping experiments. The increasing contribution of this late decay with Er^{3+} concentration and its relatively long decay-time indicated that a cross-relaxation process from a lower level was probably involved. The cross-relaxation process $W(22,50)$ (see Figure 5.4-1) has been previously reported by a number of authors (see Table 2.3-1) and seemed like the most likely source of this additional population for Level 5.

Initially, this suggestion seemed somewhat inconsistent with the predictions from the analytical modelling in low Er^{3+} concentrations. The analysis of Equation

5.2.1-0 and the corresponding fitting function indicated that in low Er^{3+} concentrations, the red numbers in Table 5.2-1, Table 5.2-2 and Table 5.2-3 actually represent the time constants of the initial and the secondary decays in the complex waveform of Level 5. The first decay is that of the population which was received from Level 6. This population decays with the normal decay rate of Level 5 (due to all processes other than those which re-populate Level 5). The second decay corresponds to population redistributed from lower levels by cross-relaxation processes such as W(22,50). Thus, according to previous discussions, it was expected that the decay time constant of this late decay would approximately correspond to one half of the decay time constant of Level 2 (actually this comment only applies to low concentrations where the decay of Level 2 follows a single exponential - Equation 5.2.1-0 is only applicable to concentrations up to 4 mol% as it is derived on the basis of an exponential decay of Level 2). A close look at the time constants for this late decay of Level 5 in low concentrations in Table 5.2-1, Table 5.2-2 and Table 5.2-3 shows that these time constants are somewhat smaller than one half of the values of the time constants fitted to the direct decay of Level 2. The decay time constant corresponding to the late decay of Level 5 looked more like one third, rather than one half, of that of Level 2. From previous discussions (see Equation 5.4.1-4) it is clear that a possible explanation would be the effect of another cross-relaxation process where the three ions originate from the same level.

Several three-ion processes, originating from Level 1 or Level 2 were investigated. In the end none of these processes were able to explain the above inconsistency with the decay at low concentrations. However, they are important for other processes and so it is instructive to consider their effects here. Process T(222,511) (see Figure 5.4-2) was initially considered. The rate constant for process could be adjusted to model reasonably well the decay of Level 5 with 800 nm pumping at high concentrations. However with this same rate constant, the process has little effect at low concentrations. Also under 975nm pumping it caused Level 1 to rise much faster than the experimental data would suggest. A similar process – T(222,610) (see Figure 5.4-1) was also considered to try to explain the late decay of Level 5. However, this process also had negligible effect at low concentrations when used with a rate constant, which was suitable to explain the decays observed at higher concentrations. In addition,

this process resulted in another inconsistency with the experimental data. When assumed to be totally responsible for the late decay of Level 5, it required a large cross-relaxation rate constant which resulted in a long decay component of the decay of Level 6. Such a decay is not observed. If the process is assumed to be only partially responsible for the late decay of Level 5 (via Level 6) then this problem does not necessarily arise. The smaller cross relaxation constant appropriate to this situation can provide some small population to Level 5 under 800 nm pumping while having a negligible effect on Level 6. However, under direct pumping of Level 2, the effect of this process would be much increased. In fact this is the only process which can satisfactorily explain the behaviour of Level 5 under direct pumping of Level 2. This process is therefore included in the model for this reason and not because it has any relevance to the decay of Level 5 under 800 nm pumping at low concentration. It is further discussed under Section 5.4.2.2.

Similarly, when the 1.5 μ m pumping was analysed, it turned out that another process, T(111,500) (see Figure 5.4-1), was needed to explain the fast rise of the population of Level 5 in these pumping conditions, especially at high concentrations. The necessary cross-relaxation constant, however, was such that it did not produce any substantial effects for 800nm pumping at any concentration.

All three-ion processes, at least when used alone, had a common problem when applied to Level 5. If the rate constant was appropriate to explain the behaviour at high concentration, the effect at low concentration was negligible. If the rate constant was appropriate for low concentration decays, the effect at high concentration was far too great. Thus other processes need to be considered if one is trying to account for the behaviour of Level 5 at low concentrations.

A further process which may have explained the decay of Level 5 at low concentration was also investigated. Since the fitted decay time of the second component in the decay of Level 5 looked very close to one-half of that of Level 4, the possibility of two ion process such as W(44,53) (see Figure 5.4.2) originating from Level 4 and populating Level 5 was also modelled. This option did not look very probable, since the red fluorescence from Level 4 was much weaker than the strong green fluorescence from Level 5. The numerical modelling confirmed these reservations. In order to make a significant contribution to the decay of Level 5, very

large values ($\sim 10^{-13} \text{cm}^3 \text{s}^{-1}$) for both cross-relaxation constants $W(21,40)$ and $W(44,53)$ were required. The large value of $W(21,40)$, however, completely depopulates Level 1 and destroys the population balance in the whole system.

We thus have no processes that can explain the observed decay rates of Level 5 at low concentrations. We now return to the discussion of Sections 4.3.1 and 4.3.2 of Chapter 4. Here we had two models which were used to explain the behaviour of the lowest three excited levels. The first used $W(22,50)$ and the second included both $W(22,50)$ and $T(220,005)$. It was not possible to distinguish these two models when one only considered Levels 0 - 3. However in the extended model containing Levels 0 - 8, it is found necessary to include a mixture of both these processes in order to correctly model the behaviour of Level 5. Only a combination of these two processes was found to adequately model both the temporal behaviour of the population of Level 2 and its balanced contribution to late components of the decay of Level 5 for the whole range of Er^{3+} concentrations studied.

The introduction of a combination of $W(22,50)$ and $T(220,005)$ does not help with the problem that the late decay constant of Level 5 at low concentrations was less than one half that of Level 2. Both processes would predict a late decay constant which was half that of Level 2 (see Equation 5.2.1-0). Despite this it was found from the modelling that the overall fit of the modelled waveforms for Level 5 to the measured ones was really very good (see fits later in this chapter). This may seem surprising but one should remember the points made earlier in this thesis about the significance of the decay times in the Tables. Because of the complex re-population processes, the numerical model is better able to follow all the interactions than the fitting of approximate analytical time constants. We made the point that the basic data was the entire waveform and the fitted decay time constants were only an aid to characterising the trends in the data in a concise way and as such they have limitations. The alternative would have been to include a very large number of waveforms and that was not considered practical. For Level 5, the fitting procedure used only the first 10 ms of the rise and decay waveform. It may be that this was somewhat insufficient to fully characterise a late decay which had a time constant of about 4 ms. If so - this could explain the slight discrepancy in the late decay time constant.

The more complex behaviour of Level 5 at high Er^{3+} concentrations, where the decay of Level 2 was non-exponential, prevented any direct comparison between decay time constants of Levels 2 and 5. It was, however, reasonable to expect the late decay rate imposed on the Level 5 to be more strongly related to the higher rate in the non-exponential decay of level 2. This is the first part of the non-exponential decay of Level 2. The reasoning here is that during the initial part of the decay of Level 2, the number of the ions was much higher and the number of ions contributed to cross relaxation processes involving Level 5 was also higher. There is in fact a reasonable correlation between the late decay time constants of Level 5 and the faster time constants in the non-exponential decays of Level 2 (see table 5.2-1)

It is useful now to summarise the situation with Level 5 so far in this discussion. We have found that the initial rise comes basically from multiphonon decay of Level 6 which gets its population mostly from ESA from Level 3. The initial decay of Level 5 was explained using a combination of processes $W(50,31)$ and $T(500,310)$. The late decay is controlled by re-population effects involving $W(22,50)$ and $T(220,005)$. When all these are fed into the extended numerical model it is found that in high concentrations one needs to also include a small contribution from an additional early population process, $W(33,60)$ to adequately model the overall balance between initial and late components of the fluorescence waveform. While both $W(33,51)$ and $W(33,60)$ cross-relaxation processes fitted the experimental data, $W(33,60)$ produced slightly better fits and was included in the model. This process, at the level included in the model, did not have any substantial effect on the lower excited levels. After inclusion of $W(33,60)$, the modelled and experimental waveforms for Level 5 were in quite good agreement for 800 nm pumping.

5.4.1.6. Levels 6 (${}^2\text{H}_{9/2}$), 7 (${}^2\text{P}_{3/2}+{}^2\text{D}_{3/2}+{}^2\text{F}_{3/2}$) and 8 (${}^4\text{H}_{9/2}+{}^4\text{G}_{9/2}$)

Some discussions on the decay of the ${}^2\text{H}_{9/2}$ level (Level 6) have already been presented in relation to the rise of Level 5 (${}^4\text{S}_{3/2}+{}^2\text{H}_{11/2}$). The energy spacing between Level 6 and the next lowest level (${}^4\text{F}_{3/2}$) is only about 2000 cm^{-1} and hence the corresponding multiphonon-assisted relaxation time constant is expected to be several

microseconds. The measured decay time-constants of between $8\mu\text{s}$ and $3\mu\text{s}$ indicated that virtually all the population of the level decays via this multiphonon-assisted relaxation to $^4\text{F}_{3/2}$ level. Since the $^4\text{F}_{3/2}$, $^4\text{F}_{5/2}$, $^4\text{F}_{7/2}$ and $^2\text{H}_{11/2}$ levels, which are between the $^2\text{H}_{9/2}$ and the $^4\text{S}_{3/2}$ levels, are very closely spaced they are strongly linked to Level 5 via fast multiphonon decay. Thus for the purposes of the model, these levels are included with Level 5. There was a relatively small change in the decay rate over the whole range of Er^{3+} concentrations under 800 nm pumping as well as under direct pumping at 403 nm. A small (linear) concentration dependence is consistent with a two-ion process involving an ion from the ground level. The cross-relaxation processes $W(60,33)$ and $W(60,51)$ ($\equiv W(60,15)$) were the most probable candidates because of the small energy mismatch. While both were able to model the temporal behaviour of the population of Level 6, it turned out that the contribution of the cross-relaxation process $W(60,51)$ ($\equiv W(60,15)$) allowed marginally better fit to the initial component in the decay of the population of Level 5 in high Er^{3+} concentration. This was considered as a sufficient justification for the inclusion of the cross-relaxation process $W(60,51)$ ($\equiv W(60,15)$) in the final version of the rate-equation model.

The explanation of the observed rise of the population of Level 6 under 800 nm pumping turned out to be a very challenging task. The rising part of the waveform of the violet fluorescence at 403 nm from Level 6 contained an instantaneous initial rise plus a later rise with a time constant of about 150 ns. While the rate of this rise was independent of the Er^{3+} concentration, its contribution to the overall waveform increased dramatically in high concentration. A similar situation was discussed in the rise of Level 4. The conclusion there was that a cross-relaxation process has to be involved to explain the observed change in the contribution. Another conclusion from the discussions about Level 4 was that cross relaxation process had to be indirectly involved in order to produce the observed constant rate of rise with concentration (i.e. the cross-relaxation process has to populate a level above Level 6 which then decays radiatively or via multiphonon-assisted relaxation into Level 6). The possibility of multiphonon assisted decay into Level 6 has to be excluded since the observations on level $^4\text{G}_{11/2}$ (see 383 nm fluorescence data in Table 5.2-1), which is directly above Level 6, showed a decay time constant of several tens of microseconds to milliseconds. This is much longer than the rise-time (or the decay-time) constant of Level 6 (see

Table 5.2-1). Thus a radiative process from a level with a substantial population, received from a cross-relaxation process, was needed to explain the rise of Level 6.

When discussing the cross-relaxation process involved, an important clue for the source-level of this process was the rate of this late rise in the decay of Level 6. If the population of this high level was decaying into Level 6 with a time constant of 150ns, that meant that this high level was itself populated with a time constant, which was faster than that. Another important consideration was the fact that a reasonable amount of population had to be shifted high up (in high concentrations this amount had to be substantially larger than the population of Level 6). All this indicated that this hypothetical process probably originated from Level 3- a level which was instantaneously populated and has the largest population for the first few microseconds. Processes such as W(33,60) and T(333,611) (see Figure 5.4-1 and 5.4-2) were initially investigated, but the modelling using these revealed a number of inconsistencies. They were affecting Level 6 directly and therefore would have imposed a rise time constant varying with concentration. The numerical modelling also revealed that to achieve a rise time constant of about 150 ns, a very large cross-relaxation constant was needed, which caused a large amount of population to be moved up to Level 6. This redistribution of population led to a sharp depletion of Level 2 and also caused the initial component in the decay of Level 5 to be boosted completely out of balance. As was mentioned with regard to the Level 5, processes W(33,60) was left in the final model since it was beneficial for the overall balance in the waveform of Level 5. It was obvious, however, that this process was not the explanation for the rise of Level 6.

It seemed that there were only two cross-relaxation processes that could satisfy the requirements described above. These were the three-ion processes T(333,107) (see Figure 5.4-2) and T(333,008) (see Figure 5.4-1). They both originated from Level 3 and excited ions up to levels above Level 6 - Level 7 ($^2P_{3/2} + ^2D_{3/2} + ^2F_{3/2}$) or Level 8 ($^4H_{9/2} + ^4G_{9/2}$).

If the cross-relaxation process T(333,107) was responsible for the late rise in the population of Level 6, two more requirements were necessary for a proper fit to the experimental waveforms to be achieved. Level 7 would have to have a short decay time of less than 1 μ s and this decay time had to be dominated by a radiative process. A brief consideration of Equation 5.4.1-4 shows that a process involving three ions from

Level 3 would produce an observed fluorescence waveform of Level 7 which would exhibit a rise time-constant of less than a microsecond and a decay constant of about 3 μ s. This decay time constant is approximately one third of the decay time-constant of Level 3. The hypothetical fluorescence from Level 7 to Level 6 would produce a rise time constant for Level 6 of a few microseconds - inconsistent with the observed risetime of Level 6 of about 150 ns.. Thus it seems that a process of the form T(333,xxx) (or W(33,xx)) cannot lead to a 150 ns rise of the population of Level 6 via a radiative decay from any Level x to Level 6.

It is time now to re-look at the origin of the 403 nm fluorescence which we had assumed was only associated with the population of Level 6. If there is more than one source of this fluorescence it may be that the 150 ns feature is actually associated with a level different to Level 6. It turns out that there are two other transitions that can give rise to fluorescence in the region of 400 nm (see Table 3.3-1 and Foldout Table). These are transitions from Level 7 to Level 1 and Level 8 to Level 3. The overlap of two independent fluorescence lines with similar decay time-constant would be dominated by the fluorescence from Level 6 in low Er^{3+} concentrations, as this is directly pumped by ESA. However, in the higher Er^{3+} concentrations more and more ions would be excited to Levels 7 or 8 via three ion processes from Level 3 and so fluorescence from one of these levels may play a significant role. We concentrate first on examining the possible fluorescence from Level 7.

When pumped by the process T(333,107), at high concentration Level 7 would be expected to have a rise which is effectively instantaneous and a decay time constant which is about 3 μ s. If the fluorescence decay time of Level 7 was around 150 ns, then fluorescence from Level 7 would nicely account for the unexplained component of the rise in the violet fluorescence waveform as well as the observed decay time constant at high concentration. The essential question is then: what is the expected fluorescence decay time of level 7? A value of 1800 s^{-1} (corresponding to 560 μ s decay time constant) was calculated for this radiative rate of Level 7, based on values for the oscillator strength in similar glasses reported by Vickers *et al.* (1992). The energy gap between Level 7 ($^2\text{P}_{3/2}+\dots$) and the nearest level below ($^2\text{G}_{7/2}$) is larger than 3500 cm^{-1} (see Foldout Table). Therefore the multiphonon assisted decay rate of Level 7 would be expected to be in the order of a few milliseconds. Thus it seems impossible that the

combined radiative and multiphonon decay rate (which determines the fluorescence risetime) could be below 1 μs . For this reason process T(333,107) was disregarded and not included in the model.

The cross-relaxation process T(333,008) (see Figure 5.4-1) was similar to process T(333,107), but would excite ions to Level 8 ($^4\text{H}_{9/2} + ^4\text{G}_{9/2}$) instead to Level 7. All the levels between Level 8 and Level 7 are closely spaced, with the largest energy gap between any two of them being less than 1700 cm^{-1} . Under these circumstances (Chapter 2) a strong multiphonon-assisted decay rate, corresponding to a time-constant of less than 1 μs was expected to dominate their decays. The discussions concerning the interpretation of Section 4.2.2 and Equation 5.4.1-4 (see relevant place in thesis where it is introduced) would imply that observation of the population of any of these levels would reveal a rise time constant of less than 1 μs and decay time constant of about 3 μs . As mentioned above, there is a transition from Level 8 to Level 3 at around 400 nm which could be responsible for the unexplained rise of the violet fluorescence. Level 8 seems to satisfy all the requirements for being a likely source of this fluorescence. The fluorescence from Level 8 would have a very fast rise because of the strong multiphoton depopulation of the level and its decay time at high concentration would be around 3 μs . The high multiphonon assisted decay rate would dominate the overall decay and the fluorescence would be expected to be weak. However, it should also be noted that the decay of Level 6 is also dominated by a multiphonon-assisted decay and therefore intensity of the violet fluorescence lines from both levels are likely to be comparable.

During the numerical modelling, a rate constant for process T(333,008) was found which, when combined with the rate constants of previous processes affecting Level 6, produced populations in these levels which agreed with the experimental measurements. These populations were such that Level 6 has the main influence on the violet fluorescence at low concentrations and level 8 dominated at high concentrations. The rate constant for process T(333,008) was such that it did not affect substantially either the decay of Level 3 nor the balance of the population of the levels below Level 3. In the final numerical model, Level 8 was assumed to have a multiphonon-assisted decay with 0.5 μs time constant and radiative decay with 20 μs time constant (corresponding to a rate of 50000 s^{-1}). We have no information as to the expected

radiative decay rate of level 8. It was found that values for this rate between 5000 s^{-1} ($200 \text{ }\mu\text{s}$) and 50000 s^{-1} ($20 \text{ }\mu\text{s}$) all allowed successful modelling of the temporal behaviour of the observed violet fluorescence line. Radiative rates higher than 50000 s^{-1} produced too fast a decay for the combined violet line, while rates of less than 5000 s^{-1} were not able to produce a fluorescence intensity sufficient to dominate this combined fluorescence in high Er^{3+} concentrations. Thus despite the lack of detailed information about Level 8 (${}^4\text{H}_{9/2}+{}^4\text{G}_{9/2}$), a feasible model of the observed violet fluorescence was developed. This model predicted well the observed temporal features of this fluorescence in all dopant concentrations.

5.4.2. Pumping wavelengths other than 800 nm

The behaviour of the $\text{Er}^{3+}:\text{ZB(L)AN}$ system under 800 nm pumping has been considered in some detail in the preceding sections. It has been possible using a combination of numerical modelling and fitting of approximate analytic solutions, to obtain a reasonably good understanding of the physical processes responsible for the behaviour of the fluorescence from the various levels (for this particular pump wavelength). At various times during the discussions, reference was made to the behaviour using other pump wavelengths - particularly under direct pumping of a particular level. This section presents a more integrated discussion of the fluorescence behaviour using pumping wavelengths other than 800 nm. The main wavelengths used were 1532 nm, 975 nm, 520 nm and 403 nm. Pumping at these wavelengths produced a very different balance of populations amongst the various energy levels than applied at 800 nm and hence a difference in the balance of importance of many of the cross relaxation processes. The numerical model to be presented later in this chapter should be able to account for the behaviour of the material under any type of pumping. While this is the case, it will be seen from the following discussions that the model has been optimised for 800 nm pumping and it performs better for this pump wavelength.

5.4.2.1. 1.5 μm pumping (into Level 1)

The analysis and the discussions below are based on the data presented in Table 5.2-4 and Table 5.2-5 which is obtained from various fits to the experimental waveforms. For 1.5 μm pumping, the values of the initial populations of Level 1, Level 3 and Level 5, used as a starting point in the modelling process are presented in Table 5.3-1.

This pumping wavelength strongly populated Level 1 ($^4\text{I}_{13/2}$) and therefore accentuated cross-relaxation processes emanating from this level such as W(11,30) and T(110,003). The non-exponential decay of Level 1, as well as the slow rate of rise of Level 2 in low Er^{3+} concentration and the rapid change of this rise with increased Er^{3+} concentration, was good confirmation of the importance of these processes. The application of the numerical model, designed for 800nm pumping, gave very good agreement with the experimental decay waveforms of Levels 1 and 2.

The weak fluorescence line at about 810 nm (Table 5.2-4) mostly originated from Level 3. The initial decay with a time constant of about 150 μs , clearly evident in 1.6 mol % concentration, indicated that fluorescence at this wavelength emanating from other levels such as Level 5 or Level 6 may also be present. The absence of this initial decay in higher Er^{3+} concentrations, as well as the evident non-exponential decay with a several millisecond time-constant, can be explained by the dominance in the higher concentrations of the fluorescence from Level 3. Under 1.5 μm pumping, this level is populated by the cross-relaxation processes like W(11,30) and T(110,003). The only unexplained feature in this fluorescence was the fast, but not instantaneous, rise time constant of about 1 μs in all concentrations. Both the previous analysis (see Equation 5.4.1-1) and the numerical model predicted a rise time constant of about 5-6 μs . One possible explanation was that the rise time of about 1 μs belonged to the rise of another 800 nm fluorescence line, overlapping the one from Level 3. A transition from Level 6 to Level 3 produces fluorescence at about 810 nm. Level 6 also was expected to be populated from the level directly above - level $^4\text{G}_{11/2}$. Level $^4\text{G}_{11/2}$ was populated instantaneously by three-stage-ESA (see Foldout Table) and since it was placed very close to Level 6 ($\Delta E < 2000\text{cm}^{-1}$), it was expected that fast multi-phonon assisted decay

to Level 6 would follow. The expected rate of this fast decay was around 1 μ s which is very close to that observed for the rise of the fluorescence at 810 nm. What remained unclear was why the rise of this fluorescence from Level 6 was comparable in magnitude with that from Level 3. A simple calculation suggested that the initial population of level ${}^4G_{11/2}$, which was populated by a multi-stage-ESA, would be orders of magnitude smaller than that of Level 3, populated by a single-stage-ESA. A 1 μ s rise in the 810 nm fluorescence from Level 6 would mean that a similar risetime should be observed with an 407 nm fluorescence emanating from this level. The observed risetime for this radiation is between about 11 μ s (low concentration) and 6 μ s (high concentration). However as will be discussed later in this chapter, the observed violet fluorescence under this pumping may originate from a level other than 6.

The slow rise (~ms) in the fluorescence intensity of the red fluorescence at about 655 nm (Table 5.2-4, Table 5.2-5) as well as the long decay time constant, decreasing only slightly with Er^{3+} concentration, were consistent with the effect of the cross-relaxation process W(21,04).

Two distinguishable contributions (each consisting of a rise and decay) were observed within the waveform of the green fluorescence of Level 5 at 520 - 550 nm (Table 5.2-4, Table 5.2-5). The initial contribution exhibited a rise which was roughly consistent to the expected decay of Level 6. The decay of this initial contribution was reasonably similar to that observed for Level 5 under 800 nm and 520 nm pumping. Numerical modelling showed that in order to successfully predict the observed balance between the two contributions to the fluorescence waveform of Level 5, an initial normalised population for Level 6 of about $n_{60}=1 \times 10^{-7}$ was required. As mentioned previously, it was not Level 6, but the level above it - ${}^4G_{11/2}$, which was initially populated by the ESA. However an approximate calculation of the ESA population of the ${}^4G_{11/2}$ level was orders of magnitude smaller than that required by the model (see Table 5.3-1). Thus we have a similar inconsistency to that mentioned previously with regard to the 810nm fluorescence. Level 5 would be expected to have an instantaneous rise produced by a two-stage ESA process. Instead one sees a slower rise which looks to be consistent with population from Level 6 which is itself populated via a three-stage ESA. It is probably that this rise in the population of Level 5 does not arise by photon-induced ESA but rather by some higher order cross relaxation process which populates

a level above Level 5 (and hence the rise of Level 5 is not too strongly dependent on concentration). The origin of this rise of Level 5 under 1.5 μm pumping has not been accounted for in this thesis. It should be remembered that the population involved is very small and this is not seen as representing a significant problem for the model.

The significant change with concentration in the rate of the rise in the second component of the fluorescence waveform of Level 5, as well as the relatively large decay time constants, was an indication that this second component in the green fluorescence was a contribution to cross-relaxation processes involving lower levels (such as W(22,50) and T(220,005)). Numerical modelling showed that for good agreement with the green fluorescence in different Er^{3+} concentrations, one more process had to be added to the model developed for 800 nm pumping – T(111,500). The first reason for this inclusion was that a process from Level 2, such as W(22,50) and T(220,005), could not explain the small decay time constants (6-2.5 ms) of the second component of the waveform. Also Level 2 itself was populated too slowly under 1.5 μm pumping to take an active part in the early part of this second component. A process was needed that originated from Level 1 and involved three ions from the same level (from Equation 5.4.1-4 it can be seen that this would impose on Level 5 a decay rate which is approximately equal to one third of the decay rate of Level 1). In addition, such a process was the only way to excite sufficient ions from Level 1 to have an effect on Level 5 which was comparable to that of T(200,005) and W(22,50) in high Er^{3+} concentration. A cross-relaxation constant for T(111,500) was found using the model which reproduced the observed balance in the green fluorescence under 1.5 μm pumping. In 800nm pumping the effect of this process turned out to be insignificant.

The weak violet fluorescence at 407nm (Table 5.2-4, Table 5.2-5) also had two obvious rise and decay components. This fluorescence was initially expected to originate from Level 6 which has an intrinsic decay time constant of about 10 μs . However, if this was the case then the observed rise in the initial component of the waveform could be explained if a level above Level 6 was decaying into Level 6 with a decay time constant of about 100 - 150 μs . According to our previous discussions (see Chapter 4, Equation 4.2-8) under these circumstances the fluorescence from Level 6 would rise with a rate which is approximately equal to the intrinsic decay rate of Level 6 and decay with a time constant of approximately 100 \div 150 μs . This explanation is at

odds with the discussion above concerning the fast rise of the 810 nm fluorescence and the rise of the initial component of the green fluorescence. These suggested a rise time of about 1 μ s and a decay time of about 10 μ s for Level 6. Another possible explanation for the initial component in the violet fluorescence was a possible fluorescence at the same wavelength from a higher excited level. The group of closely spaced levels which is labeled Level 7 ($^2P_{3/2}+^2D_{3/2}+^4F_{3/2}$) was also expected to fluoresce at about 400 nm (see Foldout Table). Despite its relatively small population the predominantly radiative decay of this level could have a fluorescence intensity comparable to that of Level 6, which decays predominantly via a multiphonon process.

The slow decay rate of the second component of the violet fluorescence waveform indicated that there was a possible contribution from a cross-relaxation process originating from some of the lower levels. The relatively weak dependence of the rise and decay with Er^{3+} concentration suggested that a two-ion process such as W(55,63) or W(51,60) was probably involved.

The lack of detailed information about the relative excited state absorption cross-sections led to a lack of reliable data for the initial populations in the levels above Level 5. The fluorescence lines at 800-820 nm and 407 nm were relatively weak and therefore not very significant for the overall model. They also involve overlapping fluorescence lines, which complicates further the modelling process. Considering all this, a detailed numerical analysis of these lines was not undertaken. The final numerical model gave reasonably good agreement between predicted and observed fluorescence for the rest of the levels (see Figure 5.5-4).

5.4.2.2. 975 nm pumping (into Level 2)

The numerical model, designed for 800 nm pumping, fitted quite well the observed dynamics of almost all fluorescence lines with 975 nm pumping (see waveform fits in Figure 5.5-5 and summary data in Table 5.2-6). The initial populations used as a starting point in the modelling process are from Table 5.3-1.

The good fits of the model to the measured fluorescence waveforms at 980 nm (Level 2) and at 1.5 μ m (Level 1) confirmed the suitability of the choice of the cross-

relaxation rate constants for the processes W(22,50), T(220,005), W(11,30) and T(110,003).

The fluorescence at ~500 nm - 560 nm and 830 nm -850 nm showed similar temporal behaviour and presumably both originated from Level 5. The decays are non exponential and were fitted with two exponentials. In 4 mol% Er³⁺ concentration the late decay rate was approximately twice than that of the decay of Level 2. At higher concentrations the decay rate increases faster than that of Level 2. The behaviour at 4 mol% is consistent with the dominance of processes W(22,50) and T(220,005) in the population of Level 5. In high concentrations it seemed that there was an additional cross-relaxation process with comparable contribution, but with a higher rate than that of these two processes. Only a three-ion process, with all ions originating from Level 2, could fulfil these two requirements. An examination of the energy spacing among the excited energy levels (see Foldout Table and Diagram) revealed that the cross-relaxation processes T(222,610) was the only suitable candidate. The numerical modelling confirmed that the inclusion of this process allowed good predictions of the experimental decay-forms of the fluorescence from Level 5 to be made for the whole range of the Er³⁺ concentrations used. This process did not have any substantial effect on the dynamics of the population of Level 1 and Level 2. The strong dependence of the effective rate of this process on the population of Level 2 also implied that its effect would be insignificant under any other pumping wavelength, where Level 2 has substantially smaller population.

The measured fluorescence rise (see Table 5.2-6) of these two fluorescence lines (with peaks at around 530 and 850 nm) turned out to be very difficult to model. This rise consisted of two components – an initial instantaneous rise, which was followed by a later rise with a time constant of a few microseconds. These two components had comparable amplitudes, with the contribution of the second component slightly increasing with Er³⁺ concentration. An examination of Table 5.3-1 would show that under 975 nm pumping Level 5 has some initial population from ESA. However, it is not Level 5, but the ⁴F_{7/2} level, which is directly populated by the ESA. Since this level is only about 1300 cm⁻¹ above Level 5 it was expected that a fast multiphonon-assisted decay to Level 5 would populate Level 5 virtually instantaneously (see Equation 2.2-1, Chapter 2). Indeed a fluorescence line was observed at 801 nm which

had only such an instantaneous rise (see the text regarding Table 5.2-6 on page 5.20). Since, of the ESA populated levels, only Level 5 had a fluorescence line at that wavelength, it can be assumed that the rise of the population of Level 5 is indeed instantaneous. If this was the case, the second component of the rise at around 530 nm and 850 nm is probably part of a fluorescence, originating from another level. There was only one level with fluorescence around both 530 nm and 850 nm and this was Level 7 (${}^2P_{3/2}+\dots$). However, with 975 nm pumping this level was expected to have an instantaneous rise itself due to pump ESA from the ${}^4F_{7/2}$ level. In addition, the population of Level 7 was expected to be much too small to be able to compete with that of Level 5. An interesting fact was that the ratio between the two components of this rise only slightly changed with concentration. One possible explanation of this could be that somehow the second component of the rise was simply a delayed part of a contribution to the population of Level 5. One mechanism for this was the cross-relaxation process $W({}^4F_{7/2} \rightarrow {}^4F_{7/2,65})$. The numerical modelling confirmed this possibility. However, it also confirmed that a very large cross-relaxation constant ($\sim 0.5 \times 10^{-9}$) was needed for a substantial amount of ions to be moved above Level 5. The need for such a large cross-relaxation constant could be explained by the fact that approximately one half of the ions in the population of level ${}^4F_{7/2}$ had to be involved in the process before the fast multiphonon-assisted decay to Level 5 takes over. This is all a bit too speculative and so was not included in the model. No other satisfactory explanation of the late rise of the fluorescence lines at about 530 nm and 850 nm could be found. As with some previous small details that could not be explained, this inconsistency between model and measurement does not have much of an effect on the overall success of the model. However, it clearly indicates that something is missing from the model and further refinement is possible.

The rise of the fluorescence intensity of the red fluorescence line at about 655 nm was consistent with the discussions in Chapter 4 (see Section 4.2.2). These discussions referred to a level which is populated from another level with a longer decay time constant. Here Level 4 is populated predominantly from Level 5, which under 975 nm pumping has a longer decay time constant than the intrinsic decay time constant of Level 4. The net result is that population Level 4 rises with a rate, corresponding to its own decay time constant and decays with a rate corresponding to the decay time

constant of Level 5. The relatively long decay time constants observed for Level 4 (they were again longer than that associated with Level 5) confirmed the presence of the cross-relaxation process W(21,40). The impact of this process, however, was delayed by the slow rise in the population of Level 1 and did not affect the rise of Level 4. The numerical modelling showed good agreement with the experimental waveforms of Level 4 for all Er^{3+} concentrations.

Under 975 nm pumping there were several excited energy levels with fluorescence at about 488 nm (see Table 5.1-1). However the observed instantaneous rise and the decay rate were very similar to that of the other fluorescence lines from Level 5. This was a clear indication that this particular 488 nm fluorescence line originated from the $^4\text{F}_{7/2}$ level. This level is only about 1400 cm^{-1} above the $^2\text{H}_{11/2}$ level (which is part of Level 5). The main consequence of this is that very fast multiphonon decay takes place immediately after the initial instantaneous population of the $^4\text{F}_{7/2}$ level via ESA. Thus the population of this $^4\text{F}_{7/2}$ level represents a very small fraction of the total population of Level 5, which is consistent with the low fluorescence intensity of the 488 nm fluorescence.

The 407 nm fluorescence was expected to originate from Level 6. However, the presence of the instantaneous component in the rise in low Er^{3+} concentration indicated an overlap was possible with a fluorescence line at similar wavelength from a different level. As was previously discussed, one such source of a fluorescence at about 400 nm was Level 7 (level $^2\text{P}_{3/2}+\dots$) which under 975 nm pumping was expected to have an instantaneous rise due to pump ESA from the $^4\text{F}_{7/2}$ level. It is believed that the cross-relaxation process T(222,610), introduced when discussing the decay of Level 5, is instrumental in populating Level 6 and contributing the long time constants in the decay of the 407 nm fluorescence. A cross-relaxation process such as W(55,63), which would have imposed on Level 6 a decay time constant approximately equal to one half of that of the decay of Level 5, may also be involved. The numerical modelling of the decays of this violet fluorescence showed reasonable agreement with the experimental waveforms for all Er^{3+} concentrations.

The fluorescence line at 450 nm was believed to originate from the $^4\text{F}_{5/2}$ level (to the $^4\text{I}_{15/2}$ level). This level was expected to be rapidly populated by multiphonon

processes from Level 6, which was mostly responsible for the fluorescence at 407 nm. This would explain the similarity of the observed fluorescence waveforms.

5.4.2.3. 520 nm pumping (into Level 5)

The summary of rise and decay time constant data obtained using this pump wavelength is shown in Table 5.2-7. During the pump pulse a number of ions are excited to Level 5 ($^4S_{3/2}+^2H_{11/2}$) via ground level pump absorption (see Table 5.3-1). A much smaller number of ions are also excited to the $^4D_{7/2}$ level via two-stage ESA, but these have been ignored in the modelling process.

With Level 5 populated much more heavily than was the case with 800 nm pumping, it was expected that the cross-relaxation processes W(50,31) and T(500,013) would dictate the population dynamics of Level 1 and Level 2. Indeed the rise of the population of these two levels exhibited similar rates, which also matched the decay rate of Level 5. In high Er^{3+} concentrations there was also a small additional contribution to the rise of the population of Level 2. This late rise could be explained by a cascading population from Level 5 to Level 2 via phonon-assisted decays. As can be seen in Table 5.2-7, in these high concentrations Level 4 rises sufficiently fast and its decay into Level 3 and consecutive multiphonon decay into Level 2 may well be able to affect the rise of Level 2. The measured decay rates of Levels 1 and 2 in low Er^{3+} concentrations were as expected. In high Er^{3+} concentrations non-exponential decays were observed. The decay waveforms predicted by the numerical modelling using rate constants optimised for 800 nm pumping were in a good agreement with the experimental waveforms for 520 nm pumping in all Er^{3+} concentrations. This provided confirmation of the adequacy of the cross-relaxation rate constants for W(50,31) and T(500,013) as well as those for all other processes which affect Level 1 and Level 2 directly.

An examination of the energies of the higher excited energy levels of Er^{3+} ions in the Foldout Table suggests that the fluorescence line at 698 nm could originate from several levels. Possible levels include the $^4F_{7/2}$ level (to level $^4I_{13/2}$), the $^2H_{9/2}$ level (to level $^4I_{11/2}$), the $^4G_{11/2}+^4G_{9/2}+^2K_{15/2}+^4G_{7/2}$ level (to level $^4I_{9/2}$) (see also Table 5.1-1) and the $^4H_{9/2}+^4G_{9/2}$ level (to level $^4F_{5/2}$). In fact the observed fluorescence could be

produced by overlapping fluorescence lines from more than one of these transitions. A very approximate calculation, based on $KT \approx 210 \text{ cm}^{-1}$ (for $T = 300 \text{ K}$) and a Boltzmann distribution, suggests that the population of the ${}^4F_{7/2}$ level would represent approximately 5×10^{-6} of the total population of Level 5. This could explain the presence of a small instantaneous component in the rise of the 698 nm fluorescence line in 0.2 mol% Er^{3+} concentration. However, the main component of the rise of the 698 nm fluorescence waveform in this Er^{3+} concentration exhibited a time constant of about 160 μs . The decay time constant following this rise was about 550 μs . It is not easy to see the origin of this 160 μs rise but it presumably arises from some overlapping fluorescence transition. However, the 550 μs decay at this 0.2 mol% concentration is consistent with the intrinsic decay of Level 5 and hence this observation is in agreement with an assumed thermal population of the ${}^4F_{7/2}$ level from Level 5.

In higher Er^{3+} concentrations a cross-relaxation process such as W(55,63) could populate Level 6 with a fast rise and a decay time constant which is half that of Level 5. It has to be remembered that the decay time constant of Level 5 is decreasing rapidly with increasing doping concentration. While the decay time of Level 6 is shorter than the time constant with which it is being filled (half of Level 5 decay time constant) the fluorescence from Level 6 will rise with its own intrinsic decay time constant and decay with about one half the decay time constant of Level 5. In high concentrations where the decay of Level 5 is short enough to violate the condition in the previous sentence, the fluorescence from Level 6 will rise with half the decay time constant of Level 5 and decay with its own intrinsic decay. The data in Table 5.2-7 is consistent with these conclusions.

The fluorescence at 655 nm, which originated from Level 4 exhibited a temporal behaviour which was fully consistent with the predictions of the model developed for 800 nm pumping. In small Er^{3+} concentration the decay rate of Level 5 was expected to be slower than that of Level 4. In these circumstances, as a rate-equation analysis similar to that in Section 4.2.2 (Chapter 4) can show, the fluorescence from Level 4 is expected to rise with a rate similar to its own decay rate and decay with the rate of the decay of Level 5. In higher Er^{3+} concentrations, however, the effect of the cross-relaxation processes W(50,13) and especially T(500,013) reduced the decay time constant of Level 5 to several microseconds. This is substantially shorter than the decay

time constant of Level 4. Under these circumstances the 655nm fluorescence is expected to rise with a rate which is similar to the decay rate of Level 5 and to decay with its own decay rate. The experimental data followed well these predictions. The late decays of the 655 nm fluorescence at 10 mol% and 18 mol% concentrations are consistent with the predictions of the model and are shown to arise due to the effects of W (21,40).

The temporal behaviour of the population of Level 5, which was responsible for the fluorescence at 520-550nm and at 800-840nm, was also consistent with the predictions of the model. The analysis of the behaviour of this level with 800nm pumping indicated that the two cross-relaxation processes, W(50,13) and T(500,013), were mainly responsible. As mentioned previously, the effect of both these processes on the decay time is dependent only on the Er^{3+} concentration and not on the population of the level. This prediction of the model is confirmed by the data of Tables 5.2-1, 5.2-7 and 5.2-8.

The two overlapping weak fluorescence lines between about 400 nm and 410 nm, as well as the weaker fluorescence at about 468 nm, had similar temporal behaviour and were believed to originate mainly from three levels – ${}^4\text{D}_{7/2}$, (${}^2\text{P}_{3/2}+\dots$) (Level 7) and ${}^2\text{H}_{9/2}$ (Level 6) (see Table 5.1-1). Level ${}^4\text{D}_{7/2}$ had fluorescence lines centered at about 468 nm (to level ${}^4\text{S}_{3/2}$) and 410 nm (to level ${}^4\text{F}_{9/2}$). The fact that the ${}^4\text{D}_{7/2}$ level gained some initial population via ESA with 520 nm pumping could explain the instantaneous component in the rise of these fluorescence lines. Level 6 (${}^2\text{H}_{9/2}$) also had a fluorescence line at about 407 nm. Level 7 has fluorescence lines at about 400 nm (to Level 1) and at about 468 nm (to Level 2). As was shown in previous discussions, calculations of the radiative and multiphonon decay rates of Level 7 indicated a lifetime of about several hundreds of microseconds. This lifetime was consistent with some of the temporal features in the waveforms of the 400 nm and 468 nm fluorescence in low concentration. Under 520 nm pumping, Level 7 is expected to be mostly populated via cascading multiphonon decay from the ${}^4\text{D}_{7/2}$ level. At high doping concentration, the processes W(55,71) and W(55, ${}^4\text{D}_{7/2}0$) are also possible but have not been considered in any detail in this thesis. The latter process would affect the ${}^4\text{D}_{7/2}$ level and both processes would affect the population of Level 7. In summary, the complicated rise and decay features of the overlapping violet lines between about 400 and 468 nm are likely

to be able to be accounted for by fluorescence from Levels 6, 7 and $^4D_{7/2}$. However, since the fluorescences are quite weak and the processes involved for 520 nm pumping do not significantly impact on important lower levels, we have not attempted to unravel all the detail involved. The final model includes only those processes that are important for the violet fluorescence under 800 nm pumping. Despite being optimised for 800 nm pumping, this model was able to successfully predict the waveforms all main fluorescences from Levels 1,2,4,5 also with 520 nm pumping(see Figure 5.5-6). The model could be further refined if the full details of the processes responsible for violet fluorescence under 520 nm pumping were also included.

5.4.2.4. 403 nm pumping (into Level 6)

The data obtained from the fits to the fluorescence waveforms recorded with this pump is shown in Table 5.2-8. With this pumping wavelength the dynamics of the system begins with some initial population in Level 6 (see Table 5.3-1).

The fluorescence line at 407nm, originating from Level 6, exhibited only a small change in decay rate throughout the range of Er^{3+} concentrations under direct pumping. This was consistent with the nature of the cross-relaxation process $W(60,51)$, the effect of which was only linearly dependant on the concentration of the Er^{3+} ions. The intensity of the fluorescence line at 698 nm exhibited the same temporal behaviour as that of 407 nm fluorescence line and it is believed that it also originated from Level 6.

The fluorescence line at 450 nm probably originated from level $^4F_{5/2}$, which is directly under Level 6 and received all its population via multiphonon-assisted decay from Level 6. This level was less than 1700 cm^{-1} above the next lower energy level, which would imply a multiphonon-assisted decay with a rate of less than several microseconds. Under these circumstances a fluorescence line from level $^4F_{5/2}$ would be expected to have a very short rise and decay with a rate, similar to the decay rate of Level 6. The experimental data for the fluorescence line at 450 nm confirmed this to be the case.

The fluorescence lines at 520-540 nm and 800-840 nm with very similar temporal behaviour are believed to originate from Level 5. As in the case of 800 nm pump, their intensity exhibited a rise with a rate which was similar to that of the multiphonon-assisted decay of Level 6. The decay time constants of these lines for all Er^{3+} concentrations were similar to that observed in the case of 800 nm and 520 nm pumping.

As in the case in the 800 nm pumping, the fluorescence at 553 nm was believed to consist of two overlapping fluorescence lines; one from Level 5 (${}^2\text{H}_{11/2}$) and another one from Level 6 (to Level 1). This explained the instantaneous rise and the double decay.

The decay of the fluorescence line at 655 nm was similar to that observed in the case of 520 nm pumping. In low Er^{3+} concentrations the decay time constant of Level 5 was longer than that of Level 4 and this was why the 655 nm fluorescence rose with a rate determined by the decay time of Level 4 and decayed with a rate consistent with the decay of Level 5. In higher Er^{3+} concentrations, where the decay rate of Level 5 was much shorter, the 655 nm fluorescence line exhibited a rise with a time constant close to the decay time of Level 5 and a decay time constant similar to the intrinsic decay time of Level 4.

The temporal behaviour of the fluorescence of the two infrared fluorescence lines at 980 nm and 1.5 μm was also similar to that observed with 520 nm pumping. Within the limitations imposed by the resolution of the detectors used, it can be seen that both infrared fluorescences rise with similar time constants. This was consistent with the presumption that from Level 6 the population quickly decays via multiphonon-assisted decay to Level 5 and from there reaches Level 1 and Level 2 via the cross-relaxation processes T(500,013) and W(50,31). When the effect of the slow decay of Level 2 into Level 1 on the fitted parameters was taken into account the decay rates of both levels were as expected (see the red numbers in Table 5.2-8). The prediction of the numerical model were in very good agreement with the observed fluorescence waveforms for all levels under 403 nm pumping (see Figure 5.5-7 and 5.5-8).

5.5. Extended rate-equation model

5.5.1. Introduction

The earlier sections of this chapter have been concerned with presenting the measured fluorescence data in a form where its main features and trends can be readily recognised. This was followed by a quite extensive discussion which attempted to explain the origin of the various fluorescence features on a level by level basis. These discussions were intended to provide a physical understanding of the processes responsible for the population of the energy levels in the material. These discussions introduced a large number of two- and three-ion processes which were found to be important for the population dynamics of the various levels under particular pump wavelengths. In many cases distinctions between processes, or elucidation of the balance between processes, required quantitative arguments which were only possible using the numerical modelling. Thus the model, and many of the aspects of processes and parameters associated with it, has already been introduced. The following sections attempt to pull together all the previous discussions and present the complete model as a set of rate equations which include all the important radiative, phonon and cross relaxation processes. The model has then been optimised and the essential output of this process is a self-consistent set of rate constants. After these have been presented, plots of measured and predicted fluorescence waveforms are presented. The waveforms presented are grouped according to pump wavelength and include the main fluorescence levels together with any levels which are directly pumped. These waveforms enable one to readily appreciate the degree to which the model predictions agree with experimental observations at each pump wavelength. The model has been optimised particularly for agreement at 800 nm.

Having obtained a set of rate constants for all the various processes, the next question to be answered is what is the accuracy of the various constants? This is not a simple question when one is dealing with numerical solutions of equations involving large numbers of parameters. A section is included where parameters have been varied one at a time to try to estimate these uncertainties. The final section discusses the

relative contributions of the various processes to the population or depopulation of the various levels. This is done by integrating the rates of the various process terms over the entire waveform to obtain a measure of the total number of ions that are involved in a particular process.

5.5.2. Non cross-relaxation constants used in the model

The values calculated in Section 5.3 were used for the initial populations of the levels which are populated via direct absorption of the pump. However, because of the large uncertainties in the calculations of the initial populations of the levels populated via ESA, these values were adjusted during modelling in order to optimise the fitting of the model to the experimental waveforms. The initial populations that were found to provide the best fits to the experimental data and were used in the final version of the model are summarised in Table 5.5-1.

Pumping λ :	Normalised initial populations:		
	Direct Absorption	<i>Excited State Absorption</i>	
800 nm	<u>$n_{30}=5 \times 10^{(-4)}$</u>	$n_{60}=8 \times 10^{(-7)}$	
1.5 μm	<u>$n_{10}=2 \times 10^{(-3)}$</u>	$n_{30}=1 \times 10^{(-6)}$	$n_{60}=1.5 \times 10^{(-7)}$
980 nm	<u>$n_{20}=1 \times 10^{(-3)}$</u>	$n_{50}=5 \times 10^{(-6)}$	
520 nm	<u>$n_{50}=3 \times 10^{(-3)}$</u>		
403 nm	<u>$n_{60}=2 \times 10^{(-4)}$</u>		

Table 5.5-1 Initial populations, modelling best the experimental data and used in the final version of the extended rate-equation model. Underlined numbers - calculated, *Numbers in italic* - adjusted for good fit.

The values of the radiative and phonon parameters used in the model, together with the corresponding references to their origin, are listed in Tables 5.5-2 and 5.5-3. The method of calculation of the radiative and multi-phonon-assisted decay rates, as

well as the branching ratios, was described in Chapter 4 for the first three levels. A similar process was followed for the other levels. The details are summarised below:

- Level 4 (${}^4F_{9/2}$)

Shinn *et al.* (1983) calculated for Level 4 a radiative decay rate of 1085 s^{-1} , which was very close to that calculated by Zou *et al.* (1993). The averaged total decay rate of Level 4 measured in our work in low erbium concentration (0.4 mol%) under direct pumping was 5650 s^{-1} (see Table 5.2-9). The multiphonon-assisted decay rate for this level was taken as the difference between the above rates ($\omega_4=4565 \text{ s}^{-1}$).

- Level 5 (${}^4S_{3/2}+{}^2H_{11/2}$)

Again values for the radiative decay rate $\sum A({}^4S_{3/2}) = 1165.3 \text{ s}^{-1}$ and $\sum A({}^2H_{11/2}) = 3264 \text{ s}^{-1}$, calculated by Shinn *et al.* (1983) were used in the modelling. These values were also very similar to those calculated by Zou *et al.* (1993). The effective radiative decay rate of both levels, which are thermally coupled at room temperature, was estimated using the expression (Reisfeld *et al.*, 1982):

$$A_{eff} = \frac{12 e^{(-\frac{\Delta E}{kT})} \sum A_{ij} {}^2H_{11/2} + 4 \sum A_{ij} {}^4S_{3/2}}{12 e^{(-\frac{\Delta E}{kT})} + 4} \text{ s}^{-1} = 1350 \text{ s}^{-1}$$

In the above formula $\Delta E=710 \text{ cm}^{-1}$ is the energy difference between both levels, $kT=207 \text{ cm}^{-1}$, $\sum A_{ij} {}^2H_{11/2} = 3264 \text{ s}^{-1}$ is the total radiative decay rate from level ${}^2H_{11/2}$ and $\sum A_{ij} {}^4S_{3/2} = 1165 \text{ s}^{-1}$ is the total radiative decay rate from level ${}^4S_{3/2}$. Since the measured decay rate in the lowest concentration was 1887 s^{-1} (see Table 5.2-7), the multiphonon-assisted decay rate was estimated using the difference of the above decay rates ($\omega_5=1887-1350=537 \text{ s}^{-1}$). The branching ratios calculated by Wetenkamp *et al.* (1992), which are similar to those used by Vickers *et al.* (1992), have been used.

- Level 6 (${}^2H_{9/2}$)

Shinn *et al.* (1983) calculated for this level a total radiative decay rate of 2285 s^{-1} . The average decay rate, measured consistently in our work in low erbium concentrations (0.2 mol% - 1.6 mol%) under various pumping conditions was about 125000 s^{-1} (see Table 5.2-1 and Table 5.2-8). The conclusion was that a multiphonon-

assisted decay rate of about 123000 s^{-1} governs the decay of this level. As in the case of Level 3, where almost the entire population of the level decays non-radiatively, the branching ratios are not very important, however for completeness the values, calculated by Shinn *et al.* (1983) were used in the model.

- Level 7 ($^2P_{3/2} + ^2D_{3/2} + ^2F_{3/2}$)

The radiative decay rate A_{7j} from Level 7 to a lower j-th level was calculated using the expression (Hilborn., 1982):

$$A_{7j} = \frac{g_j}{g_7} \frac{\omega_{7j}^2 e^2}{2\pi\epsilon_0 mc^3} f_{j7} = \frac{g_j}{g_7} \frac{\omega_{7j}^2 e^2}{2\pi\epsilon_0 mc^3} \frac{g_7}{g_j} f_{7j} = \frac{\omega_{7j}^2 e^2}{2\pi\epsilon_0 mc^3} f_{7j}$$

where f_{7j} and f_{j7} are the emission and the absorption oscillator strength of the transition, g_j and g_7 are the degeneracy factors of the levels, ω_{7j} is the resonance frequency of the transition and m is the mass of the electron. With the help of this expression and the values of the oscillator strength for the transitions from level $^2P_{3/2}$ to the lower levels, published by Vickers *et al.*(1992), a value of 1780 s^{-1} was calculated for the total radiative decay rate from Level 7. The branching ratios, presented in Table 5.5-3, were calculated from the fractional transition rate to the various levels. A multiphonon-assisted decay rate of 400 s^{-1} was obtained using Equation 2.2-1.

- Level 8 ($^4H_{9/2} + ^4G_{9/2}$)

Not much information for this level could be obtained from the literature. A calculation of the multiphonon-assisted decay rate of this level, based on Equation 2.2-1 produced a value of $1 \times 10^6 \text{ s}^{-1}$. As was already mentioned in the discussions about the violet fluorescence line under 800 nm pumping, a value of $5 \times 10^4 \text{ s}^{-1}$ for the radiative rate of Level 8 was assumed on the basis of the numerical modelling.

$A_1(s^{-1})$	101	Shinn <i>et al.</i> , 1983; Zou <i>et al.</i> , 1993; Wetenkamp <i>et al.</i> , 1992; our work
$A_2(s^{-1})$	118	Zou <i>et al.</i> , 1993; Shinn <i>et al.</i> , 1983
$A_3(s^{-1})$	140	Zou <i>et al.</i> , 1993
$A_4(s^{-1})$	1085	Zou <i>et al.</i> , 1993; Shinn <i>et al.</i> , 1983
$A_5(s^{-1})$	1350	Reisfeld <i>et al.</i> , 1982, Zou <i>et al.</i> , 1993; Shinn <i>et al.</i> , 1983
$A_6(s^{-1})$	2285	Shinn <i>et al.</i> , 1983
$A_7(s^{-1})$	1780	Vickers <i>et al.</i> , 1992; our work
$A_8(s^{-1})$	50000	Modelled
$\omega_1(s^{-1})$	0	Shinn <i>et al.</i> , 1983; Zou <i>et al.</i> , 1993; our work
$\omega_2(s^{-1})$	9	Zou <i>et al.</i> , 1993; Shinn <i>et al.</i> , 1983; our work
$\omega_3(s^{-1})$	125000	Zou and Izumitani, 1993; our work
$\omega_4(s^{-1})$	4565	Zou <i>et al.</i> , 1993; Shinn <i>et al.</i> , 1983; our work
$\omega_5(s^{-1})$	537	Zou <i>et al.</i> , 1993; Shinn <i>et al.</i> , 1983; our work
$\omega_6(s^{-1})$	123000	Shinn <i>et al.</i> , 1983; our work
$\omega_7(s^{-1})$	400	Reisfeld <i>et al.</i> , 1987
$\omega_8(s^{-1})$	1000000	Reisfeld <i>et al.</i> , 1987
b_{10}	1	
b_{20}	0.88	Zou <i>et al.</i> , 1993; Wetenkamp <i>et al.</i> , 1992
b_{21}	0.12	Zou <i>et al.</i> , 1993; Wetenkamp <i>et al.</i> , 1992
b_{30}	0.77	Zou <i>et al.</i> , 1993; Wetenkamp <i>et al.</i> , 1992
b_{31}	0.22	Zou <i>et al.</i> , 1993; Wetenkamp <i>et al.</i> , 1992
b_{32}	0.01	Zou <i>et al.</i> , 1993; Wetenkamp <i>et al.</i> , 1992
b_{40}	0.91	Zou <i>et al.</i> , 1993; Shinn <i>et al.</i> , 1983
b_{41}	0.045	Zou <i>et al.</i> , 1993; Shinn <i>et al.</i> , 1983
b_{42}	0.043	Zou <i>et al.</i> , 1993; Shinn <i>et al.</i> , 1983
b_{43}	0.002	Zou <i>et al.</i> , 1993; Shinn <i>et al.</i> , 1983
b_{50}	0.67	Wetenkamp <i>et al.</i> , 1992; Shinn <i>et al.</i> , 1983,
b_{51}	0.27	Wetenkamp <i>et al.</i> , 1992; Vickers <i>et al.</i> , 1992
b_{52}	0.02	Wetenkamp <i>et al.</i> , 1992; Vickers <i>et al.</i> , 1992
b_{53}	0.04	Wetenkamp <i>et al.</i> , 1992; Vickers <i>et al.</i> , 1992
b_{54}	0	Wetenkamp <i>et al.</i> , 1992; Vickers <i>et al.</i> , 1992

Table 5.5-2 Values and corresponding references for the parameters used in the extended rate-equation model

b ₆₀	0.41	Shinn <i>et al.</i> , 1983
b ₆₁	0.44	Shinn <i>et al.</i> , 1983
b ₆₂	0.13	Shinn <i>et al.</i> , 1983
b ₆₃	0.01	Shinn <i>et al.</i> , 1983
b ₆₄	0.01	Shinn <i>et al.</i> , 1983
b ₆₅	0	Shinn <i>et al.</i> , 1983
b ₇₀	0.06	Vickers <i>et al.</i> , 1992
b ₇₁	0.295	Vickers <i>et al.</i> , 1992
b ₇₂	0.295	Vickers <i>et a.</i> , 1992
b ₇₃	0.09	Vickers <i>et al.</i> , 1992
b ₇₄	0.09	Vickers <i>et al.</i> , 1992
b ₇₅	0.17	Vickers <i>et al.</i> , 1992
b ₇₆	0	Vickers <i>et al.</i> , 1992
b ₈₀	0.5	assumed
b ₈₁	0.1	assumed
b ₈₂	0.1	assumed
b ₈₃	0.1	assumed
b ₈₄	0.1	assumed
b ₈₅	0.1	assumed

Table 5.5-3 Values and corresponding references for the parameters used in the extended rate-equation model (continue from Table 5.5-2)

5.5.3. The rate-equation model

As was mentioned in Chapter 4, the modelling process consisted in experimenting with different combinations of cross-relaxation processes and adjusting the associated parameters in order to obtain a single set of values which predicted well the observed experimental waveforms for all the levels under all the pumping conditions in all concentrations. On some occasions there was more than one way to interpret an

$$\begin{aligned} \frac{dn_0(t)}{dt} &= \sum_{i=1..8} (b_{i0}A_i n_i(t)) + \omega_1 n_1(t) + W(11,30)Cn_1(t)^2 + W(22,50)Cn_2(t)^2 + W(21,40)Cn_1(t)n_2(t) + \\ &+ W(33,60)Cn_3(t)^2 + 2T(333,008)C^2n_3(t)^3 + T(110,003)C^2n_1(t)^2n_0(t) + 2T(111,500)C^2n_1(t)^3 + \\ &+ T(220,005)C^2n_2(t)^2n_0(t) + T(222,610)C^2n_2(t)^3 - W(60,51)Cn_6(t)n_0(t) - \\ &- W(50,31)Cn_5(t)n_0(t) - T(300,011)C^2n_3(t)n_0(t)^2 - T(500,013)C^2n_5(t)n_0(t)^2 \\ \frac{dn_1(t)}{dt} &= \sum_{i=2..8} (b_{i1}A_i n_i(t)) + \omega_2 n_2(t) - (A_1 + \omega_1)n_1(t) + W(50,31)Cn_5(t)n_0(t) + W(60,51)Cn_6(t)n_0(t) + \\ &+ 2T(300,011)C^2n_3(t)n_0(t)^2 + T(500,013)C^2n_5(t)n_0(t)^2 + T(333,441)C^2n_3(t)^3 + \\ &+ T(222,610)C^2n_2(t)^3 - 2W(11,30)Cn_1(t)^2 - W(21,40)Cn_1(t)n_2(t) - \\ &- 2T(110,003)C^2n_1(t)^2n_0(t) - 3T(111,005)C^2n_1(t)^3 \\ \frac{dn_2(t)}{dt} &= \sum_{i=3..8} (b_{i2}A_i n_i(t)) + \omega_3 n_3(t) - (A_2 + \omega_2)n_2(t) - 2W(22,50)Cn_2(t)^2 - \\ &- W(21,40)Cn_1(t)n_2(t) - 2T(220,005)C^2n_2(t)^2n_0(t) - 3T(222,610)C^2n_2(t)^3 \\ \frac{dn_3(t)}{dt} &= \sum_{i=4..8} (b_{i3}A_i n_i(t)) + \omega_4 n_4(t) - (A_3 + \omega_3)n_3(t) + W(50,31)Cn_5(t)n_0(t) + W(11,30)Cn_1(t)^2 + \\ &+ T(110,003)C^2n_1(t)^2n_0(t) + T(500,013)C^2n_0(t)^2n_5(t) - 2W(33,60)Cn_3(t)^2 - \\ &- T(300,011)C^2n_3(t)n_0(t)^2 - 3T(333,008)C^2n_3(t)^3 - 3T(333,441)C^2n_3(t)^3 \\ \frac{dn_4(t)}{dt} &= \sum_{i=5..8} (b_{i4}A_i n_i(t)) + \omega_5 n_5(t) - (A_4 + \omega_4)n_4(t) + W(21,40)Cn_1(t)n_2(t) + 2T(333,441)C^2n_3(t)^3 \\ \frac{dn_5(t)}{dt} &= \sum_{i=6..8} (b_{i5}A_i n_i(t)) + \omega_6 n_6(t) - (A_5 + \omega_5)n_5(t) + W(22,50)Cn_2(t)^2 + \\ &+ W(60,51)Cn_6(t)n_0(t) + T(220,005)C^2n_2(t)^2n_0(t) + T(111,005)C^2n_1(t)^3 - \\ &- W(50,31)Cn_5(t)n_0(t) - T(500,013)C^2n_5(t)n_0(t)^2 \\ \frac{dn_6(t)}{dt} &= \sum_{i=7..8} (b_{i6}A_i n_i(t)) + \omega_7 n_7(t) - (A_6 + \omega_6)n_6(t) + W(33,60)Cn_3(t)^2 + T(222,610)C^2n_2(t)^3 - \\ &- W(60,51)Cn_6(t)n_0(t) \\ \frac{dn_7(t)}{dt} &= -(b_{87}A_8 + \omega_8)n_8(t) - (A_7 + \omega_7)n_7(t) \\ \frac{dn_8(t)}{dt} &= -(A_8 + \omega_8)n_8(t) + T(333,008)C^2n_3(t)^3 \end{aligned}$$

Figure 5.5-1

Extended rate-equation model for Er/ZBAN glasses

■ - radiative term, ■ - multi-phonon term, ■ - two-ion process, ■ - three ion process

observed temporal feature. In these cases physical intuition had to be used together with the rate-equation analysis in order to choose the most suitable approach for every separate case. More than 30 cross-relaxation processes (see Figure 5.4-1 and Figure 5.4-2) were considered for inclusion in the model. The final model consisted of 8 coupled non-linear differential equations which included 6 two-ion and 8 three-ion cross-relaxation terms in addition to those associated with radiative and phonon decay. The final version of this system of rate-equations is presented in Figure 5.5-1. These equations have no analytic solution and hence solutions had to be obtained numerically.

The cross-relaxation rate constants, which were found to produce the best fits to the experimental waveforms, are summarised in Table 5.5-4.

W(11,30)	W(22,50)	W(33,60)*	W(21,40)** ≡W(21,04)	W(50,31) ≡W(50,13)	W(60,51)*
$1 \times 10^{-17} \text{ cm}^3/\text{s}$	$1 \times 10^{-17} \text{ cm}^3/\text{s}$	$1.5 \times 10^{-16} \text{ cm}^3/\text{s}$	$1 \times 10^{-17} \text{ cm}^3/\text{s}$	$0.4 \times 10^{-18} \text{ cm}^3/\text{s}$	$5 \times 10^{-17} \text{ cm}^3/\text{s}$
T(110,003)*	T(111,500)**		T(220,005)*	T(222,610)*	
$0.3 \times 10^{-37} \text{ cm}^6/\text{s}$	$3 \times 10^{-37} \text{ cm}^6/\text{s}$		$0.3 \times 10^{-37} \text{ cm}^6/\text{s}$	$2 \times 10^{-35} \text{ cm}^6/\text{s}$	
T(300,011)*	T(333,441)*		T(333,008)*	T(500,013)**	
$0.4 \times 10^{-38} \text{ cm}^6/\text{s}$	$1 \times 10^{-34} \text{ cm}^6/\text{s}$		$1 \times 10^{-32} \text{ cm}^6/\text{s}$	$3 \times 10^{-38} \text{ cm}^6/\text{s}$	

Table 5.5-4 Cross-relaxation parameters for Er/ZB(L)AN glasses, determined from numerical modelling with the extended rate-equation model. * - reported for first time, ** - reported for first time in fluoride glasses. The values are considered accurate to within a factor of about two (see section 5.5.5).

5.5.4. Agreement between model predictions and experimental data

The ultimate test for the quality of the model which was developed in this thesis is the ability of the model to predict the temporal behaviour of the system under a wide variety of experimental conditions. In this regard, predictions of the final version of the extended model were compared with the experimental waveforms for several different pumping wavelengths. Plots of such comparisons, where measured and predicted waveforms have been plotted together are presented in Figures 5.5-2 - 5.5-9. Because

of the large number of waveforms (more than 1000) which were measured for the various levels, concentrations and pumping wavelengths, it is necessary to present only selected representative comparisons in the figures. In general, it was decided to present experimental and predicted waveforms only for the lowest and highest concentrations available- 1.6 mol% Er^{3+} (or 0.8 mol% Er^{3+}) and 18 mol% Er^{3+} . The behaviour in intermediate concentrations is generally not substantially different from those presented and is consistent with an interpolation of the differences evident at lowest and highest concentrations. In Chapter 4 it was seen that the behaviour of Level 1 in intermediate concentrations was somewhat harder to model. For this case we also present a comparison at an intermediate concentration of 10 mol% in order to demonstrate the improvement obtained with the extensions to the model.

Figure 5.5-2 and Figure 5.5-3 compare predicted and measured waveforms for all major levels under 800nm pumping. It can be seen that there are some small disagreements between predicted and observed decay waveforms. The decay rate of Level 1 (1.5 μm fluorescence) in 18 mol% Er^{3+} concentration, for instance, was somewhat slower than that observed. The opposite case was observed for the Level 4 (655nm) and Level 6 (407nm) in 1.6 mol% Er^{3+} concentration. However, in general these deviations were not very significant and the predictions of the model followed the experimental waveforms quite closely.

To illustrate the universal applicability of the model a limited number of waveforms were also plotted for the other pumping wavelengths. Only two concentrations and only the two main levels (Level 1 and Level 2) as well as Level 5, which also played an important role in the overall dynamics of the system, were presented.

In Figure 5.5-4 the calculated and the experimental waveforms for 1.5 μm pumping are presented. The good agreement of the decay waveforms for Level 1, especially in high concentration, was an indication of the suitability of the choice of the cross-relaxation parameters $W(11,30)$ and especially $T(110,003)$ and $T(111,500)$. An indication that a suitable value for the cross-relaxation rate constant $T(111,500)$ has been used was also the good agreement of the decay of Level 5 in 18 mol% Er^{3+}

800 nm pumping

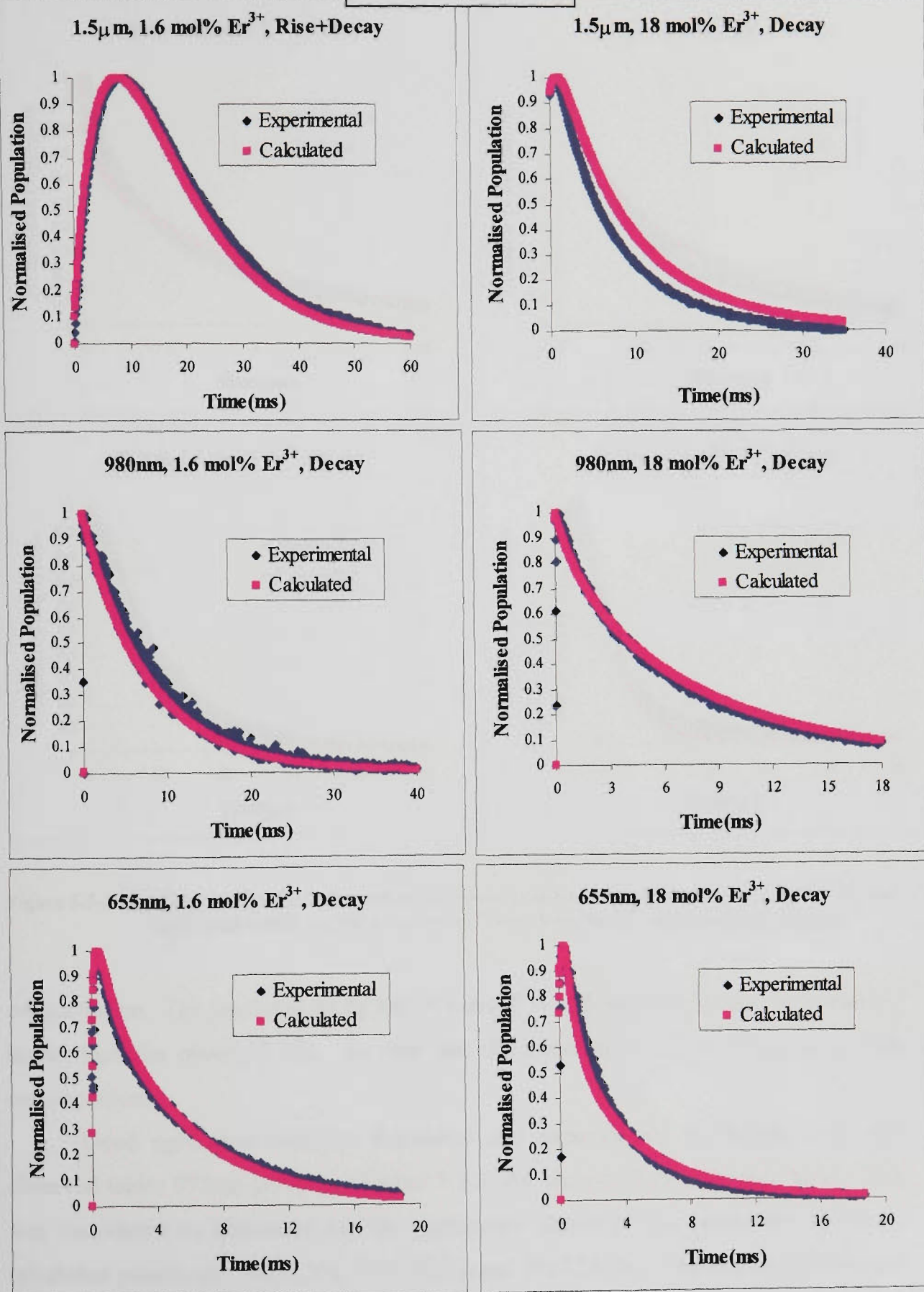


Figure 5.5-2 Calculated populations and experimental fluorescence waveforms for Level 1 (1.5 μm), Level 2 (980 nm) and Level 4 (655 nm) in 1.6 mol% Er³⁺ and 18 mol% Er³⁺ under 800nm pumping

800 nm pumping

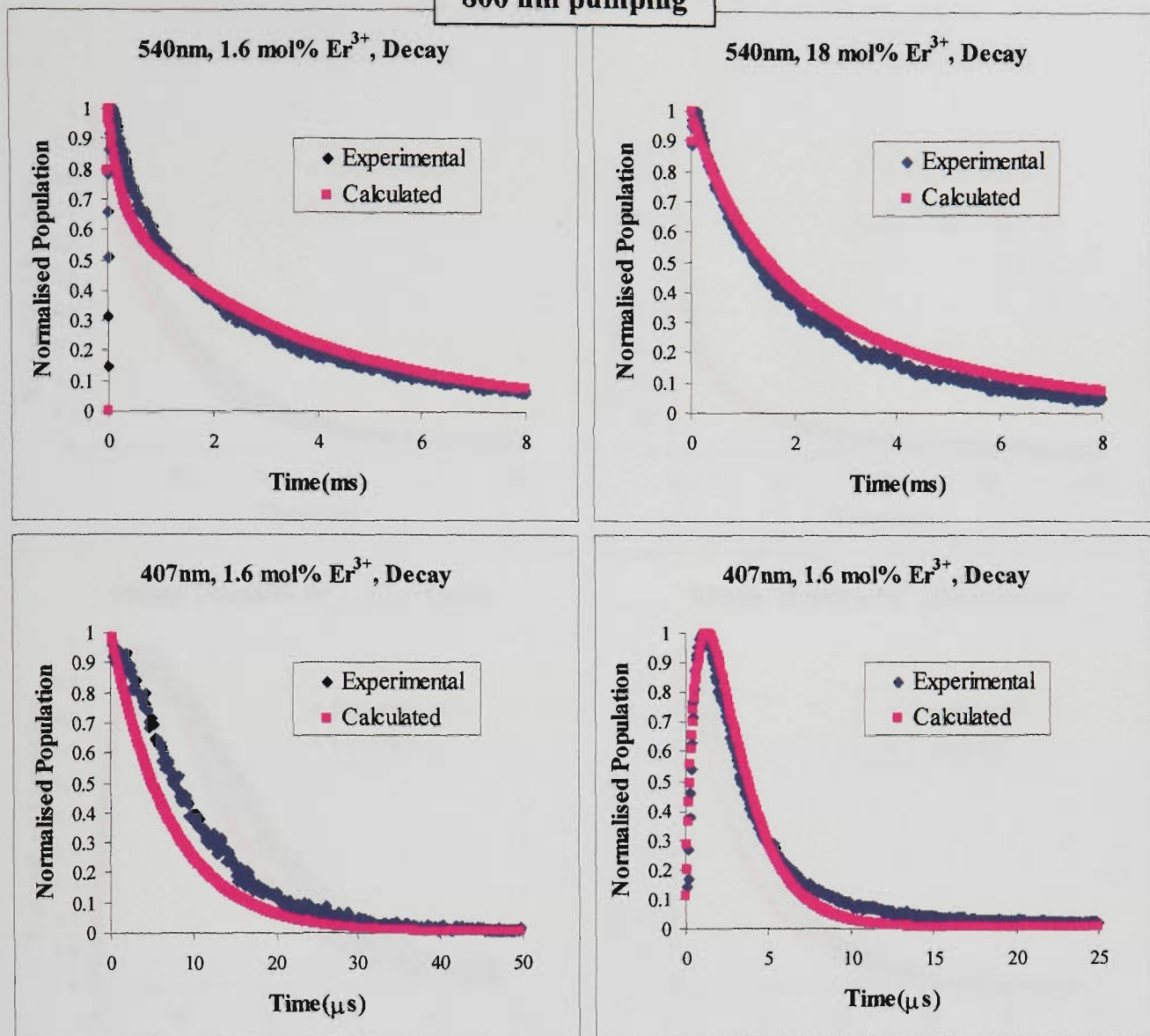


Figure 5.5-3 Calculated populations and experimental fluorescence waveforms for Level 5 (540 nm) and Level 6 (407 nm) in 1.6 mol% Er³⁺ and 18 mol% Er³⁺ under 800 nm pumping

concentration. The predicted decay rate of Level 2 in both concentrations was somehow higher than the observed one. So was also the decay rate of Level 5 again in both concentrations.

Good agreement between calculated and experimental waveforms was also observed under 975nm pumping (Figure 5.5-5) for almost all fluorescence lines. This was considered an indication for the appropriate choice of the values for the cross-relaxation parameters $W(22,50)$, $T(220,005)$ and $T(222,610)$. The difference between the decay waveforms of the 540nm fluorescence from Level 5 in low concentration indicated the lack of a sufficiently fine balance between the initial population of

1.5 μm pumping

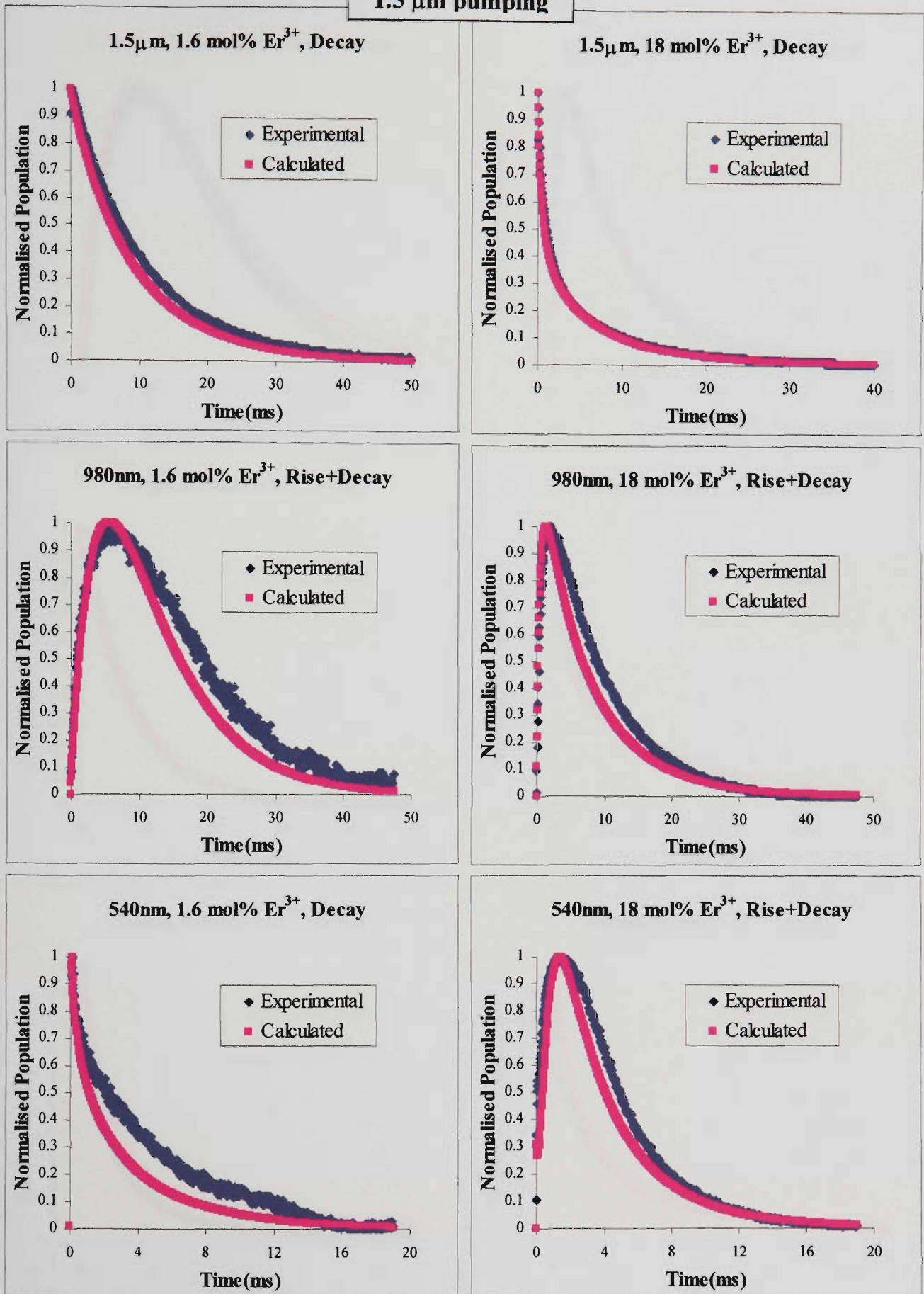


Figure 5.5-4 Calculated populations and experimental fluorescence waveforms for Level 1 (1.5 μm), Level 2 (980 nm) and Level 5 (540 nm) in 1.6 mol% Er^{3+} and 18 mol% Er^{3+} under 1.5 μm pumping

975 nm pumping

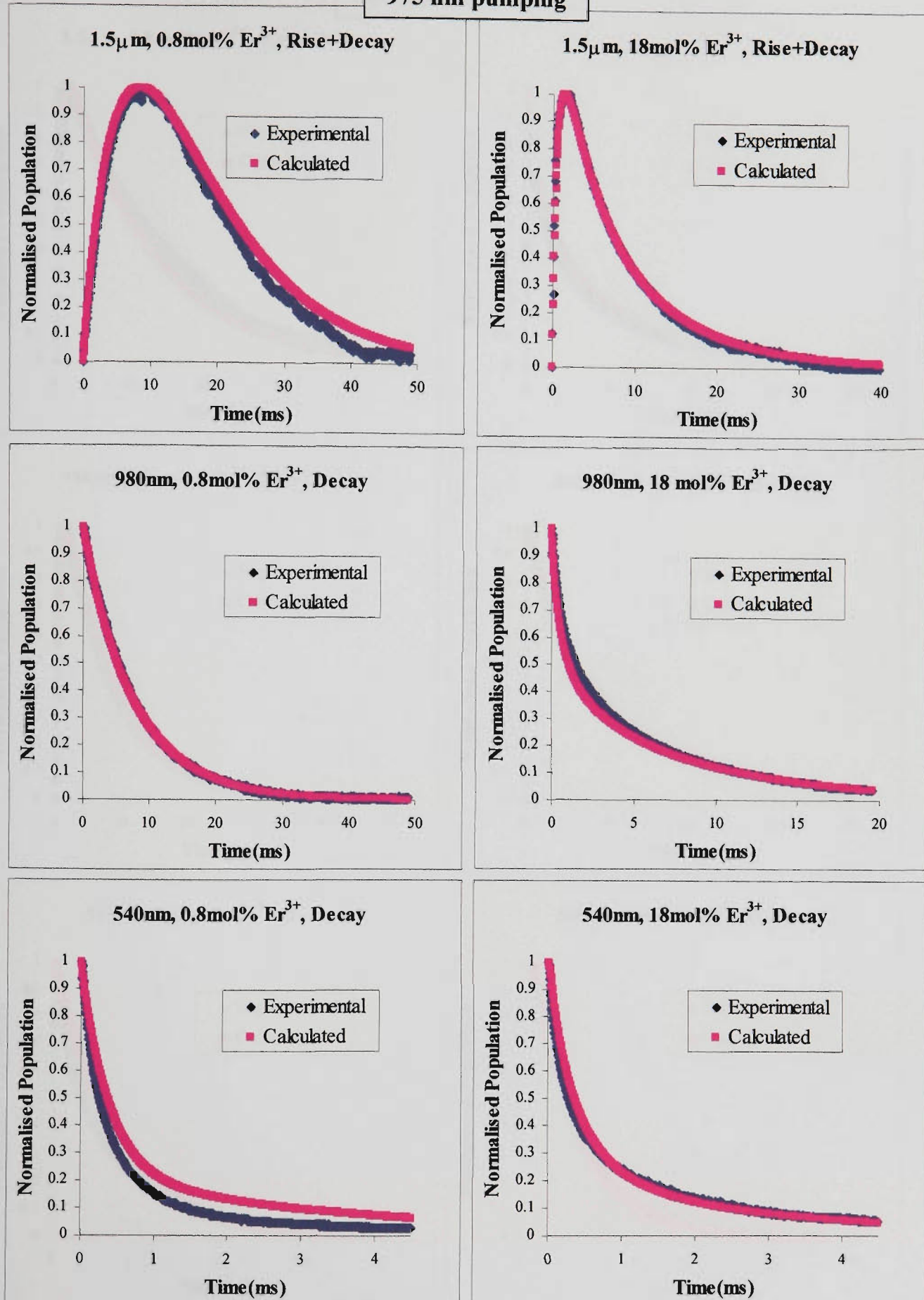


Figure 5.5-5 Calculated populations and experimental fluorescence waveforms for Level 1 (1.5 μm), Level 2 (980 nm) and Level 5 (540 nm) in 1.6 mol% Er^{3+} and 18 mol% Er^{3+} under 975 nm pumping

520 nm pumping

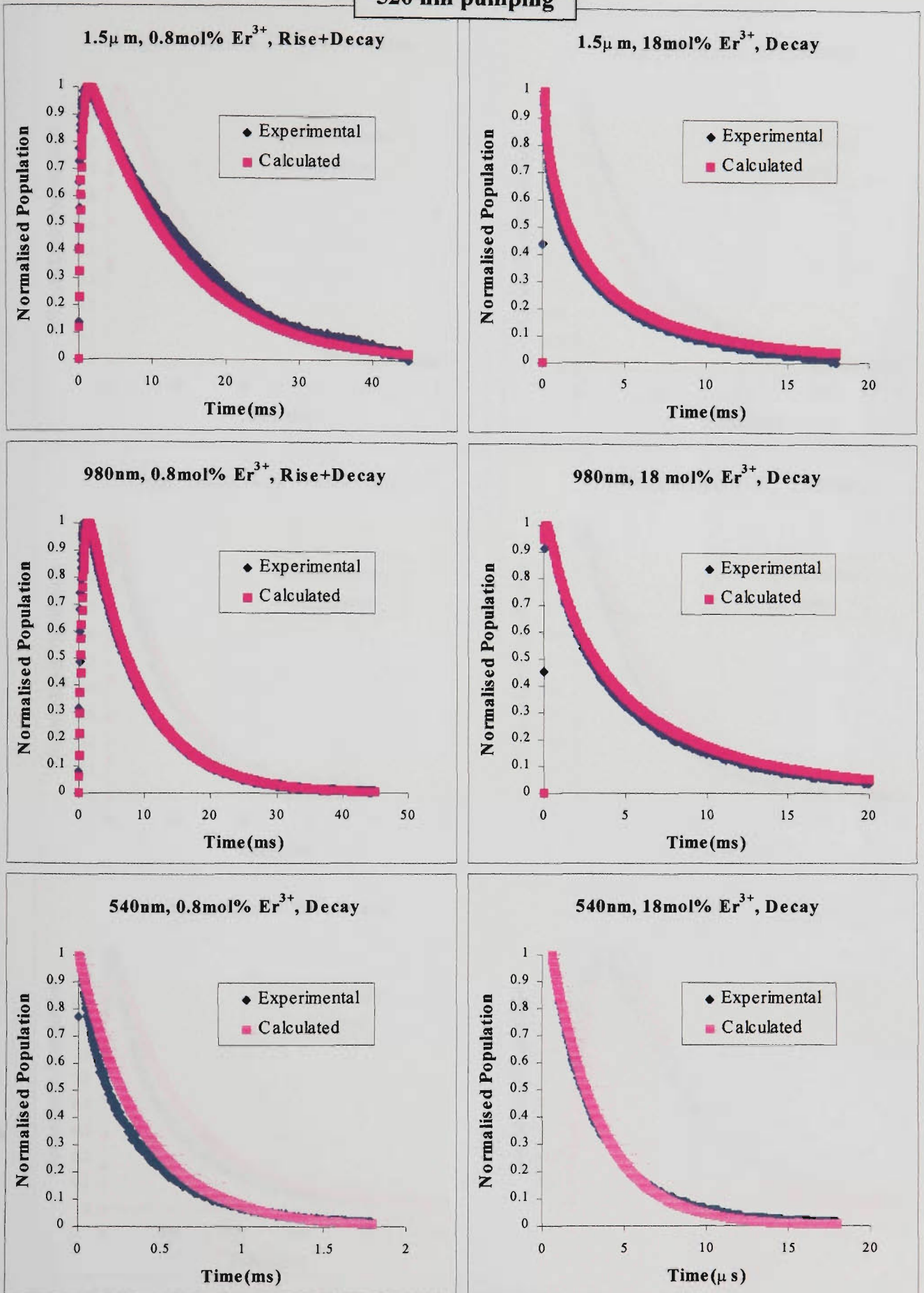


Figure 5.5-6 Calculated populations and experimental fluorescence waveforms for Level 1 (1.5 μm), Level 2 (980 nm) and Level 5 (540 nm) in 0.8 mol% Er³⁺ and 18 mol% Er³⁺ under 520 nm pumping

403 nm pumping

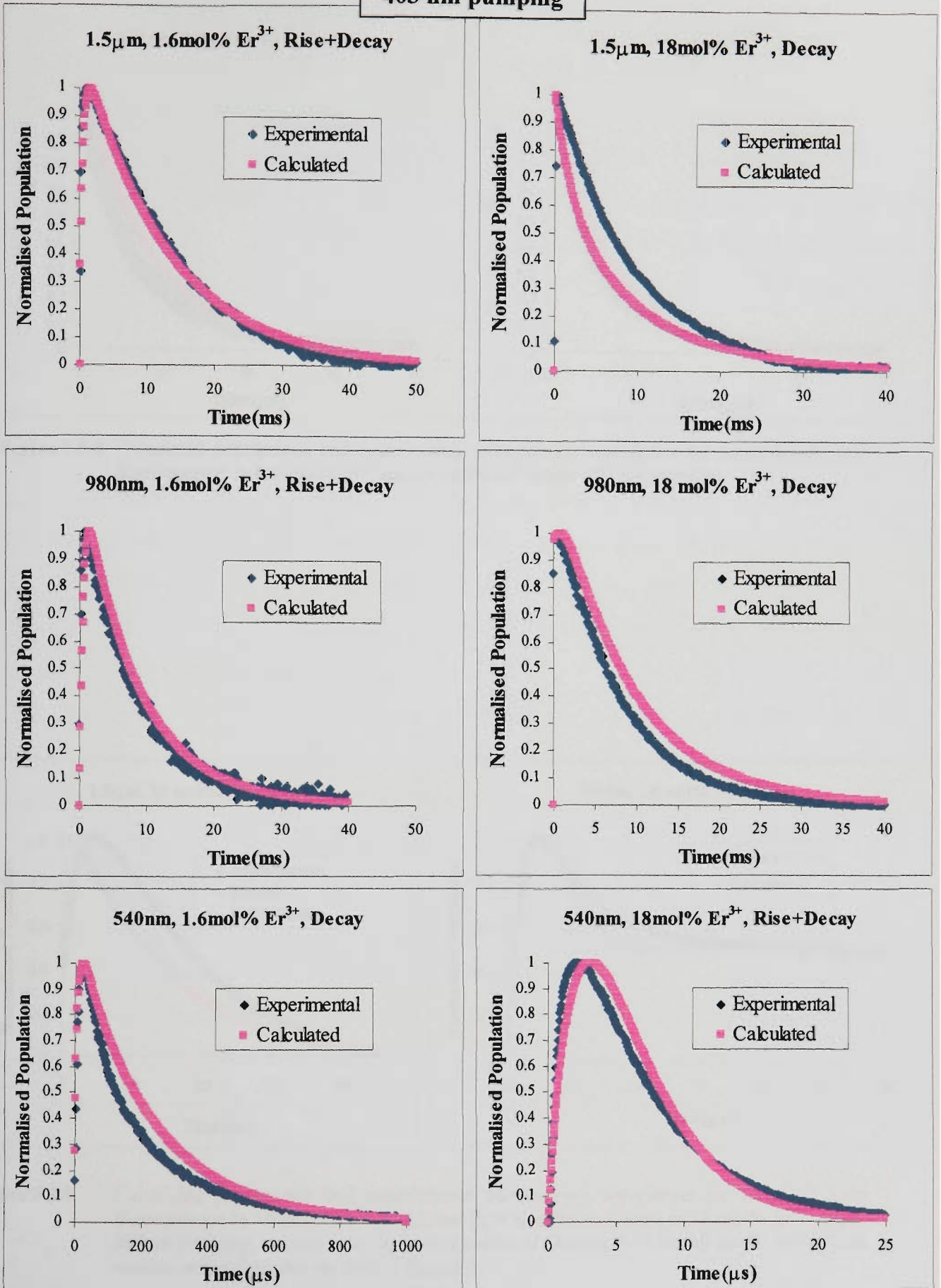


Figure 5.5-7 Calculated populations and experimental fluorescence waveforms for Level 1 (1.5 μm), Level 2 (980 nm) and Level 5 (540 nm) in 1.6 mol% Er^{3+} and 18 mol% Er^{3+} under 403 nm pumping

403 nm pumping

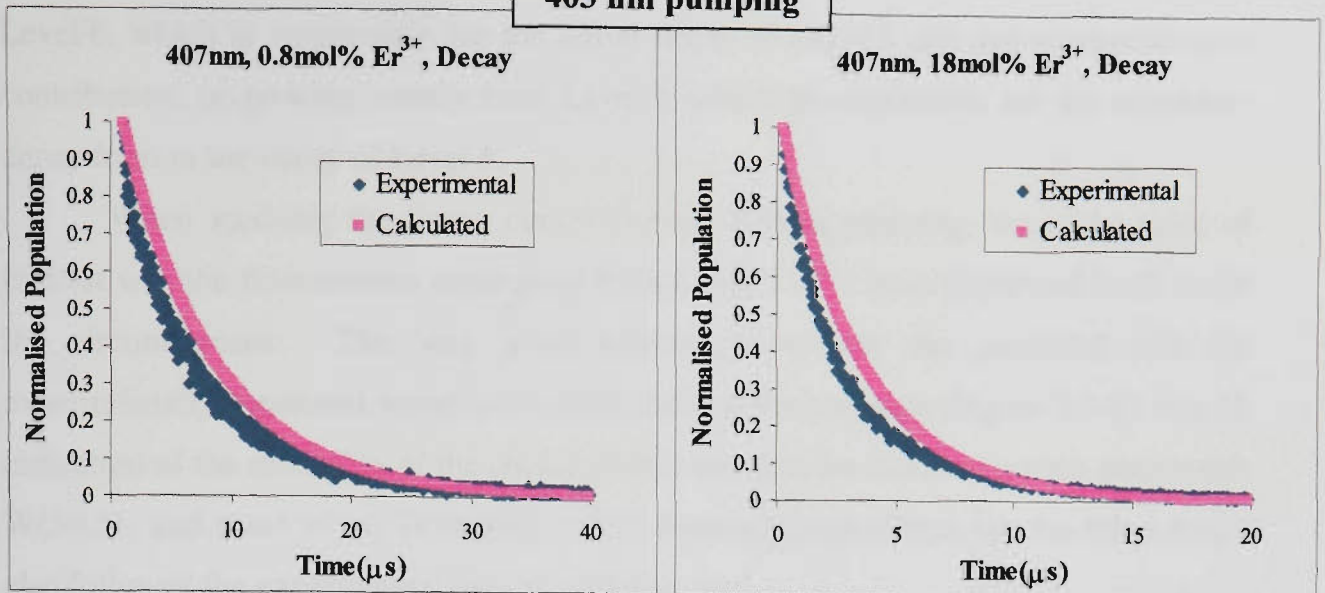


Figure 5.5-8 Calculated populations and experimental fluorescence waveforms for Level 6 (407 nm fluorescence) in 0.8 mol% Er³⁺ and 18 mol% Er³⁺ under 403 nm pumping

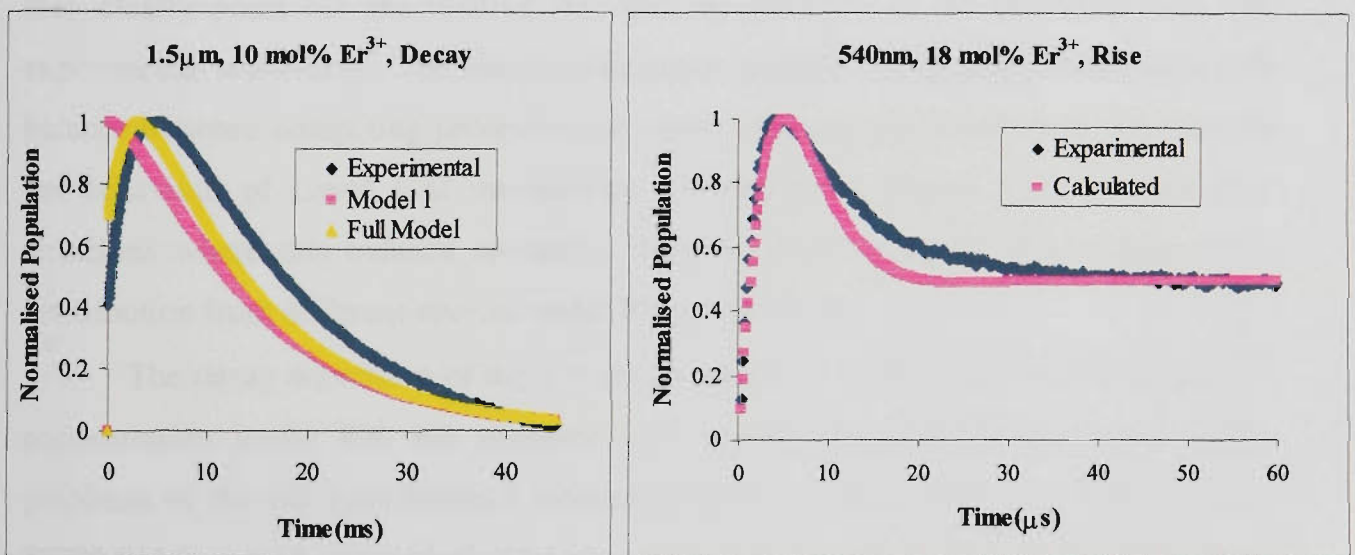


Figure 5.5-9 Calculated populations and experimental fluorescence waveforms for Level 1(1.5μm fluorescence) in 10 mol% Er³⁺ and Level 5(540nm fluorescence) in 18 mol% Er³⁺ under 800nm pumping. Model 1 is the limited model of Chapter 4. The full model is the final version of the extended model of Chapter 5.

Level 6, which is responsible for the initial decay of Level 5 and the cross-relaxation contribution, originating mostly from Level 2, which is responsible for the secondary decay form in the decay of Level 5.

When studying the decay curves for the 520nm pumping, the main point of interest was the fluorescence originating from Level 5 - the most populated level under the circumstances. The very good agreement between the predicted and the experimentally measured waveforms of the 540nm fluorescence (Figure 5.5-6) was an indication of the suitability of the choice of the values of the cross-relaxation parameters $W(50,31)$ and most of all $T(500,031)$. The calculated waveforms for the other levels also followed the experimental ones remarkably well.

The fits in the case of the 403 nm pumping were also reasonably good. This included fluorescences at 407 nm (from Level 6) and 540nm (from Level 5) (see Figure 5.5-7 and Figure 5.5-8) which are important for this pumping wavelength. From these figures it is obvious that there are some discrepancies between predicted and measured waveforms in both Er^{3+} concentrations. However, the overall agreement for all fluorescence lines was quite satisfactory.

Most of the graphs, which are presented above are in a sense self-explanatory - they clearly point out the relative size and the direction of the deviation from the experimental waveform. The need to look more carefully at situations where there is a balance between competing processes has been mentioned previously with reference to the behaviour of Level 1 at intermediate concentrations. Figure 5.5-9 presents two situations where this balance operates. Both are good examples of fine balance of contribution from different sources under 800nm pumping.

The decay waveform of the 1.5 μm fluorescence from Level 1 in 10 mol% Er^{3+} concentration under 800 nm pumping was already discussed in Chapter 4. The problems of the fits with Model 1 (including only processes $W(22,30)$, $W(22,50)$ and $T(300,011)$) and Model 2 (including also processes $T(110,003)$ and $T(220,005)$) have already been pointed out. Both these models are limited to the three lower excited energy levels and as can be seen in Figure 5.5-9, their predictions deviate considerably from the observed waveform. The predictions of the extended model developed in this chapter show much improved fits to the experimental waveform. The main reason for this is believed to be the inclusion in the model of the cross-relaxation processes

T(111,500), T(222,610) and especially T(500,013). All of these processes play significant roles in the modelling of this complex waveform. However, the deviation from the experimental waveform is still appreciable. This shows that the fine balance between the initial fast rise, caused predominantly by the cross-relaxation process T(300,011), and the later slow rise, due mainly to the radiative decay from Level 2 and also to the contribution of process T(500,013), has been predicted only approximately.

A similar fine balance of populations from different sources determines the shape of the second fluorescence waveform of Figure 5.5-9. This waveform represents the rise and the initial decay, as well as part of the late decay, of the 540 nm fluorescence from Level 5 in 800nm pumping. There is some disagreement between the predicted and the measured rate of the initial decay which is obvious in this figure. However, it should be noted that Level 5 has substantially lower population than the lower Levels 1 and 2. This makes Level 5 much more sensitive to small changes of the cross-relaxation rates of the processes which originate from these lower levels (such as W(22,50) and T(220,005)). Even processes such as T(300,011) and T(110,003) affect Level 5 indirectly since they affect Level 2 which in turn affects Level 5. In these circumstances the very presence of this initial component of the rise in the predicted waveform should be regarded as an achievement for the model.

In conclusion, from the figures presented above it is clear that the extended model provides very good agreement between predicted and measured fluorescence waveforms for a wide variety of conditions. The main aim of the work was to provide a model that could very satisfactorily predict the population behaviour of the main fluorescing levels over a wide range of doping concentrations and pumping conditions with 800 nm pumping. This has clearly been achieved. The relatively small discrepancies between prediction and measurement that are evident for all pump wavelengths are an indication that the model can still be further refined. However, in its present form it is suitable for use in designing active devices such as lasers based on these materials.

5.5.5. Accuracy of the parameters obtained from the numerical fits

As was discussed in Chapter 4, the fact that the values of the parameters in Table 5.5-4 are determined from numerical solutions of the system of equations in Figure 5.5-1 makes it very difficult to estimate the uncertainties in these values. A study of the sensitivity of the fits to the experimental waveforms to the changes in the parameters was performed in an attempt to try to quantify these uncertainties. Each parameter was separately varied by a factor of between 0.25 and 6 (up to 8 steps) and then the model was re-run. For every value of a parameter the sum of the squares of the differences (SSD) between the experimental and the predicted fluorescence waveforms was calculated. As is clear from previous discussions, there is a strong population coupling among the levels resulting from the presence of the cross-relaxation processes. Because of this coupling, for each value of a given parameter the calculations of the SSD's would ideally have involved some form of weighted summation over all possible fluorescence lines and all concentrations with all pumping wavelengths. Even when performed one parameter at a time, this involves a very large number of calculations. For example, the study of only 5 main fluorescence lines (corresponding to Levels 1,2,4,5,6) for only 3 different values of each of the 14 parameters in Table 5.4-1 in only 3 different concentrations under all 5 pumping wavelengths would require the manipulation of several thousand files. The vast amount of work involved in such a study makes it impractical. Instead, an approximate calculation of the SSDs has been performed using only the most important and most strongly affected fluorescence lines. No weighting factors have been used. In effect, weighting factors were incorporated by selecting the most strongly affected waveforms. Put another way, a proper weighted SSD would have emphasised the levels of the type selected.

The second way in which the number of calculations was limited was to calculate the SSD only for the concentration where the greatest effect of a particular cross relaxation process was expected. Calculations of the integrated contributions of the different cross relaxation terms in the rate-equations for all the main levels for 800 nm pumping were used to identify the most affected levels and concentrations for most

of the cross-relaxation processes (see next section and Table 5.5-5 for these calculations). It was clear from the very nature of the processes T(111,500), T(222,610), T(500,013) and W(60,51) that their effect is not very significant in 800nm pumping. Accordingly the calculations of the SSD's for these processes was performed under 1.5 μm , 975 nm, 520 nm and 403 nm pumping. Because of the more speculative nature of processes W(33,42), T(333,008) and T(333,441), no study of the sensitivity of the fits to their cross-relaxation rates was carried out. However, the sensitivity of appropriate fits to variations of these parameters is not likely to be very different from that of the other parameters.

Before presenting the results of the calculations of SSDs, it is useful to explain a little more clearly how Table 5.5-5 was used to select a particular fluorescence line and doping concentration in which to study the sensitivity of the solutions to variations in a particular parameter. For example, under 800 nm pumping the process W(22,50) accounted for about 41% of the total incoming population of Level 5 at 1.6 mol% doping. This is a very significant fraction and hence the sensitivity of the fits to this parameter was studied using the fluorescence waveform for this level and concentration. Similar considerations have been used in selecting waveforms with which to study the parameter sensitivity for the other cross-relaxation processes. Initially, the SSD between the experimental and the predicted waveforms was studied for values of the cross-relaxation parameters as used in the model (called in the figure "chosen values") as well as these multiplied by factor of 0.5 and 2. In the cases where too low or too high sensitivity was displayed a wider range of multiplication factors was used.

The results of this limited, but still quite extensive, sensitivity study are presented in Figure 5.5-10 (A) - (F). These figures include SSD histograms for 11 different cross relaxation processes (some processes are included more than once). In all cases except W(50,31), and possibly T(111,500), it can be seen that a factor of two change in the parameter produces substantial variations in the SSD. Thus with the exception of the above levels, it would appear that one could easily define the parameter to significantly better than a factor of 2. While one cannot really make any authoritative estimate of accuracy of parameters from this study, in general it seems that a factor of two would represent a reasonable rough estimate of the precision of the parameters

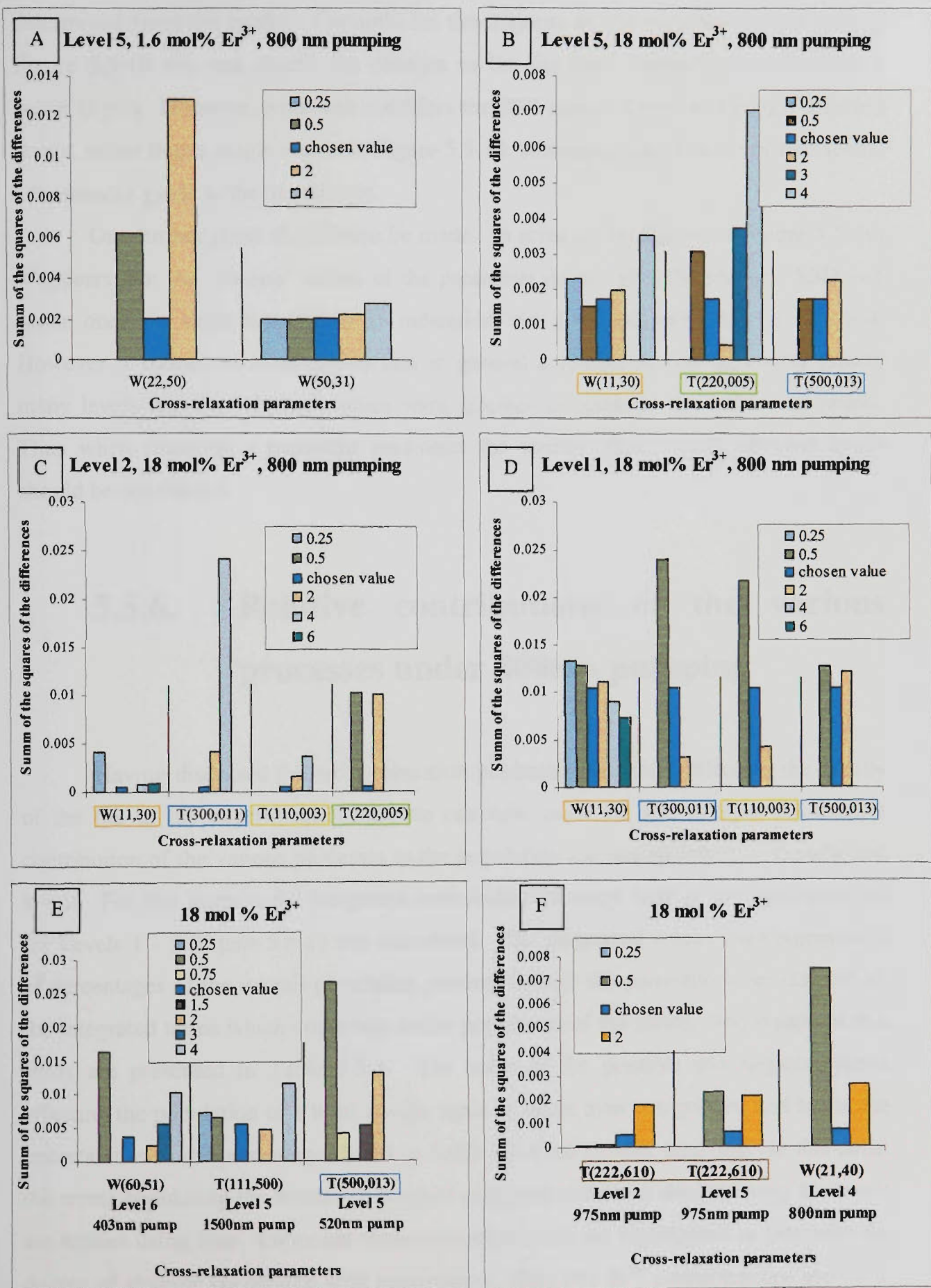


Figure 5.5-10 Sensitivity of the fits to changes in the cross-relaxation parameters. \square - For visualisation purpose frames with identical colour identify identical processes

determined from the model. Certainly for the majority of the parameters presented in Figure 5.5-10 one can clearly see changes in the fits from variations smaller than a factor of two. However, when one considers the SSD summed over all strongly affected levels, rather than a single one as in Figure 5.5-10, something like a factor of two seems a reasonable guide to the uncertainty.

One further point should also be made. In some of the figures of Figure 5.5-10, it appears that the "chosen" values of the parameter do not give the smallest SSD and hence one may think that this is an indication that a further refinement is required. However it should be remembered that in general a change in one parameter affects many levels and the "chosen" values were selected to optimise the fits for all levels. Thus when changing a particular parameter the overall effect on all affected levels should be considered.

5.5.6. Relative contributions of the various processes under 800nm pumping

Having discussed the cross-relaxation parameters and their effect on the quality of the fits to the experimental data, we can now move on and analyse the relative contribution of the various processes to the population and depopulation of the affected levels. For this purpose the integrated contribution of every term in the rate-equations for Levels 1 - 5 (Figure 5.5-1) was calculated. The integrated values were represented as percentages of the overall population passing through the particular level (sum of all the integrated terms which contribute to the population of the level). The results of this study are presented in Table 5.5-5. The sums of the positive and negative terms affecting the population of a level always agree to better than two percent and hence the uncertainties in the percentages listed in Table 5.5-5 are smaller than this. In this table, the terms populating the levels are denoted using red and those depopulating the levels are written using blue. Important cross-relaxation terms are highlighted in grey with the degree of shading correlating with importance. Only two Er^{3+} concentrations are used; 1.6 mol% and 18 mol% .

Term :	1.6 mol % Er ³⁺ Level 1 (⁴ I _{13/2})	18 mol % Er ³⁺	Term :	1.6 mol % Er ³⁺ Level 2 (⁴ I _{11/2})	18 mol % Er ³⁺
+b ₂₁ A ₂ n ₂	56.8%	5.3%	+b ₄₂ A ₄ n ₄	0.0%	0.0%
+ω ₂ n ₂	35.7%	3.0%	+b ₅₂ A ₅ n ₅	0.0%	0.0%
+b ₅₁ A ₅ n ₅	0.4%	0.0%	+b ₇₂ A ₇ n ₇	0.0%	0.7%
+b ₇₁ A ₇ n ₇	0.0%	0.8%	+b ₆₂ A ₆ n ₆	0.0%	0.0%
+W(50,31)cn ₀ n ₅	0.1%	0.1%	+ω ₃ n ₃	100.0%	99.3%
+W(60,51)cn ₆ n ₀	0.1%	1.8%	-A ₂ n ₂	91.0%	46.6%
+T(500,031) c ² n ₀ ² n ₅	3.4%	22.2%	-ω ₂ n ₂	6.9%	3.3%
+2T(300,011) c ² n ₃ n ₀ ²	2.9%	64.4%	-2W(22,50)cn ₂ ²	0.9%	3.4%
+T(222,610) c ² n ₂ ³	0.4%	2.1%	-W(21,40)cn ₁ n ₂	0.1%	1.8%
-A ₁ n ₁	99.4%	48.4%	-3T(222,610) c ² n ₂ ³	0.2%	7.0%
-2W(11,30)cn ₁ ²	0.2%	4.3%	-2T(220,005) c ² n ₂ ² n ₀	0.8%	37.9%
-W(21,40)cn ₁ n ₂	0.3%	1.6%	Level 5 (⁴ S _{3/2} + ² H _{11/2})		
-2T(110,003) c ² n ₀ n ₁ ²	0.1%	45.6%	+b ₇₅ A ₇ n ₇	0.7%	0.2%
-3T(111,500) c ² n ₁ ³	0.0%	0.1%	+ω ₆ n ₆	19.1%	6.3%
Level 4 (⁴ F _{9/2})					
+b ₈₄ A ₈ n ₈	0.2%	0.7%	+W(22,50)cn ₂ ²	41.2%	7.0%
+b ₇₄ A ₇ n ₇	0.9%	6.6%	+W(60,51)cn ₆ n ₀	2.3%	8.1%
+ω ₅ n ₅	66.6%	1.4%	+T(111,500) c ² n ₁ ³	0.0%	0.2%
+W(21,40)cn ₁ n ₂	31.7%	73.0%	+T(220,005) c ² n ₀ n ₂ ²	36.7%	78.2%
+2T(333,441) c ² n ₃ ³	0.6%	18.2%	-A ₅ n ₅	26.3%	0.4%
-A ₄ n ₄	20.4%	18.8%	-ω ₅ n ₅	12.0%	0.1%
-ω ₄ n ₄	79.6%	81.2%	-W(50,31)cn ₀ n ₅	2.3%	0.3%
			-T(500,031) c ² n ₀ ² n ₅	59.3%	99.2%

Table 5.5-5-Integrated contribution (in %) of the different terms in the rate equations for Level 1, Level 2, Level 4 and Level 5 from Figure 5.5-1 in 1.6 mol% Er³⁺ and 18 mol% Er³⁺ under 800 nm pumping. Red colour -populating terms, blue colour- depopulating terms. Grey filling - relatively important cross-relaxation process. Some terms with a relative contribution of up to 0.2% have been omitted.

Level 1 (${}^4I_{13/2}$)

As expected in low Er^{3+} concentration, Level 1 received its population predominantly from the radiative and multi-phonon assisted decay from Level 2 (${}^4I_{11/2}$) and was depopulated via its own radiative decay. The effect of the contributing process T(500,031) and especially T(300,011), appreciable even in low concentrations, increased with concentration and completely dominated at 18 mol% Er^{3+} . Process T(110,003), together with the radiative decay were mainly responsible for the depopulation of Level 1 in high concentration.

- Level 2 (${}^4I_{11/2}$)

For this 800 nm pump, almost the entire population of Level 2 (${}^4I_{11/2}$) in both 1.6 mol% Er^{3+} and 18 mol% Er^{3+} originated from the multi-phonon assisted decay from Level 3 (${}^4I_{9/2}$). Part of the reason for that was probably the fact that most of the cross-relaxation processes, originating from Level 1 (W(11,30) and T(110,003)) and Level 5 (W(50,31) and T(500,031)) terminated on Level 3. While in low concentration the radiative and the multi-phonon assisted decay completely dominated the depopulation of Level 2, in high concentration the process W(22,50) and especially T(220,005) had also a substantial contribution. Noticeably, in these high concentrations the contribution of the three ion process T(222,610) was also appreciable. This was in contrast with the contribution of process T(111,500) which, for this pumping wavelength (800nm), did not have any effect on the system.

- Level 4 (${}^4F_{9/2}$)

In low Er^{3+} concentration, Level 4 (${}^4F_{9/2}$) received its population mainly via the multi-phonon assisted decay from Level 5 and decayed via its own radiative and multi-phonon assisted decay. The effects of processes T(333,441) and especially W(21,40) were significantly enhanced at high concentrations. Also it should be noted that the values in Table 5.5-5 were integrated ones and hence take no account of the time interval over which a process acts. It is possible to have a small integrated population and still have a significant effect over a short time interval (e.g. the rise). For instance, the process T(333,441), despite its relatively small contribution in 18 mol% Er^{3+} , completely

dominated the rise of Level 4 because its effect is present only during the first 30 or so microseconds.

- Level 5 ($^4S_{3/2}+^2H_{11/2}$)

In low concentrations the two processes W(22,50) and T(220,005) are roughly equal in determining the population of this level. In high concentrations, however, T(220,005) completely dominates. In both concentrations the cross-relaxation process T(500,031) was by far the most important in depopulating Level 5. As was mentioned in earlier discussions, the effect of process W(50,31) was relatively small and only noticeable in low Er^{3+} concentration

5.6. Conclusions

This chapter has presented a comprehensive study of the population dynamics of the main fluorescing energy levels in highly-doped $Er^{3+}/ZB(L)AN$ glasses. This study has involved extensive measurements of fluorescences from important energy levels, clarification of the physical processes responsible for the details of each fluorescence waveform and finally the development of a model which can predict fluorescence waveforms which agree quite well with those measured over a wide variety of conditions. The main results of the study were as follows:

- A large number of fluorescence waveforms for eight fluorescence levels of the system $Er^{3+}/ZB(L)AN$ have been collected for 5 different pumping wavelengths in samples with Er^{3+} concentrations from 0.2 mol% to 18 mol%.
- These fluorescence waveforms have been fitted using analytical functions, derived from a simplified rate-equation analysis. Where no analytical solutions could be found, a simple-exponential- or combination of rise + decay-exponential-function fits have been used. These fits have been used to summarise the principal features of the waveforms in tabular form.
- The data from the fits to the experimental waveforms have been analysed in detail to provide a physical understanding of the processes responsible for the features evident in the tabulated data. The dominant ion-ion exchange processes have been

identified. A complex rate-equation model, consisting of nine coupled non-linear rate-equations, has been developed.

- In the process of the modelling, 2 two-ion cross-relaxation processes and 6 three-ion cross-relaxation processes were, to our knowledge, introduced for the first time in explaining the population dynamics of the Er^{3+} ions. In addition, 3 other processes were applied for the first time for Er^{3+} ions in fluoride glasses.

- The cross-relaxation rate constants in this model have been varied until good agreement with the experimental waveforms has been achieved. A single self-consistent set of rate constants was obtained for the 14 cross-relaxation processes implemented in the model. Modelling with this set of constants produced waveforms which agreed quite well with those measured for the main fluorescent levels over the whole range of Er^{3+} concentrations used.

- The sensitivity of the SSD between predicted and measured waveforms to changes in the values of the cross-relaxation rate constants has been studied. This has allowed estimation of the accuracy of the rate constants obtained from the model. The parameters are considered accurate to within a factor of about two.

- The integrated contributions of the various process terms in the rate equation model for Levels 1,2,4 and 5 with 800nm pumping have been calculated. These calculations quantified the overall importance of the various processes involved in population and de-population of the different excited energy levels.

The studied $\text{Er}^{3+}/\text{ZB(L)AN}$ system exhibited a large number of fluorescence lines, some of which were overlapping, and had quite complex fluorescence waveforms. While still capable of further refinement, the rate equation model makes a significant contribution to the identification and quantification of the dominant mechanisms in the population dynamics of this system.

Chapter 6

Conclusion

Knowles and Jenssen (1992) in a study of Er, Pr:BaY₂F₈ stated that erbium has proven to be a very difficult system to understand, especially when high doping concentrations are involved. The present research confirmed this to be the case. The low multiphonon rates in the fluorozirconate glasses result in a high quantum efficiency of the energy levels of the erbium ions. These high quantum efficiencies give rise to numerous fluorescence lines, many of which are non-existent in other glasses, including silica glasses. Some of these fluorescence lines are overlapping because of the resonant spacing between many energy levels in erbium. These overlapping fluorescence lines are evident also in the lifetime measurements, where complex waveforms with multiple rises and decays are observed. This study confirmed that the resonant spacing also gives rise to a large number of two-ion and three-ion cross-relaxation processes, which are especially important in the high erbium concentrations used in this research. These cross-relaxation processes cause a continuous redistribution of population among all the levels. This results in complex population dynamics which is very difficult to analyse

and model. The need for the present research was justified by the previous lack of very detailed analysis of these cross-relaxation processes in glasses. Knowledge of these processes and the associated cross-relaxation rate-constants is very important for the design and optimisation of future optoelectronic devices using these materials. Thus this study has concentrated on investigation of the temporal behaviour of the fluorescence from highly doped Er/ZB(L)AN glasses and the effect of various cross-relaxation processes on this behaviour. A short summary of this study is presented below.

Brief summary of the work:

Chemically stable ZB(L)AN glasses with excellent optical qualities and erbium concentration from 0.2 mol% to 18 mol % have been produced.

Fluorescence and absorption spectra of these glasses have been studied. The absorption cross-sections for the main pumping wavelengths are presented below (the uncertainties are 10%):

Pumping λ	1.5 μm	980 nm	800 nm	520 nm	403 nm
σ (cm^2)	4.5×10^{-21}	1.9×10^{-21}	0.6×10^{-21}	11×10^{-21}	1.3×10^{-21}

While pumping at 800 nm, the fluorescence intensities of the main fluorescence lines have been studied as a function of the erbium concentration and pump power. All of the fluorescence lines studied exhibited an increase in intensity up to a doping level of about 12-14 mol% and a decrease beyond that concentration. Log/log plots of the fluorescence intensity vs pump power at 800 nm revealed that, as expected, the pump process for excitation of the $^4\text{I}_{13/2}$ and $^4\text{I}_{11/2}$ levels was characterised by absorption of an average of approximately one pump photon per excited ion. Similar plots showed that the excitation process for the $^4\text{F}_{9/2}$ and ($^4\text{S}_{3/2} + ^2\text{H}_{11/2}$) levels required an average absorption of about two pump photons per excited ion. The fluorescence at 407 nm required an average of more than two pump photons per fluorescence photon. Later lifetime measurements of this violet line indicated that the fluorescence at this

wavelength probably originates from two different levels; the $^2H_{9/2}$ level, populated by two excitation photons, and a higher $^4D_{9/2}$ level, which was populated by a process requiring the absorption of three excitation photons.

Numerous decay waveforms were measured for all main fluorescence lines in samples covering the whole range of concentrations under 800 nm, 1.5 μ m, 980 nm, 520 nm and 403 nm pumping. The effects of the various cross-relaxation processes on the population dynamics of the $Er^{3+}/ZB(L)AN$ system were analysed in detail. In some cases this analysis allowed simplified analytical functions to be derived and fitted to the observed decay curves. However, for most of the fluorescence waveforms the analysis was too complex and no analytical fitting functions could be derived. Single or multiple rise and decay exponential functions were fitted to the experimental waveforms in these cases. The fitting of these functions allowed the fluorescence waveform data to be summarised in tabular form.

Under 800 nm pumping, most of the excited erbium ions were presumed to be in the first three excited energy levels. For that reason the first attempt of modelling used a system of rate equations involving only these levels. Despite the limited number of levels, the inclusion of three-ion processes led to non-linear equations which could not be solved analytically and hence numerical routines were used. Two important conclusions were drawn from the numerical modelling involving these three excited states. The first conclusion was that in high doping concentrations the three-ion cross-relaxation process T(330,001) was mainly responsible for the fast rise of the population of Level 1 ($^4I_{13/2}$) with 800 nm excitation. The second conclusion was that in the population dynamics of the $Er^{3+}/ZB(L)AN$ system in high doping concentrations, there was a strong indication of the presence of two other three-ion processes, T(110,003) and T(220,005).

This first model was found to be unsatisfactory for two main reasons:

- The limited number of levels under consideration did not introduce sufficient constraints on the modelling so that there was a unique model which could duplicate the measured waveforms. As a result the model could not distinguish between similar processes

- While the model produced reasonable fits to the measured waveforms at both high and low concentrations, the agreement at intermediate concentrations was not adequate, especially in the case of the waveform of the $^4I_{13/2}$ level (Level 1)

It was clear from this first modelling attempt using only three excited states that higher energy levels were involved in the processes that affected Levels 1 - 3. With this in mind the range of fluorescence measurements was extended to include all detectable fluorescence waveforms (with appreciable fluorescence intensity). Some of these waveforms originated from levels as high as the $^4D_{7/2}$ level (Level 8). This fluorescence data was used to extend the initial model to include these higher excited states. More than 30 different cross-relaxation processes (see Fig. 5.4-1 and Fig.5.4-2, Chapter5) and their effects on the population dynamics of the relevant levels were investigated. An extended rate-equation model (see Fig. 5.5-1, Chapter 5), including 8 excited levels and 14 cross-relaxation processes, was constructed. The values of the cross-relaxation rate constants which best modelled the experimental waveforms are presented in the table below (see also Table 5.5-4, Chapter 5).

W(11,30)	W(22,50)	W(33,60)*	W(21,40)** ≡W(21,04)	W(50,31) ≡W(50,13)	W(60,51)*
$1 \times 10^{-17} \text{ cm}^3/\text{s}$	$1 \times 10^{-17} \text{ cm}^3/\text{s}$	$1.5 \times 10^{-16} \text{ cm}^3/\text{s}$	$1 \times 10^{-17} \text{ cm}^3/\text{s}$	$0.4 \times 10^{-18} \text{ cm}^3/\text{s}$	$5 \times 10^{-17} \text{ cm}^3/\text{s}$
T(110,003)*	T(111,500)**		T(220,005)*	T(222,610)*	
$0.3 \times 10^{-37} \text{ cm}^6/\text{s}$	$3 \times 10^{-37} \text{ cm}^6/\text{s}$		$0.3 \times 10^{-37} \text{ cm}^6/\text{s}$	$2 \times 10^{-35} \text{ cm}^6/\text{s}$	
T(300,011)*	T(333,441)*		T(333,008)*	T(500,013)**	
$0.4 \times 10^{-38} \text{ cm}^6/\text{s}$	$1 \times 10^{-34} \text{ cm}^6/\text{s}$		$1 \times 10^{-32} \text{ cm}^6/\text{s}$	$3 \times 10^{-38} \text{ cm}^6/\text{s}$	

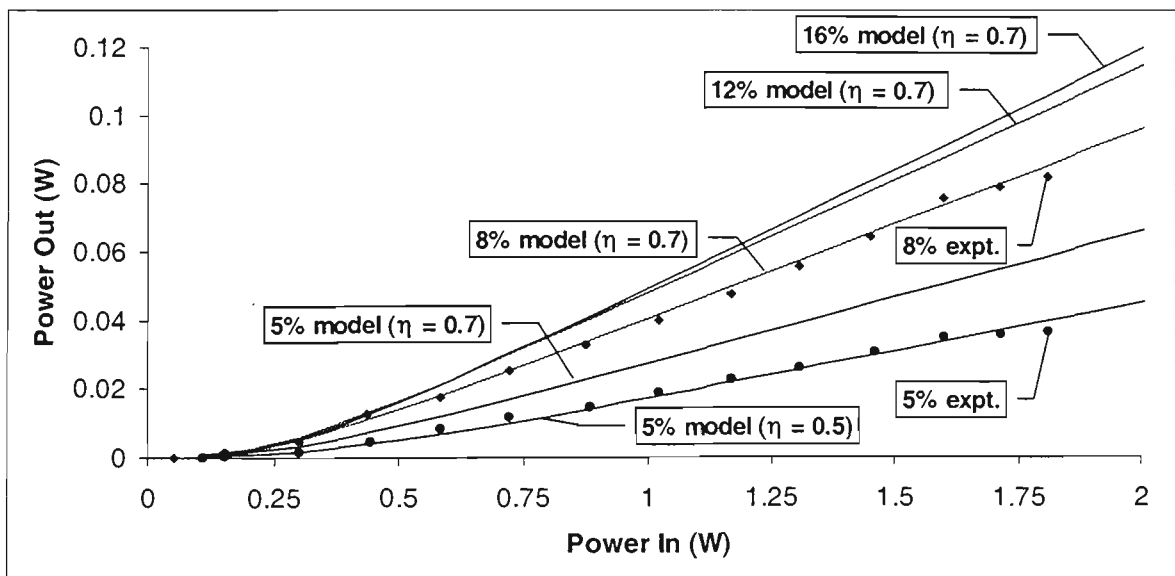
Because of the use of numerical routines it was difficult to estimate the uncertainties in the above parameters. However, a study of the sensitivity of the fits to the experimental waveforms to change in these parameters indicated that these are accurate within about a factor of two. The integrated contributions of the various processes affecting the population of the main fluorescing levels were calculated for 800 nm pumping. This calculation allowed the relative importance of the different processes affecting a particular level to be quantified.

In conclusion - a very detailed study of the population dynamics in heavily-doped $\text{Er}^{3+}/\text{ZB(L)AN}$ glasses has been carried out. A large number of ion-ion exchange processes were found to be important for the population dynamics of the system. The dominant processes were identified and values for their rate constants were obtained. Most of these processes are reported for first time in this thesis and associated publications (see Table 5.5-2, Chapter 5). The relative importance of these processes for the population dynamics of the affected levels with 800 nm excitation has been evaluated.

The dynamics of the $\text{Er}^{3+}/\text{ZB(L)AN}$ system in these high concentrations is very complex. Because of this, and also because of the numerical nature of the modelling process, the possibility of the existence of more than one self-consistent set of rate constants which adequately model the measured waveforms could not be completely excluded. However, from the discussions in Chapter 5 it is apparent that the complex re-population mechanisms imposed tight restrictions on the cross-relaxation rate constants of all processes introduced in the system. Also it should be remembered that the single set of cross-relaxation rates obtained in this thesis satisfies reasonably well measured waveforms of many fluorescing lines for 5 different pumping wavelengths in samples with erbium concentrations varying by two orders of magnitude. These requirements also imposed severe limitation on the choice of cross-relaxation processes included in the model, as well as on the values of the corresponding rates. Thus, while the existence of a different set of cross-relaxation processes or rate constants can not be completely ruled out, all the indications are that it is very unlikely.

The main contribution of this work is that it provides a much more-detailed understanding of the population dynamics in Er^{3+} glasses than has previously been published. There are also a number of possible applications of the cross-relaxation rate constants obtained in this work. These rate constants could be used for determining an unknown doping concentration (or concentration profile) in a sample from fluorescence measurements in a way similar to that described by Petreski *et al.*, (1997) and Mitchell *et al.* (1999). Knowledge of the cross relaxation processes and their rate constants should also enable future detailed modelling and optimisation of heavily-doped erbium systems in devices such as lasers, amplifiers and waveguides.

The model has already been used for laser modelling and it has shown some promising results. While a laser based on the ZB(L)AN glasses studied in this thesis is yet to be constructed, Sandrock *et al.*(1999) recently reported two bulk lasers lasing at 2.7 μm - 2.8 μm in very similar materials. Er^{3+} concentrations of 5 mol% and 8 mol% were used for these lasers. A slightly modified version of the rate-equation model presented in this thesis fitted reasonably well the experimental laser data presented by Sandrock *et al.* Some of the experimental parameters such as pump coupling efficiency and diffraction losses had to be adjusted in order to optimise the agreement. However, all the values used were well within the range expected for the particular experimental setup. The figure below presents experimental and modelled input/output characteristics of Er^{3+} :ZB(L)AN lasers for several doping concentrations. The continuous lines represent output vs input power for 5 mol%, 8 mol%, 12 mol% and 16 mol% predicted by the model. The dots represent the experimental data for 5 mol% and 8 mol% from the publication of Sandrock *et al.* It could be noticed that two different values of pump coupling efficiency (η) were needed in the model to achieve a good fit to the experimental points for 5 mol% and 8 mol%. It was not clear from the publication of Sandrock *et al.* if such a difference in η was present in the experimental setup for both lasers. However, the fact that only a simple scaling factor allows good predictions for the performance of two different lasers to be made was considered as very encouraging indication for the overall good performance of the model.



Calculated (continuous lines) and experimental (dotted lines) input/output characteristics of Er^{3+} :ZB(L)AN lasers for the indicated doping concentrations. The experimental data is from Sandrock *et al.*(1999). η – pump coupling efficiency used in the calculations.

Another good indication was that the model predicted the observed non-linear behaviour in the threshold region. Also, as could be seen in the figure above, the model predictions indicated that a concentration of 16 mol% is very close to the optimum concentration with respect to the slope efficiency of the particular laser setup used. This was in agreement with the trends discussed by Sandrock *et al* for YLF crystals.

Future work

There are several different areas where further work is required to extend this research.

- One of the problems in the experimental work of this thesis was the non-uniform power distribution within the pump beam. This resulted in relatively large uncertainty in the estimate of the area of the beam spot. A beam homogeniser, not available for this thesis, could be used in future experiments to improve the uniformity of the pumping beam. This would allow more precise estimate of the energy density of the pump, which would reduce the associated uncertainties in the estimates of the initial populations of the various levels. A beam analyser could also be used. While it would not improve the uniformity of the pump beam, it would substantially improve the accuracy of our estimate of the beam size and therefore of the pump densities used. This will ultimately allow more precise values of the cross-relaxation rate constants to be obtained.
- A coherent model was developed, which predicted well the temporal population behaviour of the 5 lowest energy levels in the erbium ions. However, a really detailed analysis was carried out only for the case of 800 nm pumping. As can be seen from the discussions in Chapter 5, there are still some inconsistencies between model predictions and experimental data, especially for pumping wavelengths other than 800 nm. More detailed studies at these wavelengths, as well as new wavelengths (i.e. 650 nm), would allow further refinement of the model. Such studies could result in fine tuning of rate constants already introduced or perhaps even add small effects due to other processes. Processes, which are prominent at pump wavelengths other than the five used in this thesis could have a noticeable effect at some of these five pumping wavelengths. This may help remove

remaining inconsistencies between measurement and predictions of the existing model.

- Another useful study would be that of the fluorescence properties of Level 7 under direct pumping at around and 314 nm. As was mentioned previously, the radiative and multiphonon decay rates of this level suggest an overall decay time of several hundred microseconds. If this is the case, this level may play an important role in the overall population dynamics under UV pumping.
- Another study that would produce interesting information involves the effect of temperature on the overall population dynamics of the $\text{Er}^{3+}/\text{ZB(L)AN}$ system. Temperature variations result in redistribution in the population of the Stark levels and also in altered phonon-assisted decay rates. It has been shown for crystals (Lupei, 1990) that temperature affects the efficiency of the various cross-relaxation processes and different cross-relaxation processes can dominate the population dynamics of a particular level at different temperatures.
- As it was discussed previously, the model developed here predicted reasonably well the experimental output characteristics of the 2.7 μm lasers, reported by Sandrock *et al.*(1999). However, another important test and application would be to use the model to predict the laser dynamics in potential glass materials. Thus, one possible extension of the present work would be to study the suitability of the $\text{Er}^{3+}/\text{ZB(L)AN}$ glasses, studied in this thesis, for laser applications. The model could then be used to optimise various parameters, such as doping concentration with respect to the particular laser wavelength. While the immediate interest could concentrate on 1.5 μm and 2.7 μm emission wavelengths, other wavelength could also be studied at a later stage.

References

- Adam L.** and Sibley W.A., "Optical properties of rare earth ions in fluorozirconate glasses, Proceedings of the 3th Intern. Symp. Halide Glasses, France, 1985
- Aggarwal I.D.** and Lu G. (ed.), "Fluoride Glass Fibre Optics", Academic Press, San Diego 1991.
- Allain J.Y.**, Monerie M. and Poignant H., "Lasing at 1.00 μm in erbium-doped fluorozirconate fibre", *Electron. Lett.*, 25, 318, 1989
- Almeida R.M.** (ed.), "Halide Glasses for Infrared Fiber Optics", NATO ASI Series E, No.123 (Martinus Nijhoff, Dordrecht) 1987.
- Auzel F.**, Meichenin D. and Poignant H., "Laser cross-section and quantum yield of Er^{3+} at 2.7 μm in a ZrF_4 -based fluoride glasses", *Electron. Lett.*, 24, 909, 1988a
- Auzel F.**, Meichenin D. and Poignant H., "Tunable continuous-wave, room-temperature Er^{3+} -doped ZrF_4 -based glass laser between 2.69 μm and 2.78 μm ", *Electron. Lett.*, 24, 1463, 1988b
- Auzel F.**, "Rare earth in fluoride glasses", Proceedings 6-th Intern. Symp. Halide Glasses, 1989
- Barnes W.L.**, Poole S.B., Townsend J.E., Reekie L., Taylor D.J. and Payne D.N., " Er^{3+} - Yb^{3+} and Er^{3+} doped fiber lasers", *Journal of Lightwave Technology*, 7, 1461, 1989
- Brenier A.**, Moncorge R. and Pedrini C., " Er^{3+} - Tm^{3+} energy transfer in YLiF_4 (YLF), *IEEE J. Quantum Electron*, 26, 967, 1990
- Brierley M.C.** and France P.W., "Contonuous wave lasing at 2.7 μm in an erbium-doped fluorozirconate fibre", *Electron. Lett.*, 24, 935, 1988
- Brunel M.I.**, Vallet M., Bretenaker F., Le Floch A., Adam Jean-Luc, Duhamel-Henry N. and Allain Jean-Yves, "A simple method to measure the lifetime of excited levels of rare earth ions in fluorophosphate glasses", *Opt. Mat.* 5, 209, 1996
- Chen C.Y.**, Petrin R.R., Yeh D.C., Sibley W.A. and Adam J.L., "Concentration - dependent energy -transfer processess in Er^{3+} - and Tm^{3+} - doped heavy metal fluoride glass", *Opt. Lett.*, 14, 422, 1989

- Desurvire E.**, "Erbium-doped fibre amplifiers: Principles and applications", Wiley-Interscience, New York, 1994
- Dexter D.L.** "A theory of sensitized luminescence in solids", J.Chem.Phys., vol.21, 5, 836, 1953
- Di Bartolo B.**, "Energy transfer Processes in condensed matter", Plenu Press, New York, 1984
- Digonet M.J.F.**, "Rare Earth doped fiber lasers and amplifiers", Marcel Dekker, New York, 1993
- Di Pasquale F.**, "Modeling of highly-efficient grating-frdback and Fabry-Perot Er³⁺-Yb³⁺ co-doped fibre laser", IEEE J.Quantum Electron., 32, 326, 1996
- Eyal M.**, Raisfeld R., Jorgensen C.K. and Bendov B., "Laser properties of holmium and erbium in thorium -, zinc- and yttrium - based fluoride glass", Chem. Phys. Lett., 139, 395, 1987
- Fluck R.**, Haring R., Paschotta R., Gini E., Melchior H. and Keller U., "Eye-safe pulsed microchip laser using semiconductor saturable absorber mirrors", Appl. Phys. Lett., 72(25), 3273, 1998
- Fong F.K.** and Diestler D.J., "Many-body processes in nonradiative energy transfer between ions in crystals", J.Chem.Physics, 56, 2875, 1972
- France P.W.**, Brierley M.C., Carter S.F., Moore M.W and Williams J.R., "Fluoride Fibre Lasers for Sources over the Wavelength Range 1.0 to 3.0 μm ", SPIE 1048, IR Fibr. Opt., 124, 1989
- France P.W.**(Ed), "Fluoride Glass Optical Fibres", Blackie, London, 1990
- France P.W.** (Ed), Optical fibre lasers and amplifiers, Blackie and Son Ltd, 1991
- Gapontsev V.P.**, Matitsin S.M., Isineev A.B. and Kravchenko V.B., "Erbium glass lasers and their applications", Opt. Laser Techn., 189-196, 1982
- Gapontsev V.P.**, Matitsin S.M., Isineev A.B., "Channels of energy losses in erbium laser glasses in the stimulated emission process", Optics Comm., 46, 226 - 230, 1983
- Georgescu S.**, Lupei V., Lupei A., Zhekov V.I., Murina T.M. and Studenkin M.I., "Concentration effects on the up-conversion from the $^4\text{I}_{13/2}$ level of Er³⁺ in YAG", Optics Comm., 81, 186, 1991
- Haixing Z.** and Fuxi G., "Luminescence of Er³⁺ and Ho³⁺ ions in fluoride glasses", Proceedings of the 3Th. Intern. Symp. Halide Glasses, 1985, France

- Hanna D.C.**, Kazer A., Shepherd D.P., "A 1.54 μm Er glass laser pumped by a 1.064 μm Nd:YAG laser", *Optics Comm.*, 63, 417, 1987
- Hecht J.**, "Rare earths create useful long wavelength lasers", *Laser Focus World*, 135, 1993
- Heumann E.**, Ledig M., Ehrt D., Seeber W., Duszinsky E.W., Heide H.-J.v.d. and Huber G., CW laser action of Er in double sensitised fluoroaluminate glass at room temperature, *Appl. Phys. Lett.*, 52, 255, 1988
- Hilborn R.C.**, "Einstein coefficients, cross sections, f values, dipole moments and all that", *Amer. J. Phys.*, 50, 982, 1982
- Inokuti M.** and Hirayama F., "Influence of energy transfer by the exchange mechanism on donor luminescence", *J.Chem.Phys.*, 43, 1978, 1965
- Jiacheng Z.**, Chengfang L. and Bauki L., "Study of Heavy Metal Fluoride Glasses doped with Er³⁺", *Proceedings of the 8th Intern. Symp. Halide Glasses*, France, 1992
- Judd B.R.**, "Optical absorption intensities of rare earth ions", *Phys. Rev.*, 127, 750, 1962
- Kimura Y.** and Nakazawa M., "Gain characteristics of erbium-doped fibre amplifiers with high erbium concentration", *Electron. Lett.*, 28, 1420, 1992
- Knowles D.S.** and Janssen H.P., "Upconversion vs Pr-deactivation for efficient 3 μm laser operation in erbium", *IEEE J. Quantum Electron.* 28, 1197, 1992
- Koechner W.**, "Solid-state laser Engineering", Springer Verlag, 1992
- Laporta P.**, Silvestry S.De, Magni V. and Svelto O., "Diode-pumped cw bulk Er:Yb:glass laser", *Opt. Lett.*16, 1952, 1991
- Laporta P.**, Taccheo S., Longhi S. and Svelto O., "Diode-pumped microchip Er-Yb:glass laser", *Opt. Lett.*18, 1232, 1993
- Laporta P.**, Taccheo S., Longhi S., Svelto O. and Svelto C., "Erbium-ytterbium microlasers:optical properties and lasing characteristics", *Optics Mater.*, 11, 269, 1999
- Layne C.B.**, Lowdermilk W.H. and Weber M.J., "Multiphonon relaxation of rare earth in oxide glasses, *Phys.Rev.B*,16,10-20, 1977
- Lupei A.**, Lupei V.,Georgesku S., Ursu, I., Zhekov V.I.,Murina T.M. and Prokhorov A.M., "Many body energy transfer processes between Er³⁺ ions in yttrium aluminium garnet", *Phys.Rev.* 41/16, 10923, 1990

- Lupei V.**, Georgescu S. and Florea V., "On the dynamics of population inversion for 3 μm Er^{3+} lasers", *IEEE J. Quantum Electron.*, 29,426, 1993
- Newman P.N.**, private communication, 1999
- MacFarlane D.R.**, Javorniczki J.S., Newman P.J., Bogdanov V.K., Booth D.J. and Gibbs W.E.K., "High Er^{3+} content ZBN glasses for microchip laser applications", *J. Non-Cryst. Solids* 213 & 214, 158, 1997
- Millar C.A.**, Brierley M.C., Hunt M.H. and Carter S.F., "Efficient up-conversion pumping at 800nm of an erbium-doped fluoride fibre laser operating at 850nm", *Electron. Lett.*, 26, 1871, 1990
- Miniscalco W.J.**, Andrews L.J., Thomson B.A., Wei T. and Hall T., " $^4\text{I}_{13/2} \rightarrow ^4\text{I}_{15/2}$ emission and absorption cross sections for Er^{3+} -doped glasses", *OSA Proceedings on Tunable Solid State Lasers*, .5, 354, 1989
- Miniscalco W.J.**, Chapter: "Rare earth doped glasses: optical properties" in "Rare earth doped fibre lasers and amplifiers" by Ed. M.J.F.Digonnet, Marcel Dekker, New York, 1993
- Mitchell I.R.**, PhD thesis, "A spectroscopic study of Nd^{3+} and Pr^{3+} doped fluorozirconate glasses", Victoria University, Melbourne, 1999
- Moine B.**, Brenier A. and Pedrini C., "Fluorescence dynamics of Er^{3+} and Ho^{3+} ions and energy transfer in some fluoride glasses", *IEEE J. Quantum Electron.*, 25, 88, 1989
- Nakazawa M.**, Kimura Y. and Susiki K., "High gain erbium fibre amplifier pumped by 800 nm band", *Electron. Lett.*, 26, 549, 1990
- Nilsson J.**, Scheer B., Jaskorzynska, "Modelling and optimisation of short Yb^{3+} -sensitised Er^{3+} -doped fiber amplifiers", *IEEE Photon.Technol.Lett.* 6, 383, 1994
- Offelt G.S.**, "Intensities of crystal spectra of rare earth ions", *The J. Chem. Phys.*, 37, 511, 1962
- Okada K.**, Miura K., Masuda I. and Jamashita T., "Upconversion fluorescence in AlF_3 - ZrF_4 based fluoride glass containing ErF_3 ", *Proc. 5th Intern. Symp. Halide Glasses*, Japan, 1988
- Oomen E.W.J.L.**, Le Gall P.M.T. and van Dongen A.M.A., "On the origin of the red emission band from erbium doped fluoride glasses excited with 800 nm", *J Lumin.*, 46, 353, 1990

- Petreski B.P.**, Schilders S.P., Farrel P.M. and Gu M., "Imaging concentration profiles of praseodymium-doped optical fibres", *Electron. Lett.*, 33, 889, 1997
- Pollack S.A.** and Robinson M., "Laser emission of Er^{3+} in ZrF_4 -based fluoride glasses", *Electron. Lett.*, 24, 320, 1988
- Pollnau M.**, "The Route toward a Diode-Pumped 1-W Erbium 3 μm Fiber Laser", *IEEE J. Quantum Electron.*, 33, 1982, 1997
- Pope C.L.**, Reddy B.R., Nash-Stevenson S.K., Efficient violet upconversion signal from a fluoride fiber doped with erbium, *Opt.Lett.*, 22, 295, 1997
- Poppe E.**, Srinivasan B. and Jain R.K., "980 nm diode pumped continuous wave mid-IR(2.7 μm) fibre laser", *Electron. Lett.*, 34(24), 2331, 1998
- Poulain M.**, Poulain M., Lucas J. and Brun P., *Mater. Res. Bull.*, 10, 243, 1975
- Poulain M.**, Chap.2, in "Fluoride Glasses" by Comyns A.E., Wiley, 1989
- Quimby R.S.** Drexhage M.G and Suscavage M.J., Efficient frequency up-conversion via energy transfer in fluoride glasses, *Electron; Lett.*, 23, 32, 1987
- Reisfeld R.** and Jorgensen C.K., "Lasers and Excited States of Rare Earths", Springer, Berlin, 1977
- Reisfeld R.**, Katz G., Spector N., Jorgensen C.K., Jacoboni C. and De Pape R., "Optical transition probabilities of Er^{3+} in fluoride glasses", *J. Solid State Chem.*, 41, 253, 1982
- Reisfeld R.** and Jorgensen C.K., "Excited States Phenomena in Vitreous Materials", Elsevier, Amsterdam, 1987
- Samek L.**, Wasilak J. and Marczuch K., "Optical properties of fluorozirconate glasses activated with rare earth elements" *J Non-Cryst. Solids*, 140, 243, 1992
- Sandrock T.**, Dening A. and Huber G., " Laser emission of erbium-doped fluoride bulk glasses in the range from 2.7 to 2.8 μm ", *Opt. Lett.*, 24/6, 382, 1999
- Shi W.Q.**, Bass M. and Birnbaum M., "Effects of energy transfer among Er^{3+} ions on the fluorescence decay and lasing properties of heavily doped $\text{Er}:\text{Y}_3\text{Al}_5\text{O}_{12}$ ", *J. Opt. Soc. Amer. B*, 7, 1456, 1990
- Shinn M.D.**, Sibley W.A., Drexhage M.G and Brown R.N., Optical transitions of Er^{3+} ions in fluorozirconate glass", *Phys. Rev. B*, 27, 6635, 1983
- Smart R.G.**, Carter J.N., Hanna D.C. and Trooper A.C., "Erbium-doped fluorozirconate fibre laser operating at 1.66 and 1.72 μm ", *Electron. Lett.* 26, 649, 1990
- Snitzer E.** and Woodcock R., "Yb $^{3+}$ -Er $^{3+}$ glass laser", *Appl.Phys Lett* 6 (1965) 45-46

- Srinivasan B.**, Tafoya J. and Jain R.K., "High power Watt-Level CW operation of diode pumped 2.7 mm fiber lasers using efficient cross-relaxation and energy transfer mechanisms", *Optics Express*, 4(12),10, 1999
- Stone J.** and Burrus C.A., "Neodymium-doped silica lasers in end-pumped fiber geometry", *Appl. Phys. Lett.*, 23,388, 1973
- Taira T.**, Mukai A., Nozawa Y. and Kobayashi T., "Single - mode oscillation of laser-diode-pumped Nd:YVO₄ microchip lasers", *Opt. Lett.*, 1, 1955, 1991
- Taccheo S.**, Laporta P., Longhi S., Svelto O., and Svelto C, "Diode pumped bulk erbium-ytterbium lasers", *Appl. Phys. B*, 63, 425, 1996
- Vickers D.J.** and McFarlane R.A., "Intensity parameter measurements for Er, Ho, Tm and Pr in fluorozirconate glass", *OSA Proceedings on Advanced Solid State Lasers*, 13, 280, 1992
- Van Dongen A-M.**, Oomen E. and Gall P.le, "Upconversion in rare-earth doped fluoride glasses", *SPIE, 1513: Glasses for Optoelectronics*, 330, 1991
- Watts R.K.** and Richter H.J., "Diffusion and transfer of optical excitation in YF₃:Yb,Ho", *Phys.Rev.B*, 6, 1584, 1972
- Weber M.J.**, "Luminescence decay by energy migration and transfer:observatuion of diffusion limited relaxation, *Phys.Rev.B*, 4, 2932, 1971
- Wetenkamp L.**, PhD Thesis, 1991
- Wetenkamp L.**, West G.F. and Tobben H., "Co-doping effects in Er³⁺- and Ho³⁺-doped ZBLAN glasses", *J. Non-Cryst. Solids*, 140, 1992 a.
- Wetenkamp L.**, West G.F. and Tobben H., "Optical properties of rare earth-doped ZBLAN glasses", *J. Non-Cryst. Solids*, 140, 1992 b
- Whitley T.J.**, Miller C.A., Wyatt R., Brierley M.C. and Szebesta D., "Upconversion pumped green lasing in erbium doped fluorozirconate fibre", *Electr. Lett.*, 27/20, 1785, 1991
- Wright J.C.**, "Up-conversion and excited state energy transfer in rare-earth doped materials" in "Radiationless processes in molecules and condensed phases" by Fong F.K., Springer-Verlag, 1976
- Yanagita H.**, Okada K., Miura K., Toratani H. and Yamashita T., "Er³⁺ doped fluorozirco-aluminate glasses", *Proceedings 6-th Intern. Symp. Halide Glasses*, 1989

- Yanagita H.**, Toratani H., Yamashita T. and Masuda I., "Diode-pumped Er glass laser at 2.7 μm ", *SPIE, 1513: Glasses for Optoelectronics*, 386, 1991
- Yokota M.** and Tanimoto O., "Effects of diffusion on energy transfer by resonance", *J.Phys.Soc.Japan*, 22, 779, 1967
- Zayhowski J.J.** and Mooradian A., "Single-frequency microchip Nd laser", *Opt. Lett.*, 14, 24-26, 1989
- Zhekov V.I.**, Lobachev V.A., Murina T.M. and Prokhorov A.M., "Cooperative phenomena in yttrium erbium aluminium garnet crystals", *Sov. J Quantum Electr.*, 14, 128, 1984
- Zhekov V.I.**, Murina T.M., Prokhorov A.M., Studenikov M.I., Georgescu S., Lupey V. and Ursu I. "Cooperative processes in $\text{Y}_3\text{Al}_5\text{O}_{12}:\text{Er}^{3+}$ crystals", *Sov J. Quantum Electron.*, 16, 274, 1986
- Zhekov V.I.**, Murina T.M., Prokhorov A.M., Studenikov M.I., Georgescu S., Lupey A. and Lupey V. "Nonradiative transfer of excitation energy in crystals with the interaction of three optically active centres", *JETP Lett.*, 52, 670, 1990
- Zou X.** and Izumitani T., "Spectroscopic properties and mechanisms of excited state absorption and energy transfer upconversion for Er^{3+} -doped glasses", *J Non-Cryst. Solids*, 162, 68, 1993

Symbols and Acronyms

*- a number with very large fitting uncertainties

a – host dependent parameter

^A – assumed value

A_i – radiative decay rate

A_{ij} - the spontaneous emission rate from state i to state j

b – host dependent parameter

b_{ij} – branching ratio for fluorescence from Level i to Level j

c - constant ($w(R)=cR^{-5}$)

C – erbium concentration

C^* – constant $=n_{20}(\omega_2+b_{21}A_2)$

D –thickness of the sample

D^* –diffusion coefficient

E – energy of the pump pulse,

E_{abs} - absorbed pumping energy

ESA – excited state absorption

f_{ij} (f_{ji}) - emission (absorption) oscillator strength of the transition from level i to level j (or vice versus).

g_i - degeneracy factors of level i

g_j - degeneracy factors of Level j

$h\nu$ – pump photon energy

k – constant ($k=(4/3)\pi\Gamma(1-3/s)N_aR_o^3\tau_o^{-3/s}$)

K – cross-relaxation coefficient corresponding to W(22,50) or W(11,30)

K' – constant $=(2KC)$

K_d – coefficient (see Equations 2.3-7 ÷2.3-10)

m - mass of the electron.

N_0 - the absolute population of the ground level

NA – non available

N_a – number acceptor ions per unit volume

N_d – donor concentration
 NE – non-exponential
 N_{ei} – the number of excited ions
 $N_{ei/v}$ - the number of excited ions per unit volume
 N_i – absolute population of i-th Level
 n_i – normalised population of i-th Level (normalised with the Er^{3+} concentration)
 n_{i0} – initial normalized population of i-th Level
 p – the number of photons required to bridge an energy gap
 P, Q – constants
 R – repeated measurements for repeatability check
 R^2 – correlation coefficient
 R_n – donor - acceptor separation
 s – constant ($s=6, 8$ or 10 depending on the type of multipolar interaction)
 S – pumped area of the sample
 SSD – sum of the squares of the differences
 T – three ion cross-relaxation process
 t – time
 t_i – time constants
 U – constant (see Equation 2.3-10)
 v – sample volume
 V_i - measured voltage, corresponding to relative population n_i
 W – two-ion cross-relaxation process
 $w(R_n)$ – probability for direct donor - acceptor energy transfer
 $x = D * c^{-1/3} * t^{2/3}$
 Z – constant $= V_1(t) / n_1(t)$
 $ZBLAN$ - Zirconium Barium Lanthanum Aluminium Sodium

$v(\mathbf{r} - \mathbf{r}_n)$ – the probability for energy transfer from an excited donor to the n^{th} acceptor at position \mathbf{r}_n

$\Phi(\mathbf{r},t)$ – excitation density

Γ – gamma function

α – absorption coefficient

λ_{ij} – the wavelength for the transition from level i to level j

λ – wavelength

σ_{ij}^λ – the pick cross-section at wavelength λ for absorption from level i to level j

σ – absorption cross-section,

σ^l – integrated absorption cross-section

τ_0 – intrinsic decay rate(the decay time in absence of energy-transfer processes)

τ_r (τ_d) – rise (decay) time constants of exponential functions

ω_i – multiphonon decay rate from i -th level

ω_{ij} – the resonance frequency of the transition from Level i to Level j

Publications

1. Resulting from the work of this thesis

a) Journal articles:

- **V.K.Bogdanov**, W.E.K.Gibbs, D.J.Booth, J.S.Javorniczki, P.J.Newman and D.R.MacFarlane, “Energy exchange processes in Er^{3+} -doped fluorozirconate glasses”, Journal of Non-Crystalline Solids, v.256 & 257, 288-293, (1999)
- D.R.MacFarlane, J.S.Javorniczki, P.J.Newman, **V.K.Bogdanov**, D.J.Booth and W.E.K.Gibbs, “High Er^{3+} content ZBN glasses for microchip laser applications”, Journal of Non-Crystalline Solids 213 & 214, 158-163, (1997)
- **V.K.Bogdanov**, W.E.K.Gibbs, D.J.Booth, J.S.Javorniczki, P.J.Newman and D.R.MacFarlane, “Fluorescence from highly-doped erbium fluorozirconate glasses pumped at 800 nm”, Optics Communications 132, 73-76, (1996)
- J.S.Javorniczki, P.J.Newman, D.R.MacFarlane, D.J.Booth and **V.K.Bogdanov**, “High erbium content heavy metal fluoride glasses”, Journal of Non-Crystalline Solids, 249, (1995)

b) Conferences/Workshop presentations:

- **V.K.Bogdanov**, W.E.K.Gibbs, D.J.Booth, J.S.Javorniczki, P.J.Newman and D.R.MacFarlane, “Rate-equation modelling of fluorescence in Er^{3+} -doped fluorozirconate glasses”, DSTO-workshop, Salisbury, August, 1998

- **V.K.Bogdanov** , W.E.K.Gibbs , D.J.Booth , J.S.Javorniczki, P.J.Newman and D.R.MacFarlane, “Energy level processes in heavily-doped Er^{3+} fluorozirconate glasses”, AOS conference, Adelaide, 1997

2. Resulting during the course of the work of this thesis

- Ian R.Mitchell, **Valentin K.Bogdanov** and Peter M.Farrell, “Energy transfer in praseodymium and neodymium co-doped fluorozirconate glass”, Optics Communications 155, 275-280 (1998)
- S.A.Wade, **V.K.Bogdanov**, S.F.Collins and G.W.Baxter and G.Monnom, “Thermalisation of the $^5\text{D}_0$ and $^5\text{D}_1$ excited states in europium-doped optical fibre”, 13th National Congress of the Australian Institute of Physics, Fremantle Sept. 1998
- S.A.Wade, P.M.Farrell, **V.K.Bogdanov**, S.F.Collins and G.W.Baxter, “Modelling of the temperature dependent lifetimes of thermally coupled levels in Eu^{3+} -doped silica fibre”, Submitted to ACOLS 98, Christchurch, NZ, December 1998

